



The
University
Of
Sheffield.

Access to Electronic Thesis

Author: Gary Dunderdale
Thesis title: Autonomous Motion of Small Particles through Surface Interaction Gradients
Qualification: PhD

This electronic thesis is protected by the Copyright, Designs and Patents Act 1988. No reproduction is permitted without consent of the author. It is also protected by the Creative Commons Licence allowing Attributions-Non-commercial-No derivatives.

This thesis was embargoed until 20 July 2012.

If this electronic thesis has been edited by the author it will be indicated as such on the title page and in the text.

Autonomous Motion of Small Particles through Surface Interaction Gradients



Gary Dunderdale

Department of Chemistry, The University of Sheffield

Submitted for the degree of Doctor of Philosophy

September 2011

Declaration

The work described in this thesis was undertaken at The University of Sheffield between October 2008 and September 2011 under the supervision of Dr. Patrick Fairclough and Dr. Jonathan Howse. Unless stated, all the work is the authors and has not been submitted in whole or in part for any other degree at this or any other institution.

Acknowledgements

I would like to thank the following people for their assistance and help during my research:

Patrick Fairclough for providing me with the opportunity to study for a Ph.D, supervising me over the last three years and allowing the research to be pursued in directions which interested me. Andy Parnell for help with Atomic Force Microscopy measurements and fitting gathered ellipsometry results. Steven Ebbens for help with optical microscopy, particle tracking and preparation of janus particles. Mike Weir for help with polymer brush preparation and kinetic ellipsometry measurements. Joseph Adams for help in preparing gold surfaces and thiol monolayers. Damien Dupin for help in preparing latex particles and with zeta potential measurements. Adam Blanz for help with Gel Permeation chromatography. Chris Hill for help with Scanning Electron Microscopy.

Abstract

A theoretical design by Balazs et al (ACS Nano, 2008), in which two particles are propelled forward by changing their interaction with a compliant surface by releasing nanoparticles, was attempted to be implemented.

Initial studies showed that the design needed to be altered slightly to overcome the friction encountered between the particles and the surface, and to alter the surface by a way other than by the adsorption of nanoparticles. These alterations to the design included changing the interactions present from totally adhesive, to partially or completely repulsive to overcome friction, and substituted a catalytic chemical reaction for the release of nanoparticles used in theoretical design.

An implementation of the theoretical design which used repulsive van der Waals forces to change the particle-surface interaction from adhesive to repulsive, by the catalytic conversion of benzene and bromine to bromobenzene, was investigated. It was found that although the particle-surface interaction could be converted from attractive to repulsive, the rate of the catalytic reaction was too slow to surround the catalytic particles with enough bromobenzene to propel particles forward.

Electrostatic repulsions between a particle and surface were investigated and found to be unable to significantly change the particle-surface interaction, so were of no use in implementing the theoretical design.

Another implementation of the theoretical design which used the steric forces exerted between a particle and surface to alter the particle-surface interaction was investigated. It was found that these steric interactions could significantly influence particles and were able to control their position on a surface. Ways to change the steric interactions from repulsive to more repulsive by a chemical reaction were found and catalytic particles which could release the required reagent created. In all cases it was found that the rate of catalytic reaction was too slow to modify the surface in the correct way to produce propulsion.

It was concluded that substituting a catalytic chemical reaction for the release of nanoparticles in the theoretical design is not a viable alternative which can be used to alter a surface and thus change the particle-surface interaction to create propulsion.

Contents

Chapter 1:	Introduction to Nanopropulsion	1
1.1	Theoretical and Exploratory Research into Nanopropulsion	5
1.2	Scaling-down Existing Technology	9
1.3	Propulsion of Small Objects	11
1.4	Nanorods which Propel themselves through Solution	13
1.5	Increasing the Speed of Nanorods	16
1.6	Controlling the Motion of Nanorods	18
1.7	Making use of Self propelling Nanorods	22
1.8	Other Propulsion Mechanisms	24
1.9	Nano Swarms	27
1.10	A Design to Work From	31
Chapter 2:	Preliminary Experiments into Creating Propulsion Along a Surface Gradient	
2.1	Reversibility of Adhesion	38
2.2	Frictional Forces Between a Particle and Surface	44
2.3	The use of Nanoparticles to alter Surfaces and Particle-Surface Interactions	50
2.4	Summary and Conclusions	54
2.5	Experimental Details	56
Chapter 3:	Propulsion using Repulsive van der Waals Forces	
3.1	Introduction	60
3.2	A Combination of Materials to use	66
3.3	Calculation of Dielectric Response Functions and Hamaker Constants	68
3.4	Confirmation of Repulsive van der Waals forces	73
3.5	Catalysts	77
3.6	Measuring the Rate of Bromination	82
3.7	Rate of Reaction Necessary to Create Repulsive van der Waals Forces	85
3.8	Is Propulsion of Catalytic Particles Observed?	88
3.9	Gold / Iron Janus Particles	91
3.10	Summary of using Repulsive van der Waals Forces to Create Propulsion	93
3.11	Experimental Details	95

Chapter 4: Propulsion using Electrostatic interactions

4.1	Introduction	98
4.2	Particle-Surface Interaction Calculations	101
4.3	Creating Surfaces which can alter their Surface Charge	105
4.4	Sedimentation Experiments	110
4.5	Repulsion-Repulsion Surface Interaction Patterns	117
4.6	Adhesion-Repulsion Surface Interaction Patterns	122
4.7	Adhesion-Adhesion Surface Interaction Patterns	125
4.8	Summary and Conclusions	131
4.9	Experimental Details	133

Chapter 5: Propulsion using Steric Interactions

5.1	Introduction	136
5.2	Achieving Colloidal Stability on Polymer Brushes	138
5.3	Can Polymer Brushes Influence Small Particles?	141
5.4	Altering the Thickness of a Polymer Brush by pH	160
5.5	Swelling by Chemical Modification with Methyl Iodide	181
5.6	Creating a Polymer Brush by Grafting-to	185
5.7	Summary and Conclusions	188
5.8	Experimental Details	191

Chapter 6: Summary, Discussion and Conclusions

6.1	Summary	200
6.2	Discussion	202
6.3	Conclusion	207
6.4	Future Work	208

Appendix 1: Calculation of Forces F and f from Chapter 5 210

1 Introduction to Nanopropulsion

Propulsion of small objects through liquids is essential to achieve, if technology such as that proposed by many nanotechnologists is to become reality rather than science fiction. Authors such as Drexler¹ describe tiny machines which are able to do incredible feats, such as *assemblers* which construct objects from a feedstock of materials and *doctor* machines which travel around the human body repairing broken cells. Many have criticised Drexler and say that this future will never appear, but acquiring better knowledge of propelling small objects around will still be of great use if achieved.

Propulsion of small objects is much different to the propulsion of large objects which we are accustomed to. Macroscopic heat engines such as a combustion engine cannot be simply scaled down to nanoscopic sizes, as they rely on temperature gradients to convert chemical energy to mechanical. At small length scales the temperature differential becomes so large that it is impossible to maintain². Therefore a different propulsion method must be designed.

An often quoted obstacle to be overcome by a small object to enable it to under go propulsion is the low Reynolds number of the potential vehicle. Reynolds number describes how fluids flow around an object and is given by the equation:

$$\Re = \frac{av\rho}{\eta}$$

eq. 1

where a is the size of the vehicle, v the velocity of the vehicle, ρ the density of water or continuous fluid, and η the dynamic viscosity of water or the continuous fluid.

Two distinct regimes of fluid flow can be identified based on Reynolds number. When the vehicle is large and moves quickly, as in macroscopic vehicles, $\Re > 1$. The flow of liquid around the vehicle is said to be turbulent, as the inertial forces created by the vehicle moving through water dominate over the viscous forces in water, and so the water

is *sheared*. When the size of the vehicle is reduced and the velocity is slower, $\Re \ll 1$. Under these conditions the flow of water around the vehicle is said to be laminar, as the fluid flows in straight smooth lines around the vehicle. Now the viscous forces of water dominate over inertial forces created by the vehicle.

A submarine travelling through the sea has a Reynolds number of around $\sim 10^8$ and so the submarine experiences turbulence around its hull. If the engine is stopped in the submarine while it is moving it will coast to a stop over hundreds of meters. Whereas a bacterium has a Reynolds number of $\sim 10^{-5}$ and experiences lamella flow where the viscosity of water dominates. Thus, if a spermatozoa were to suddenly stop swimming through solution it could come to a stop instantly³. The distance coasted can be calculated to be $\sim 0.04\text{\AA}$, which is less than the atomic radii of a single atom.

The second obstacle to be overcome is Brownian motion⁴. This is the seemingly random motion of small particles through a liquid, which causes them to diffuse from one area to another and also be rotated. This random motion is caused by collisions between molecules of the liquid and the small particle, which pass on a small kinetic energy to the particle causing it to move. The result of many collisions causes the particle to become displaced by a certain distance which follows Einstein's equation in two dimensions:

$$\langle \Delta L \rangle^2 = 4Dt \tag{eq. 2}$$

where $\langle \Delta L \rangle^2$ is the average length displaced squared, t the amount of time and D the diffusion coefficient given by:

$$D = \frac{kT}{6\pi\eta r} \tag{eq. 3}$$

where k is the Boltzmann constant, T is the temperature, η the viscosity of the surrounding liquid and r is the particles radius.

From Einstein's equation it can be seen that the distance displaced is proportional to the square root of time, therefore it takes a particle four times as long to travel a distance twice as far. This means that a bacteria will diffuse a distance of its own body length by Brownian motion, in around one millisecond. Whereas to be displaced a large distance requires many hours.

Brownian motion also causes small objects to be rotated about their position, according to the equation:

$$\langle \theta \rangle^2 = 2D_r t$$

eq. 3

where $\langle \theta \rangle^2$ is the average angle rotated squared, D_r the rotational diffusion coefficient and t time. From this equation it can be calculated that a 1 μm diameter particle is rotated 90° in less than a second.

The consequences of Brownian motion for a small vehicle are great, the vehicle will be buffeted from side to side and up and down which may interfere with the propulsion mechanism. It will also be rotated, meaning that it cannot simply head off in the direction of its destination and hope to get there, as it will be quickly rotated causing it to propel itself in the wrong direction. As the vehicle will also have no sense of direction, rotational Brownian motion will also cause the vehicle to become disorientated.

Nature has overcome these problems of low Reynolds number and Brownian motion and many examples of motion can be observed in bacteria and cellular biology.

Kinesin is a motor protein found in eukaryotic cells and is able to propel itself along microtubules. It is responsible for moving organelles around a cell within the cytoplasm. The Kinesin motor protein moves along the microtubule via two connection points, which take it in turn to disconnect from the tube and migrate further along the tubule; thus Kinesin is said to move in a hand over hand fashion.

The protein moves along the microtubule in steps of 8nm, consuming one molecule of its energy source adenosine triphosphate per step, giving a propulsion velocity of 0.3 $\mu\text{m s}^{-1}$. The protein takes around 100 steps along the microtubule before disconnecting and drifting away. Block and Guydosh⁵ have studied the motion of Kinesin along a microtubule by attaching a macroscopic silica bead to the protein. It was observed using light microscopy that the bead was propelled along the microtubule.

E. Coli usually have six flagella attached to the outside of their bodies. By rotating all the flagella anticlockwise the bacterium is able to bundle them together and be propelled forward. By rotating the flagella clockwise, the flagella no longer bundle together and cause the bacteria to rotate about its centre faster than normal. These two modes of flagella motion give rise to motions known as runs and tumbles⁶.

E. Coli makes use of these two different modes to enable it to beat Brownian motion. Its body is coated with receptors for specific chemical species which allows it to measure the 'quality' of its current environment every four seconds. If the quality of its environment has improved over the last four seconds, the bacterium executes a short tumble before carrying on with a run in a similar direction. If the environment gets worse

after four seconds the bacteria executes a larger tumble before the next run, meaning that its direction of propulsion is changed significantly⁷. Using this run and tumble strategy, E. Coli can migrate from one area to another in response to a chemical species, this is known as chemotaxis.

Bacteria and other structures in nature are exquisite examples of creating mobility that currently cannot be reproduced synthetically due to their complex structures involved. To achieve mobility a much simpler mechanism must be used based on synthetically feasible chemistry.

Motion caused by chemical reactions in a synthetic environment has been observed before. For example, when mercury droplets are placed on the surface of a potassium dichromate and nitric acid solution they are observed to be propelled forward in a random motion^{8,9}. A similar motion has also been observed when a small piece of camphor is placed on the surface of water¹⁰⁻¹².

Whitesides et al¹³ were some of the first researchers to produce motion by a chemical reaction on relatively small objects. They created disks of plastic 1cm in diameter, with an asymmetric placement of platinum on their surface. When these disks were floated on top of a solution of hydrogen peroxide, the platinum decomposed H₂O₂ to water and bubbles of oxygen. These bubbles released from the disk asymmetrically causing it to be propelled forwards. The group also created disks of plastic which were chiral and observed that disks self-assembled with other disks only of their own chirality.

Motion on liquid droplets has also been created by placing the droplet on a surface with a chemical or thermal gradient^{14,15}. The droplet migrates along the gradient to an area of lower surface energy if a chemical gradient is used, or an area of higher surface energy if a thermal gradient is used. Sumino et al¹⁶ have created droplets that create a gradient of surface energy underneath themselves by removing surfactant from the surface. In this way they are able to propel themselves forward and also migrate greater distances than if the surface gradient is fixed. If a curved circular surface was used the droplets were observed to propel themselves around the circle and perform loop-the-loops.

Much work by researchers has also gone into manipulating small objects in liquids using externally applied fields. In this way particles can be propelled through solution from one area to another.

Optical forces have been widely used to control the placement and freedom of small particles in so called *optical tweezers*¹⁷. These optical tweezers exert forces on particles by illuminating them with a highly focused laser. As the photons of light incident on the

particle they are refracted, causing a change in their momentum. As all forces have an equal and opposite force, the particle experiences a force in the opposite direction of the refracted light due to its change in momentum.

The flow of a liquid is a simple way to achieve motion of small particles. Ropp et al¹⁸ have created a flow cell in which very small particles can be either held in place or propelled from one region to another by controlling the flow of liquid in the cell. Lee et al¹⁹ have used a microfluidic device with three input channels having different flow rates, to focus a dispersion of small particles into a thin line of single particles.

Electrophoresis²⁰, thermophoresis²¹ and magnetophoresis²² are all transport phenomenon of small particles dispersed in liquids caused by the external application of either a temperature gradient or electrical or magnetic field, and can be used to transport particles through a liquid. But with the application of an external field all particles experience an equal force in the same direction meaning that they must all exhibit identical motions. To move in an individual way particles must be capable of propelling themselves forward.

1.1 Theoretical and Exploratory Research into Nanopropulsion

Many researchers have proposed theoretical designs to achieve motion at the nanoscale which take into account factors such as low Reynolds number and Brownian motion. Purcell's 3-link swimmer²³ is the most famous of these designs which he described in his lecture *Life at low Reynolds number*. During this lecture he highlighted the problems which would be encountered in creating a small object which deforms to propel itself through a liquid including the problem of breaking the *time-reversibility* of the swimmer's deformations.

He states that a small object similar to a scallop which consists of two rigid sections joined together by a hinge so that the object can deform by opening and closing like a book, would not be able to deform in a fashion which would lead it to be propelled forward through solution, due to the low Reynolds number. If the 'scallop' opens, this produces a force which causes the object to move forward slightly but as the scallop closes an opposite force is created which moves the scallop backwards by the same amount as it was initially moved forward. This means that a swimming strategy used by the scallop of simply opening and closing would lead to the scallop oscillating backwards

and forwards around one position as it opens and closes, instead of the desired propulsion forward.

This oscillation is a direct consequence of the swimmer's deformations being *time-reversible* – the closing deformation is the same as the opening deformation but in reverse. Perhaps it might be thought that altering the speed at which the scallop opens and closes will break the time-reversibility, but it does not due to the low Reynolds number - opening the scallop is equal to closing the scallop at any speed.

Scallops in real life are able to propel themselves forward by an opening and closing mechanism because they are macroscopic and so at high Reynolds number and experience turbulent flow of liquid around themselves. Due to this turbulence the opening and closing processes are slightly different each time, and along with inertia which is significant at high Reynolds number, the time-reversibility of the motion is broken.

To break the time-reversibility Purcell proposed a swimming strategy for a small object consisting of three rigid sections joined together by two hinged sections, as shown below in Figure 1. By having the extra hinged segment the object can deform in a way which breaks the time-reversibility.

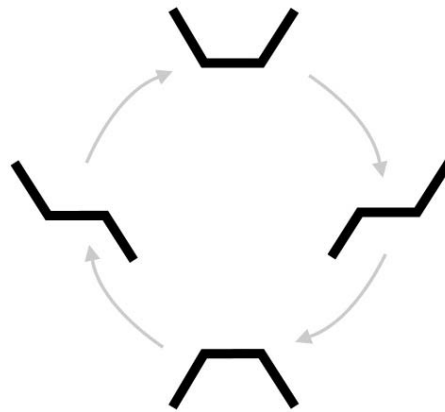


Figure 1 Schematic of Purcell's three link swimmer deforming in a non-time reversible way.

Golestanian and Najafi²⁴ have designed a swimmer which is very similar to Purcell's, except in this design three spheres are joined together by two deformable linkages which can change their lengths. This substitution was made in an effort to make an experimental realisation of the strategy more accessible but it remains still very synthetically challenging. The swimmer propels itself by shortening and lengthening the

deformable linkages in a cycle which alters the distance between spheres in a non time-reversible way. The authors found that the velocity at which the swimmer was propelled is dependant on the change in distance between the connected spheres.

Much work has also concentrated on designing objects which can propel themselves forwards using a mechanism which does not rely on the physical deformation of the object. Golestanian et al²⁵ have proposed that a chemical reaction catalysed on the surface of an object can create a gradient of chemical potential or particle mobility, which would result in the propulsion of the object. They studied how the shape of the object and the placement of catalyst effects the subsequent propulsion, finding that the symmetry of the chemical potential and/or mobility around the particle must be broken by the asymmetrical placement of the catalyst. Several different designs were suggested including i) a Janus particle where one hemisphere is functionalised with a catalyst, ii) a design in which a spherical particle has an equatorial belt containing catalyst and two hemispheres which have different mobility's for the products of the catalysed reaction, and iii) a design in which a substance is created at one pole and consumed at the other.

A spherical geometry was suggested to be better than a rod shape with the longest dimension the same length as the particle diameter. Propelled velocity was proposed to be independent of the objects size.

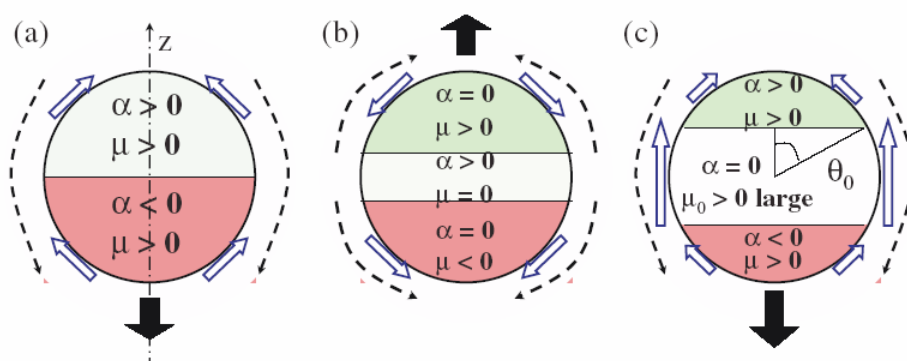


Figure 2 Three spherical swimmers proposed by Golestanian et al, reproduced from ref²⁵. a) Janus swimmer where a chemical reaction occurs on the top hemisphere b) Saturn swimmer where catalyst is in an equatorial belt c) swimmer in which a substance is created and then consumed at the poles.

Kapral et al²⁶ have also proposed vehicles which are propelled forward by a chemical reaction. In one scheme two particles come into close proximity, one particle is catalytic whereas the other is inert. The catalytic particle converts solvent molecules A to solvent

B, thus also changing the interactions between the solvent and particles. Following simulations using multiple particle collision dynamics, the authors found that the conversion of A to B lead to propulsion of the pair of particles by the preferential migration of solvent B towards either the catalytic particle or the non catalytic particle, depending on which interaction between the solvent and the particles is stronger.

This design is extremely simple in that it only requires two particles which could be created separately to come into close proximity, meaning that it should be synthetically accessible. Although perhaps it would be difficult to find a chemical reaction catalysed by a substance which could be immobilised onto a particle which has the correct rate of reaction and gives the correct interaction with the different particles. Interactions were also modelled by a simple Lennard-Jones interaction consisting of a very short ranged repulsion due to the Born condition that two atoms cannot occupy the same space and a single long range interaction. This modelling may be too simplistic to describe the total interaction between a molecule and particle which consist of many interactions such as dispersion forces, Coulomb interactions, hydrogen bonding etc with differing decay lengths.

The same authors have also published a related design in which the second inert sphere is replaced with a polymer chain²⁷. Again the catalytic sphere converts the solvent A to solvent B, changing the interactions between the tethered polymer chain and the surrounding liquid. From simulations the authors found that the swimmer propelled itself forward in the direction of the catalytic head group by the preferential migration of the tethered polymer chain towards the catalytic head group. Propelled velocity was also fastest when the length of the polymer chain was small when in a poor solvent and when the size of the catalytic head group was increased up to a certain size after which the velocity decreased due to the extra viscous drag.

Work by Coq et al²⁸ into the fluid physics of flagellas which rotate to create propulsion, has shown that a helical shaped flagella is not needed to create propulsion. Using a cylindrical soft filament of macroscopic size, they observed a transition from straight to helical shape as the filament was rotated. This induced helicity is caused by viscous resistance of the liquid on the filament's surface and generates a propulsive force along the axis of rotation. By altering the frequency of rotation the 'tightness' of the helix could also be controlled. This work has highlighted that a swimmer needs only a flexible tail which rotates, rather than a complex helical shaped tail which is synthetically challenging to construct.

1.2 Scaling-down Existing Technology

Much work has gone into the design and fabrication of so called ‘Nanocars’²⁹, which are essentially scaled down versions of macroscopic cars. They generally consist of a rigid chassis made from a single organic molecule joined to alkyl groups which act as ‘bearings’ for the wheels allowing free rotation due to their triple carbon-carbon bond. Wheels are attached to these bearings which normally consist of spherical molecules like fullerenes such as C₆₀ or carboranes.

When placed on an atomically smooth surface such as gold and heated above 200°C while being observed by Scanning Tunnelling Microscopy (STM), these nanocars apparently then start to move around and migrate from one area to another on the surface³⁰. The reason why these molecules move around is not clear and has not been addressed. As they do not contain any engine capable of propelling themselves forwards the only mechanism of motion is diffusion, but the published results seem to show these objects moving only forwards instead of the expected forwards and backwards. No

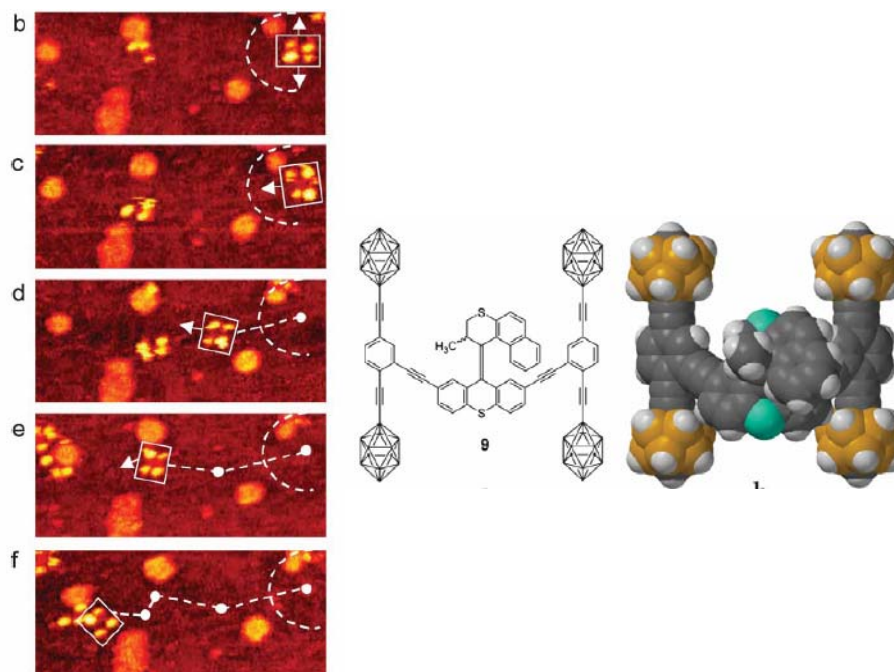


Figure 3 STM images of a nanocar migrating over a gold surface at 200°C over the course of 10 minutes, reproduced from ref³⁰ (left) and chemical structure of a nanocar equipped with a photo-isomerisable engine, reproduced from ref³¹ (right).

motion is observed until the surface temperature is raised to 200°C which does not seem logical. Heating increases the nanocars' thermal energy, meaning that an energy barrier to motion could be overcome but it presumably also increases the strength of interactions between the nanocar and the surface, increasing the energy barrier to motion.

The nanocars were imaged using STM meaning that the motion was captured at a very low frame rate ~1 frame per minute, and the distance travelled by the nanocar between individual frames is around three of its own diameters. As there are multiple nanocars in close proximity to each other, the low frame rate means that an observer cannot be sure if a nanocar in sequential image frames is in fact the same one. From the published images it can be seen that objects which look like nanocars appear and disappear intermittently on the surface, raising serious questions about whether the observed 'motion' is in fact the nanocars propelling themselves forward.

Several 'engines' have been incorporated into these nanocars in an effort to drive them forward. One such engine was a molecule containing a photo-isomerisable group which in response to light of a certain wavelength rotates uni-directionally about a double bond³¹. Sterically large groups were attached to this molecule making it act like a 'paddle wheel' as it rotated, which it was proposed would drive the nanocar forward when incorporated into its chassis. But no propulsion was observed when the engine was incorporated.

Another engine consisted of incorporating a Ring Opening Metathesis Polymerisation catalyst into the nanocar's chassis³² which was expected to propel the nanocar forward by the pressure created behind the vehicle by a growing polymer chain. While the attached catalysts were shown to be effective polymerisation catalysts, no propulsion of the nanocars was observed.

The production of these described nanocars is extremely difficult due to their complex structure, requiring state-of-the-art organic synthesis techniques to be used. The synthesis is also problematic due to the low solubility of the fullerene wheels in almost all solvents. With this difficulty in mind and the so far unsuccessful attempts to propel the nanocars forward, it is questionable if this strategy of miniaturising macroscopic vehicles is the best to take. As has already been discussed, much simpler swimming strategies have been proposed which are synthetically much easier to implement.

1.3 Propulsion of Small Objects

Dreyfus et al³³ were some of the first to create a microscopic object capable of propelling itself forwards through a liquid. They achieved this by connecting several superparamagnetic particles together using strands of DNA through biotin-streptavidin linkages, which formed a line of particles which were connected together but still able to bend. This line of particles was then connected to a red blood cell to be propelled forward. By exposing the red blood cell connected to the line of particles to an externally applied oscillating magnetic field, the line of particles could beat like a flagella. Oscillating the magnetic field in a certain fashion meant the beating of the flagella was cyclic but non time-reversible, which as has already been discussed is essential to create a motion which moves objects forward rather than simply oscillate about one position. This resulted in the red blood cell being propelled with the flagella leading the direction of motion, whereas organisms such as spermatozoa move with the flagella trailing behind.

Ghosh and Fischer³⁴ have taken a similar approach of using magnetic fields to create motion. They constructed a helical screw shape connected to silica particle head by a dynamic shadow-growth mechanism. A thin layer of cobalt was then deposited onto one side of the created helices making the 'screws' magnetic. Upon exposure to a rotating magnetic field, the screws experience a torque force which caused them to rotate also. In this fashion they were 'screwed' through the liquid like a propeller, propelling them forwards. By altering the frequency of the external rotating magnetic field they found that the velocity of the helix could be controlled. At a rotation frequency of 150Hz the helix was propelled forward at the sizeable velocity of $40\mu\text{m s}^{-1}$. Also by altering the direction of the applied magnetic field the direction of propulsion could be altered. This allowed the authors to move helices in a prescribed trajectory and mark out the symbols 'R', '@' and 'H'.

Tierno et al³⁵ have also used magnetic fields to propel small objects through solution, although they have made use of a much simpler fabrication method to create an object which moves in a way to break the time reversibility of its motion. They create a colloidal doublet by joining two paramagnetic particles of different sizes together using DNA bridges. Applying an external rotating magnetic field then causes these doublets to rotate in one of the vertical planes.

When the doublet is in bulk solution this rotation does not lead to any propulsion as the force generated forwards at the top of the particle due to hydrodynamics is equal and opposite to the force generated at the bottom of the particle acting backwards. When the

doublet is close to a horizontal surface however, the hydrodynamic forces acting on the bottom of the doublet become larger than the forces acting on the top due to the increase hydrodynamic resistance experienced by the doublet's bottom surface and the horizontal surface. Thus the doublet is propelled forward in the direction of rotation with a velocity of $3.2\mu\text{m s}^{-1}$.

Zhang et al³⁶ have also studied a very similar situation in which nickel nanowires which sediment close to the bottom surface of an observation chamber are magnetised and then rotated by an external magnetic field. Again the proximity of the observation chamber's bottom surface breaks the symmetry of the viscous resistance acting on the nanorod, leading it to be propelled forward in the direction of rotation. By applying the rotating magnetic field in the horizontal, the nanorod could be tumbled head over tail, rotating about the nanorod's centre. This lead to propulsion of the nanorod with velocities which were dependant on the frequency of the rotating magnetic field, at the highest frequency used velocities of $35\mu\text{m s}^{-1}$ were observed.

The nanorod stopped instantly when the magnetic field was turned off due to the low Reynolds number and the direction of motion could be controlled by either altering the direction of the magnetic field or could be reversed by reversing the direction of the rotating magnetic field, allowing the nanorod to be steered over a predefined course. The group also found that a polystyrene latex particle could be attached to the nanorod to act as a model cargo which could be carried by the nanorod without a significant loss of velocity. They also created topographically patterned surfaces which contained 'hills' and 'valleys' and found that the nanorod could navigate over these features against the sedimentation effects caused by gravity.

Agrawal et al³⁷ have used a similar scheme to Whitesides et al¹³ to propel smaller $800\mu\text{m}$ polystyrene particles. The studies are identical except for the size of objects propelled, both using the decomposition of hydrogen peroxide to generate oxygen bubbles which propel the objects forward. The authors functionalised the polystyrene particles symmetrically with the platinum catalyst necessary by the in situ reduction of a soluble platinum salt to insoluble nanoparticles which are attached on the larger particles' surface. Investigation of these catalytic particles in solutions of hydrogen peroxide showed interesting behaviour. Initially the bead sedimented to the bottom of the solution as it is slightly more dense than the solution, but then as the catalyst generated oxygen, small bubbles of the gas started to form on the particles' surface. After a certain amount of time the amount number of bubbles attached to the particle was sufficient to make the particle buoyant which following further production of gas bubbles made the particle float to the top surface of the solution. Upon reaching the top surface the bubbles

attached to the particle burst causing the particle to sediment back to the bottom of the liquid.

In this way an autonomous cyclic motion was created which is highly desirable in nanoscale applications. The authors also found that the frequency of these cycles of motion could be 'tuned' by altering the viscosity of the liquid.

Burgo et al³⁸ have studied the anomalous diffusion of Poly(ethylene oxide) (PEO) on hydrophilic-hydrophobic surface gradients. Using fluorescence correlation spectroscopy the group measured the diffusion coefficients of fluorescently labelled PEO chains, finding that diffusion was fastest when the polymer chains were not bound to a surface and much slower when the chains were attached. The measured diffusion coefficient also depended on the surface identity. On a hydrophobic surface diffusion was found to be slowest and on a hydrophilic surface up to 9 times faster, although the spread in data gathered from repeats of the experiments were quite large. These results were rationalised by measuring the interaction energies between a PEO chain and the different surfaces which found a strong adhesion for the hydrophilic surface and a weak adhesion for the hydrophobic surface.

When the diffusion of PEO on a surface which consisted of a gradient from hydrophilic to hydrophobic was investigated, PEO was found to diffuse 100 times faster in the direction of increasing hydrophilicity than the direction of decreasing hydrophilicity. Therefore it was proposed that PEO chains experience a net propulsion along the gradient from a hydrophobic area to a hydrophilic area.

1.4 Nanorods which Propel themselves through Solution

Sen et al³⁹ have created small cylinders consisting of half gold and half platinum arranged in segments which they call 'nanorods'. These were created by the electrochemical deposition of either gold or platinum from a soluble metal salt into an alumina filter membrane which had been converted to an electrode by depositing a layer of silver on the back. This membrane contains many small cylindrical pores which act as a template for the deposition of the metal onto the underlying silver layer. Sequential depositions of platinum and gold gave a cylinder of platinum attached to a cylinder of gold within the membrane template. The lengths of these metal cylinders and so their relative proportions could be controlled through the deposition time and the current used.

These nanorods could then be released from the template-electrode by dissolving the silver electrode using concentrated nitric acid followed by dissolving the alumina template in sodium hydroxide.

When these nanorods were dispersed in an aqueous solution of hydrogen peroxide they were found by video microscopy to be propelled forwards. Thus, this group were the first to create propulsion of small objects in aqueous solution via a chemical reaction. The propelled velocity was found to increase with increasing concentrations of hydrogen peroxide, up to around $8\mu\text{m s}^{-1}$ in 5% hydrogen peroxide. Further analysis of the motion showed that the rods were propelled along their longest axis with the platinum segment leading the direction of motion, in direct contrast to the work of Whitesides et al¹³ who found that their disks moved with the platinum segment trailing.

Further experiments were carried out by the group to explain the observed motion. Nanorods consisting of three metal segments in the order Pt-Au-Pt were found to not propel themselves forward, neither were nanorods consisting of a single metal segment of platinum or gold. Therefore the authors concluded that asymmetry of the nanorod was necessary to create propulsion. H_2O_2 and the platinum segment, which are known to participate in the catalytic decomposition of H_2O_2 forming oxygen and water, are also necessary.

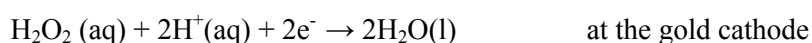
To explain the observed propulsion the authors used an interfacial tension propulsion mechanism where in oxygen generated by the catalytic decomposition of H_2O_2 by platinum lowers the interfacial tension between water and the nanorod at the platinum end. This interfacial tension causes the nanorod to be propelled forward and the interfacial tension gradient is re-established by the fast chemical reaction. This propulsion mechanism was later suggested to be wrong and a new mechanism proposed.

Further study of the mechanism of propulsion showed that a propulsion mechanism due to bubble formation could be discounted as the direction of motion in which the nanorods were propelled was the opposite of that observed for macroscopic objects propelled forward by the formation of bubbles on a platinum surface. Calculation of the concentration of chemical species created by the platinum segment around the nanorod by the same group of authors apparently showed that nanorods are not propelled forward by diffusiophoresis. Although later Howse et al⁴⁰ showed that diffusiophoresis could propel particles forward (discussed later).

These observations lead the researchers to believe that propulsion of the nanorods was either due to the interfacial tension gradient that they had already proposed or due to a self-electrophoretic propulsion mechanism⁴¹. In this propulsion mechanism hydrogen peroxide is decomposed by both the platinum and gold segments of the nanorod in a bipolar redox reaction. It was proposed that the platinum segment in the nanorod acts as an

anode and accepts electrons from an oxidation reaction catalysed on the platinum surface, whereas gold acts as a cathode and donates electrons to a chemical species in solution in a reduction reaction. With the platinum segment constantly receiving electrons and gold constantly donating electrons there is a flow of charge from the platinum segment to gold segment. Propulsion of the particle was therefore proposed to be due to the flow of electrons inside the nanorod which cause a flow of cations in the surrounding fluid to maintain charge neutrality.

The self-electrophoretic propulsion mechanism later gained further credit as a plausible propulsion mechanism when Sen et al⁴² carried out investigation into the redox properties of platinum and gold using cyclic voltammetry. Proposing that the relevant redox half-reactions were:



This means that gold needs to have a more positive electrical potential than platinum to act as the cathode and that nanorods should move with their platinum segment facing forwards, both of these were observed using cyclic voltammetry and optical microscopy, giving strong evidence for self-electrophoresis. Investigation of nanorods constructed of different combinations of other metals such as Rh, Ni, Ru and Pd showed that nanorods always moved forwards with the most electropositive metal which acts as the anode at the front.

The velocity of propulsion should increase as the difference between the two segments acting as electrodes in the nanorod increases, as the larger the potential difference the larger the electrical field is around the particle. This trend was confirmed in the study showing that nanorods constructed of materials which gave large potential differences propelled themselves forwards at larger velocities. Although the trend in the data suggest that when the potential difference is zero, the propelled velocity will not be zero but instead the sizeable velocity of $\sim 11 \mu\text{m s}^{-1}$. This was not addressed in the study but could possibly be due to convection currents in the observation chamber which propel nanorods through solution even when they are not propelling themselves.

1.5 Increasing the Speed of Nanorods

Wang et al⁴³ have also created gold / platinum nanorods and studied their propulsion through a liquid. They found that incorporating carbon nanotubes into the platinum segment of a nanorod increased the average propelled velocity from $7\mu\text{m s}^{-1}$ to $57\mu\text{m s}^{-1}$ in 15 wt% hydrogen peroxide. Investigation of the electrochemistry showed that the addition of carbon nanotubes had changed the electrical potential of the platinum segment from 297mV to 244mV meaning that H_2O_2 is more easily oxidised by the platinum electrode. This addition therefore also significantly changed the potential difference between the platinum segment from 19 to 72mV resulting in faster propulsion.

The same authors also found that the speed of nanorods containing carbon nanotubes could be significantly increased by adding hydrazine to the fuel mixture. This increased the average velocity of nanorods containing nanotubes to $93\mu\text{m s}^{-1}$. Although at these propulsion speeds the trajectory of the nanorods changed from approximately straight to highly circular, meaning that they would be less effective at travelling large distances quickly as they veer off course and travel in the wrong direction. Finally this problem was overcome by the authors by incorporating a nickel segment into the nanorods allowing them to be aligned in a weak magnetic field (discussed later) and the direction of motion to be fixed in a straight line. While held in this fixed orientation a small fraction of the nanorods were found to travel extremely quickly, at velocities greater than $200\mu\text{m s}^{-1}$.

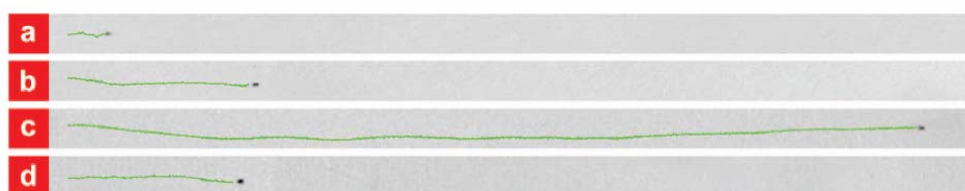


Figure 4 Trajectories of nanorods oriented by a magnetic field over time. A) nanorod not containing carbon nanotubes, B) nanorod containing carbon nanotubes, C) nanorod containing nanotubes with added hydrazine, D) nanorods not containing nanotubes with added hydrazine.

The velocity of nanorods has also been increased by altering the gold segment of metal nanorods. Wang et al⁴⁴ altered the gold segment by incorporating silver using a gold-silver alloy for the ‘gold’ segment. Again investigation of the electrochemistry showed that the potential of the ‘gold’ segment could be changed from 243mV to become more electropositive at 274mV, when the electrode contained 75vol % silver. This effectively

doubled the potential difference from 56mV to 98mV. This led to a vast increase in the observed propulsion velocity from 10 to 87 $\mu\text{m s}^{-1}$.

Investigation of nanorods containing different amounts of silver in the 'gold' segment showed that their velocity increased linearly with the amount of silver in the segment up to 75vol %, after which the velocity decreased to zero at 100vol % silver. The authors rationalised this result by comparing the nanorods to literature sources of gold-silver catalysts, which are extremely effective up to a point where they consist mostly of silver, at which point they are no longer catalytic.

Zacharia et al⁴⁵ have investigated how surface area affects the propulsive velocity of similar nickel-gold nanorods. In these nanorods nickel is used instead of platinum which also catalyses the decomposition of hydrogen peroxide. By adding small silica particles to the electrodeposition solution they found that they became incorporated into the nanorod, and following etching with hydrofluoric acid which dissolves the silica, created small holes in the nanorod surface increasing their surface area. Adding 50% silica to the electrodeposition mixture increased the surface area from 5.3 $\text{m}^2 \text{g}^{-1}$ to 200 $\text{m}^2 \text{g}^{-1}$, as measured by BET measurements using nitrogen gas. The authors expected the increase in surface area to increase the rate of hydrogen peroxide decomposition and enhance the velocity of propulsion. This was found to be true, as a linear increase in propulsion velocity was observed with increasing surface area of the nanorods nickel segment, up to a point at which the propelled velocity reached a plateau at surface areas larger than $\sim 100 \text{m}^2 \text{g}^{-1}$. When the gold segment of nanorods was roughened using the same procedure, no increase in propulsion velocity was observed, suggesting that propulsion velocity is limited by the rate of reaction on the nickel segment of the nanorod. Although an increase in velocity was observed with increasing surface roughness and so increasing surface area, the increase in velocity was actually quite small only $\sim 2 \mu\text{m s}^{-1}$.

Fragrino et al⁴⁶ have also studied how surface area effects propelled velocity. In this study they created silica particles which propel themselves forwards by functionalising the surface with an area of gold and an area of platinum that were connected together allowing the self-electrophoretic propulsion identified in nanorods to take place. Using their fabrication technique they were able to change the surface area of gold by altering the fraction of the sphere which was coated with gold. Unlike Zacharia et al⁴⁵ they found that the propelled velocity of the spheres increased as the surface area of gold increased from 1.2 $\mu\text{m s}^{-1}$ at zero gold coverage to 2.8 $\mu\text{m s}^{-1}$ at maximum coverage.

A few different strategies to improve the propelled velocity of objects which 'swim' have been highlighted, the most successful have been the strategies by Wang et al^{43,44} which have significantly increased the speed at which nanorods are propelled through solution. All strategies have the common theme of trying to increase the rate of hydrogen

peroxide decomposition, although other strategies have been proposed by Pumera⁴⁷. Considering the self-electrophoretic propulsion mechanism, the relative permittivity and viscosity of the liquid should influence the propelled velocity. Pumera predicts the fastest motion would be observed in acetonitrile closely followed by water, with ethanol giving the slowest propelled velocity. He predicts increasing the ionic strength of the liquid should slow propulsion and that increasing the concentration of hydrogen peroxide should increase the rate of reaction and so velocity, up to a certain concentration after which the velocity should be decreased by the hydrogen peroxide also increasing the viscosity of the liquid.

1.6 Controlling the Motion of Nanorods

Sen et al⁴⁸ have incorporated nickel metal segments 100nm in length into nanorods, which cause them to align in the direction of a weak externally applied magnetic field. As the nickel segments are smaller than the critical domain size of 150nm, they consist of a single magnetic domain and due to the nickel segment length being smaller than the nanorod width (400nm), the nanorod becomes magnetized normal to its length upon exposure to an externally applied magnetic field. The authors found that these nanorods preferentially aligned themselves with a weak externally applied magnetic field due to the magnetic torque induced by the nickel segments which is 4 times larger than the force exerted on the nanorods by rotational Brownian motion.

When these nanorods were dispersed in a hydrogen peroxide solution they propelled themselves forwards travelling in straight lines at short time scales which changed to a random trajectory at long time scales due to rotational Brownian motion. This behaviour could be changed by the application of the external magnetic field which orientated the nanorods in the direction of the magnetic field and caused them to travel forward with much straighter trajectories at long time scales. Also by changing the orientation of the external field by rotating the magnet, the direction in which nanorods travelled could be changed, leading to the ability to remotely control nanorods.

Using this technique, the authors were able to remotely control the motion of nanorods propelling themselves forwards to mark out a trajectory in the shape of the letters 'PSU' (Penn State University) on a length scale of 50 μ m. Wang et al⁴⁹ also used this technique

to maneuver a nanorod in a complex path around a microfluidic channel and transport a cargo from one location to another.

Wang et al⁵⁰ have developed a system in which the velocity of nanorods can be controlled externally by placing a gold electrode in close proximity to a nanorod undergoing propulsion. When an electrical potential is applied to the electrode, the redox chemistry of the nanorod is affected either retarding or accelerating the rod. In this way as the potential was changed in the electrode from +1V to -0.4V, the rods velocity could be altered from 4 to 22 $\mu\text{m s}^{-1}$, whereas with no applied potential the velocity was 9 $\mu\text{m s}^{-1}$.

The authors explained this behaviour by proposing that the potential applied in the electrode changes the concentration of oxygen in the solution surrounding the nanorod. At an applied potential of +1V they propose that hydrogen peroxide in solution is oxidised releasing oxygen and at a potential of -0.4V oxygen in solution is reduced lowering its concentration. They then go on to propose that these changes in oxygen concentrations affect the anodic reactions occurring at the platinum surface, changing the potential difference between the anode and cathode in the nanorod, which has been suggested earlier to be responsible for propulsion.

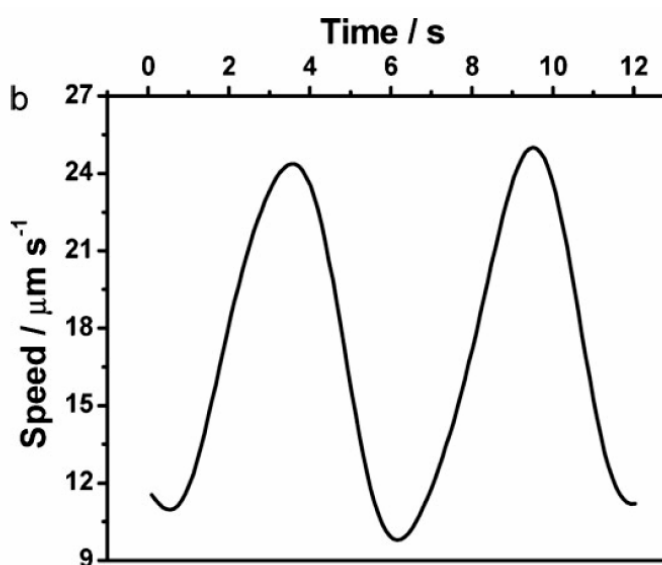


Figure 5 Speed of a nanorod close to the surface of a heating filament during heat pulses 3 seconds long at times 0 and 6 seconds. Reproduced from ref⁵¹.

Wang et al⁵¹ have also controlled the velocity at which a nanorod is propelled through solution by altering the temperature of the surrounding fluid. In these experiments a heating filament was placed inside the observation chamber and the motion of nanorods close to the filament studied. They found that the velocity could be increased from its

normal value of $14\mu\text{m s}^{-1}$ at 25°C to $45\mu\text{m s}^{-1}$ at 65°C , attributing the observed increase in velocity to both an increase in the rate of hydrogen peroxide decomposition with temperature and a decrease in the viscous drag experienced by the nanorod as it moves through the liquid with temperature. Measurement of the potential difference between the platinum and gold electrode at different temperatures showed an increase consistent with the observed increase in velocity. The change in velocity occurred fairly quickly with application of the electric current meaning that this technique could be used to remotely control the velocity at which a nanorod moves.

Bacteria exhibit directed motion in response to gradients of a chemical substance, known as chemotaxis. Sen et al⁵² claim that they have observed this chemotactic behaviour for platinum-gold nanorods which are placed in a concentration gradient of hydrogen peroxide. In these experiments a small piece of agarose gel was soaked in a hydrogen peroxide solution and added to an observation chamber to act as a source of hydrogen peroxide. Apparently over the course of 4 days the nanorods migrate from all areas in the observation chamber to a position very close to the agarose gel. After 4 days they authors measured that 70% of the nanorods were accumulated at the gel surface. Control experiments were carried out, such as repeating the experiment using pure gold nanorods which do not propel themselves forwards, and also repeating the experiment without soaking the agarose gel in hydrogen peroxide. In both cases no chemotaxis was observed.

Although these control experiments were carried out in an attempt to prove that the observed motion was chemotaxis, no other group has published results which have repeated these experiments. Inspection of the experiments carried out published by the group raise several concerning questions. Firstly the nanorods are mostly oriented perpendicular to the hydrogen peroxide gradient and travel sideways towards the source of hydrogen peroxide and also do not seem to be propelled forwards along their length. This is in complete contradiction to the way in which nanorods were found to move in solutions of hydrogen peroxide. Secondly they seem to migrate towards the agarose gel at the same speed irrespective of their initial distance away from the gel. This seems surprising as the concentration should be proportional to $1/\text{distance}$ and as the nanorod velocity is directly proportional to hydrogen peroxide concentration; nanorods should migrate towards the gel, moving quickly when they are close to the gel and slowly when they are far way from the gel.

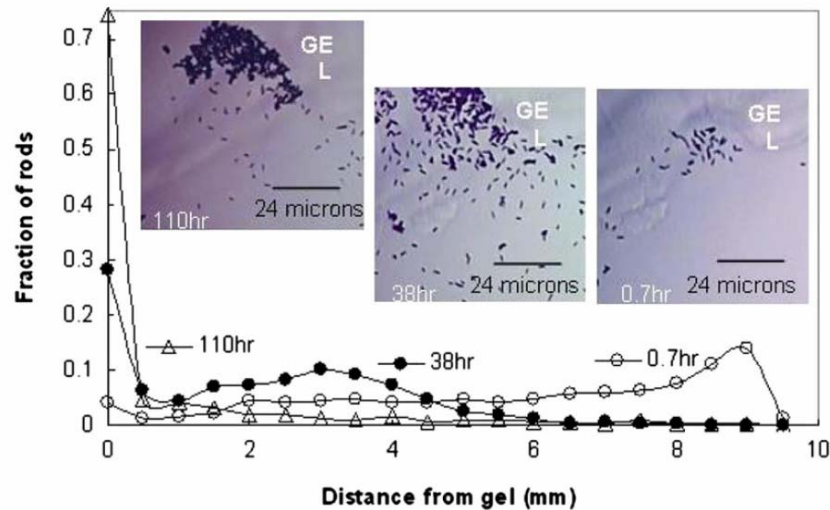


Figure 6 The distribution of nanorods which apparently exhibit chemotaxis towards a piece of agarose gel soaked in hydrogen peroxide which is placed in the top left of the optical micrographs. Reproduced from ref⁵².

During this study the actual existence of a concentration gradient was never confirmed, and surely after 4 days any gradient that did exist would have vanished? Explanations other than chemotaxis seem much more realistic. For example perhaps the nanorods adhere to the gel surface meaning that as the nanorods diffuse around over time, the gel acts like fly paper adsorbing the nanorods allowing a high concentration to build up over time, although this should have been observed in the control experiments. The most likely explanation for the observed motion is sedimentation; the prepared nanorods are very dense and will be propelled down a sloped surface. As we shall see in chapter 4, the slope needed to propel small dense particles along a surface at a reasonable speed is very small, less than one degree of incline. If the bottom surface of the observation chamber used in these experiments was not perfectly aligned in the horizontal, nanorods will migrate from one area to another at a small but constant speed.

1.7 Making use of Self propelling Nanorods

Sen et al⁵³ have used nanorods to investigate the rheological behaviour of liquid interfaces. By measuring nanorod velocities at the interface between decane and water the surface shear viscosity could be inferred by numerical treatment of the data gathered. Addition of a surfactant to the liquid interface was shown to increase the surface shear viscosity by observing a decrease in nanorod propulsion velocity, which the authors attributed to an increase in the viscous drag around the nanorod. Although this may not be the case as the nanorods are propelled through solution by the surface catalysed decomposition of hydrogen peroxide, adding a substance to the liquid which has high surface activity (a surfactant) may reduce the catalytic activity of the nanorod and thus decrease its velocity. This could easily have been investigated by a control experiment which measured nanorod velocity in aqueous solution with different amounts of surfactant added but was not carried out.

Using nanorods to probe the rheology of liquids and interfaces maybe particularly useful in situations where conventional techniques cannot be used, for example due to the small size of the system where a nanorod could perform the measurement but a rheometer could not.

Sen et al⁵⁴ have investigated if the motion of nanorods can be used to carry a cargo, transport it to a specific location and then release it. To achieve this they attached a positively charged polystyrene latex particle to the gold segment of a nanorod through electrostatic bonds using a polypyrrole linkage and observed the cargo laden nanorod's motion. They found that the nanorod did in fact still propel itself forward when it was laden with cargo and so could transport the cargo around, although the velocity of the nanorod was reduced by the extra viscous drag caused by the cargo. Consistent with this hypothesis nanorod velocity decreased further as larger latex particles were attached. Even with the cargo attached the velocity of the nanorods was still reasonable, for a cargo of a $1\mu\text{m}$ latex particle, the nanorod velocity was measured to be $4\mu\text{m s}^{-1}$. They also used a biotin-streptavidin linkage to join nanorods and cargo together, meaning that the bonds formed between nanorods and latex particle was highly specific and that the nanorods would only transport a specific cargo.

By adding nickel segments to the nanorod, the direction of motion could be controlled by the application of an externally applied magnetic field. This had two advantages, firstly an unladen nanorod could now be driven into a latex cargo particle to form the cargo laden nanorod, whereas without this control the nanorod and cargo had to come into contact through diffusion to join together. Secondly, the direction in which the

nanorod transports the cargo could now be controlled, although the magnetic field affects all of the nanorods in the dispersion and so they must all move in the same direction simultaneously due to the magnetic field.

The authors also claimed that the cargo laden nanorods were capable of transporting their cargo up a concentration gradient of hydrogen peroxide towards the source by chemotaxis, although as discussed above, insufficient evidence has been provided to ascertain if this actually occurs.

This research allowed a latex particle cargo to be picked up and transported to a specific location by magnetically steered nanorods, but it did not allow the nanorod to be separated from its cargo once it had been delivered to the desired location. Later Sen et al⁵⁵ developed nanorod-cargo linkages which are photo-cleavable, meaning that the cargo could now be released from the nanorod. One of these linkages made use of a silver segment in the nanorod which could be dissolved by UV irradiation in aqueous solution allowing nanorod and cargo to separate. In another linkage a photo-cleavable *o*-nitrobenzyl group was used, also allowing separation of the nanorod and cargo upon exposure to UV light. Once exposed to UV light the nanorod released its cargo and could no longer transport any other cargo, meaning that the developed nanorods were for single use only. Cleavage of the linkages using UV light was also not spontaneous, dissolving the silver linkage took 10-20 seconds and cleavage of the *o*-nitrobenzyl linkage 60-100 seconds.

This cleavage time limits the usefulness of the cargo transporters as the ability to target a specific drop-off point is significantly reduced by the time taken to separate the nanorod and cargo which are travelling at $2.3\mu\text{m s}^{-1}$. Wang et al⁴⁹ found that cargo could be 'loaded' onto a nanorod by a magnetic linkage, then could be transported to a specific location by the magnetic steering of the nanorod through an externally applied field and then quickly 'unloaded' from the nanorod by executing a fast change in direction which breaks the weak magnetic link between the cargo and the nanorod.

1.8 Other Propulsion Mechanisms

The phenomena known as diffusiophoresis⁵⁶ has long been known to be responsible for the transport of small particles dispersed in solution from an area of high concentration of a solute, to an area lower in concentration. Howse et al⁴⁰ have made use of this phenomena to propel latex particles through solution. By coating one hemisphere of a latex particle with platinum using thermal evaporation of the metal, they created Janus particles capable of decomposing hydrogen peroxide to oxygen and water on only one side of the sphere. When these Janus particles were dispersed in a solution of hydrogen peroxide they were found to propel themselves forwards at speeds up to $3\mu\text{m s}^{-1}$.

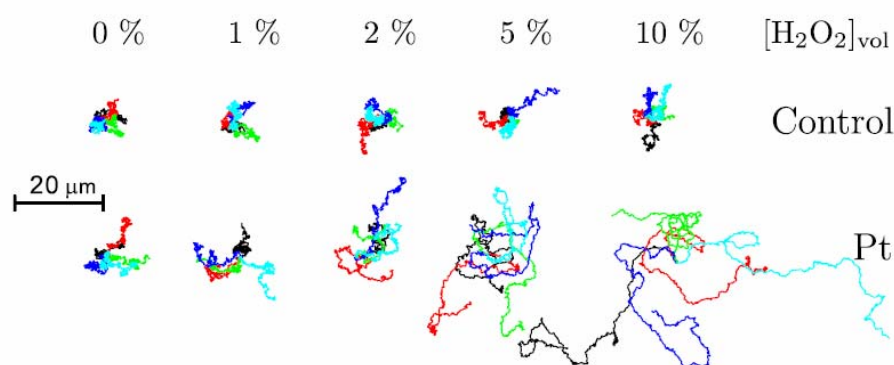


Figure 7 The trajectory of five platinum-latex Janus over 25 seconds in varying concentrations of hydrogen peroxide. Reproduced from ref⁴⁰.

The decomposition of hydrogen peroxide asymmetrically on the Janus particle leads to the production of a chemical gradient around the particle of reactants to products. As the reaction converts two molecules of hydrogen peroxide to two molecules of water and one molecule of oxygen, the chemical reaction converts two molecules into three. The resulting gradient of reactants to products is therefore also a gradient of concentration. To dilute this higher concentration of substance around the platinum hemisphere and return the solution to equilibrium, water flows into the area from solution and most importantly over the surface of the particle. This flow of water over the particles surface results in propulsion of the particle through solution; by Galilean invariance the particle must be propelled forwards if water is propelled backwards.

The authors found that Janus particles moved through solution in a combination of Brownian motion and propulsion, which could be explained by mathematical treatment of the data. At short time scales the particles moved in straight lines whereas at long time

scales the direction of propulsion was rotated due to rotational Brownian motion leading to a random walk with an enhanced diffusion coefficient.

Propulsion of the particles was found to be slower than that observed by researchers investigating nanorods at $3\mu\text{m s}^{-1}$, consistent with a different propulsion mechanism. Particles created in this study have an advantage of a low density, enabling them to be propelled in all three dimensions (x, y, z), compared to dense platinum-gold nanorods which sediment to the bottom of an observation chamber meaning they can only move in two dimensions.

The rotation of Janus particles was found to be faster than expected due to an angular velocity created by the chemical reaction. This was found to be useful in creating particles which could propel themselves forwards to undergo motion leading to a circular trajectory⁵⁷. These observed circular trajectories could very useful in creating devices which ‘fetch and carry’, as the travel away from their initial starting point and eventually return to the same point.

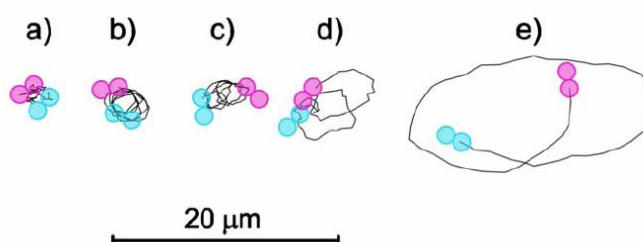


Figure 8 Circular trajectories captured from movies of platinum-latex Janus particles over 25 seconds. Reproduced from ref⁵⁷.

As well as self-diffusiophoresis and self-electrophoresis another propulsion mechanism of propulsion based on the decomposition of hydrogen peroxide has been proposed. Feringa et al⁵⁸ attached a manganese catalyst which decomposes hydrogen peroxide, to the surface of a relatively large silica beads (40-60 μm) and observed motion of these beads in hydrogen peroxide solutions. Unlike the Janus particles of Howse et al⁴⁰, the placement of the catalyst was symmetrical over the particles surface and unlike in any of the nanoscale propulsion methods described so far, the researchers observed bubbles forming at the particles surface.

Based on these observations the authors suggested a different propulsion mechanism to those already described. The manganese catalyst decomposes hydrogen peroxide which releases oxygen into solution. Once the solution has become saturated with oxygen,

bubbles start to form on the silica particles surface, grow in size and then detach causing the particles to be propelled forward by a bubble recoil force. Investigation of mixtures of catalyst functionalised and non functionalised particles showed that bubbles only formed on the surface of the particles with catalyst, suggesting that functionalisation of the surfaces creates bubble nucleation points.

Other notable propulsion mechanisms include one by Mano and Heller⁵⁹ wherein a carbon fibre is functionalised with two different enzymes which catalyse chemical reactions, which creates an electric field around the fibre leading it to be propelled forward by the self-electrophoresis mechanism, as has been used for the propulsion of nanorods. The authors found that propulsion of the fibre ceased if an insulator was incorporated into the fibre breaking the electrochemical linkage between the two enzymes at the ends of the fibre.

Pantarotto et al⁶⁰ have also made use of enzymes to create propulsion by functionalising carbon nanotubes with catalase which decomposes hydrogen peroxide. They also observed bubbles forming on the nanotubes, suggesting that bubble formation was also the mechanism of propulsion in this case also. By attaching a second enzyme which produces hydrogen peroxide from glucose - glucose oxidase, they found that the carbon nanorods could be propelled forward using glucose as the fuel.

Finally Mei et al⁶¹ have also made use of bubbles to propel objects through a liquid. They created hollow tubes of metals using a novel method which rolls up a planar sheet of the metal. These hollow tubes emit bubbles preferentially at one end through the conversion of hydrogen peroxide to oxygen using a platinum surface inside the tube. The created tubes are quite large $\sim 20\mu\text{m}$ but are capable of very fast propulsion velocities of up to 2mm s^{-1} .

1.9 Nano Swarms

As well as research into small objects which can propel themselves through solution, much work has gone into researching ways to create groups of small objects which can group or 'school' together in response to a stimulus. All except one of these systems in which this occurs consist of particles which are photo-catalytic.

Sen et al⁶² first reported this type of behaviour for silver chloride particles dispersed in water. The group found that spherical silver chloride particles propel themselves forward upon exposure to UV light, even though the particles are symmetrical and so should not be propelled forward. Even more interestingly they also observed that the particles propelled themselves towards each other, forming 'schools' of many particles in several areas. If a small area was exposed to UV light, silver chloride particles were found to migrate to this area and form a school from far away. When the UV light was turned off the particles were able to diffuse away from the school and re-disperse in solution. This process could be repeated multiple times.

To explain this behaviour the authors state that the UV light exposure triggers a photo-catalytic reaction in the silver chloride particles which causes them to dissolve as ions, creating a local high concentration of ions around the particle. As discussed in an earlier section, this alone would not create propulsion of the particles due to the symmetry of the ion concentration around the particle, therefore the authors suggested that the concentration is slightly asymmetrical due to either the roughness of the particles or differences in the intensity of UV light around the particle, resulting in different rates of reaction on the particle surface, breaking the symmetry. This resulting slightly asymmetrical distribution of ions around the particle creates an electric field due to the different rates at which cations (protons) and anions (chloride ions) diffuse through water, in which the particle is propelled forward by electrophoresis.

To support this suggested propulsion mechanism the group carried out experiments with photo-catalytically inert particles such as silica and polystyrene. They found that upon exposure to UV light the positively charged polystyrene particles were propelled towards a silver chloride particle whereas negatively charged silica particles were propelled away from a silver chloride particle. These experiments suggest that silver chloride particles do create an electric field around themselves when exposed to UV light and that the direction of the field is towards the silver chloride particle. Also if the silver chloride particle was replaced with a magnesium oxide particle, the direction of the electric field could be reversed due to the diffusion of the anion (OH^-) now being faster than that of the cation (Mg^{2+}).

While the groups proposed propulsion mechanism may be fairly new and un-ratified, there is clear evidence that exposing silver chloride particles to UV light creates propulsion and can be used to induce swarming in dispersions of particles.

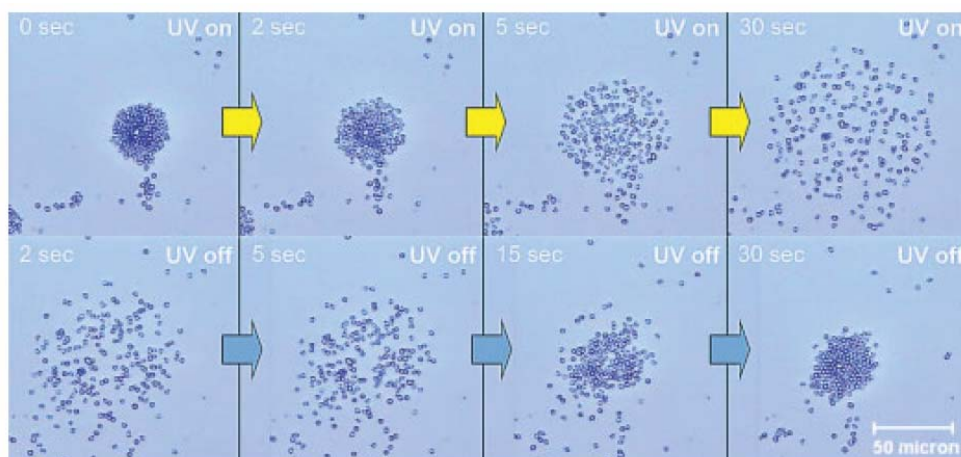


Figure 9 SiO₂ / TiO₂ Janus particles which aggregate in the absence of UV light and then repel each other when the UV light is turned on. Reproduced from ref⁶³.

Sen et al⁶³ have also studied a very similar system consisting of titanium dioxide particles which produce electrons in response to exposure to UV light. These titanium dioxide particles were found to propel themselves forward with velocities up to $10\mu\text{m s}^{-1}$ upon exposure to UV light. Propulsion was proposed to be due to a higher concentration around the particle of a chemical species such as hydroxide radicals formed by the donation of an electron to a water molecule, which causes diffusiophoresis. In this case the propulsion - which must be caused by asymmetry - was rationalised by the ‘lumpy’ non spherical shape of the titanium dioxide powder used.

Schooling behaviour was also observed but in a manner reverse of that already described for silver chloride particles, as silica and also cationic polystyrene particles both initially adhered to titanium dioxide particles then were repelled away upon exposure to UV light. This initial attraction of both the negatively charged silica particles and the positively charged polystyrene particles was rationalised by the authors by stating that the attractions were due to electrostatic attractions between oppositely charged surfaces. This explanation seems weak, as to attract both cationic and anionic particles the surface of titanium dioxide must be zwitterionic, whereas the authors measured zeta potentials which ranged from strongly negative to weakly positive for the titanium dioxide particles. Also during adsorption of charged particles onto a surface of opposite charge, a monolayer forms reversing the surface charge from oppositely charged to

having the same surface charge of the particles, which blocks further adsorption⁶⁴. This doesn't seem to fit with the group's observed results which clearly show that multi-layers of particles form and that a monolayer does not prevent further adhesion.

Sen et al⁶⁵ have also studied silver particles attached to a magnetically doped polystyrene particle forming a so called 'nano diamer'. When exposed to UV light the silver particle decomposes hydrogen peroxide:



Which due to the different diffusion coefficients of Ag^+ and HOO^- , leads to the formation of an electric field through which the charged nano diamer is propelled by electrophoresis. Propulsion velocities up to $3\mu\text{m s}^{-1}$ were observed.

When in fairly concentrated dispersions, exposed to UV light and a magnetic field, silver particles were unexpectedly observed to cluster together forming a tight school of particles. Experiments which changed several variables could not pinpoint the reason why these aggregates formed but highlighted that UV light, a magnetic field and hydrogen peroxide were necessary for this to occur.

Mixtures of these silver particles and magnetically doped polystyrene particles were found to form chain structures without UV light exposure, which then 'exploded' upon UV exposure releasing many of the contained particles back into dispersion from the chains. The authors could not explain this observed behaviour.

Wang et al⁶⁶ are the only group which have so far published a system capable of swarming or schooling that doesn't use a photo-catalytic reaction. In this system they disperse small gold particles in a mixture of hydrogen peroxide and hydrazine and observe that the particles aggregate together over time into small clusters $\sim 20\mu\text{m}$. After a certain amount of time the clusters redisperse back into solution and the whole process can be repeated by a further addition of hydrazine. Also individual particles were observed to be propelled forwards at velocities up to $16\mu\text{m s}^{-1}$.

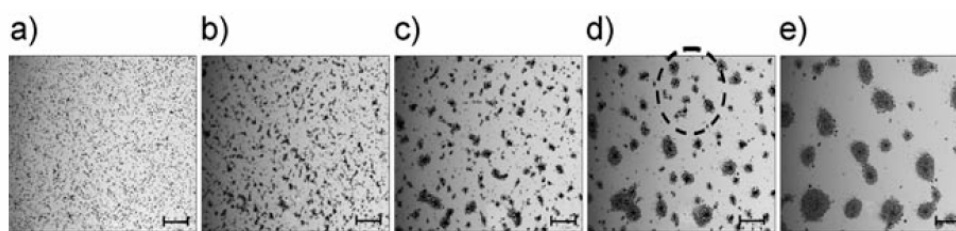


Figure 10 Clusters forming of gold particles by the addition of hydrazine. Reproduced from ref⁶⁶.

Control experiments showed that both hydrazine and hydrogen peroxide were necessary to induce clustering and the authors suggested a similar clustering mechanism to that of Sen et al⁶³. In the proposed mechanism gold decomposes hydrogen peroxide in the presence of hydrazine leading to a decrease in the solution pH and the formation of an ionic gradient due to the different diffusion coefficients of anions and cations. The gold particles migrate through this ionic gradient due to diffusiophoresis. Finally the group observed that chemically modifying the gold surface using self assembling monolayers of alkyl thiols, it was possible to alter the rate at which clusters formed and the final size of the formed clusters.

1.10 A Design to Work From

This thesis will be concerned with creating propulsion of small objects through solution. Instead of starting from scratch, a theoretical design by Balazs et al⁶⁷ shall be attempted to be implemented, which has been shown computationally to generate propulsion.

In this design, Balazs et al⁶⁷ have designed a system in which two polymeric microcapsules adsorbed onto a surface, work as a pair to undergo propulsion. The two particles are not connected together physically but instead communicate between themselves using a combination of nanoparticles released from their interior and hydrodynamic interactions to create propulsion (see Figure 11). If this design could be implemented, it would be the first example of a synthetic small vehicle which propels itself along a surface and it would also be the first example of communication between synthetically created small particles.

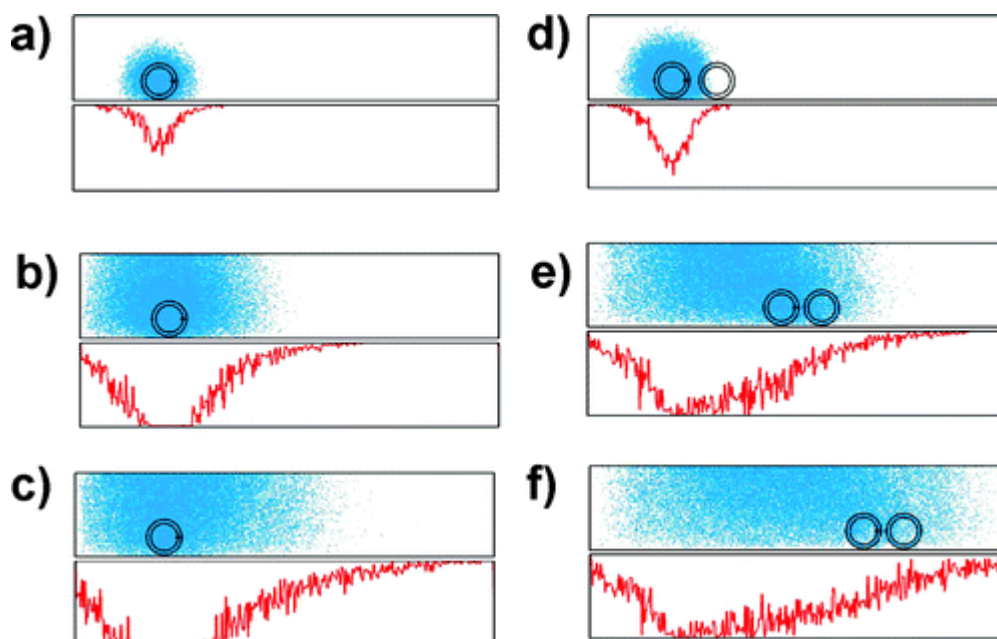


Figure 11 Snapshots of a single motor capsule (a-c) and a motor capsule and target capsule (d-f) adsorbed on a surface. Released nanoparticles are shown in blue and the microcapsule-surface interaction strength vs. position is shown below each snapshot. Reproduced from ref⁶⁷.

Propulsion of the microcapsules is created through their interaction with the surface onto which they are adsorbed as follows. Initially one of the polymeric microcapsules, named the *motor* capsule, is filled with a large number of dispersed nanoparticles which

are able to diffuse out of the motor capsule through the porous membrane which makes up the capsules. Once released, these nanoparticles can chemisorb onto the surface and alter its properties. Specifically the adsorption of nanoparticles alters the surface in a fashion which decreases the interactions between the surface and both of the microcapsules.

As the nanoparticles are released from a point source, their concentration is highest close to the motor capsule and decays to zero far away from the capsule. Due to this, a gradient of adsorbed nanoparticle density on the surface is created around the motor capsule, leading to a gradient of microcapsule adhesion. The second microcapsule adsorbed onto the surface, named the *target* capsule, responds to this created gradient of adhesion by migrating away from its original position to regions on the surface unmodified by the nanoparticles.

Figure 11 shows snapshots from computational modelling of the proposed design. When a single motor capsule is adsorbed onto the surface and subsequently releases nanoparticles which adsorb onto the surface, the distribution of nanoparticles can be seen in Figure 11 a-c. The diffuse cloud of nanoparticles gradually migrates outwards over time functionalising the surface, but at all times the distribution is symmetrical about the motor capsule. As this distribution of nanoparticles is symmetrical, so is the capsule-surface interaction, meaning that no propulsion is observed.

However, a second capsule positioned in close proximity to the motor particle (the target capsule) will have the surface underneath it functionalised asymmetrically, leading to a gradient of capsule-surface interaction. According to the computational modelling, this should cause the target capsule to be propelled away from the motor particle, as shown in Figure 11 (d-f). As the two capsules are at low Reynolds number, the movement of the target particle to the right, also causes the motor capsule to follow through hydrodynamic interactions. As the capsules move to a new area, further nanoparticles are released which adsorb onto the surface, leading to propagation of the gradient across the surface.

From computational modelling using different values of key variables, three types of propulsion were found. The first of which is *arrested motion*, where the capsules are observed to move initially and then stop moving. This is caused by the surface gradient created by the adsorption of nanoparticles propagating across the surface faster than the microcapsules can move. In other words the gradient overtakes the microcapsules, leaving them on a homogeneously functionalised surface.

The second type of motion was found if the microcapsules were able to migrate across the surface faster than the surface gradient can propagate. This leads to an oscillatory type motion where the capsules go through cycles of move, stop, move. Separating these

two motions is *sustained motion*, where the surface gradient propagates and the microcapsules migrate at the same speed, leading to propulsion at a constant velocity.

This theoretical design introduces many interesting concepts which have not been experimentally realised so far. Particles are said to exhibit communication between each other through the release of nanoparticles, and this has so far not been observed in synthetically created nanoswimmers, perhaps with the exception of nanoswimmers which form swarms⁶⁸⁻⁶⁰. But communication is commonly observed between two or more biological cells and enables them to undergo chemotaxis towards each other⁶⁹.

Propulsion through a surface interaction has also not been observed in nanoswimmers but has been studied for polymer chains³⁸, and has also been used at larger sizes to create surfaces over which liquid droplets are propelled¹⁴. The different types of motion of which particles are predicted to move, has also not been observed in synthetic nanoswimmers. Howse et al⁴⁰ have observed a change from ballistic type propulsion at short time scales to super-diffusive behaviour at long time scales but the observed motions are not as useful as those predicted in the theoretical design.

Further computational modelling based on this design has shown that large groups of particles can be propelled along a surface in response to a nearby motor particle⁷⁰ and that microcapsules filled with nanoparticles can also propagate chemical signals across large arrays of capsules^{71,72}. Study of these systems could also be related to designs in which the particles are driven along the surface through flow of a liquid^{67,73-80}.

For these reasons, this particular design by Balazs et al⁶⁷ is a very attractive theoretical design to implement. In chapter 2 some preliminary studies shall be carried out to investigate if the propulsion mechanism is feasible and then following some changes to the design, implementations investigated in chapters 3-5.

References

- (1) Drexler, K. *Engines of Creation*; Anchor, 1987.
- (2) Jones, R. A. L. *Soft Machines*; Oxford University Press, 2004.
- (3) Berg, H. C. *Random Walks in Biology*; Princeton University Press, 1983.
- (4) Duplantier, B. In *Poincare Seminar 2005*; Damour, T., Darrigol, O., Duplantier, B., Rivasseau, V., Eds. Paris, FRANCE, 2005, p 201-293.
- (5) Block, S. M.; Goldstein, L. S. B.; Schnapp, B. J. *Nature* **1990**, *348*, 348-352.
- (6) Macnab, R. M.; Ornston, M. K. *Journal of Molecular Biology* **1977**, *112*, 1-30.
- (7) Block, S. M.; Segall, J. E.; Berg, H. C. *J. Bacteriol.* **1983**, *154*, 312-323.
- (8) Watanabe, N.; Kutsumi, K.; Sano, O. *Journal of the Physical Society of Japan* **1994**, *63*, 2955-2963.
- (9) Sano, O.; Kutsumi, K.; Watanabe, N. *Journal of the Physical Society of Japan* **1995**, *64*, 1993-1999.
- (10) Nakata, S.; Hiromatsu, S.; Kitahata, H. *Journal of Physical Chemistry B* **2003**, *107*, 10557-10559.
- (11) Kohira, M. I.; Hayashima, Y.; Nagayama, M.; Nakata, S. *Langmuir* **2001**, *17*, 7124-7129.
- (12) Nakata, S.; Kawagishi, N.; Murakami, M.; Suematsu, N. J.; Nakamura, M. *Colloids and Surfaces a-Physicochemical and Engineering Aspects* **2009**, *349*, 74-77.
- (13) Ismagilov, R. F.; Schwartz, A.; Bowden, N.; Whitesides, G. M. *Angewandte Chemie-International Edition* **2002**, *41*, 652-+.
- (14) Chaudhury, M. K.; Whitesides, G. M. *Science* **1992**, *256*, 1539-1541.
- (15) Brochard, F. *Langmuir* **1989**, *5*, 432-438.
- (16) Sumino, Y.; Magome, N.; Hamada, T.; Yoshikawa, K. *Physical Review Letters* **2005**, *94*.
- (17) Cohen, A. E.; Moerner, W. E. *Applied Physics Letters* **2005**, *86*.
- (18) Ropp, C.; Probst, R.; Cummins, Z.; Kumar, R.; Berglund, A. J.; Raghavan, S. R.; Waks, E.; Shapiro, B. *Nano Letters*, *10*, 2525-2530.
- (19) Lee, G. B.; Chang, C. C.; Huang, S. B.; Yang, R. J. *Journal of Micromechanics and Microengineering* **2006**, *16*, 1024-1032.
- (20) Dekker, M. *Interfacial Electrokinetics and electrophoresis*; New York, 2002.
- (21) Piazza, R. *Journal of Physics-Condensed Matter* **2004**, *16*, S4195-S4211.
- (22) Watarai, H.; Suwa, M.; Iiguni, Y. *Analytical and Bioanalytical Chemistry* **2004**, *378*, 1693-1699.
- (23) Purcell, E. M. *American Journal of Physics* **1977**, *45*, 3-11.
- (24) Najafi, A.; Golestanian, R. *Physical Review E* **2004**, *69*, 4.

- (25) Golestanian, R.; Liverpool, T. B.; Ajdari, A. *New Journal of Physics* **2007**, *9*.
- (26) Tao, Y.-G.; Kapral, R. *J Chem Phys* **2008**, *128*, 164518.
- (27) Tao, Y. G.; Kapral, R. *ChemPhysChem* **2009**, *10*, 770-773.
- (28) Coq, N.; du Roure, O.; Marthelot, J.; Bartolo, D.; Fermigier, M. *Physics of Fluids* **2008**, *20*.
- (29) Shirai, Y.; Morin, J. F.; Sasaki, T.; Guerrero, J. M.; Tour, J. M. *Chemical Society Reviews* **2006**, *35*, 1043-1055.
- (30) Shirai, Y.; Osgood, A. J.; Zhao, Y. M.; Yao, Y. X.; Saudan, L.; Yang, H. B.; Chiu, Y. H.; Alemany, L. B.; Sasaki, T.; Morin, J. F.; Guerrero, J. M.; Kelly, K. F.; Tour, J. M. *Journal of the American Chemical Society* **2006**, *128*, 4854-4864.
- (31) Morin, J. F.; Shirai, Y.; Tour, J. M. *Organic Letters* **2006**, *8*, 1713-1716.
- (32) Godoy, J.; Vives, G.; Tour, J. M. *Acs Nano*, *5*, 85-90.
- (33) Dreyfus, R.; Baudry, J.; Roper, M. L.; Fermigier, M.; Stone, H. A.; Bibette, J. *Nature* **2005**, *437*, 862-865.
- (34) Ghosh, A.; Fischer, P. *Nano Letters* **2009**, *9*, 2243-2245.
- (35) Tierno, P.; Golestanian, R.; Pagonabarraga, I.; Sagues, F. *Physical Review Letters* **2008**, *101*.
- (36) Zhang, L.; Petit, T.; Lu, Y.; Kratochvil, B. E.; Peyer, K. E.; Pei, R.; Lou, J.; Nelson, B. J. *Acs Nano*, *4*, 6228-6234.
- (37) Agrawal, A.; Dey, K. K.; Paul, A.; Basu, S.; Chattopadhyay, A. *Journal of Physical Chemistry C* **2008**, *112*, 2797-2801.
- (38) Burgos, P.; Zhang, Z. Y.; Golestanian, R.; Leggett, G. J.; Geoghegan, M. *ACS Nano* **2009**, *3*, 3235-3243.
- (39) Paxton, W. F.; Kistler, K. C.; Olmeda, C. C.; Sen, A.; St Angelo, S. K.; Cao, Y. Y.; Mallouk, T. E.; Lammert, P. E.; Crespi, V. H. *Journal of the American Chemical Society* **2004**, *126*, 13424-13431.
- (40) Howse, J. R.; Jones, R. A. L.; Ryan, A. J.; Gough, T.; Vafabakhsh, R.; Golestanian, R. *Phys Rev Lett* **2007**, *99*, 048102.
- (41) Paxton, W. F.; Sen, A.; Mallouk, T. E. *Chemistry-a European Journal* **2005**, *11*, 6462-6470.
- (42) Wang, Y.; Hernandez, R. M.; Bartlett, D. J.; Bingham, J. M.; Kline, T. R.; Sen, A.; Mallouk, T. E. *Langmuir* **2006**, *22*, 10451-10456.
- (43) Laocharoensuk, R.; Burdick, J.; Wang, J. *ACS Nano* **2008**, *2*, 1069-1075.
- (44) Demirok, U. K.; Laocharoensuk, R.; Manesh, K. M.; Wang, J. *Angewandte Chemie-International Edition* **2008**, *47*, 9349-9351.
- (45) Zacharia, N. S.; Sadeq, Z. S.; Ozin, G. A. *Chemical Communications* **2009**, 5856-5858.
- (46) Gibbs, J. G.; Fragnito, N. A.; Zhao, Y. P. *Applied Physics Letters*, *97*.
- (47) Pumera, M. *Nanoscale*, *2*, 1643-1649.

- (48) Kline, T. R.; Paxton, W. F.; Mallouk, T. E.; Sen, A. *Angewandte Chemie-International Edition* **2005**, *44*, 744-746.
- (49) Burdick, J.; Laocharoensuk, R.; Wheat, P. M.; Posner, J. D.; Wang, J. *Journal of the American Chemical Society* **2008**, *130*, 8164-+.
- (50) Calvo-Marzal, P.; Manesh, K. M.; Kagan, D.; Balasubramanian, S.; Cardona, M.; Flechsig, G. U.; Posner, J.; Wang, J. *Chemical Communications* **2009**, 4509-4511.
- (51) Balasubramanian, S.; Kagan, D.; Manesh, K. M.; Calvo-Marzal, P.; Flechsig, G. U.; Wang, J. *Small* **2009**, *5*, 1569-1574.
- (52) Hong, Y.; Blackman, N. M. K.; Kopp, N. D.; Sen, A.; Velegol, D. *Physical Review Letters* **2007**, *99*.
- (53) Dhar, P.; Fischer, T. M.; Wang, Y.; Mallouk, T. E.; Paxton, W. F.; Sen, A. *Nano Letters* **2006**, *6*, 66-72.
- (54) Sundararajan, S.; Lammert, P. E.; Zudans, A. W.; Crespi, V. H.; Sen, A. *Nano Letters* **2008**, *8*, 1271-1276.
- (55) Sundararajan, S.; Sengupta, S.; Ibele, M. E.; Sen, A. *Small*, *6*, 1479-1482.
- (56) Ebel, J. P.; Anderson, J. L.; Prieve, D. C. *Langmuir* **1988**, *4*, 396-406.
- (57) Ebbens, S.; Jones, R. A. L.; Ryan, A. J.; Golestanian, R.; Howse, J. R. *Physical Review E*, *82*.
- (58) Vicario, J.; Eelkema, R.; Browne, W. R.; Meetsma, A.; La Crois, R. M.; Feringa, B. L. *Chemical Communications* **2005**, 3936-3938.
- (59) Mano, N.; Heller, A. *Journal of the American Chemical Society* **2005**, *127*, 11574-11575.
- (60) Pantarotto, D.; Browne, W. R.; Feringa, B. L. *Chemical Communications* **2008**, 1533-1535.
- (61) Solovev, A. A.; Mei, Y. F.; Urena, E. B.; Huang, G. S.; Schmidt, O. G. *Small* **2009**, *5*, 1688-1692.
- (62) Ibele, M.; Mallouk, T. E.; Sen, A. *Angewandte Chemie-International Edition* **2009**, *48*, 3308-3312.
- (63) Hong, Y. Y.; Diaz, M.; Cordova-Figueroa, U. M.; Sen, A. *Advanced Functional Materials*, *20*, 1568-1576.
- (64) Adamczyk, Z.; Jaszczolt, K.; Michna, A.; Siwek, B.; Szyk-Warszynska, L.; Zembala, M. *Advances in Colloid and Interface Science* **2005**, *118*, 25-42.
- (65) Chaturvedi, N.; Hong, Y. Y.; Sen, A.; Velegol, D. *Langmuir*, *26*, 6308-6313.
- (66) Kagan, D.; Balasubramanian, S.; Wang, J. *Angewandte Chemie-International Edition*, *50*, 503-506.
- (67) Usta, O. B.; Alexeev, A.; Zhu, G.; Balazs, A. C. *ACS Nano* **2008**, *2*, 471-476.
- (68) Sen, A.; Ibele, M.; Hong, Y.; Velegol, D. *Faraday Discussions* **2009**, *143*, 15-27.
- (69) Shields, J. D.; Fleury, M. E.; Yong, C.; Tomei, A. A.; Randolph, G. J.; Swartz, M. A. *Cancer Cell* **2007**, *11*, 526-538.

- (70) Bhattacharya, A.; Usta, O. B.; Yashin, V. V.; Balazs, A. C. *Langmuir* **2009**, *25*, 9644-9647.
- (71) Bhattacharya, A.; Balazs, A. C. *Physical Review E*, *82*.
- (72) Bhattacharya, A.; Balazs, A. C. *Journal of Materials Chemistry*, *20*, 10384-10396.
- (73) Alexeev, A.; Verberg, R.; Balazs, A. C. *Journal of Polymer Science Part B-Polymer Physics* **2006**, *44*, 2667-2678.
- (74) Verberg, R.; Alexeev, A.; Balazs, A. C. *J. Chem. Phys.* **2006**, *125*.
- (75) Alexeev, A.; Verberg, R.; Balazs, A. C. *Soft Matter* **2006**, *2*, 499-509.
- (76) Alexeev, A.; Verberg, R.; Balazs, A. C. *Physical Review Letters* **2006**, *96*.
- (77) Smith, K. A.; Alexeev, A.; Verberg, R.; Balazs, A. C. *Langmuir* **2006**, *22*, 6739-6742.
- (78) Usta, O. B.; Alexeev, A.; Balazs, A. C. *Langmuir* **2007**, *23*, 10887-10890.
- (79) Zhu, G. D.; Alexeev, A.; Kumacheva, E.; Balazs, A. C. *J. Chem. Phys.* **2007**, *127*, 10.
- (80) Alexeev, A.; Verberg, R.; Balazs, A. C. *Langmuir* **2007**, *23*, 983-987.

2 Preliminary Experiments into Creating Propulsion along a Surface Gradient

To investigate if the theoretical design could be implemented, some preliminary studies were carried out into the key components of the propulsion mechanism. As the design relies on a particle adsorbing and desorbing from a surface to create propulsion, in section 2.1 the reversibility of particle adhesion to surfaces shall be investigated. In section 2.2 the friction encountered between a particle sliding along a surface will be investigated to find if it is necessary for the particle to be released from the surface to migrate along an adhesion gradient. Finally as a gradient of particle adhesion is created in the theoretical design through the adsorption of nanoparticles released from a microcapsule, section 2.3 will discuss the release of nanoparticles from a microcapsule and investigate if these released nanoparticles modify surfaces, and lead to a change in the interaction between a particle and a surface.

2.1 Reversibility of Adhesion

It was investigated if particles could attach to a surface and then detach from the surface spontaneously by the input of a chemical stimulus.

Poly(styrene) latex particles with a surface coating of poly(dimethylamino ethyl methacrylate) (PDMA) were created by dispersion polymerization using a PDMA block copolymer as a steric stabiliser, following a protocol by Armes et al^{1,2}. These particles are cationic at pH values below ~ 7 and so adsorbed onto an anionically charged glass surface when dispersed at pH 5, through the attractive electrostatic forces (See chapter 4). This leads to a sparse coverage of latex particles on the glass surface as shown in Figure 1 (left).

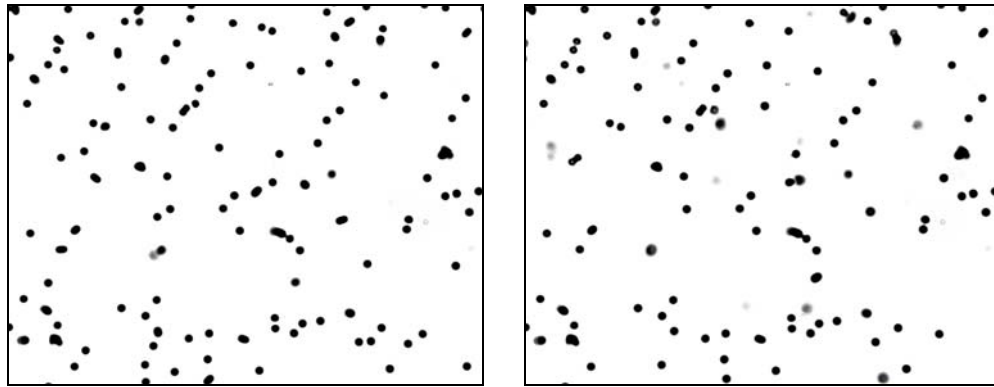


Figure 1 Optical micrograph of PDMA functionalised latex particles adsorbed onto glass at pH 5 (left) and with sodium hydroxide added ~pH 10 (right).

In an attempt to release the particles from the surface, the pH of the solution was raised by adding a drop of sodium hydroxide solution. This rise in pH should lead to the deprotonation of PDMA chains, causing the particle to lose its cationic charge and become negatively charged. In this way the attractive force between the particle and surface should be broken. Zeta potential measurements of the particles confirmed the charges of the particles, changing from +47mV at pH 3 to -32mV at pH 11. But as can be seen in Figure 1 (right), most of the adsorbed particles remained adhered to the glass surface, showing that they do not spontaneously release from the surface.

This irreversible adhesion can be explained by the relevant surface forces acting on the particle when in contact with the glass surface. Electrostatic forces are present which draw the particle and surface together at pH 5, where they are oppositely charged. When the pH is raised to around pH 10, the particle and surface become negatively charged and repel each other. Therefore if only electrostatic forces were present the particle should spontaneously release from the surface. But another force present between the particle and surface is van der Waals force, which is discussed in more detail in the next chapter.

This van der Waals force dominates over electrostatic forces when the particle is in contact with the surface and is mostly unaffected by changes in the solution pH. So when the pH of the solution is changed from 5 to ~10, the attraction between the particle and surface due to van der Waals force remains constant. As van der Waals force is much stronger than the electrostatic forces, particles remain adhered to the surface.

Investigation of Adhesion by Atomic Force Microscopy

To further investigate the reversibility of particle attachment to a surface further, colloidal probe Atomic Force Microscopy (AFM)^{3,4} was used. In these experiments a small polystyrene particle was glued to a triangular AFM tip as shown in Figure 2, creating a flexible probe that can be used to measure the force exerted on a particle by a surface.

This probe was then loaded into the Atomic Force Microscope and moved by the piezo electrics within the instrument up and down, moving the particle attached to the tip from a position in solution to come into contact with the surface. While this occurred the instrument measured the forces exerted on the particle by measuring how much the flexible tip was bent. For a fuller explanation see reference³.



Figure 2 Optical micrograph of a polystyrene particle attached to an AFM tip allowing the force-distance profiles between a particle and surface to be measured.

Figure 3 shows the force measured by the AFM instrument as the particle is brought into contact with the surface at pH 10. Initially the force acting on the particle is zero when it is in solution and then suddenly increases as the particle comes into contact with the surface. Forces due to the electrostatic repulsion as the two charged surfaces approach each other are not clearly visible due to the scale of the figure.

When the direction of the piezo electrics are reversed and the particle functionalised tip is moved away from the surface, the force is reduced through zero to become more negative. This is caused by the particle adhering to the surface, causing the flexible tip to bend. At a certain point the force reaches its minimum value, the particle is pulled from the surface and the force returns back to zero (see Figure 4). The minimum force reached is known as the *pull-off force*.

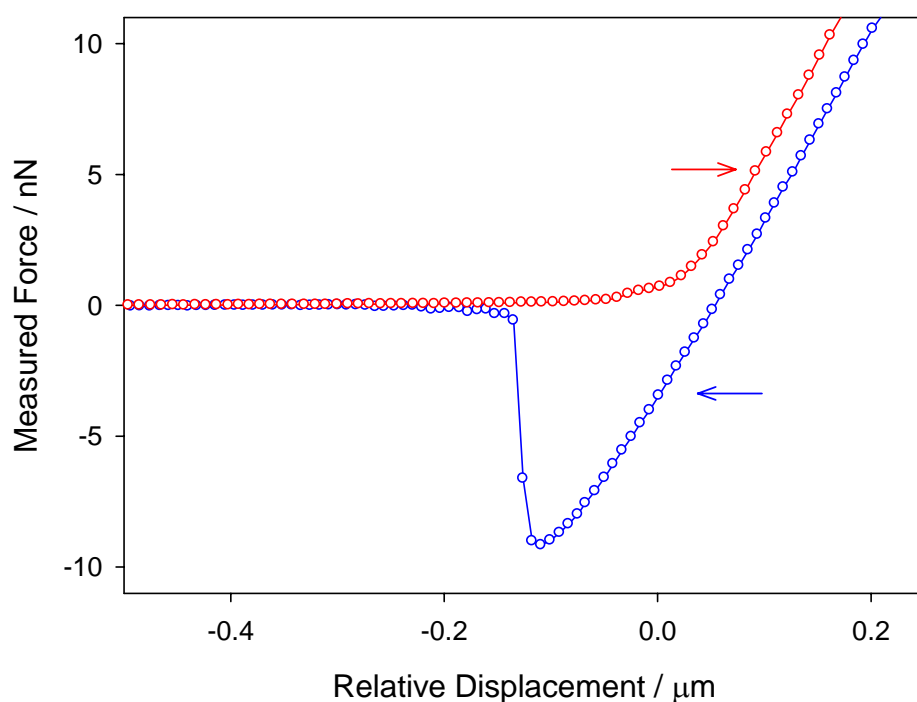


Figure 3 A typical measured force-distance profile between a polystyrene particle and a planar silica surface. Data points in red show the measured force as the particle is advanced towards the surface, and blue data points the measured force as the particle is withdrawn from the surface.

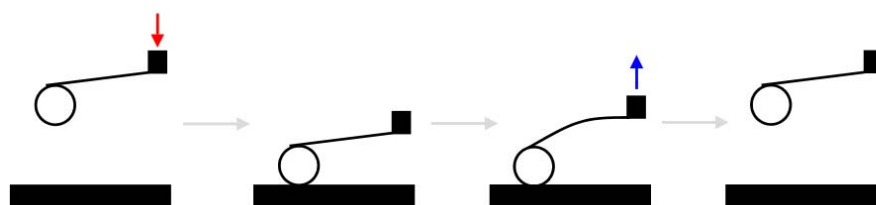


Figure 4 Schematic illustration of a particle functionalised AFM tip. From the left: tip advances towards surface; tip in contact with surface; tip is retracted and particle adheres to the surface causing the flexible tip to bend; particle detaches from surface.

Taking an average of 200 repeats of this experiment, a mean pull-off force of 9nN was found. This shows that a particle adsorbed onto a surface cannot be spontaneously released by changing the solution pH. Although electrostatic forces can be effectively switched on and off by changing the pH, van der Waals force remains constant, meaning that particles must be pulled from the surface to be removed.

This irreversible adhesion of particles to a surface is not taken into account in the theoretical model. Instead in the model, the particle-surface interaction can be reduced to zero, leading to the spontaneous release of a particle from a surface. The theoretical model uses a Morse potential to describe the particle-surface interaction, meaning that the interaction is modelled on a single interaction with a specified decay length. In the systems studied so far, the particle-surface interaction depends on a combination of two interactions with different decay lengths – van der Waals force and electrostatic repulsion. Therefore the real interaction is not well described by a single Morse potential.

An implementation of the theoretical design will have to make use of a particle which is either: adhered to the surface and slides along the surface, remaining in contact at all times; or a particle which is repelled away from the surface and never comes into contact with the surface. Under both these conditions the particle-surface interaction is dominated by a single interaction and can be well described by a Morse potential.

Can Polymer Chains Desorb from Surfaces?

Polymer chains were also investigated to find if they would be of any use in implementing the theoretical design. As has already been shown, particle adhesion is irreversible but perhaps a particle could be tethered to a surface by a polymer chain which migrates along a surface gradient, as has been shown possible by Burgos et al⁵. Or alternatively, perhaps a particle constructed of the polymer chain could be used, such as microcapsules created by layer-by-layer deposition. For either of these to work a polymer must be able to reversibly bind to a surface.

Poly(dimethylamino ethyl methacrylate) (PDMA) was chosen as a polymer to study due to its water solubility and its amine groups which can be protonated leading to a cationic surface charge. This polymer was dissolved in water at pH 3 and introduced to a silicon surface. As shown in Figure 5, this led to the PDMA adsorbing onto the surface of the silicon due to its opposite charge, giving a dry thickness of 1.7nm, when studied using ellipsometry. This surface was then rinsed extensively with water at pH 11 and dried in a stream of nitrogen gas. This process will deprotonate the adsorbed polymer chain breaking the electrostatic attraction to the surface, which should enable the polymer chains to desorb from the surface. But as shown in the Figure 5, the ellipsometric height only decreased by a small amount, indicating that most of the polymer chains have remained adhered to the surface and not been released. Repeating this process several

times resulted in further decreases in the measured ellipsometric height but did not remove all the adsorbed polymer.

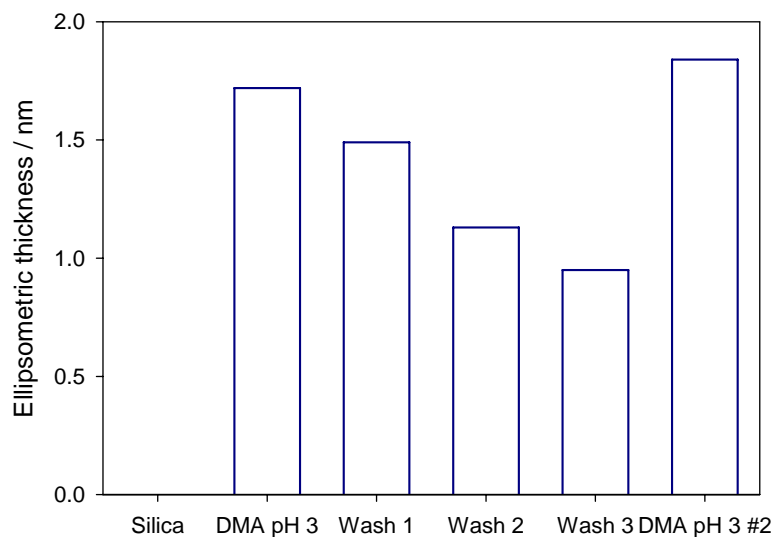


Figure 5 Measured ellipsometric height of an adsorbed PDMA layer, followed by washings with pH 11, followed by a further PDMA adsorption.

As a control experiment, the surface was reintroduced to the PDMA solution at pH 3 and then dried. PDMA re-adsorbed onto the surface filling the spaces created by polymer chains which had desorbed giving a new thickness of 1.8nm very close to the original thickness of 1.7nm.

This experiment shows that polymer chains cannot spontaneously release from a surface. Similar to particles, their interaction with the surface is due to a combination of forces such as electrostatics, dipole interactions and dispersion interactions⁶. Altering the pH only changes the electrostatic interactions, meaning that the polymer can still be attracted to the surface through other interactions making it irreversible. This suggests that polymer chains will not be able to migrate across a surface by reversibly binding, but they may be able to migrate across a surface by the reversible binding of one segment of the polymer chain, rather than the whole chain. This was not investigated further.

2.2 Frictional Forces Between a Particle and Surface

It has been shown in the previous section that particles cannot be adsorbed onto a surface and then be released. Therefore any motion of an adsorbed particle has to occur by the particle sliding or rolling along the surface, during which time it is expected that it will encounter significant friction. Presumably a particle will slide using a mixture of sliding and rolling encountering different amounts of friction depending on whether the particle slides or rolls.

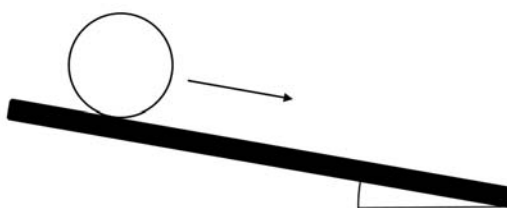


Figure 6 Schematic representation of a gold particle on an inclined surface as described in the text.

To investigate if a particle sliding or rolling along a surface is feasible, experiments were carried out into the friction encountered between the particle and surface. A very simple experiment involved dispersing $4\mu\text{m}$ gold particles in a 0.1M sodium chloride solution and allowing the dense particles to sediment onto an inclined glass surface. Due to gravity and the sloped surface, a force of $mg \sin\theta$ acts on the gold particle parallel to the surface. By inclining the surface at angles of up to 5.7° , the force acting on the particle could be increased up to 1.1pN . Video microscopy showed that these gold particles did not move from their original position as the glass was inclined, showing that the frictional force experienced by the gold particle is greater than 1.1pN . Although this force seems small, it can be calculated that this force is large enough to propel a gold particle through solution at $24\mu\text{m s}^{-1}$ – a similar speed to most of the nanoswimmers highlighted in the introduction.

Another experiment involved subjecting polystyrene particles adsorbed onto a glass surface to a flow of water. This flow exerts a force on the particle parallel to the surface due to the hydrodynamic drag and also a force perpendicular to the surface due to the shear force exerted on the liquid by the stationary glass surface⁷. These two forces are opposed by the friction between the particle and the surface, and the pull-off force respectively, as shown in Figure 7.

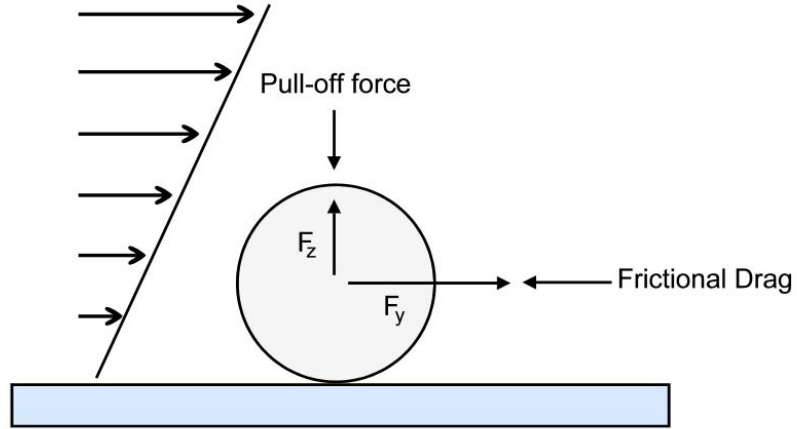


Figure 7 Schematic of the forces acting on a particle adsorbed onto a glass surface by a flow of water.

Particles were observed by video microscopy while the flow rate of water over the surface was increased from 0 up to 27ml min^{-1} . At flow rates less than 15ml min^{-1} , particles remained in their original positions and did not slide along the glass surface. At a flow rate of 15ml min^{-1} some particles were observed to move from their original positions along the glass surface, and at flow rates of 20ml min^{-1} or greater all particles adsorbed to the surface were observed to move from their original positions. Results typical of those gathered are shown in Figure 8.

The force acting on the particle parallel to the surface F_y , which is opposed by the friction force can be calculated by:

$$F_y = 6\pi\eta Rv$$

eq. 1

where η is the viscosity of water, R the particle radius and v the velocity of water flowing at one radius above the surface. The force acting normal to the surface F_z , can be calculated by⁷:

$$\text{Lift Force} = \rho R^4 \sigma^2 \times 9.257$$

eq. 2

where ρ is the density of water, R particle radius, σ the shear stress of water at the surface.

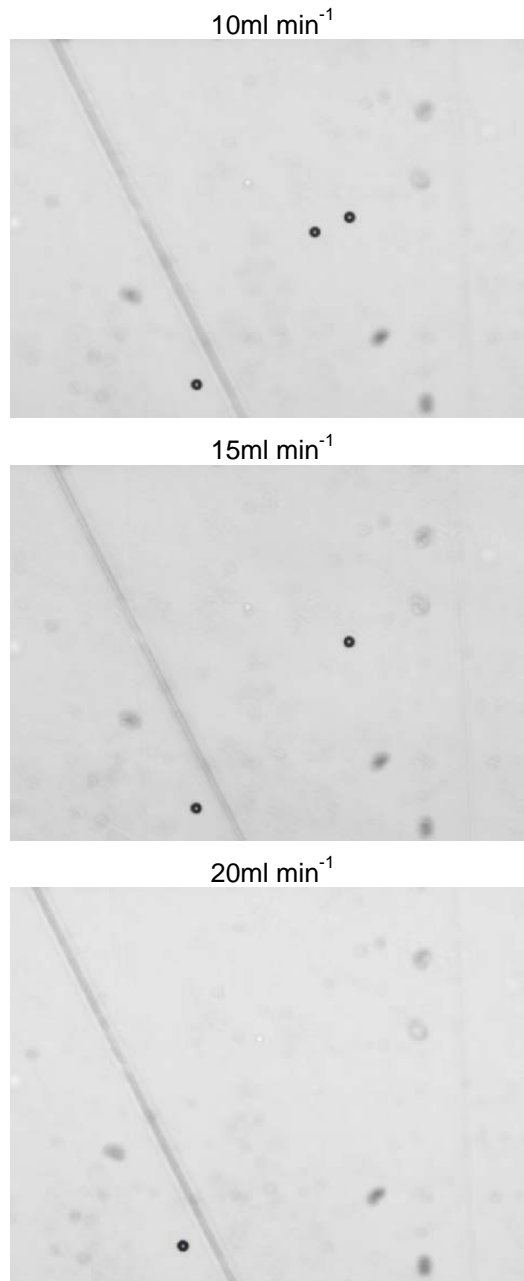


Figure 8 Typical experimental results from investigating the frictional force between a particle and a surface by introducing a flow of water over the surface.

Using these equations, a force parallel to the surface of $F_y = 1.7\text{nN}$ is calculated when the flow of water is 10ml min^{-1} . At this flow rate, the particles remain adhered to the surface and do not move, indicating that the frictional force between the particle and surface must be greater than 1.7nN , otherwise the particle would be observed to move along the surface at a velocity slower than the velocity of the moving water.

At 15ml min^{-1} , when some of the particles are observed to start moving from their original positions, the lift force F_z can be calculated to be 0.69nN . This value is an order

of magnitude smaller than the pull-off force measured for identical polystyrene particles, suggesting that the particles have not been pulled off the surface and slide along the surface. The force F_y can be calculated to be 2.6nN.

From these results it is tempting to conclude that particles remain bound to the surface as the flow of water increases and begin to slide when the force exerted on them becomes large enough. If this was the case the measured frictional force between the particle and surface would be 1.7 – 2.6 nN, but a further observation indicates that particles do not remain adhered to the surface. If the velocity of the ‘sliding’ particles is measured, it is found to be very close to the velocity of the water flowing over the surface, i.e. the frictional force is zero. This does not make sense, as at lower flow rates the frictional force was measured to be greater than 1.7nN.

Therefore it is suggested that particles which are initially bound to the glass surface, experience a force F_y which is insufficient to overcome the frictional force. When the flow rate is increased, particles are pulled off the surface allowing them to travel in the direction of flow at the same velocity as the stream of water. It was calculated that the force F_z is an order of magnitude smaller than the pull-off force but it was neglected that the flow of water may not be constant due to ‘slip and stick’ nature of the syringe pump used. Therefore, the average flow rate does not give a flow which is strong enough to lift the particles off the surface but the flow may have an instantaneous flow rate which does.

From the experiments used to investigate the friction encountered between a particle and surface, it can be concluded that for 4 μ m gold particle, the frictional force is greater than 1.1pN and for polystyrene particles greater than 1.7nN. To move a particle along a surface, a propulsive force of greater than this frictional force is required. It is not known if a force this large could be created by altering the interactions between a surface and a particle but even if a force large enough could be generated, pulling a particle across a surface is a vast waste of energy and will make propulsion slow and inefficient. A propulsive force of greater than 1.7nN is required to get a polystyrene particle to start sliding along a surface, whereas if the same particle was not in contact with the surface but instead a small distance above, it would be propelled by the same force at 15,500 μ m s⁻¹!

Nordgren and Rutland⁸ have studied the frictional forces between a particle and surface which are coated in a polymer brush, and found the frictional force to be ~3nN. Feiler et al⁹ have also studied the friction between a particle and surface, finding a larger frictional force of 15nN. This confirms the results gathered from experiment – frictional forces are large compared to the force needed to propel the particle through solution.

There have been many reports in the literature of biological cells and phospholipid vesicles which are driven along a surface by a flow of water¹⁰⁻¹². Rieu et al¹³ have studied the frictional forces between phospholipid bilayers and found that the bilayer reduced friction significantly. With these reports in mind, giant vesicles were created of the lipid phosphatidylcholine and their behaviour on surfaces investigated.

The vesicles were created by rehydrating a layer of phosphatidylcholine with an aqueous solution containing sucrose at pH 5, which led to the spontaneous self-assembly of the giant vesicles with sizes up to $\sim 50\mu\text{m}$, as shown in Figure 9. This aqueous solution containing vesicles was then diluted 1000x with water (pH 5) and added to a microscope observation chamber with a glass microscope slide as the bottom surface. This dilution reduced the concentration of sucrose in the solution and lowered its density, while the concentration of sucrose inside the vesicles and therefore the density remained unchanged. This caused the vesicles to sediment to the bottom of the observation chamber, where they were found by video microscopy to not adhere to the surface, instead they were free to diffuse around.

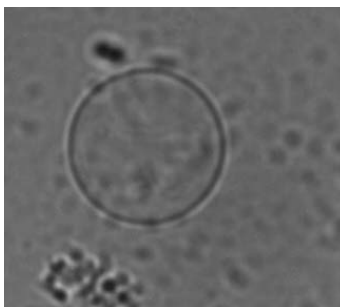


Figure 9 Optical micrograph of a prepared phosphatidylcholine vesicle.

This freedom of giant vesicles on silica surfaces was unexpected, as the surface of the vesicles should be zwitterionic and have a net positive charge of $\sim +1\text{mV}^{14}$, causing them to be attracted to the anionic silica surface. This result can be rationalised by recalling that for a vesicle to exist, there must be lipid in the solution with a concentration of at least the critical micelle concentration⁶. This lipid in solution will be attracted to the surface and will self-assemble into a supported lipid layer¹⁵, onto which giant vesicles will be repelled. It was confirmed by ellipsometry that a lipid layer forms on the silica surface over the course of 5 minutes with a thickness of 5.2nm.

Adding 0.1M sodium chloride to suppress electrostatic repulsion between vesicles and silica surfaces coated with a layer of lipid, also did not result in vesicles adhering to the

silica substrate. Therefore as vesicles do not adhere to a surface, they are of no use in implementing the theoretical design.

In this section it has been shown that friction between a particle and a surface is large compared to the forces required to propel a particle through solution. Any implementation of the theoretical design which relies on particles sliding across a surface will be very inefficient due to the energy wasted through friction, and will require the generation of a large propulsion force. It is not known if a force this large could be generated, as all existing nanoswimmers make use of very small forces. To implement the design an approach in which the particle is repelled away from the surface should be used. This will enable the particle to move across the surface with only viscous drag acting against the propulsion force.

2.3 The use of Nanoparticles to alter Surfaces and Particle-Surface Interactions

In the theoretical design, the motor particle releases nanoparticles which then adsorb onto the surface and alter the interactions between target particle and the surface. To investigate if particles can adsorb onto a surface and alter the particle-surface interactions, surfaces were created, then functionalised with nanoparticles and the surface properties measured.

Silicon surfaces which are anionically charged were firstly coated with poly(allyl amine) through electrostatic self assembly to make a cationic surface. Nanoparticles were created by the miniemulsion polymerisation of styrene, giving 64nm polystyrene particles which are anionically charged due to persulfate groups on the particles surface. These particles should adsorb onto the created cationic surfaces through electrostatic self assembly and alter the surface properties of the surface, as shown schematically in Figure 10.

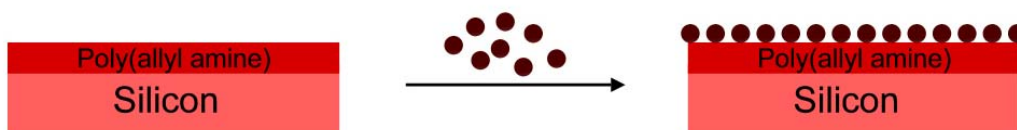


Figure 10 Schematic representation of the created surfaces with polystyrene particles adsorbing onto the surface.

Ellipsometry showed that the adsorption of poly(allyl amine) gave a layer of polymer 2nm thick, and that after exposure to the polystyrene particles an extra layer 18nm thick was created. The layer is thinner than the diameter of the adsorbed particles due to the data being fitted with a continuous layer model, rather than discrete particles of polystyrene but still shows that a layer of the nanoparticles are adsorbing onto the surface.

Static contact angle measurements with water showed a change from 17° before to 78° after nanoparticle adsorption, suggesting that the surface has become more hydrophobic as expected from a surface being functionalised with polystyrene. Although this may not be the case, as contact angle measurements also depend on surface roughness as well as hydrophilicity. Upon functionalising the surface with nanoparticles, the surface has changed from very smooth to have a roughness of one particle diameter – 64nm.

To measure if the surface charge changes when functionalised with the nanoparticles, silica particles were functionalised in the same way as the planar surface and then were used in zeta potential measurements. This showed that the surface charge of the silica particles surface changed from +33mV to -45mV. This suggests that the surface changes from cationic to anionic upon functionalisation with the nanoparticles, but the zeta potential is the potential of the surface at the slipping plane, and this changes significantly after the adsorption of nanoparticles, from a few Angstroms above the surface to approximately one particle diameter above the surface $\sim 64\text{nm}$.

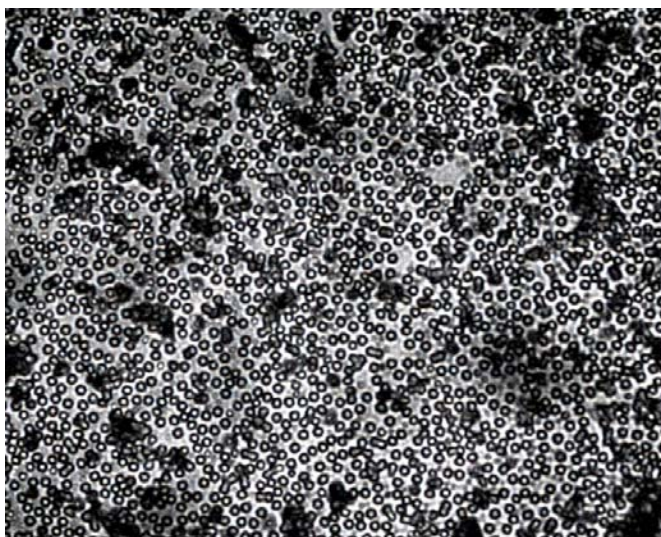


Figure 11 Optical micrograph of a surface functionalised with $1\mu\text{m}$ anionically charge polystyrene particles from aqueous dispersion.

Taking the results from the two experiments above literally, it might be concluded that the adsorption of nanoparticles onto a surface changes the properties of the surface from hydrophilic and cationic, to a surface which is hydrophobic and anionic. But for the reasons discussed, these results may be misleading and the nanoparticle functionalisation probably creates a surface which has a mixture of surface properties from the nanoparticles and the original surface. This would cause the surface to become amphiphilic and zwitterionic upon functionalisation with the nanoparticles.

To enable the functionalisation of surfaces to be visualised, larger $1\mu\text{m}$ anionic polystyrene particles were adsorbed onto a surface. Figure 11 shows an optical micrograph of the functionalised surface. The adsorbed particles do not completely cover the entire surface, instead they form a random distribution on the surface with relatively large gaps between particles. This is caused by the electrostatic repulsions between

particles which blocks another from coming into close proximity. Counting the number of particles per unit of area, it was calculated that only 22% of the surface area had been functionalised by the adsorption of the particles.

In the theoretical design, nanoparticles are released from the motor microcapsule and are adsorbed onto the surface to change the particle-surface interaction. The number of nanoparticles contained in the microcapsule can be calculated by:

$$\text{Number of Nanoparticles} = \frac{V_{micro} \times \sigma}{V_{np}} = \left(\frac{R_{micro}}{R_{np}} \right)^3 \times \sigma$$

eq. 3

where V_{micro} and V_{np} are the volumes of a microcapsule and a nanoparticle respectively, σ the packing efficiency (0.74 for hexagonal close packing, <0.5 for colloidal dispersions), R_{micro} and R_{np} the radii of the microcapsule and nanoparticle respectively.

As these nanoparticles are released from the microcapsule and are adsorbed onto the surface modifying its properties, the area modified can be calculated by multiplying the number of nanoparticles by the area that they modify:

$$\begin{aligned} \text{Area Modified} &= \text{Number of Nanoparticles} \times \pi R_{np}^2 \times \frac{1}{\alpha} \\ &= \left(\frac{R_{micro}}{R_{np}} \right)^3 \times \sigma \times \pi R_{np}^2 \times \frac{1}{\alpha} \end{aligned}$$

eq. 4

where α is the surface coverage of the nanoparticles on the surface (found to be 0.22 from experiments above). Dividing by the cross-sectional area of the microcapsule gives the area of the surface modified in units of microcapsule areas:

$$\begin{aligned} \text{Area Modified} &= \left(\frac{R_{micro}}{R_{np}} \right)^3 \times \sigma \times \frac{\pi R_{np}^2}{\pi R_{micro}^2} \times \frac{1}{\alpha} \\ &= \left(\frac{R_{micro}}{R_{np}} \right) \times \frac{\sigma}{\alpha} \end{aligned}$$

eq. 5

Using eq. 5 it is possible to calculate that a 5 μ m microcapsule filled with a 50% v/v nanoparticle dispersion of 5nm particles, would modify an area equivalent to 2,273 of the microcapsules areas. This value seems large enough for the nanoparticles to alter enough of the surface for the microcapsule to be propelled a significant distance. But if the parameters are changed to a 1 μ m microcapsule filled with a 50vol % dispersion of 50nm nanoparticles, an area of only 45 microcapsules would be modified. This area of surface modification seems too small for the microcapsule to be propelled any significant distance.

Another question which arises from the use of a microcapsule which releases nanoparticles to alter the surface is, how will the nanoparticles be released from the microcapsule? Studies of membrane permeability have shown that small ions or molecules can pass through the membrane and the rate of release can be tailored by altering the pH of the surrounding solution or treatment with a solvent¹⁶. Whereas large molecules or nanoparticles cannot pass through the membrane¹⁷ and will need to be released either through a hole or a pore in the membrane.

Pores are present in many biological cell membranes but as of yet, have not been incorporated into microcapsules. Holes or tears can be created in the microcapsules membrane during their preparation, which would allow nanoparticles to pass through the membrane and be released. But the rate of release would be uncontrollable due to the high osmotic pressure created inside the microcapsule by the high concentration of nanoparticles which will force nanoparticles out of the microcapsule very rapidly.

De Geest et al¹⁸ have created microcapsules filled with nanoparticles which degrade in alkali conditions. This causes the membrane of the microcapsule to rupture releasing the nanoparticles into solution. Although this is not particularly useful for implementation of the theoretical design, as the time at which the membrane ruptures is not controllable and the release of nanoparticles only occurs once, instead of the constant release required.

For the reasons discussed above, it seems unlikely that nanoparticles could be released from a microcapsule, and from experiments carried out above, that they do not alter surfaces significantly upon adsorbing onto them. Therefore an alternative way to alter the surfaces shall be needed. However the surface is modified, the source of the modification needs to originate from a particle which acts as the motor particle in the theoretical design.

2.4 Summary and Conclusions

In this chapter experiments have been carried out which investigate the feasibility of the theoretical design. Three key points have been investigated which form the basis of the propulsion mechanism:

In section 2.1 the adhesion of cationic polystyrene particles to anionic silica surfaces was found to be irreversible. Particles did not spontaneously release from the surface when sodium hydroxide was added, which breaks the electrostatic attraction of particles to the oppositely charged surfaces. Atomic force microscopy also showed that the adhesion of a particle to a surface was irreversible and did not occur spontaneously. The particles used in this experiment had to be pulled off the surface with a force of 9nN.

These results have strong implications on the implementation of the theoretical design as they show that the behaviour of particles is markedly different to that described in the theoretical model. The differences between the results of the computational study and these experiments arise because the particle-surface interaction is based on a single interaction in the computational work, whereas in the experimental studies the interaction is caused by a combination of two interactions.

In section 2.2 the friction encountered between a particle and surface in contact was investigated. Using a flow cell experiment it was found that the force required to slide a particle along a surface was large at $>1.7\text{nN}$. Therefore to propel a particle across a surface, a propulsive force greater than this frictional force would be required. Due to this friction, any propulsion created would be slow and very inefficient. Phospholipid vesicles were also investigated to find if they could slide across surfaces with less friction but it was found that these vesicles did not adhere to surfaces, making them of no use in implementing the theoretical design.

It is therefore concluded that for the theoretical design to be implemented, a particle must be repelled away from the surface to allow it to migrate along the created surface interaction gradient. A particle-surface interaction which consists of a single interaction which can be changed from adhesive to repulsive must be found. Implementations based on this type of interaction will be the focus of chapter 3, which makes use of van der Waals forces to alter particle-surface interactions from adhesive to repulsive.

Alternatively, an implementation of the design in which the particle never comes into contact with the surface could be used. The particle should be repelled away from the surface at all times and the interaction altered from repulsive to more repulsive. Implementations of the design based on these types of interaction will be the focus of

chapters 4 and 5, where a particle is repelled away from the surface using electrostatic or steric forces respectively.

In section 2.3 the release of nanoparticles from a microcapsule was discussed and found not to be currently synthetically possible. The adsorption of nanoparticles onto an oppositely charged surface was studied and it was found that surfaces treated with the particles acquired new properties based on a mixture of the nanoparticle and the original surfaces properties. Results found from experiments with larger particles showed that only a small fraction of the surfaces became functionalised with the particles due to the electrostatic repulsions between particles.

It is therefore concluded that for the theoretical design to be implemented, a procedure which modifies the surfaces properties using a method other than the adsorption of nanoparticles should be used. This could be achieved through the use of a chemical reaction which transforms functional groups on the surface or a chemical reaction which alters the properties of the liquid separating the particle and surface. Conveniently if a chemical reaction is used, the chemical species could be generated through a catalytic reaction on the motor particle's surface, rather than through release of a chemical contained within the motor particle. Using a chemical reaction is also appealing due to the wide range of chemical reactions which can be achieved.

In this chapter, key points of the theoretical design have been studied and problems with implementing this design highlighted. Several solutions to these problems have been suggested which change the theoretical design. These include altering the particle-surface interaction from using differences in adhesion, to using either interactions which change from adhesive to repulsive, or from repulsive to more repulsive. Instead of changing these interactions by releasing nanoparticles from the motor particle, a chemical species will be released or generated by a catalytic reaction on the motor particle surface. The following chapters investigate different implementations of the theoretical design using these initial changes.

2.5 Experimental Details

Group Transfer Polymerisation of Poly(Dimethylamino ethyl methacrylate)-b-(Methyl methacrylate) (PDMA-b-MMA). Before polymerization, tetrahydrofuran (THF), dimethylamino ethyl methacrylate (DMA) and methyl methacrylate (MMA) were distilled, mixed with calcium hydride overnight and then distilled again. Following Armes et al,¹ a total of 100ml THF, 10mg tetrabutylammonium bibenzoate and 0.2ml 1-methoxy-1-trimethylsiloxy-2-methyl-1-propene were added to a 500ml reaction vessel which had previously been dried and evacuated. 18ml DMA was then added slowly via a side-arm over approximately 5 minutes. This caused the temperature of the liquid mixture to rise by 13°. After one hour the temperature had returned to room temperature indicating near complete polymerization of DMA, at this point 3ml of MMA was added. Again the liquid mixture temperature raised and returned back to room temperature after another hour. After a total of 2 hours polymerisation time ethanol was added via a side arm to quench polymerisation.

The prepared block copolymer was then isolated by removing solvent by rotary evaporation and further dried under high vacuum to remove unreacted monomer. Gel permeation chromatography indicated a molecular weight of the homopolymer to be 22,023 g mol⁻¹, with a polydispersity index of 1.11, the diblock copolymer was found to be 26,597 g mol⁻¹, with a polydispersity index of 1.10. ¹H NMR analysis showed that the block copolymer was 30mol % MMA.

Dispersion Polymerisation of Styrene using a Poly(Dimethylamino ethyl methacrylate)-b-(Methylmethacrylate) Steric Stabiliser. Following Armes et al,² 0.5g of the prepared PDMA-b-MMA block copolymer and 50ml of ethanol were added to a 3-necked round bottom flask fitted with reflux condenser and magnetic stirrer bar. After one hour the block copolymer had dissolved and 50mg azobisisobutyronitrile dissolved in 5g styrene added. The flask was then sealed and degassed by bubbling nitrogen gas through the reaction liquid for 30 minutes. Then the flask was heated to 60°C for 24 hours before polymerisation was quenched by opening the flask to the air.

The prepared particles were then purified by three repeat cycles of centrifuging, decanting the supernatant and redispersing in water at pH 3. Dynamic light scattering showed that the particle had a mean diameter of 4.2µm and a polydispersity of 1.16.

Investigation of Surface Forces using Atomic Force Microscopy. 20µm polystyrene particles were attached to triangular Veeco tipless probes using a UV curable glue (Norland optical adhesive) using a Digital Instruments Nanoscope IV multimode instrument as a micromanipulator. Probes with a particle attached were then exposed to

UV light for one hour to cure the glue. The probe was then loaded into a Digital Instruments 1D force puller and the spring constant of the cantilever measured using the 'thermal' method included in the instruments software. The probe was then surrounded with water adjusted to pH 10 using sodium hydroxide and the spring constant remeasured. The tip was then lowered to close proximity of a clean glass surface and 200 cycles of data collected as the tip was moved a distance of $5\mu\text{m}$ at $2\mu\text{m s}^{-1}$. An average pull-off force was then calculated using the software.

Radical Polymerisation of Dimethylamino Ethyl Methacrylate in Bulk. 1g of dimethylamino ethyl methacrylate and 50mg azobisisobutyronitrile were mixed together in a 50ml glass sample tube. This tube was then heated to 50°C in an oven for 24 hours resulting in polymerisation of the monomer. The produced polymer was used without further purification.

Adsorption of PDMA onto Silicon Surfaces and Determination of Thickness using Spectroscopic Ellipsometry. 0.5g PDMA was dissolved in 50ml of water adjusted to pH 3 using dilute hydrochloric acid overnight. The thickness of any organic layer on a piece of clean silicon was measured using a spectroscopic ellipsometry and fitting data with a Cauchy layer model. The same piece of silicon was then submerged in the PDMA solution for 20 minutes, rinsed with water at pH 3 and then dried in a stream of nitrogen gas. The thickness of the adsorbed layer was then measured using ellipsometry and again after being rinsed with water at pH 11 and dried. This was repeated a further two times and then finally the piece of silicon was resubmerged in the PDMA solution for 20 minutes, rinsed with water at pH 3, dried in a stream of nitrogen and the ellipsometric height measured.

Investigation of Frictional Forces on Gold Particles on Inclined Surfaces. $4\mu\text{m}$ gold particles were dispersed in a solution of 0.1M sodium chloride to suppress electrostatic repulsions from surfaces. A small amount of this dispersion was then sandwiched between two clean glass microscope slide using double sided adhesive as a gasket, to create an observation chamber. This observation chamber was then inclined at various angles and the position of particles measured using video microscopy.

Investigation of Frictional and Pull-off Forces by Applying a Flow of Water over a Surface. $20\mu\text{m}$ polystyrene particles were dispersed onto a clean microscope from a dry powder. A flow cell was created by sandwiching two pieces of Perspex together using 1mm thick rubber as a gasket. Holes were drilled in the top piece of Perspex to create an inlet and an outlet. The inlet was then connected to an Aladdin 1000 syringe pump fitted with a 60ml 26mm diameter syringe and the glass surface with particles loaded into the flow cell.

The flow cell was then carefully filled with a solution of 0.1M sodium chloride using the syringe pump at a low flow rate. Position of the particles was then monitored using video microscopy at 5x magnification while liquid was pumped through the flow cell at different rates of up to 27ml min⁻¹. The dimensions of the flow cell channel was measured to be 0.96mm wide, with an estimated 1mm height.

Preparation of Giant Phosphatidyl Choline Vesicles. 0.1g of phosphatidyl choline was dissolved in a small amount ~0.5ml dichloromethane in a glass sample tube. Then the lid was removed and the liquid evaporated by a stream of nitrogen gas while the tube was simultaneously rotated to allow the liquid to coat all of the glass surface. Once dry the tube was placed in an oven at 60°C for 2 hours to ensure complete evaporation. 10ml of water was then added to the tube and a magnetic stirrer bar used to rapidly stir the liquid. After 24 hours giant vesicles were visible by light microscopy with diameters up to 50µm.

Preparation of Nanoparticles by Miniemulsion Polymerisation. A total of 1g styrene, 4g water, 25mg ammonium persulfate, 0.5g sodium dodecylsulphonate and 100µl decahydronaphthaline were added to a test tube fitted with a magnetic stirrer bar. The mixture was then emulsified by rapid stirring for 20 minutes, followed by sonication for 1 hour. After which the mixture was degassed for 30 minutes by bubbling nitrogen gas through the solution and was then heated to 65°C overnight. Dynamic light scattering gave a mean diameter of 64nm.

References

- (1) Baines, F. L.; Dionisio, S.; Billingham, N. C.; Armes, S. P. *Macromolecules* **1996**, *29*, 3096-3102.
- (2) Amalvy, J. I.; Unali, G. F.; Li, Y.; Granger-Bevan, S.; Armes, S. P.; Binks, B. P.; Rodrigues, J. A.; Whitby, C. P. *Langmuir* **2004**, *20*, 4345-4354.
- (3) Cappella, B.; Dietler, G. *Surface Science Reports* **1999**, *34*, 1.
- (4) Ducker, W. A.; Senden, T. J.; Pashley, R. M. *Nature* **1991**, *353*, 239-241.
- (5) Burgos, P.; Zhang, Z. Y.; Golestanian, R.; Leggett, G. J.; Geoghegan, M. *ACS Nano* **2009**, *3*, 3235-3243.
- (6) Israelachvili *Intermolecular & Surface Forces*; 2nd ed.; Academic Press.
- (7) Yahiaoui, S.; Feuillebois, F. *Journal of Fluid Mechanics*, *662*, 447-474.
- (8) Nordgren, N.; Rutland, M. W. *Nano Letters* **2009**, *9*, 2984-2990.
- (9) Feiler, A.; Larson, I.; Jenkins, P.; Attard, P. *Langmuir* **2000**, *16*, 10269-10277.
- (10) Lawrence, M. B.; Springer, T. A. *Cell* **1991**, *65*, 859-873.
- (11) Abkarian, M.; Lartigue, C.; Viallat, A. *Phys. Rev. E* **2001**, *63*.
- (12) Abkarian, M.; Viallat, A. *Biophysical Journal* **2005**, *89*, 1055-1066.
- (13) Trunfio-Sfarghiu, A.-M.; Berthier, Y.; Meurisse, M.-H.; Rieu, J.-P. *Langmuir* **2008**, *24*, 8765-8771.
- (14) Jin, Q.; Xu, J.-P.; Ji, J.; Shen, J.-C. *Chemical Communications* **2008**, 3058-3060.
- (15) Cremer, P. S.; Boxer, S. G. *J. Phys. Chem. B* **1999**, *103*, 2554-2559.
- (16) Sukhorukov, G. B.; Antipov, A. A.; Voigt, A.; Donath, E.; Mohwald, H. *Macromol. Rapid Commun.* **2001**, *22*, 44-46.
- (17) Radtchenko, I. L.; Giersig, M.; Sukhorukov, G. B. *Langmuir* **2002**, *18*, 8204-8208.
- (18) De Geest, B. G.; De Koker, S.; Demeester, J.; De Smedt, S. C.; Hennink, W. E. *Polymer Chemistry*, *1*, 137-148.

3 Propulsion using Repulsive van der Waals Forces

3.1 Introduction

As has been shown in the previous chapter, particles need to be repelled away from a surface to enable them to move free of friction. It was also shown that particles adsorb onto surfaces irreversibly due to van der Waals forces which dominates when the particle is in close proximity to the surface. Therefore it is van der Waals force which must be altered from adhesive to a zero force, to allow particles to be released from a surface. Further, the van der Waals force must be converted from adhesive to repulsive, to repel a particle above a surface and allow it to move. In this chapter ways to implement the theoretical design based on changing van der Waals force from attractive to repulsive shall be investigated.

Van der Waals force has a electrodynamic origin being caused by the interactions between electrical dipoles. There are three types of interactions which contribute to the force: Permanent dipole - permanent dipole interactions (Keesom force), permanent dipole-induced dipole (Debye force) and instantaneous dipole-induced dipole (London force). The interaction energy between two molecules is calculated using Hamaker theory from the equation:

$$w = \frac{-C}{r^6} \quad \text{eq. 1}$$

Where C is the strength of the molecule pair interaction and r is the distance separating them.

To find the interaction between two macroscopic bodies such as a small particle and a planar surface which consist of many molecules, it is necessary to account for the interaction between all molecules in one body with all molecules in the other body.

Following this so called *pairwise additivity*, the interaction energy between a small particle and a planar surface can be calculated using the equation:

$$W = \frac{-A_{132}R}{6D} \quad \text{eq. 2}$$

Where R is the particle radius, D the distance separating the particle and surface, and A_{132} is the Hamaker constant for a body of material 1 acting across a media of material 3 with another body of material 2. The Hamaker constant can be calculated for the interaction between two molecules from their polarizabilities using Hamaker theory, but for large collections of molecules this treatment is insufficient due to the neighbouring effects of nearby molecules. Lifshitz theory is of more use in this situation as it treats the two interacting surfaces as a continuous media rather than consisting of individual molecules and derives the forces acting between the two bodies from their refractive index and dielectric constant. Following Lifshitz theory, the Hamaker constant can be calculated from the equation:

$$A_{132} = \frac{3kT}{2} \sum_{n=0}^{\infty} \sum_{m=1}^{\infty} \frac{1}{m^3} \left(\frac{\epsilon_1(i\xi n) - \epsilon_3(i\xi n)}{\epsilon_1(i\xi n) + \epsilon_3(i\xi n)} \times \frac{\epsilon_2(i\xi n) - \epsilon_3(i\xi n)}{\epsilon_2(i\xi n) + \epsilon_3(i\xi n)} \right)^m \quad \text{eq. 3}$$

Where k is Boltzmann's constant, T temperature, n and m are integers from a series expansion. $\epsilon(i\xi n)$ is the dielectric response function of the material shown in subscript.

Essentially the dielectric response function describes the dielectric properties of the material at all frequencies. In these calculations it is evaluated at fixed frequency intervals of $\xi = 4\pi^2 kT/h$, where h is Planck's constant. Using these sampling frequencies gives one static frequency term, one term at infra-red frequency, two terms in at visible frequency, with the rest being at UV frequencies.

The dielectric response function can be calculated using the Ninham-Parsegian two oscillator approximation from limited optical data¹ using tabulated data, see Bergstrom² for example.

$$\epsilon(i\xi n) = 1 + \frac{C_{IR}}{1 + (\xi/\omega_{IR})^2} + \frac{C_{UV}}{1 + (\xi/\omega_{UV})^2} \quad \text{eq. 4}$$

Where C_{IR} and C_{UV} are the adsorption strengths and ω_{IR} and ω_{UV} are the adsorption frequencies of the materials (units of rad/s).

Repulsive van der Waals Forces

From the above explanation of van der Waals forces it has been proposed that the force experience by two bodies separated by a liquid could be repulsive, even through van der Waals forces are always attractive. This interesting situation occurs when the Hamaker constant is negative, thus giving an interaction energy which increases as the two bodies are brought together as in eq. 2.

Eq. 3 tells us that the Hamaker constant can be negative if the dielectric response function of the intervening liquid, is intermediate between the dielectric response functions of the two bodies it is separating:

$$\varepsilon_1(i\xi n) < \varepsilon_3(i\xi n) < \varepsilon_2(i\xi n) \quad \text{or} \quad \varepsilon_1(i\xi n) > \varepsilon_3(i\xi n) > \varepsilon_2(i\xi n)$$

This situation is quite rare meaning that until recently repulsive van der Waals forces were only predicted and no real life examples were known.

The first example of repulsive van der Waals forces were found when liquid helium was placed in a metal container. The liquid helium was found to climb the walls of the container and flow outside the vessel, completely draining the container. Following calculation of van der Waals forces it was confirmed that they were repulsive and could be used to explain this strange phenomena³.

Meurk et al⁴ were the first group to study repulsive van der Waals forces by Atomic Force Microscopy (AFM) using inorganic surfaces separated by variety of halogenated liquids. Using the same mathematical method described above they calculated Hamaker constants for several combinations of materials, finding that when two surfaces of the same material (silicon nitride or silicon) interacted across either diiodomethane or 1-bromonaphthalene a positive Hamaker constant was predicted, whereas if the surfaces were made of different materials a negative Hamaker constant was predicted when separated by both of the liquids. This is consistent with theory; the liquid's dielectric response function cannot be intermediate of the two surfaces dielectric response function

if they are made of the same material, so attractive van der Waals forces should be observed.

Data from AFM revealed a small attraction between surfaces which were identical, as predicted and hysteresis was observed in the data captured as the tip was moved either towards or away from the surface, consistent with adhesion. When the AFM tip and the planar surface were of different material the attraction towards the surface was no longer observed and the hysteresis in the data disappeared, suggesting that attractive van der Waals forces were no longer present. Although they did not observe any repulsion between the surfaces either. This is probably due to the AFM tips they used which had only a small 50nm diameter, meaning that any repulsive forces experienced would be very small and below the resolution of the instrument.

Lee and Sigmund^{5,6} have studied van der Waals forces between a PTFE surface and a AFM tip functionalised with a small particle consisting of either silica or alumina separated by cyclohexane. Calculation of the dielectric response functions of the materials showed that cyclohexane's dielectric function is intermediate of PTFE's and alumina's or silica's. Following Lifshitz theory they predicted negative Hamaker constants of -2.36×10^{-20} J for the alumina-cyclohexane-PTFE system and a weaker -0.87×10^{-20} J for the silica-cyclohexane-PTFE system. AFM study of the force-distance profiles of the two surfaces as they were brought together showed that the two surfaces were repelled from each other at close distances consistent with repulsive van der Waals forces. The experimentally obtained data fitted well with theoretical distance dependency and calculated Hamaker constants, if retardation of the force was taken into account.

Milling et al⁷ have studied van der Waals forces between PTFE surfaces and gold spheres again by AFM. When the two surfaces are separated by air or a polar liquid such as water they found attractive van der Waals forces, whereas when non-polar liquids such as cyclohexane or bromobenzene separated the surfaces, repulsive forces were observed. Generally, the experimental findings from AFM data agreed with the theoretical prediction from Lifshitz theory. In the case where experiment and theory disagreed, the limited optical data or the Ninham-Parsegian approximation not adequately describing the dielectric response function of the material was thought to be responsible.

Munday et al⁸ studied the forces between silica and gold separated by bromobenzene, again finding the expected repulsive van der Waals force. They also studied the surfaces by electrostatic force microscopy which measures the forces experienced by an AFM tip due to surface charge, in an attempt to prove that the repulsion between surfaces is due to repulsive van der Waals forces and not electrostatic repulsion between two charged surfaces. Using this technique they found that a silica or gold surface had a 'roughness' in

the distribution of charge on the surface, when in water. Whereas in bromobenzene, the surfaces appeared smooth. They attribute these differences in the surfaces 'roughness' to the surfaces being charged in polar liquids and not charged in non-polar liquids. This assumption seems weak as they have only shown that the surfaces have an inhomogeneous distribution of charge in polar liquids and either no charge or a homogeneous charge distribution in non polar liquids. Surely the best evidence that the observed force is due to van der Waals force is how well the data fits with the force law?

So far the study of repulsive van der Waals forces has been mostly to confirm that they exist, what groups of materials they exist between, and that they are not in fact an electrostatic force. Although there has been some research into making use of these forces.

Feiler et al⁹ have used repulsive van der Waals forces to reduce the friction between a gold sphere and a PTFE surface separated by cyclohexane. They have repeated the work of Lee and Sigmund⁵, confirming that repulsive van der Waals forces are observed for this combination of materials. Using friction AFM they found that the friction experienced between the gold sphere and the PTFE surface was reduced to below the resolution of the AFM ($< 1\text{nN}$), whereas if ethanol was used as the intervening liquid much higher frictional forces were observed.

Cho et al¹⁰ have proposed that repulsive van der Waals forces could be used to create electronic devices that self assemble from a dispersion of a mixture of colloidal particles. They also created a prototype battery using platinum and LiClO_4 surfaces as electrodes, and carbon based particles as an insulating material. The insulating particles experienced attractive van der Waals forces towards the platinum surface and repulsive forces towards the LiClO_4 surface and so self-assembled onto the platinum surface insulating it. This allowed the LiClO_4 surface to be charged-up and used as a store of electricity.

For a particle to propel itself forward it will be necessary to change van der Waals interactions. Sernelius¹¹ has proposed that van der Waals forces can be altered by irradiation with microwaves, which leads to the force being enhanced, and Kimura¹² has also proposed that van der Waals forces can be enhanced by irradiation with light at a Mie resonant frequency. But both of these ways of changing van der Waals force are not suitable to be implemented as a practical solution to the theoretical design. As the microwaves or light would have to be generated at the motor particle and would not decay with distance away from the particle, as a concentration of nanoparticles would to give the desired adhesion gradient. Therefore the most sensible way to change van der Waals force is to change one media of the system to another.

In this chapter repulsive van der Waals forces shall be explored as a way to change a particle's interaction with a surface, leading it to be propelled forward as in the theoretical design. The change in interaction must be from strong to weak and therefore from attractive to repulsive van der Waals forces. This transformation must be via a chemical reaction either of the surface or the surrounding liquid and should be catalysed by the motor particle. Modification of the surface is extremely difficult, for example changing a polyethylene surface to poly(tetrafluoroethylene) surface would result in a change from attractive to repulsive van der Waals force for a silica particle surrounded by cyclohexane, but this reaction is difficult to achieve at room temperature and pressure. It is much easier to alter the liquid surrounding the particle.

Almost all liquids result in attractive van der Waals forces between a particle and a surface so can be used as reactants to create a specific liquid such as cyclohexane, which results in repulsive van der Waals forces. Therefore it makes most sense to start with a combination of materials in which van der Waals force has been studied and found to be repulsive, then use retrosynthesis to devise a chemical route to form this specific liquid from reactants.

From the literature sources discussed above we know that repulsive van der Waals forces have been observed for cyclohexane, bromobenzene, 1-bromonaphthalene, diiodomethane and 2-butanone. One of these liquids will have to be formed by a chemical reaction, preferably at room temperature and pressure by a chemical reaction catalysed by or on the motor particles surface. This would change van der Waals from attractive to repulsive locally around the motor particle.

Fortland and Askivik¹³ have studied the van der Waals forces in mixture of liquids finding that the results could be explained by combining the dielectric properties of each component in the mixture according to the Clausius-Mosotti equation.

3.2 A Combination of Materials to use

To implement the design it will be necessary to identify a combination of materials which result in repulsive van der Waals forces and then identify a synthetic route to create this combination of materials through a chemical reaction. The combination of materials used as 'reactants' should result in attractive van der Waals forces which are then converted by chemical reaction to repulsive van der Waals forces. As stated above a chemical reaction on the liquid separating two surfaces will be the easiest to achieve, rather than on the surfaces. Therefore retrosynthetic analysis has been performed on liquids which have been highlighted in literature sources to result in repulsive van der Waals forces, to find the most suitable material combination and a chemical reaction which forms these.

Table 1 shows the liquids which can be used to separate two surfaces made of selected materials which result in repulsive van der Waals forces and possible ways to create these liquids by a chemical reaction. Bromobenzene gives repulsive van der Waals forces for the combinations of materials PTFE - Bromobenzene - Gold and Silica - Bromobenzene - Gold, whereas for 1-Bromonaphthalene the relevant combination of materials is silicon nitride - 1-bromonaphthalene - Silica. Both Bromobenzene and 1-Bromonaphthalene can be easily created by the bromination of benzene or naphthalene using a Lewis acid catalyst such as AlCl_3 at room temperature (Route 1) or bromobenzene can be created by the bromination of benzene via a radical reaction using AIBN (Azobisisobutyronitrile) and N-Bromosuccinimide at elevated temperatures (Route 2). Route 1 is much more desirable as it occurs at room temperature and makes use of a catalyst which could be attached to the motor particle to create a local high concentration.

p-Xylene has been reported to create repulsive van der Waals forces in the materials combination PTFE - p-Xylene - Gold and can be created through the methylation of either toluene (as shown) or dimethylation of benzene again using a Lewis acid catalyst. Although over substitution can take place in both reactions leading to trimethylbenzene. In addition selectivity is quite poor leading to ortho and meta isomers of xylene as well as the desired para isomer. This reaction is less desirable for use in the design due to these selectivity problems.

Van der Waals forces in cyclohexane have been extensively studied, making it highly desirable for use in the implementation of the design. It has been reported to lead to repulsive van der Waals forces for the combination of materials PTFE - Cyclohexane - Silica, PTFE - Cyclohexane - Alumina and PTFE - Cyclohexane - Gold. It is difficult to create by chemical reaction but one synthetic route could be the hydrogenation of

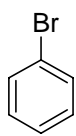
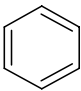
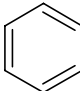
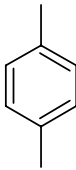
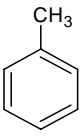
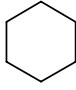
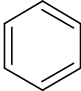
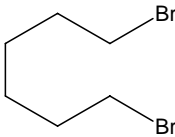
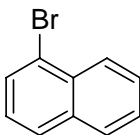
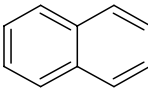
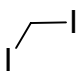
Liquid	Synthetic Route
 Bromobenzene	 + Br ₂ + Lewis Acid (Route 1)  + N-Bromosuccinimide + AIBN (Route 2)
 p-Xylene	 + CH ₃ Cl + Lewis Acid
 Cyclohexane	 + H ₂ (Route 1)  + Na ⁽⁰⁾ (Route 2)
 1-Bromonaphthalene	 + Br ₂ + Lewis Acid
 Diiodomethane	CH ₃ I + Na ₂ AsO ₃ + NaOH (Route 1) CH ₂ Cl ₂ + 2NaI (Route 2)

Table 1 Liquids which can be used to create repulsive van der Waals forces between surfaces and possible synthetic routes to generate these via a chemical reaction.

benzene (route 1), although this reaction requires high temperatures and pressures along with a catalyst, meaning that it is undesirable for use in the design. Another route is by a Wurtz reaction of dibromohexane which leads to ring formation via a radical reaction to produce cyclohexane (route 2). However, this is also unsuitable as the reaction does not require a catalyst to proceed, so to create a local high concentration of cyclohexane around itself the motor particle must be made of sodium.

Diiodomethane has been reported to create repulsive van der Waals forces between surfaces in the combination of materials silicon nitride – diiodomethane – silica and can be produced either by the reduction of iodoform with sodium arsenite (route 1) or by a Finkelstein reaction in which chlorine is exchanged for iodine (route 2). Again both routes are undesirable because they do not require a catalyst.

Of all the liquids highlighted bromobenzene seems the most attractive liquid to use in combination with the materials gold and silica because it is relatively easy to create by the bromination of benzene. There are a wide variety of Lewis acid catalysts which could be potentially immobilised to the motor particle surface allowing it to generate a local high concentration of bromobenzene around itself. The combination of materials used in the bromobenzene system is also particularly attractive as particles and surfaces made of silica and gold are easy to obtain from commercial sources or prepare in house. For example a glass microscope slide could be used for a silica surface or a gold coating could be added by thermal evaporation to give a gold surface. Silica particles are commercially widely available and a limited range of gold particles are also available. Whereas to use PTFE as a surface requires mechanical polishing to achieve a smooth surface.

For these reasons highlighted the combination of materials silica – bromobenzene – gold shall be investigated. A catalyst immobilised onto the motor particle surface will convert a mixture of benzene and bromine to bromobenzene changing van der Waals interactions from attractive to repulsive, potentially leading to propulsion of particles along surfaces.

3.3 Calculation of Dielectric Response Functions and Hamaker Constants

To investigate if van der Waals force between gold and silica is attractive when separated by the reactants benzene and bromine then repulsive when separated by bromobenzene, Lifshitz theory of van der Waals force was used to calculate Hamaker constants. First representative dielectric response functions were calculated using eq. 4 and optical data from a variety of sources outlined in Table 2. Due to the sampling frequencies being spaced 2.4×10^{14} rad/s apart most of the points lie in the UV region and

so it is the values of C_{UV} and ω_{UV} which are most important in constructing a representative dielectric response function. Where two sources of optical data have been gathered both have the same values of C_{UV} and, ω_{UV} , meaning that they give essentially the same dielectric response function as each other.

The calculated dielectric response functions of the two surface materials silica and gold are shown in Figure 1. Gold has a high dielectric response characteristic of a metal, whereas silica has a low dielectric response. As outlined earlier, to achieve repulsive van der Waals forces the dielectric response function of the surrounding liquid must be intermediate of these two dielectric responses and so lie in the region marked out with hashing in Figure 1.

Substance	C_{IR}	ω_{IR} (10^{15} rad/s)	C_{UV}	ω_{UV} (10^{16} rad/s)	Reference
Gold	3.980	5.880	1.873	3.570	5
	1.750	1.270	1.873	3.570	7
Silica	0.829	0.087	1.098	2.030	2
Bromobenzene	2.967	0.547	1.335	1.290	7
Benzene	0.819	0.554	0.501	0.013	13
	0.067	0.554	0.501	0.013	
Bromine	na	na	na	Na	

Table 2 Dielectric parameters of materials used in this study

The dielectric response function of benzene was also calculated and is shown in Figure 2 to lie outside the dielectric responses of the two surfaces, and so should lead to attractive van der Waals forces. No data could be found for bromine as it is not amenable to this kind of analysis due to its strong absorptions in the visible light spectrum. It is expected that the dielectric response function will not lie in the repulsive region, as liquids with this dielectric response are rare. Therefore dispersing gold particles in mixtures of benzene and bromine should result in attractive van der Waals forces between the particle and a silica surface.

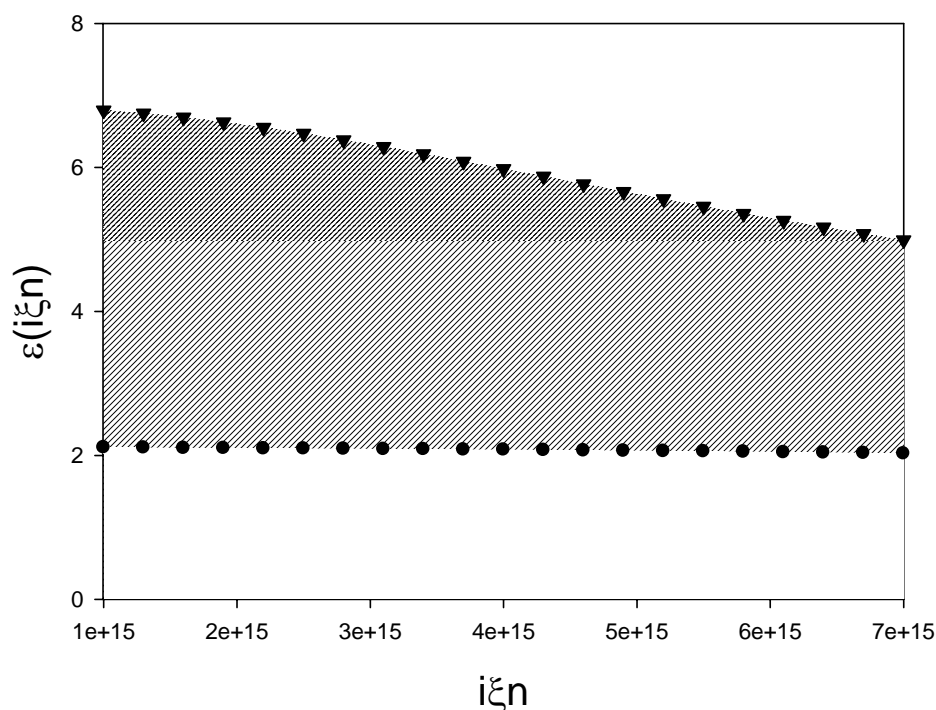


Figure 1 Dielectric response function of gold (triangles) and silica (circles). The hashed area shows values of the dielectric response function which are intermediate of gold and silica in which repulsive van der Waals forces occur.

The dielectric response of bromobenzene was calculated and is also shown in Figure 2. Unlike most liquids, it is unusual in that it lies intermediate between that of gold and silica in the region highlighted by hashing and should therefore lead to repulsive van der Waals forces.

Data was also not available for the by-product of the reaction hydrogen bromide, and so its dielectric function was also not calculated. It is expected that the concentration of hydrogen bromide will be low, as it has a low solubility in the liquid and therefore most of the hydrogen bromide will form bubbles and not be part of the media separating a silica and gold surface. Due to this low concentration van der Waals forces will be dominated by the interactions of bromobenzene.

As shown in Figure 2, a mixture of benzene and bromine should lead to an adhesion between a silica and gold surfaces which when converted to bromobenzene and hydrogen bromide by chemical reaction, should be converted to a repulsive force which forces the silica and gold surfaces apart.

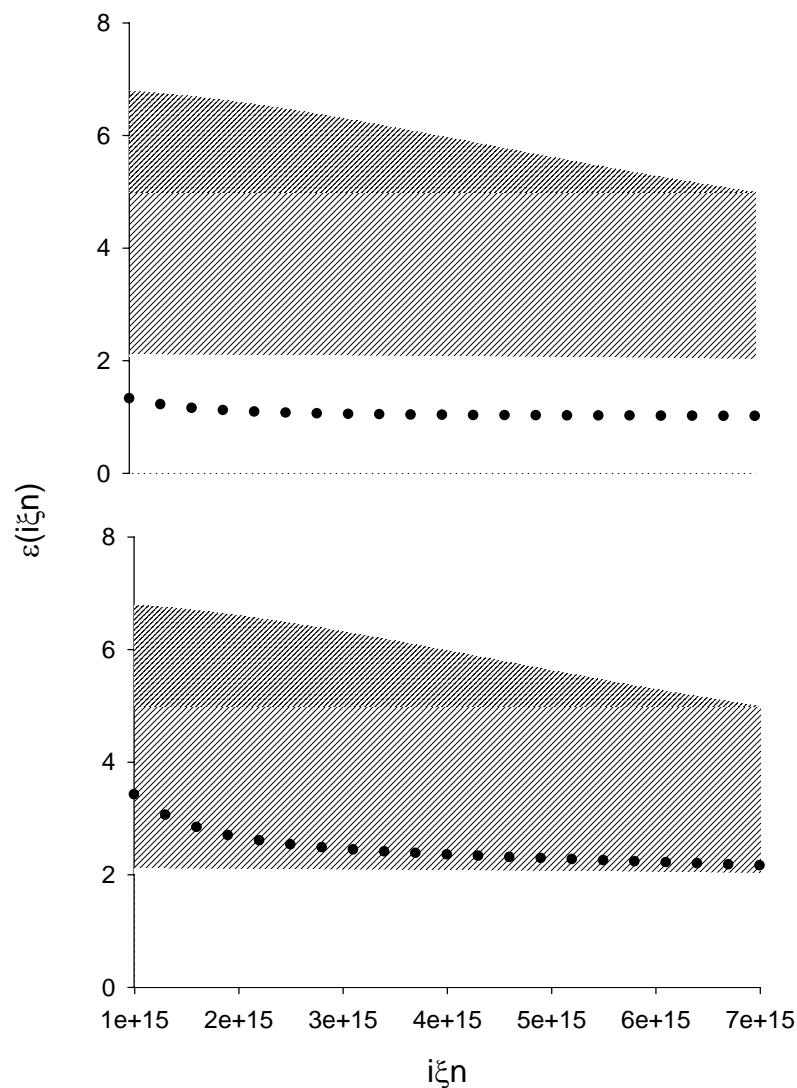


Figure 2 Dielectric response functions of reactants (Benzene only) and products (Bromobenzene). The hashed area shows the values of the dielectric response function which the liquid must be to contribute to repulsive van der Waals forces between silica and gold.

Following calculations of the relevant dielectric response functions, Hamaker constants for the interaction between a gold surface and a silica surface when surrounded by the reactants or products were calculated using eq. 3, with the summation indexes $n = 0-50$ and $m = 1-4$.

When surrounded by the reactants of the chemical reaction benzene and bromine, which is approximated as just benzene due to no information for bromine, a positive Hamaker constant of $+5.78 \times 10^{-20}$ J was found. This indicates that the gold particle should experience an attraction to the silica surface. Whereas a negative Hamaker constant of -0.57×10^{-20} J was found when the liquid converted to the product of the reaction,

bromobenzene. This calculated Hamaker constant is around 10x smaller than that found in the experiments of Munday et al⁸ but still indicates that repulsive van der Waals forces should be experienced and that gold particles should be repelled away from the silica surfaces.

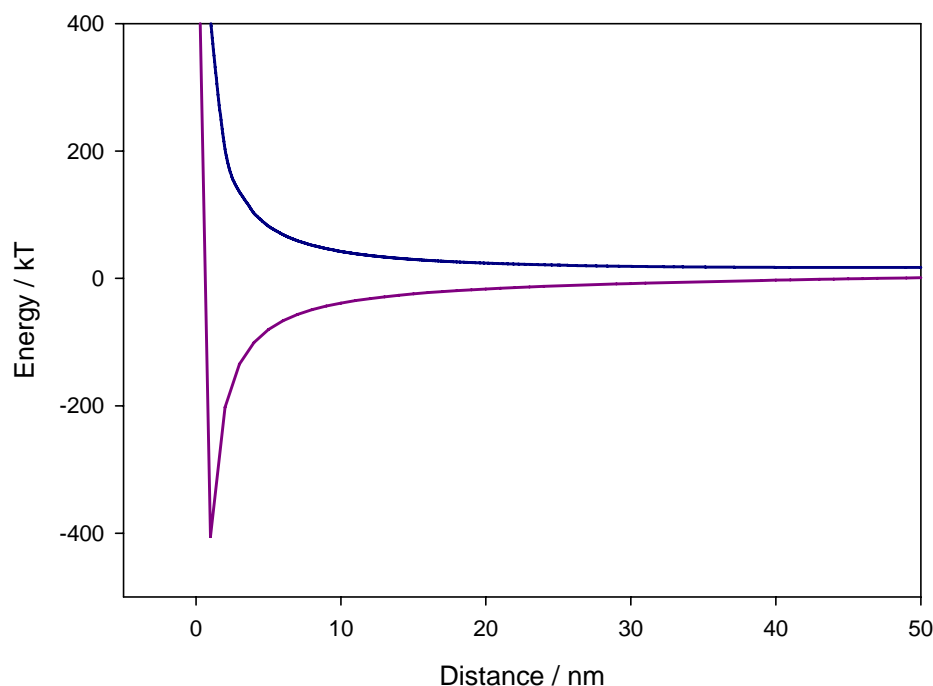


Figure 3 Energy-distance dependency of the interaction between gold and silica when dispersed in benzene (purple) and bromobenzene (blue).

Figure 3 shows the interaction profiles of a gold particle and a silica surface calculated using eq. 2. When the intervening liquid is benzene and bromine, the particle sediments down through the liquid due to its higher density and is then attracted to the surface. It comes to a rest when in contact with the surface. Whereas when the intervening liquid is the product of the reaction, bromobenzene, the particle sediments down as before and experiences a repulsion from the surface which increases as it gets nearer. Now the particle should come to rest at a point above the surface at a position where its gravitational force mg is equal to the repulsive force from the surface. This will be approximately 20nm above the surface.

The change in energy for a particle as the liquid surrounding it changes from benzene to bromobenzene is over 450 kT. Although the particle cannot make use of all of this energy to propel itself forward, as until the interaction becomes slightly repulsive the

particle will experience friction and be unable to slide along the surface. This energy is much smaller $\sim 50kT$, but should be sufficient energy to create a force which drives the particle across the surface.

3.4 Confirmation of Repulsive van der Waals forces

To confirm that van der Waals forces are repulsive for a gold particle and a silica surface when surrounded by bromobenzene and attractive when surrounded by benzene or a mixture of benzene and bromine, the behaviour of small gold particles ($4\mu\text{m}$) was investigated.

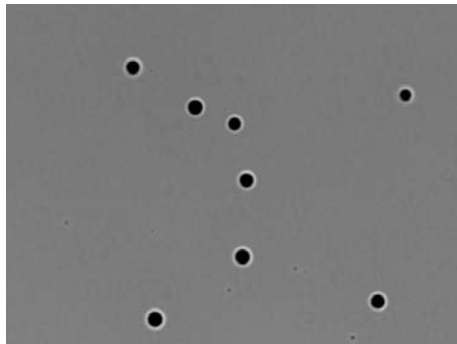


Figure 4 Trajectory of gold particles dispersed in benzene.

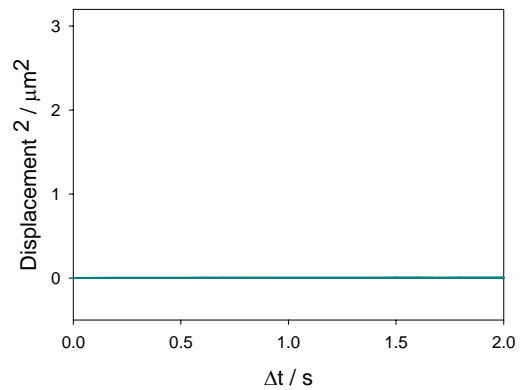


Figure 6 Mean squared displacement of gold particles dispersed in benzene.

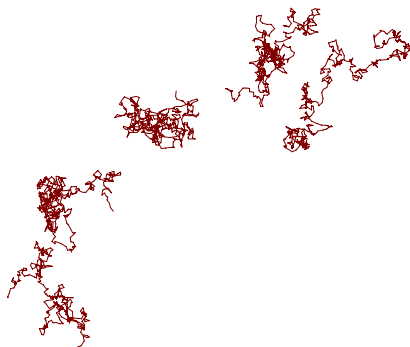


Figure 5 Trajectory of gold particles dispersed in bromobenzene.

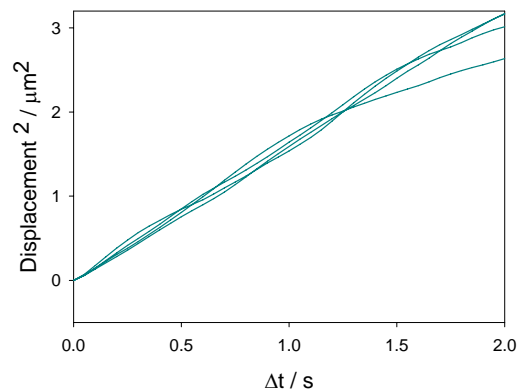


Figure 7 Mean squared displacement of gold particles dispersed in bromobenzene.

When gold particles were dispersed in benzene they quickly sedimented to the bottom surface of the observation chamber where they adhered to the surface and did not undergo Brownian motion. Figure 4 shows the trajectory of particles in benzene over 2 minutes and illustrates that they do not move during the observation period. Figure 5 shows the calculated mean-squared displacement (MSD) of the particles in figure 4. For a particle undergoing Brownian motion, the MSD should follow Einstein's equation for diffusion observed in two dimensions,

$$\text{MSD} = 4D\Delta t$$

where D is the diffusion coefficient and t is time.

Analysis of the slopes of lines in figure 4 gives the measured diffusion coefficient of the particles. In all cases the diffusion coefficient of particles were found to be zero to two decimal places - $D = 0.00\mu\text{m}^2 \text{ s}^{-1}$, showing that particles are adhered to the surface and are unable to move by Brownian motion due to the high friction encountered between the particle and the surface. If they were to undergo Brownian motion they should have a diffusion coefficient of $0.16\mu\text{m}^2 \text{ s}^{-1}$, as calculated by the Stokes-Einstein equation

$$D = \frac{kT}{6\pi\eta R}$$

Where kT is the thermal energy, η the viscosity of the liquid, and R the particle radius.

Therefore due to the low mobility of gold particles it is possible to confirm that they are in contact with the silica surface and due to this fact that van der Waals forces have either a positive Hamaker constant (attractive forces) or that van der Waals forces are repulsive but very small in magnitude allowing the mass of the particle to force it into contact with the silica surface.

In contrast to these results gold particles were repelled away from the surface enabling them to undergo Brownian motion when dispersed in bromobenzene. Figure 5 shows the trajectories of gold particles dispersed in bromobenzene showing that they were able to migrate from one area to another over time due to Brownian motion. Figure 7 shows the MSD of these particles which give a straight line plot showing that the observed motion follows Einstein's equation.

Analysis of the slopes of these lines gives an average diffusion coefficient of $0.26\mu\text{m}^2 \text{ s}^{-1}$ which is significantly faster than that predicted by the Stokes-Einstein equation of

$0.10\mu\text{m}^2\text{ s}^{-1}$. It is not understood why this diffusion is faster than expected but it is clear from this experiment that gold particles are not in contact with the silica surface and are able to migrate from one area to another. Therefore, they do not come into contact with the surface the particles must be repelled away from the surface by repulsive van der Waals forces, confirming that the Hamaker constant under these conditions is negative.

One particular point to note is the exceeding high level of surface cleanliness necessary to observe repulsive van der Waals forces. Glass microscope slides used as the silica substrates had to be clean using the extremely harsh conditions (Piranha solution) to achieve a situation in which gold particles could levitate above a the surface and undergo Brownian motion. Cleaning the substrates under milder conditions such as sonicating in surfactant solution resulted in a loss of colloidal stability and gold particles adhering to the silica surface when surrounded by bromobenzene.

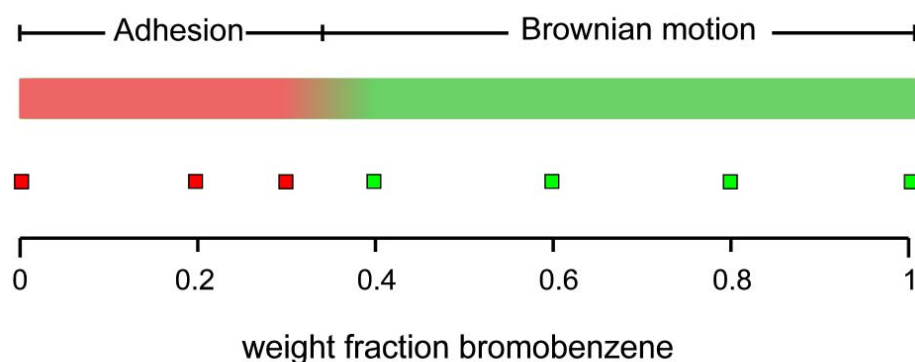


Figure 8 Behaviour of gold particles dispersed in different weight fractions of bromobenzene with the remainder of the fraction consisting of a mixture of 30wt % bromine and 70wt % benzene. Squares indicate individual results of particles which adhere to the silica surface (red) or do not adhere to the surface and are free to undergo Brownian motion (green).

A series of experiments were performed to investigate the concentration of bromobenzene required to convert van der Waals forces from attractive to repulsive, and thus lift a gold particle up off the silica surface enabling it to undergo Brownian motion. The motion of gold particles was tracked while they were dispersed in varying weight fractions of bromobenzene, with the remaining fraction of the liquid made up of 70wt % benzene and 30wt% bromine. This particular mixture of benzene and bromine was used instead of the stoichiometric amount of 49wt% benzene to 51wt% bromine due to the

optical opaqueness of bromine which didn't allow the particles to be visualised in high concentrations.

Figure 8 shows the behaviour of gold particles in these mixtures with red squares indicating that particles adhered to the surface and were unable to diffuse and green squares indicating that particles didn't adhere and were able to undergo Brownian motion. The transition from where particles experience attractive van der Waals forces to where particles experience repulsive van der Waals forces occurs at around 30 – 40 wt% bromobenzene. The transition is broad with some of the particles undergoing Brownian motion at 30 wt%, which by 40 wt% changes to the majority of particles. The exact amount of bromobenzene required to lift a particle above a surface probably depends on the individual particle as surface roughness vastly affects van der Waals forces.

From the experiments described above we know that gold particles adhere to silica when surrounded by benzene or benzene/bromine mixtures, whereas they do not adhere when surrounded by bromobenzene. So if a mixture of benzene and bromine is converted to bromobenzene, gold particles should release from the silica surface.

To investigate if the adhesion of gold particles to a silica surface is reversible as is predicted from the energy-distance profiles plotted above, gold particles were dispersed in benzene and introduced to an observation chamber with a clean silica plate as the bottom surface. The gold particles sedimented onto the silica plate within a fraction of a second where they adhered to it as predicted and did not undergo Brownian motion. Bromobenzene was then introduced via a micropipette to create a local high concentration of bromobenzene around selected particles; see Figure 9. It was possible to see bromobenzene being emitted from the micropipette as a 'haze' effect due to differences in the refractive indices of the two liquids, confirming that the concentration of bromobenzene was higher around the micropipette tip. Although it was not possible to know the exact concentration of bromobenzene. Under these conditions the gold particles remained adhered to the surface in the same position and did not release as expected. Of 16 gold particles in close proximity to the micropipette 16 remained in the same position.

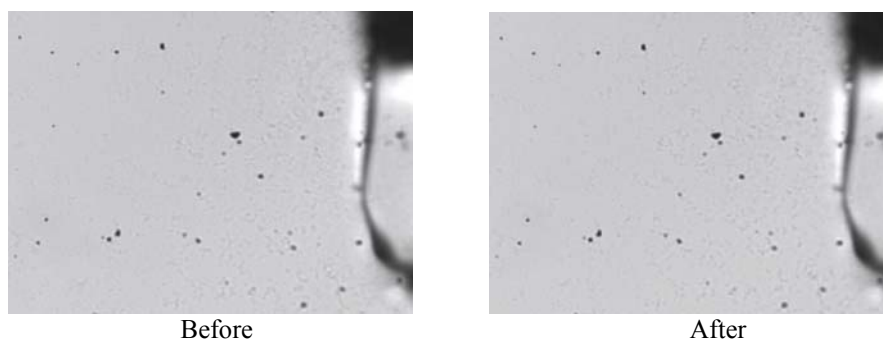
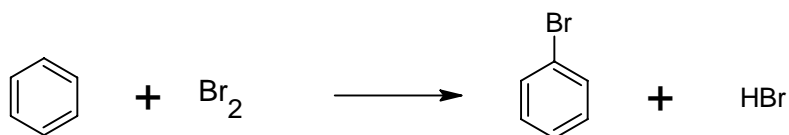


Figure 9 Gold particles dispersed in benzene before and after an injection of bromobenzene

This unexpected irreversibility of the gold particles adhering to silica could be due to surface contamination by greasy molecules which adsorb onto surfaces from the air and lead to bridging flocculation of the particles to the silica surface. From experiments done with gold particles dispersed in bromobenzene we know that the surface must be very clean for the particles to levitate above the silica surface and undergo Brownian motion where the particle and surface are separated by approximately 15nm. Perhaps the surfaces must be even cleaner for a particle to come into contact with silica and then be released.

This obtained result puts doubt into a design which works via repulsive van der Waals forces as the particle must adsorb and then release from the surface in a continuous manner to undergo propulsion.

3.5 Catalysts



To convert benzene to bromobenzene it was necessary to find a catalyst which could be immobilised onto a particle's surface to create a motor particle. This will allow the motor particle to act as a source of bromobenzene and convert van der Waals forces from attractive to repulsive as in the theoretical design.

Pyridine is commonly used for this purpose and is an excellent homogeneous catalyst. ¹H NMR analysis of the reaction showed that pyridine can convert benzene to bromobenzene to greater than 99% conversion (NMR signals from benzene were not visible) after 24 hours, as shown in Table 3. Following this initially promising result, an attempt was made to attach pyridine to a gold particle through a thiolate linkage to form a heterogeneous catalyst. Thus mercaptovinyl pyridine was investigated as a potential catalyst for the bromination of benzene but it was found that upon mixing Mercaptovinyl pyridine with the reactants that an orange solid formed. NMR analysis showed that the bromination reaction hadn't proceeded at all and no signal from the bromobenzene was observed. This orange solid was observed for both 2 and 4-mercaptovinyl pyridine indicating that the position of the ring substitution didn't affect the reaction products as is often observed in aromatic compounds. 4-mercaptopyridine was also allowed to self-assemble on gold particles to form a monolayer and these particles were also found to be an ineffective catalyst.

Poly(4-vinyl pyridine) was also investigated as a potential catalyst which could be tethered to a particle either through electrostatic assembly in aqueous dispersion or tethering to the surface through surface initiated polymerisation. This also proved to be an ineffective catalyst, again forming an orange solid with 0% conversion by NMR.

Pyridine is a highly conjugated molecule meaning that electron-donating or electron-withdrawing groups added to different position on the ring will greatly affect the electronic properties and therefore catalytic properties of the pyridine ring. To investigate these effects a variety of pyridine containing molecules was investigated.

4-Dimethylamino pyridine has an electron donating group in the para ring position, whereas isonicotinic acid has an electron withdrawing group in the para ring position. Both were found to be ineffective catalysts. Isonicotinic acid was not soluble in the reaction mixture meaning any catalysis has to be heterogeneous and NMR analysis gave 0% conversion. 4-dimethylamino pyridine formed an orange solid with the reactants and 0% conversion by NMR. Other molecules such as 2,2'-bipyridine and 4-vinyl pyridine also gave 0% conversion although presumably the vinyl group in 4-vinyl pyridine becomes brominated.

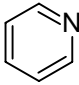
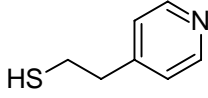
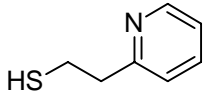
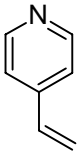
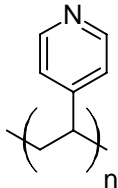
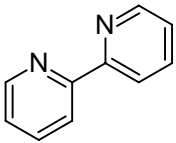
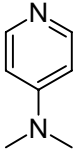
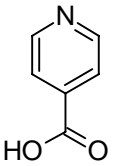
Molecule		Result
 Pyridine	$\xrightarrow{\text{Benzene, Br}_2}$	>99% conversion after 24 hours
 4-Mercaptovinyl pyridine	$\xrightarrow{\text{Benzene, Br}_2}$	0% conversion Orange solid formed
 2-Mercaptovinyl pyridine	$\xrightarrow{\text{Benzene, Br}_2}$	0% conversion Orange solid formed
 4-vinyl pyridine	$\xrightarrow{\text{Benzene, Br}_2}$	0% conversion Yellow solid formed
 Poly(4-vinyl pyridine)	$\xrightarrow{\text{Benzene, Br}_2}$	0% conversion Orange solid formed
 2,2'-Bipyridine	$\xrightarrow{\text{Benzene, Br}_2}$	0% conversion
 4-Dimethylamino pyridine	$\xrightarrow{\text{Benzene, Br}_2}$	0% conversion Orange solid formed
 Isonicotinic Acid	$\xrightarrow{\text{Benzene, Br}_2}$	0% conversion Isonicotinic acid not soluble in reaction mixture

Table 3 Molecules investigated as potential pyridine based catalysts for the bromination of benzene. Conversion was determined by ^1H NMR in chloroform.

In summary, none of the pyridine based catalyst were suitable for the proposed reaction. Many of them formed an orange or yellow solid which could be a complex of the pyridine containing molecule and bromine. If pyridine was then added to reaction mixtures which contained the orange solid, it disappeared to give a clear liquid which ^1H NMR analysis showed to be bromobenzene.

Control experiments showed that a catalyst is necessary for the reaction to proceed as a mixture of benzene and bromine gave 0% conversion after 24 hours, and that gold particles are an ineffective catalyst also giving 0% conversion after 24 hours.

Some metals are also catalysts for the bromination of benzene. Iron particles were found to be effective as a catalyst, converting benzene to bromobenzene with >99% conversion after 24 hours. Iron is not the actual catalyst but instead reacts with bromine at the particle surface to form the heterogeneous catalyst iron tribromide (Scheme 1). True to the nature of a catalyst, more reactants could be added to the iron particles and again >99% conversion observed.



Aluminium particles were also investigated and found to be effective catalysts giving >99% conversion after 24 hours. Although this catalyst is not heterogeneous, as aluminium reacts with bromine in a similar way to iron giving the catalyst aluminium tribromide, which is soluble in the reaction solution. It was thought that although this catalyst is soluble in the reaction solution that it could still be used, as an aluminium particle could act as a source of the catalyst and that a high concentration of catalyst would exist around aluminium particles. But further investigation showed that the catalyst is only sparingly soluble and when aluminium is used as a catalyst crystals form in the solution which presumably consist of the catalyst, aluminium tribromide, as shown in Figure 10.

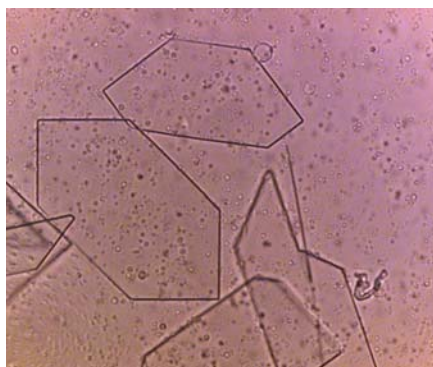


Figure 10 Crystals formed in the reaction solution when aluminium particles are used as a catalyst

Therefore it is desirable to use iron as the catalyst to convert a mixture of bromine and benzene to bromobenzene and change van der Waals forces from adhesive to repulsive, which should lead to propulsion. Perhaps gold particles could be coated with a thin layer of iron to create a catalytic ‘motor’ particle, but this is unnecessary. Iron is a metal like gold and so will have a similar high dielectric response function characteristic of a metal. Therefore iron particles should also experience repulsive van der Waals forces when surrounded by bromobenzene and attractive van der Waals forces when surrounded by a mixture of benzene and bromine. Repeating experiments of dispersing particles in benzene or bromobenzene showed this to be true – iron particles behaved identically to gold particles and can therefore be used directly as the motor particle.

3.6 Measuring the Rate of Bromination

The rate at which iron particles convert benzene to bromobenzene was monitored by removing aliquots from a reaction vessel at different times and determining the relative amounts of benzene, bromine and bromobenzene present by gas chromatography with UV detection. As shown in Figure 11 the rate of bromination is initially fast and is a vigorous reaction from which orange gas is evolved. After 30 minutes of reaction time, the rate of reaction has decreased to a slower rate which gives a roughly linear increase in bromobenzene with time.

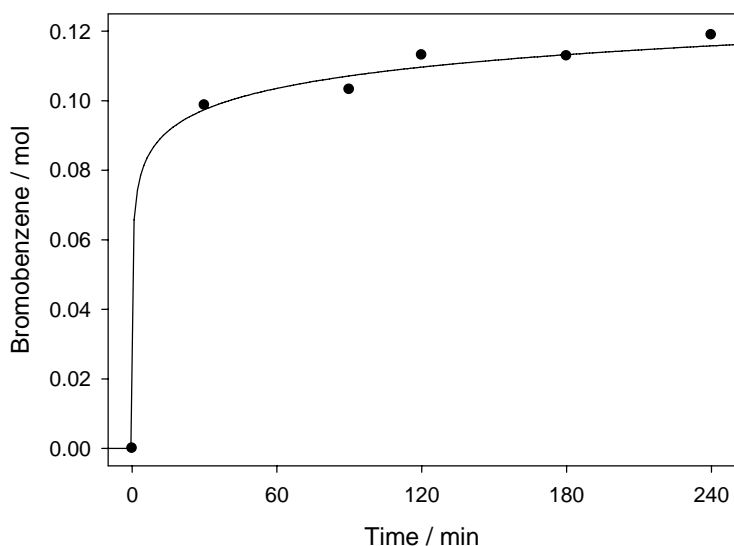


Figure 11 Bromination of benzene by iron particles at room temperature followed by GC-UV

A rough analysis of the reaction can be used to estimate the rate of reaction. At times greater than 30 min the rate of reaction can be estimated by a linear fit to the data points as $3.0 \times 10^{-18} \text{ mol s}^{-1}$ per particle, and at times shorter than 30 min an average rate can be measured by joining the data point at $t = 30 \text{ min}$ to the origin giving $1.0 \times 10^{-16} \text{ mol s}^{-1}$ per particle. Although at times close to $t = 0$ this will underestimate the rate of reaction and at times near 30 minutes over estimate the rate.

A fuller analysis reveals that the reaction should follow the rate equation

$$-\frac{\partial[\text{Benzene}]}{\partial t} = k[\text{Benzene}][\text{Bromine}][\text{Catalyst}] \quad \text{eq. 5}$$

which can be simplified if the concentration of the catalyst is assumed to be constant and is incorporated into the rate constant to give a new rate constant k' . Further simplification can be made by noticing that the initial concentrations of benzene and bromine are equal and that due to the 1:1 stoichiometry of the reaction that they remain equal at all times, giving:

$$-\frac{\partial[\text{Benzene}]}{\partial t} = k'[\text{Benzene}]^2 \quad \text{eq. 6}$$

from which the integrated pseudo-second order rate equation with respect to benzene can be found as:

$$\frac{1}{[\text{Benzene}]} = \frac{1}{[\text{Benzene}]_0} + k' t \quad \text{eq. 7}$$

Therefore a plot of $1/[\text{Benzene}]$ vs. time should give a linear plot with a gradient of k' in the units $1/\text{M s}$.

As shown in Figure 12 this gives a linear plot at times greater than 30 minutes but not at times 0-3 minutes. It is not known why the data doesn't fit the expected pseudo second order reaction kinetics at these short time scales but Bradfield¹⁴ also found that the bromination of benzene did not fit second order kinetics as expected but had a non-integer order.

From this analysis of the reaction kinetics it is possible to find the rate constant which when multiplied by the initial concentration of benzene squared and divided by the number of particles in the reaction gives the rate of reaction to be $1.9 \times 10^{-15} \text{ mol s}^{-1}$ per particle, although as stated earlier this analysis doesn't follow these kinetics at times shorter than 30 minutes.

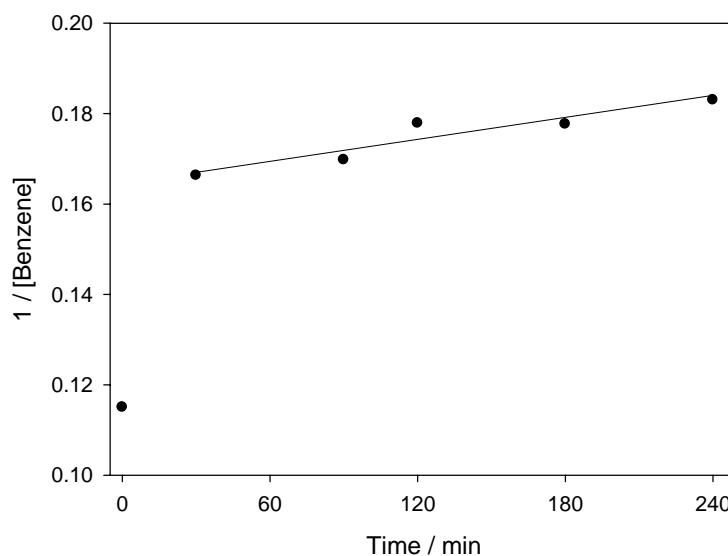


Figure 12 $1/[\text{Benzene}]$ vs. time for data shown in figure 1.

Due to the large error that comes from using the rough method and the experimental data not fitting the expected pseudo second order reaction kinetics, it is difficult to define the rate of reaction that has any meaning. In most of the experiments performed in this chapter iron particles are mixed with reactants and then observed in the first 30 minutes after this time, meaning that the rough analysis at long times will give a rate of reaction which is slower than the actual rate. Rough analysis of the first 30 minutes is probably the most useful because it gives an average rate over the time in which particles would be observed in experiments. Analysis of the rate of reaction by the integrated pseudo second order rate equation gives meaningless results as the kinetics do not fit the results during the first 30 minutes when a particle would be observed.

As to referring to a literature reference, most research that is done on the rate of bromination of organic molecules is done in a solvent such as chloroform rather than in bulk (no solvent). Normally a large excess of either bromine or benzene is added so that the concentration of this reagent remains constant, then the reaction follows so called 'forced' first order kinetics with respect to the other reagent. For these reasons literature sources are of no use here in predicting the rate of bromination of the iron particles studied.

3.7 Rate of Reaction Necessary to Create Repulsive van der Waals Forces

For an iron particle to be released from the silica surface it will need to surround itself with a concentration of bromobenzene greater than 35wt % by converting benzene and bromine to bromobenzene. The concentration of bromobenzene around an iron particle at distance r from the surface at any time t should follow the equation^{15,16}:

$$\text{Conc}_{(r,t)} = \frac{\text{Rate}}{4\pi Dr} \operatorname{erfc} \frac{r}{\sqrt{4Dt}} \quad \text{eq. 8}$$

Where concentration is measured in mol m⁻³, Rate is the rate of reaction (mol s⁻¹) and D is diffusion coefficient (m² s⁻¹) of the released species. erfc is the complimentary error function.

After a sufficient amount of time the concentration around the iron particle should reach a steady state, as the amount of bromobenzene released by the particle is equal to the amount removed from the vicinity of the particle by diffusion and should obey the equation;

$$\text{Conc}_{(r)} = \frac{\text{Rate}}{4\pi Dr} \quad \text{eq. 9}$$

as t becomes infinitely large $r/\sqrt{4Dt} = 0$ and $\operatorname{erfc}(0) = 1$. The concentration of bromobenzene changes by less than 1% when $\operatorname{erfc} r/\sqrt{4Dt} = 0.99$, or when $r/\sqrt{4Dt} = 0.01$. This occurs in less than a second at distances up to $r = 500\text{nm}$. Therefore at all times observed by video microscopy the concentration of bromobenzene around an iron particle should follow eq. 9 and be highest at the surface and decrease at a rate proportional to $1/r$ to 0 some distance away from the particle.

Figure 13 shows the concentration of bromobenzene around an iron particle calculated from the rates measured by experiment. The diffusion coefficient of bromobenzene in the reactant mixture has been estimated from the molecules size, using the Stokes-Einstein equation and the viscosity of benzene. The concentration is highest around the particle for the highest rate of reaction estimated using pseudo second order kinetics and lowest for the slowest rate of reaction estimated using a linear fit of GC-UV data at times greater than 30 minutes. In all cases the concentration of bromobenzene is below the critical

35wt % ($3,333 \text{ mol m}^{-3}$) necessary to release particles from the surface even at distances away from the surface as small as 1nm.

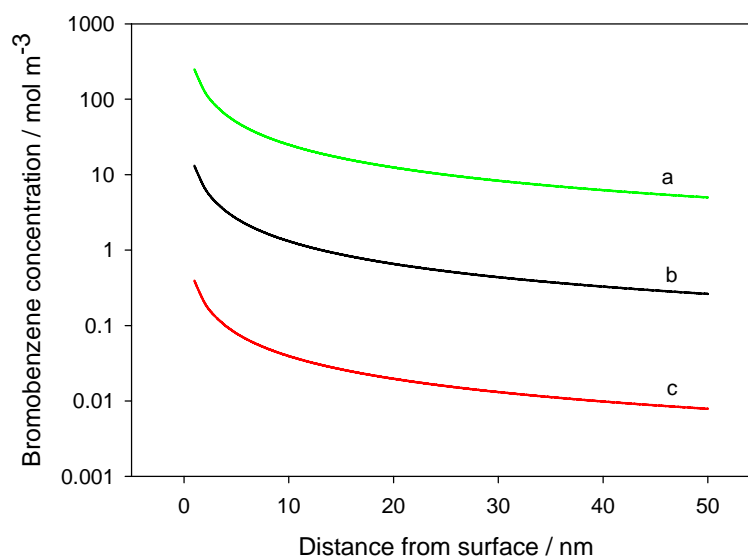


Figure 13 Concentration of bromobenzene vs. distance from an iron particles surface at steady state with rates of release measured from GC-UV a – fitting data with 2nd order kinetics, b – rate estimated over the first 30 min, c – rate estimated at times greater than 30 min.

It is not known what distance away from the surface that the bromobenzene concentration must exceed 35wt % for the particle to be repelled but it is known that van der Waals forces are short ranged and occur primarily in the first 30nm, therefore it can be estimated that if the concentration of bromobenzene at 30nm exceeded 35wt %, repulsive van der Waals forces would be observed. Entering the relevant numbers into eq. 9 gives a rate of reaction at which the iron particle would surround itself with bromobenzene and undergo Brownian motion. This number is $7.6 \times 10^{-13} \text{ mol s}^{-1}$ which is 400x faster than the rate estimated by 2nd order kinetics and 7,600x faster than the average rate over the first 30 minutes.

To act as a motor particle in the theoretical design, iron particles should release bromobenzene to create an adhesion gradient which causes the target particle positioned $1.5\mu\text{m}$ away to migrate. For this target particle to migrate the concentration of bromobenzene around it must exceed 35wt %. Again the rate of reaction necessary to achieve this can be calculated from eq. 9, giving a rate which is 381,000x faster than the average rate measured over the first 30 minutes.

As iron particles cannot migrate across a surface until they are repelled above the surface, they cannot migrate until they have converted reactants to 35wt % bromobenzene and in effect any energy used converting reactants to bromobenzene up to this point is wasted as particles cannot move. Therefore just less than 35wt % bromobenzene can be added to the liquid mixture to reduce the amount of bromobenzene that a particle has to produce to surround itself with a sufficiently high concentration to release from the surface. Although adding bromobenzene to the liquid mixture doesn't lower the rate of release necessary significantly. For example adding 30wt % bromobenzene reduces the increase in concentration necessary around the particle by a significant amount from $3,333 \text{ mol m}^{-3}$ to 476 mol m^{-3} but the rate of release necessary only reduces from $7.6 \times 10^{-13} \text{ mol s}^{-1}$ to $1.1 \times 10^{-13} \text{ mol s}^{-1}$, still 57x faster than the fastest rate estimated. Further bromobenzene cannot be added to reduce the rate as the transition between attractive and repulsive van der Waals forces is broad ranging from 30-40wt %.

It should also be noted that the rate of reaction on particles will be slower than that measured because while particles are observed under the microscope they are not stirred, meaning that the rate is limited by the diffusion of reactants to the catalytic surface. The concentration of bromobenzene will also be lower around the particle than predicted because the rate of reaction does not equal the rate of release. As reactants are converted to products the concentration of reactants around the particle falls, decreasing the rate of reaction. Due to these reasons the calculated concentration of bromobenzene around an iron particle should be a maximum which in practice will not be achieved.

Increasing the viscosity of the liquid medium may help iron particles to surround themselves with the necessary concentration of bromobenzene by slowing the rate at which bromobenzene can diffuse away from the motor particle. Viscosity of liquids is normally increased by adding a substance such as fructose or a macromolecule such as poly(ethylene oxide), which would change the dielectric response function of the liquid significantly and alter van der Waals forces. As well as slowing that rate at which the product diffuses away from the motor particle, it will also slow the rate at which reactants diffuse toward the particle, slowing the rate of reaction and therefore the rate of release. For these reasons, increasing the viscosity of the liquid medium was not investigated.

Surface roughness will also play a significant role in van der Waals forces. Increasing surface roughness decreases the strength of the force because the interaction volume is effectively reduced. This means that a rough particle will require a higher concentration of bromobenzene surrounding it to release from the surface and will experience less of an attraction to the surface when surrounded by reactant mixture, therefore the change in energy experience by the particle upon converting reactants to bromobenzene is reduced.

3.8 Is Propulsion of Catalytic Particles Observed?

When iron particles are dispersed in a mixture of benzene and bromine, they sediment onto the bottom silica surface of the observation chamber where they adhere to the surface and do not undergo Brownian motion as shown in Figure 14. Although a few particles seem to migrate in one particular direction a few micrometres over the course of the observation (500 sec), analysis of their motion gives diffusion coefficients of $0.00\mu\text{m}^2\text{ s}^{-1}$ for all particles shown.

This is unexpected as the iron particles should convert benzene and bromine to bromobenzene creating a local high concentration of bromobenzene around themselves which change van der Waals forces from attractive to repulsive allowing them to undergo Brownian motion. It may be that iron particles require a certain amount of time to convert a sufficient amount of reactants to products and to surround themselves with bromobenzene but even after 10 minutes the iron particles remain in the same position as they initially sedimented onto the surface.

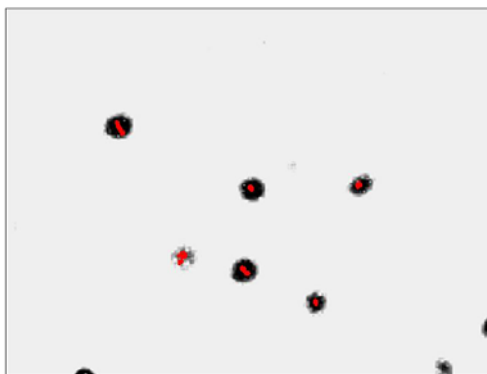


Figure 14 Trajectories of iron particles (red dots) dispersed in 70wt % benzene, 30wt % bromine over 500 sec.

The observed migration of a few micrometres could be due to convection currents or sedimentation along the surface which is not precisely orientated horizontally. The particles should not propel themselves forward, as without the second target particle in close proximity the distribution of bromobenzene and therefore the adhesion gradient is symmetrical. Migration also seems to be in a straight line which would not be expected if it were propulsion due to the particle rotating by Brownian motion as it moves.

When using a dilute dispersion of iron particles the conversion of benzene to bromobenzene remains low and particles must create a local high concentration of bromobenzene around themselves to be able to undergo Brownian motion, but if a concentrated dispersion of iron particles is used then the bulk of the liquid surrounding iron particles can be converted from benzene to bromobenzene and it is not necessary to have a local high concentration. From experiments described above it is known that particles are repelled above the surface in concentrations higher than ~35wt % bromobenzene, so over the course of the bromination reaction a concentrated dispersion of iron particles should become repelled from the surface.

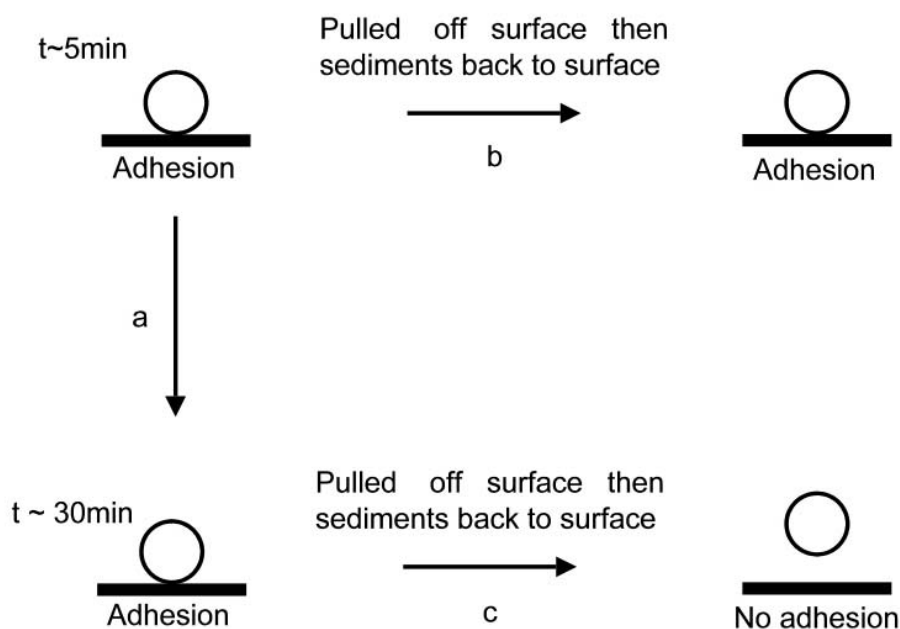


Figure 15 Illustration of the behaviour of a concentrated dispersion of iron particles in initially a mixture of benzene and bromine

Figure 15 illustrates the observed behaviour under these conditions. When iron particles are initially mixed with reactants conversion is low leading to attractive van der Waals forces and particles which adhere to the silica substrate. Following the arrow labelled *a* the bulk of the liquid is converted to a high fraction bromobenzene over 30 minutes meaning that particles should experience repulsive van der Waals forces and Brownian motion be observed but like in the dilute case described above, particles do not spontaneously release from the surface and remain in the same position.

This experiment shows that the iron particles are converting benzene and bromine to bromobenzene, as we have shown by NMR analysis, but that they are not creating a local high concentration of bromobenzene around themselves, otherwise iron particles would be colloidally stable towards surface aggregation when dispersed in reactants.

Interesting results are obtained if the particles are forcibly removed from the silica surface by inverting the observation chamber upside down and tapping on the surface, then allowing particles to sediment from solution back onto the silica substrate.

If this procedure is carried out early in the course of the reaction ~ 5 min, when the conversion is low (arrow labelled *b*), particles simply sediment back onto the surface and readsorb. Whereas if this is done after ~ 30 min, when a high fraction of the liquid has been converted to bromobenzene (arrow labelled *c*), a significant fraction of the particles no longer adhere to the surface and undergo Brownian motion.

These experiments show not only that iron particles are not surrounding themselves with bromobenzene but that adhesion to the silica surface may not be as reversible as expected from Lifshitz theory. When the particles and surface are forced apart the particles do not re-adhere when a sufficient amount of bromobenzene has been produced but they do not spontaneously break free of the surface.

Another point to note is the necessity of a target particle to be in close proximity with the motor particle or in this incarnation of the design an iron particle must come into close proximity with a gold particle for propulsion to take place. This is difficult to achieve in practice due to the low probability of an iron particle sedimenting onto the silica surface in close proximity to a gold particle but also without any other particles being in the same area to interfere in the distribution of bromobenzene created. Using concentrated dispersions of a mixture of iron and gold particles lead to common instances of two particles being close together but always with other particles also nearby. Using more dilute dispersions resulted in no instances of two particles being in close proximity to each other.

For this reason it was not attempted to assemble a target particle next to a motor particle and any motion observed or not-observed studied. To create this arrangement of particles it would probably be necessary to invoke the use of a micromanipulation technique such as optical tweezers¹⁷ rather than to rely on two particles coming into close proximity by chance.

3.9 Gold / Iron Janus Particles

To try to circumvent the problems encountered above gold / iron Janus particles were created, which avoids the problem of finding an iron and a gold particle in close proximity to each other. To try to overcome the problem of iron particles not surrounding themselves with bromobenzene making them able to undergo Brownian motion, a mixture of 40wt% bromobenzene and 60% reactants was used. Under these conditions janus particles were able to undergo Brownian motion whilst converting reactants to bromobenzene changing their van der Waals interactions from repulsive to more repulsive.

Observation of the produced Janus particles showed a Brownian like motion of the particles which needs to be analysed mathematically to ascertain if the particles are simply undergoing Brownian motion or a combination of Brownian motion and propulsion. If the particles are undergoing Brownian motion their mean-squared-displacement should give a straight line obeying Einstein's equation for diffusion observed in two dimensions:

$$\langle \Delta L^2 \rangle = 4Dt \quad \text{eq. 10}$$

Where D is the diffusion coefficient and t time. Whereas if the particle is undergoing a combination of Brownian motion and propulsion the mean-squared-displacement should follow the equation¹⁸:

$$\langle \Delta L^2 \rangle = 4Dt + \frac{v^2 \tau_r}{2} \left[\frac{2t}{\tau_r} + e^{-2t/\tau_r} - 1 \right] \quad \text{eq. 11}$$

where v is the propulsion velocity and τ_r is the inverse of the rotational diffusion coefficient. Which reduces at short time scales to:

$$\langle \Delta L^2 \rangle = 4Dt + v^2 t^2 \quad \text{eq. 12}$$

and at long time-scales:

$$\langle \Delta L^2 \rangle = (4D + v^2 \tau_r) t \quad \text{eq. 13}$$

Figure 16 shows the mean-squared-displacement of some Janus particles under the conditions described above. This shows that most of the particles have approximately linear plots confirming that they are simply undergoing Brownian motion. Measurement of the slope gives the diffusion coefficient of $0.27 \mu\text{m}^2 \text{s}^{-1}$, in close agreement to that calculated by the Stokes-Einstein equation of $0.22 \mu\text{m}^2 \text{s}^{-1}$. Other particles have curved plots suggesting that they are being propelled forward, which when fitted with eq. 12 gives velocities of up to $0.7 \mu\text{m} \text{s}^{-1}$. Although analysis of the particle trajectory suggests that this velocity is not due to the particle propelling itself forward but convection within the cell, as the particles motion is uni-directional instead of the expected propulsion in changing directions as the particle is rotated by rotational Brownian motion.

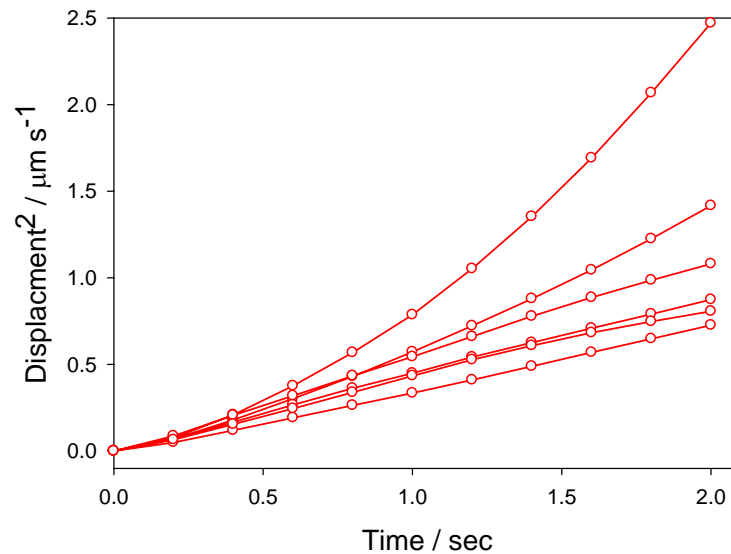


Figure 16 Mean-squared-displacement of iron/gold Janus particles in a mixture of benzene and bromine.

3.10 Summary of using Repulsive van der Waals Forces to Create Propulsion

From analysis of van der Waals forces through Lifshitz theory, it has been found that a gold particle should experience attractive van der Waals forces to a silica surface when surrounded by a mixture of benzene and bromine. Then when this mixture of reactants is converted to bromobenzene by a chemical reaction Lifshitz theory predicts that the particle will be repelled from the surface and experience repulsive van der Waals forces.

This prediction was confirmed to be correct by observation of gold particles dispersed in mixtures of benzene / bromine or bromobenzene. When dispersed in benzene / bromine mixtures, particles adhered to the surface and did not undergo Brownian motion, whereas when dispersed in bromobenzene the particles were repelled from the surface and could undergo Brownian motion with the expected diffusion coefficient.

Iron particles were found to be effective catalysts for the bromination of benzene and observation of these particles dispersed in bromobenzene confirmed that they behave like gold and experience repulsive van der Waals forces, so can be used as the motor particle in the theoretical design. Following further investigation of iron particles, it was found that they are colloidally unstable in dispersions of mixtures of benzene and bromine and adhere to the silica surface. It was suggested that this adhesion was due to the particles producing bromobenzene at a rate which is insufficiently fast enough to surround themselves with the concentration of bromobenzene necessary to generate repulsive van der Waals forces.

Experiments using mixtures of gold and iron particles did not find any propulsion of pairs of particles as expected from the theoretical design. It was also found that occurrences of a gold particle being in close proximity to an iron particle without any other particles nearby was extremely rare.

To circumvent the problems of rate of release and finding a motor and target particle next to each other, gold-iron janus particles were created. Investigation of these particles dispersed in 40wt % bromobenzene and 60wt % reactants allowed particles to undergo Brownian motion while altering their interaction with the surface by converting reactants to bromobenzene but showed that particles only underwent Brownian motion and did not propel themselves forwards.

Therefore it is suggested that a design based upon repulsive van der Waals forces will not lead to propulsion of particles due to the high rate at which bromobenzene must be generated by the motor particle to surround itself with bromobenzene. Substituting a chemical species such as bromobenzene for the surface altering nanoparticles in the

theoretical design results in an increase in diffusion coefficient of ~ 100 fold, meaning that a chemical species must be released from the motor particle faster than nanoparticles.

3.11 Experimental Details

Materials. Microscope slides were purchased from Menzel glass. Gold particles (3-5 μm) were purchased from Alfa Aeser, gold particles (1 μm) from Sigma-Aldrich, iron particles (2-3 μm) were purchased from PolySciences inc., aluminium powder from Alfa Aeser. CoverWells (0.1mm) from Grace-Bio labs. All chemicals were purchased from Sigma-Aldrich and used as received.

Cleaning Glass Microscope Slides. Microscope slide were rinsed with deionised water to remove dust from the packaging material and then submerged in Piranha solution (1:3 30% hydrogen peroxide to 10M sulphuric acid) for 14 hours. They were then rinsed with copious amounts of ultrapure water followed by ethanol, then they were dried in a warm oven (70 °C) for 2 hours. Microscope slides were used immediately after being cleaned.

Dispersion of Metal Particles in Solvents, Construction of Observation Chambers and Observation of Particle Motion. A small amount of the metal powder was transferred to a 1ml glass vial using a glass pipette as a spatula. In this way magnetisation of the ferromagnetic iron particles was avoided. A small amount of the chosen solvent was then added sealed with a PTFE cap and then sonicated for 5 minutes. A CoverWell was adhered to a cleaned glass microscope slide and the resulting chamber filled with the particle dispersion so that the level of fluid was above the gasket. A second slide was then used to seal the chamber top and was applied at an angle so that the liquid in the chamber made contact with the slide first at one side quickly followed by the other side. This procedure sealed the chamber excluding any air bubbles. Particles in the chambers were then observed under a microscope (Nikon Eclipse ME2000) at 50x magnification using diascope illumination. Movies of the motion were recorded using a Pixelink PL-A742 machine vision camera. The motions of particles were tracked after movie capture using a custom built LabView script which determined the position of particles in each frame of the movie.

Preparation of Iron / Gold Janus Particles. Iron particles were dispersed in ethanol and sonicated to aid dissolution. A monolayer of iron particles was then assembled on a clean glass microscope slide from this dispersion by spin-coating at 5000 rpm for 60 seconds. Slides with a monolayer of iron particles were then placed in a thermal evaporator and 20 nm of gold evaporated at 0.03 nm s^{-1} onto them to form janus particles. The particles were then removed from the glass slide by lightly scrapping across the surface with piece of wetted lens tissue which was then washed into a glass vial using benzene, resulting in the janus particles being transferred from the slide to the vial.

Measurement of Rate of Bromination. 24g Benzene and 25g Bromine were added to a two-arm round bottom flask fitted with reflux condenser and magnetic stirrer bar. A bung was placed in the top of the reflux condenser to stop the escape of hydrogen bromide. 37mg of iron powder was dispersed in 1g of benzene and added to the mixture via side arm at $t = 0$. A vigorous reaction was observed over the first few minutes which then decreased to a moderate rate. Aliquots of the reaction mixture were taken at different time intervals, immediately diluted with ethanol and then analysed by gas chromatography – UV detection immediately. With the particular GC-UV set up ethanol had an elution time of 1.1 minutes, benzene 2.1 minutes, Bromobenzene 12.0 minutes and isomers of dibromobenzene 15 -16 minutes. The amount of benzene compared to bromobenzene was then measured from the chromatogram and using a calibration graph to converted into the real amounts.

Reversible Adhesion Studies using Micropipettes. Micropipettes were created by heating glass capillary tubes in a flame until they glowed red then quickly stretching the tube, creating a much smaller tube. Breaking the smaller tube in two lead to micropipettes with diameters around 50 μ m. An micropipette was then attached to a manual pneumatic syringe pump capable of dispersing small amounts of liquid and was filled with bromobenzene. Iron particles were dispersed in a mixture of 70wt % benzene and 30wt % bromine and introduced to an observation chamber containing a micropipette tip and sealed with allowing a small air bubble in the observation chamber so that extra liquid could be injected. After a certain period of time an amount of bromobenzene was injected into the cell while particles were observed by video microscopy.

References

- (1) Hough, D. B.; White, L. R. *Advances in Colloid and Interface Science* **1980**, *14*, 3-41.
- (2) Bergstrom, L. *Advances in Colloid and Interface Science* **1997**, *70*, 125-169.
- (3) Dzyaloshinskii, I. E.; Lifshitz, E. M.; Pitaevskii, L. P. *Adv. Phys.* **1961**, *10*, 165-209.
- (4) Meurk, A.; Luckham, P. F.; Bergstrom, L. *Langmuir* **1997**, *13*, 3896-3899.
- (5) Lee, S.; Sigmund, W. M. *J. Colloid Interface Sci.* **2001**, *243*, 365-369.
- (6) Lee, S. W.; Sigmund, W. M. *Colloids and Surfaces A-Physicochemical and Engineering Aspects* **2002**, *204*, 43-50.
- (7) Milling, A.; Mulvaney, P.; Larson, I. J. *Colloid Interface Sci.* **1996**, *180*, 460-465.
- (8) Munday, J. N.; Capasso, F.; Parsegian, V. A. *Nature* **2009**, *457*, 170-173.
- (9) Feiler, A. A.; Bergstrom, L.; Rutland, M. W. *Langmuir* **2008**, *24*, 2274-2276.
- (10) Cho, Y. K.; Wartena, R.; Tobias, S. M.; Chiang, Y. M. *Advanced Functional Materials* **2007**, *17*, 379-389.
- (11) Sernelius, B. E. *Physical Chemistry Chemical Physics* **2004**, *6*, 1363-68.
- (12) Kimura, K. *J. Phys. Chem.* **1994**, *98*, 11997-12002.
- (13) Fodand, P.; Askvik, K. M. *Colloids and Surfaces a-Physicochemical and Engineering Aspects* **2008**, *324*, 22-27.
- (14) Bradfield, A. E.; Jones, B. *Transactions of the Faraday Society* **1941**, *37*, 0726-0743.
- (15) Carslaw, H. S. J., J. C *Conduction of heat in solids*; 2nd ed.; Oxford, 1959.
- (16) Crank, J. *The Mathematics of Diffusion*; 2nd ed.; Oxford, 1975.
- (17) Ashkin, A.; Dziedzic, J. M.; Bjorkholm, J. E.; Chu, S. *Opt. Lett.* **1986**, *11*, 288-290.
- (18) Howse, J. R.; Jones, R. A. L.; Ryan, A. J.; Gough, T.; Vafabakhsh, R.; Golestanian, R. *Phys Rev Lett* **2007**, *99*, 048102.

4 Propulsion using Electrostatic Interactions

4.1 Introduction

When surrounded by a polar liquid most surfaces acquire a charge. When two surfaces of the same charge come into close proximity, they are repelled away from each. The repulsion is so strong that it can over-power the van der Waals force between the two surfaces. This repulsion is not caused by the Coulombic interactions of two electrical charges but from the changes which they induce in the properties of the liquid.

A surface can become charged by three mechanisms or a combination of the three. The first of which is due to the ionisation of functional groups attached to the surface when placed in water. Examples may include sulphonic acid groups, which dissociate in water to form a cationic proton and a surface bound sulphony anion, and primary amine groups, which become protonated to form surface bound cations. The second mechanism by which a surface can become charged is by preferential adsorption of an ion over the adsorption of ions of the opposite charge. This normally occurs for hydrophobic surfaces which preferentially adsorb hydroxide ions from aqueous solution over cations, leading to a negative surface charge. The third mechanism is through ion exchange, where ions of higher valency replace surface bound ions.

A surface that has become charged due to either of these mechanisms will attract ions of opposite charge (counterions) through a Coulombic attraction. This attraction is balanced by a repulsive entropic pressure which attempts to prevent the counterions migrating towards the surface and so becoming more concentrated in solution. The number of ions attracted to the surface will be the number required to cancel out the surface charge and to achieve charge neutrality. A small proportion of these counterions will be bound to the surface in an enthalpically favourable but entropically unfavourable position, forming the *Stern Layer*. The rest of these counterions will be present in close

proximity to the surface but not adsorbed, forming a *diffuse layer*. This combination of *Stern layer* and *diffuse layer* are known as a double layer and is shown in Figure 1.

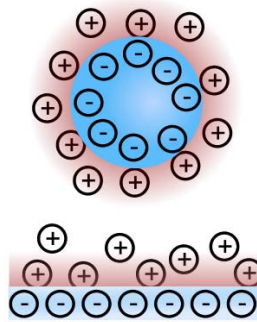


Figure 1 Schematic depiction of the double layer formed around a negatively charge particle and surface. The diffuse layer of counterions is shown in red.

The charged surface creates an electrical potential ψ , in the nearby solution which dictates the concentration of counterions present by a Boltzmann distribution:

$$\rho = \rho_0 e^{-ze\psi/kT}$$

eq. 1

Where z is the valency of the ion, e the electronic charge, ρ the concentration of counterion at position x away from the surface and ρ_0 the concentration of counterion in bulk solution.

These counterions present also change the electrical potential at each position away from the surface in the solution, according to the Poisson equation:

$$\frac{\partial^2 \psi}{\partial x^2} = \frac{-ze\rho}{\epsilon\epsilon_0}$$

eq. 2

Where ϵ is the relative permittivity of the solution.

Substituting the Boltzmann distribution into the Poisson equation and rearranging gives the Poisson-Boltzmann equation:

$$\frac{\partial^2 \psi}{\partial x^2} = - \left(\frac{ze\rho_0}{\epsilon\epsilon_0} \right) e^{-ze\rho/kT}$$

eq. 3

Solving this second-order differential equation allows the electrical potential, electrical field and most importantly the concentration of counterions to be found.

Solving this second-order differential equation is not trivial and requires two boundary conditions. The mathematics of solving this equation will not be discussed further here, instead the reader is directed to the appropriate literature sources. Approaches to solving this equation using analytical expressions have been used by Zypman¹ and also Hogg, Healy and Fuersten², whereas Bhattacharjee and Elimelech³ have used a surface element integration numerical method.

Repulsive forces are experienced when two surfaces of the same charge are brought into close proximity. This is caused by the confinement of the two diffuse layers into a single volume. In this way the concentration of counterions is increased leading to an entropic or osmotic pressure between the two surfaces which force them apart. From a solution of the Poisson-Boltzmann equation the concentration of ions can be calculated at any point away from the two surfaces, which following further calculations, which won't be discussed here, can give the repulsive pressure and so the force acting between the two surfaces.

An important consideration is, as the surfaces approach each other, do the counterions readsorb back onto the surfaces? If they do, the potential remains constant but the charge falls; conversely if the counterions do not readsorb, the charge remains constant but the potential does not. These two limiting cases are known as constant charge and constant potential limits. From experiments which measure the forces between surfaces, it is known that the actual repulsive force lies between these two limits. These differences are only of importance below separations of one Debye length (~15nm in water⁵).

In this chapter, electrostatic interactions will be explored as a potential interaction which can be changed through a chemical reaction to produce a gradient of interaction energy, which could lead to the propulsion of small particles as in the theoretical design. As the interaction is entirely repulsive, changes in interaction can only repel a particle away from a surface. To create a difference in particle energy these repulsive interactions will have to do work against an opposing force. It will be suggested that by using dense metal particles that this opposing force can be gravity.

We shall start with calculations of the forcing acting on a particle and surface.

4.2 Particle-Surface Interaction Calculations

The total interaction energy of a dense particle and a nearby surface is the sum of all the interactions occurring between them such as attractive van der Waals force, the repulsive electrostatic force and also the gravitational force:

$$\text{Interaction Energy} = V_A + V_R + mgh \quad \text{eq. 1}$$

where m is the mass of the particle; g gravitational acceleration; h height above the surface; V_R is the repulsive interactions caused by the overlapping double layers; V_A is the attraction between surfaces caused by van der Waals given by:

$$V_A = \frac{-A_{132}R}{6D} \quad \text{eq. 2}$$

where A_{132} is the Hamaker constant, R is the radius of the particle and D is the distance separating the particle and surface.

The repulsive interactions caused by the overlapping of two double layers can be calculated using the following equation, which has been modified from Hogg, Healy and Fuersten² to calculate the interaction between a sphere and a surface, rather than two spheres. This was done via the Derjaguin approximation, equating the original

term $\frac{R_1 R_2}{R_1 + R_2}$, where R_1 and R_2 are the radii of the two spheres, for $R_1 \gg R_2$, i.e. sphere 1

is a planar surface so has an infinitely large radii. The result of which simply gives R_2 . Substituting this back into the equation gives:

$$V_R = \frac{2\varepsilon R}{4} (\psi_1^2 + \psi_2^2) \left[\frac{2\psi_1\psi_2}{(\psi_1^2 + \psi_2^2)} \text{Ln} \left(\frac{1 + \exp(-\kappa D)}{1 - \exp(-\kappa D)} \right) + \text{Ln}(1 - \exp(-2\kappa D)) \right] \quad \text{eq. 3}$$

Where ε is the relative permittivity of the medium; R particle's radius; ψ the surface charges of surfaces 1 and 2; κ is the inverse Debye length (m^{-1}); D is the distance separating the surface and sphere.

Particles which are denser than the liquid in which they are dispersed will sediment down towards the bottom surface of the container. As they come closer to the bottom surface they will start to experience a repulsion due to the overlapping of the double layers on both surfaces, which increases approximately exponentially. The particle will come to rest at a position where the forces acting downwards - gravity and van der Waals force - are balanced by the repulsive electrostatic forces acting upwards. This position can be called the *equilibrium height*.

At the equilibrium height the particle may diffuse around, both from side to side and also up and down but will spend most of its time at approximately the point where the electrostatic forces are equal to the gravitational force. If the surface repulsion is increased the particle will be repelled further away from the surface to a new equilibrium position of greater height above the surface. Therefore by increasing surface repulsions the particle has been caused to gain gravitational potential energy.

If the particle is constructed of a material which has a density close to the liquid in which it is dispersed, its effective buoyant mass will only be small and raising the particle by increasing surface repulsions shall only increase its gravitational potential energy by a small amount. Conversely if the particle is very dense and so has a relatively large mass, raising the particle by increasing surface repulsions shall result in a larger change in energy.

It is useful to introduce a number called the *gravitational length*, which is the height through which the particle must be raised to result in a gain in gravitational potential energy of one thermal energy (kT). For a $4\mu\text{m}$ gold particle this is rather small at only 0.7nm , whereas for a polystyrene particle of the same size, it is significantly larger at 250nm . Highlighting the fact that to achieve a large change in energy by increasing surface repulsion experienced between a particle and surface, the particle should have the largest mass possible. This can be achieved by using relatively large particles made of dense materials.

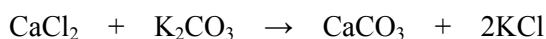
To change the surface repulsions experienced by a particle from a surface, examination of eq. 3 shows that several variables can be changed.

Changing the relative permittivity of the medium separating the particle and surface will alter the strength of surface repulsions and could be achieved by converting one liquid to another via a chemical reaction. For example an imaginary chemical reaction which converts methanol to water would change the relative permittivity from 30 to 78, more than doubling the repulsive forces experienced by a particle.

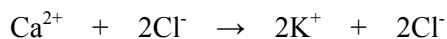
Changing the particles radius would change the experienced repulsive forces but is not an appealing strategy. Although particles could be created of a material which can

expand in response to a chemical stimulus such as a weak polyelectrolyte⁴, these materials are of low density, so increasing the repulsion raises them away from the surface but does not significantly alter the particles energy as mgh is small.

Altering the inverse Debye length does not change the strength of electrostatic repulsions but instead alters the rate at which they decay away from a surface by screening the interactions. So by changing the inverse Debye length, the magnitude of the repulsions at the equilibrium height can be altered, causing the particle to move to a new equilibrium height. The inverse Debye length can be altered by the addition of salts to the liquid separating the particle and surface, although this would decrease surface repulsions. To increase the surface repulsions, dissolved ions would have to be removed from solution which is synthetically challenging. For example, potassium carbonate could be added initially to the intervening liquid to screen electrostatic interactions causing a small repulsive force at the equilibrium height. Then calcium chloride could be added, forming insoluble calcium carbonate which will precipitate out of solution:



In this way, divalent calcium ions have been removed from solution and replaced with twice the number of monovalent potassium ions:



Although this chemical reaction has not reduced the ionic strength of the solution separating the particle and surface, it would still alter the repulsive forces due to monovalent ions being much less effective at screening electrostatic interactions than divalent ions. This phenomena has been observed during experiments into the flocculation of colloidal particles, where it was found that screening of electrostatic interactions is proportional to the valency of ions to the sixth power – known as the Schultz-Hardy rule⁵.

A strategy like this could be used but would be problematic due to the precipitation of calcium carbonate from solution which would ‘dirty’ the surfaces of the particle and planar surface. This precipitation may also block the release of calcium chloride from a potential motor particle.

Changing the charges of surfaces can lead to differences in repulsion experienced, by either changing one or both of the surfaces to become more charged, a particle will be repelled further from the surface causing it to gain gravitational potential energy. Using eq. 1-3, the interaction energy between a 4 μm gold particle with a surface charge of

-30mV, and surfaces with a charge of -30mV or -60mV was calculated and is shown in Figure 2.

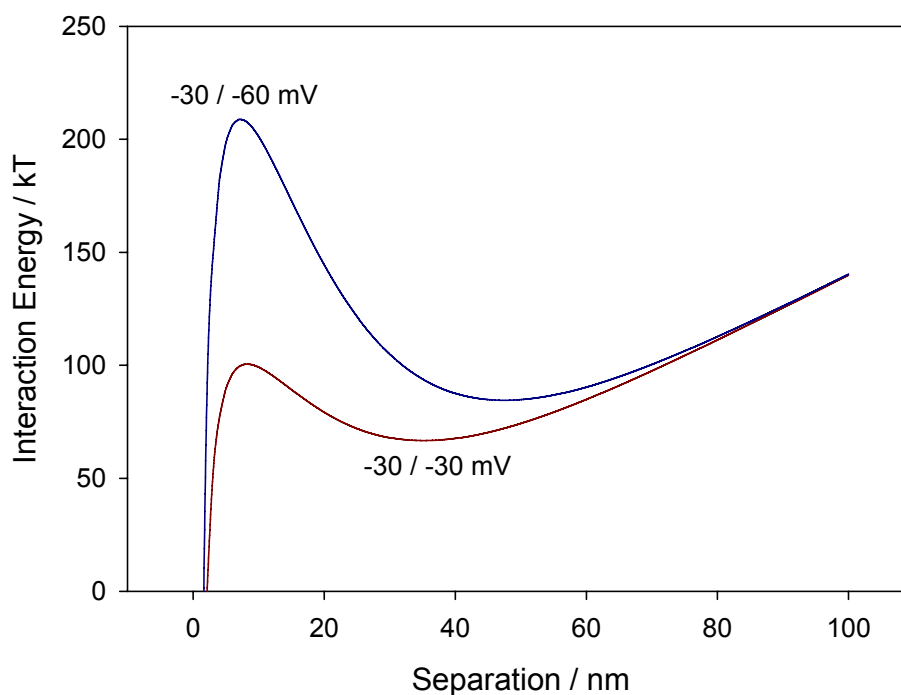


Figure 2 Interaction energy of a particle (-30mV) and planar surfaces of different surface charge (-30mV or -60mV).

As can be seen from this figure, the particle's energy is reduced by sedimenting down closer to the surface until it reaches a point 30-50 nm above the surface. Approaching closer to the surface from this point raises the particle's energy as the electrostatic repulsion caused by the overlapping double layers becomes large. This increase in particle energy continues until the separation becomes small enough that van der Waals force begins to dominate the interaction at separations of less than 15nm. The dense gold particle has two separation distances where the slope of the interaction energy plot, i.e. the force acting on the particle, is zero. One of these energy minima is at 0 nm where the particle and surface are in contact, known as the *primary minima*, and the other between 30 and 50 nm above the surface where electrostatic repulsions are equal to the gravitational force, sometimes called a *gravitational minima*.

The position of this gravitational minima changes depending on the surface charge. For the -30mV gold particle above a surface with the same charge, the position of the gravitational minima is 37nm above the surface. Whereas for the gold particle above a

surface with a -60mV surface charge, the position is shifted higher to 48nm. Therefore converting a surface with an initial surface charge of -30mV to -60mV will cause the particle to experience an increase in repulsion equivalent to raising the particle by 11nm or increasing the particle's energy by 15kT.

The increase in particle energy upon converting a surface of low charge to a higher surface charge can be maximised by minimising the initial surface charge and maximising the chemically-altered surface's charge. Although if the surface charge is too low on the initial surface, the particle may be able to pass from the gravitational energy minima to the primary minima, as the energy barrier preventing it from doing this becomes smaller. Therefore an initial surface charge of at least -30mV should be used. Creating a surface with the highest possible surface charge is limited to surface charges less than ~80mV, due to the size of functional groups which create this charge, they cannot be packed on the surface at any higher density to give a higher surface charge.

4.3 Creating Surfaces which can alter their Surface Charge

To create an implementation of the theoretical design which makes use of the highlighted electrostatic repulsions to propel particles forward, it will be necessary to create surfaces that can have their surface charge increased by a chemical reaction. Therefore it will be necessary to introduce some kind of functionality to the surface, which enables the surface charge to be increased by the chemical transformations.

A common way to create surfaces with different functionality is by the spontaneous assembly of small molecules from solution onto a substrate, to form a self-assembled monolayer. One of the most widely studied groups of self-assembled monolayers are alkyl thiols which self-assemble onto gold substrates by the formation of a thiolate bond (see Figure 3). Unlike silane monolayers which form on glass surfaces, a wide range of functional groups can be included at the tail end of the thiol molecule which do not interfere with the self-assembly process⁶. This makes alkyl thiol monolayers particularly attractive for use in creating surfaces which can alter their surface charge through a chemical reaction.

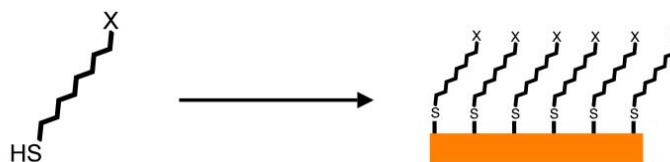


Figure 3 The Self-assembly of alkyl thiols onto gold surfaces to create monolayers. X is the tail group functionality.

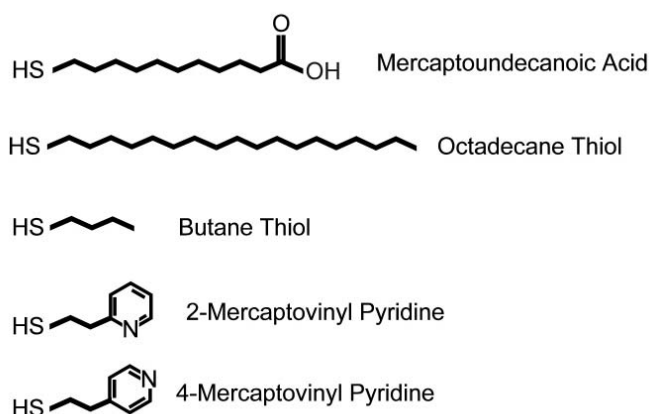


Figure 4 Different thiol molecules used to create surfaces with different functionalities

Surfaces with mercaptoundecanoic acid, 2-mercaptopvinyl pyridine, 4-mercaptopvinyl pyridine, butane thiol, octadecane thiol were created (see Figure 4). The quality of the monolayer formation was assessed by measuring the static contact angle with water and comparing with literature values. All monolayers created had static contact angles similar to those reported in the literature⁶ and so functionalisation of the surfaces was considered to be successful and of high quality.

To measure the surface charge of planar surfaces, streaming potential measurements can be made by applying a flow of water across the surface and measuring the voltage created between two electrodes. Unfortunately this equipment was not available and so an alternative procedure was used. In this procedure, small spherical gold particles <1 μ m were functionalised with alkyl thiols in exactly the same manner as the created planar surfaces. The zeta potential of these particles was then measured using a commercial instrument. As the particle radius is much larger than the dimensions of the adsorbed thiol layer, it will appear to be a planar surface to the thiol molecule, much like the Earth seems flat to a human standing on it.

The zeta potential is a measure of surface charge but is only valid at distances away from the particle's surface greater than the position of the slipping plane. As the gold particles are smooth and should not contain any attached soluble polymer layer, the position of the slipping plane should be just a few Angstroms away from the surface, at the edge of the so called *Stern* layer. A 4 μm gold particle will never come this close to a planar gold surface due to the electrostatic repulsions, therefore the zeta potential of small gold particles should be equal to the surface charge of planar gold surfaces experienced by a 4 μm gold particle.

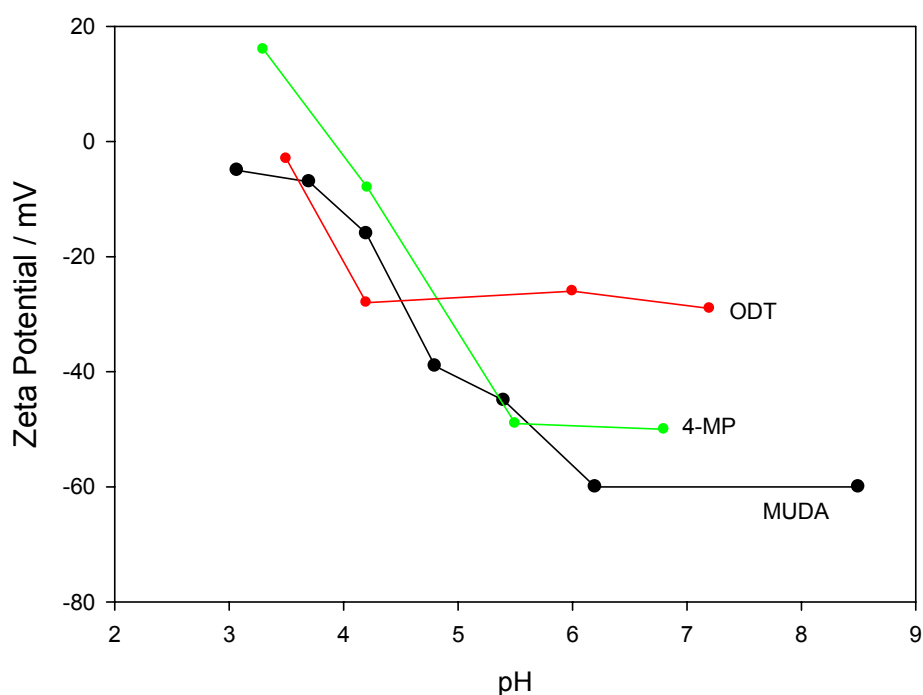


Figure 5 Zeta potentials of different surfaces. ODT – Octadecanethiol, 4-MP – 4-Mercaptovinylpyridine, MUDA – Mercaptoundecanoic acid

Figure 5 shows the measured zeta potentials of small gold particles functionalised with different thiol monolayers at different pH values. Mercaptoundecanoic acid (MUDA) contains tail groups with a carboxylic acid functionality. These carboxylic acid groups are protonated at low pH and deprotonated at high pH, meaning that the surface is ionised at high pH and therefore highly charged. Zeta potentials of around -60mV were measured above pH 6. At low pH the carboxylic acid groups are protonated and therefore the surface has a low surface charge. At pH 3 a zeta potential of -4mV was measured. Vezenov et al⁷ measured a pK_a of 5.5 for mercaptoundecanoic monolayers but in results

gathered from zeta potential measurements in this study, the pK_a seems to be slightly lower.

Static contact angle measurements with water adjusted to different pH values using sodium hydroxide and hydrochloric acid also confirmed a change in the physical properties of the mercaptoundecanoic acid monolayer at high and low pH, changing from 13° at pH 11 to 20° at pH 3. Although this change in contact angle is small, it perhaps indicates a change in the ionisation state of the carboxylic acid groups in the monolayer.

Monolayers of 4-mercaptovinyl pyridine (4-MP) contain the weak base group pyridine and so can also be protonated or deprotonated depending on the pH, although now the surface becomes ionised at low pH. Xia et al⁸ have determined the pK_a of this monolayer to be 5.3 and Bryant et al⁹ determined a pK_a of 4.6, both are much higher than the pK_a of 1.4 measured for mercaptovinyl pyridine in solution¹⁰. Consistent with these studies, zeta potential measurements showed that particles functionalised with 4-MP had a positive surface charge of +17mV at pH 3.4. Upon increasing the pH, particles became less positively charged due to the deprotonation and neutralisation of pyridine groups, then at pH values greater than ~ 4 became negatively charged. This negative charging increased to plateau at -50mV at pH's higher than 5.5. This unexpected negative charging of the surface is probably due to the adsorption of hydroxide ions from solution by the hydrophobic surface⁵. Consistent with this hypothesis, static contact angles with water showed that the surface was moderately hydrophobic, have a contact angle of $\sim 60^\circ$. Unlike MUDA monolayers the contact angle did not change significantly at high and low pH.

So far it has been shown that monolayers containing either weak acids or bases can become charged by altering the pH which can lead to ionisation of the surface, but the surface charge can also be altered on surfaces containing no ionisable functional groups. For example, octadecane thiol has a terminal methyl group which cannot be protonated or deprotonated, but as can be seen from Figure 5, its zeta potential changes from ~ 0 mV at pH 3.5 to become negatively charged at pH 4 with a zeta potential of ~ -30 mV. Like 4-MP monolayers, this charging is due to the adsorption of hydroxide ions onto the hydrophobic surface.

Guire et al¹¹ have studied surfaces with similar functionality and found that the zeta potential of surfaces with a carboxylic acid tail group changed from +5mV at pH 3 to -50mV at pH 7, in close agreement to the data obtained in this study. They also studied surfaces with primary amine groups which can be protonated like 4-MP monolayers, finding the zeta potential changed from +50mV at pH 5 to +10mV at pH 7. This result is quite different from those gathered for 4-MP but could be explained by differences in the functional groups studied (primary vs. tertiary amine).

Finally in a separate experiment unfunctionalised gold particles were found to have a zeta potential of -37mV at pH 7.

It has been shown in this section that surfaces can be created of different surface charge, which should lead to differences in the repulsive force experienced by a dense particle above them. To create propulsion as in the theoretical design, it will be necessary to convert a surface of low surface charge to one of higher surface charge. This could be achieved in several ways:

A MUDA surface could have its charge increased by an increase in the solution pH. On going from pH 3 to 7, the surface charge would change from -5mV to -65mV . Although the colloidal stability of the gold particle would be poor at pH 3 due to the small surface charge, meaning that surface coagulation may be observed. A better strategy would be to alter the pH from 4.5 to 7, changing the zeta potential from $\sim -30\text{mV}$ to -65mV . This gives a change in surface charge which is smaller but gives a lowest surface charge of -30mV , on which colloidal stability should be good.

A 4-MP surface could be made more cationically charged by reducing the solution pH from 4 to 3, but this results in a change in surface charge of only $\sim 0\text{mV}$ to $\sim +20\text{mV}$. Again the surface charges are low which risks surface coagulation of particles. Counter-intuitively 4-MP surfaces can have a negative surface charge which can be increased from $\sim 0\text{mV}$ at pH 4 to -50mV at pH 6.

Finally a surface of ODT, which has no ionisable surface functionality, can be made more negatively charged by increasing the solution pH from 3 to 5. This results in a change in surface charge of $\sim 0\text{mV}$ to -30mV , probably by the preferential adsorption of hydroxide ions from solution.

An unfunctionalised gold surface could have its surface charge increased from -37mV to -65mV , by the self-assembly of MUDA on its surface. This strategy is quite appealing as the transformation is irreversible, unlike all the other strategies proposed, and only requires a very small concentration of the chemical species to occur.

Considering all the ways to convert a surface with a low surface charge to one with higher surface charge, the two which are most suited to be used in the theoretical design are changing a MUDA surface charge by increasing the solution pH, and functionalising a gold surface with MUDA at pH 7. In both cases the initial surface charge is greater than -30mV , which should give good colloidal stability of gold particles towards surface coagulation, and the change in surface charge is relatively large at $\sim 30\text{mV}$. These changes in surface charge are similar to those used in the particle-surface interaction calculations, which predicted that changes in surface charge should change particle energies by $15kT$ by raising the particles by 1nm .

4.4 Sedimentation Experiments

From particle-surface interaction calculations, it was predicted that a particle can be raised a small height by increasing the charge of a surface. For a 4 μ m gold particle on a surface which changes from -30 to -60mV, this change in height was predicted to be 11nm.

To produce propulsion from this small change in height, a gradient will need to be created of surface charge, leading to a gradient of particle height above the surface. The shape of this gradient may not be linear and will be dictated by the diffusion and rate of reaction of the chemical species released from the motor particle. Nevertheless it will have a maximum height of 11nm and the length of the gradient can be estimated to greater than one particle diameter, as this is the distance between the motor and target particles. Making the assumption that the gradient is linear, with a height of 11nm and a length of one diameter, 4 μ m, the angle of incline created is $\tan^{-1}(11/4000) = 0.16^\circ$. This angle is extremely small but will still result in the propulsion of particles down the gradient, although it would be slow and masked by Brownian motion of the particles. The slope could be greater than this value if the gradient of surface charge created leads to a non-linear gradient of particle height but it is clear that it will still be small and only a few degrees of incline.

The velocity at which a particle sediments through a liquid can be calculated by equating the force pushing the particle through the liquid to the viscous resistance:

$$\begin{aligned}\text{Force} &= \text{viscous resistance} \\ mg &= 6\pi\eta rv \\ \frac{4}{3}\pi r^3(\rho_{particle} - \rho_{liq.})g &= 6\pi\eta rv\end{aligned}$$

which, rearranging to make velocity the subject of the equation and cancelling terms, leads to the following equation, sometimes called the Svedburg or Stokes equation.

$$\text{Sedimentation velocity} = \frac{2r^2(\rho_{particle} - \rho_{liq.})g}{9\eta}$$

eq. 4

But in these experiments, the particle will be observed from above as it sediments along a sloped surface, so the force propelling the particle across the sloped surface becomes $mg \tan \theta$, and eq. 4 becomes:

$$\text{Velocity} = \frac{2r^2(\rho_{particle} - \rho_{liq.})g}{9\eta} \tan \theta$$

eq. 5

where θ is the angle of incline between the slopes surface and the horizontal.

To investigate if gradients of particle height as small as those estimated using rough calculations can propel a particle forward, it was necessary to produce a gradient of particle height that has the same slope of inclination but which is much longer in length and which does not change over time. To reproduce this gradient of height and allow the motion of the gold particles to be studied, a glass microscope slide was inclined to varying degrees and the motion of 4 μm gold particles observed.

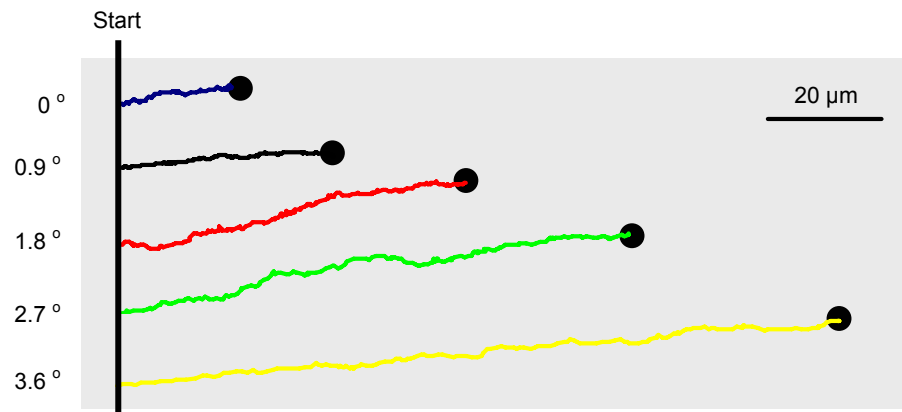


Figure 6 Typical trajectories of 4 μm gold particles sedimenting across a glass surface inclined at various angles over a time period of 35 seconds.

As shown in Figure 6, particles sedimented down the slope moving from left to right when observed from above. The larger the angle of incline the faster particles travelled. Even when the substrate was not inclined at all, gold particles still moved from left to right suggesting that the microscope was not initially level, even though an effort was made to level it. Particles also migrate in a direction perpendicular to the direction of sedimentation due to diffusion by Brownian motion.

It is not clear from the captured motion how the particles move in close proximity to the surface, either by sliding or rolling. As they are electrostatically repelled from the surface they should slide easily across the surface, but as the bottom of the particle experiences a higher viscous resistance due to the proximity of the glass surface, particles should also experience a torque force causing them to roll along the surface. Abkarian et al¹² have studied the sedimentation of large vesicles along sloped surfaces and found that motion was a combination of mostly sliding and some rolling.

Analysis of captured movies of the sedimentation using a custom made LabView script, which finds the position of the particles in each frame of the recorded movies, allowed the mean-squared-displacement of the particles to be found. Figure 7 shows this plotted against the observation time interval.

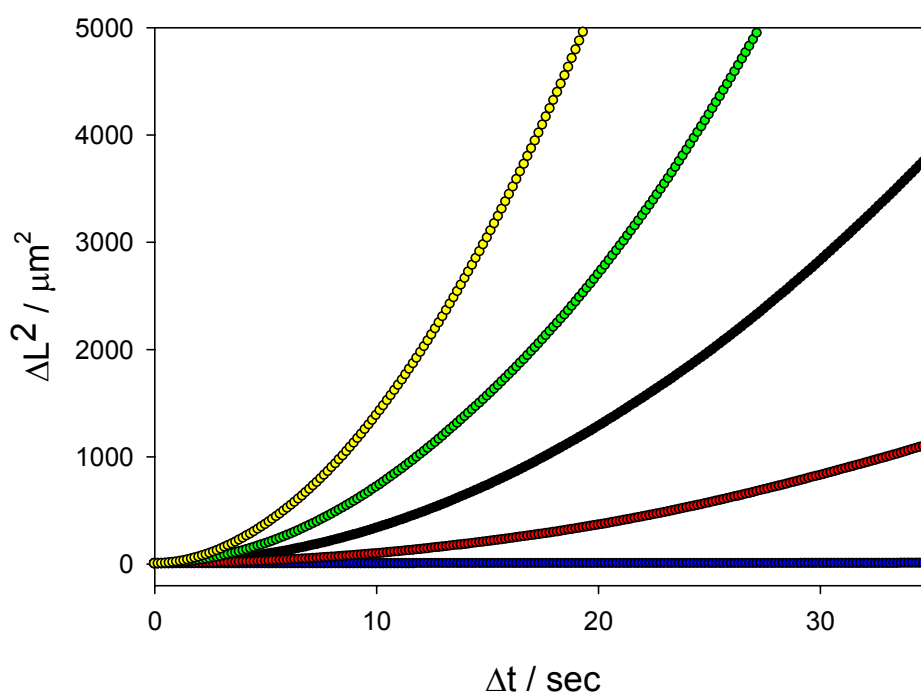


Figure 7 Typical mean-squared-displacements of 4μm gold particles sedimenting down a surface inclined to 3.6° (yellow); 2.7° (green); 1.8° (black); 0.9° (red); 0° (blue).

Particles underwent a combination of Brownian motion and sedimentation down the sloped surface. Therefore a simple analysis of the particles velocity by measuring the distance travelled divided by time (velocity = distance / time), gave results which differed quite significantly, depending on the two positions or times the velocity was measured between. To extract meaningful velocities both Brownian motion and sedimentation

must be taken into account. The mean-squared-displacement $\langle \Delta L \rangle^2$ of a particle diffusing is given by Einstein's equation $\langle \Delta L \rangle^2 = 4D\Delta t$. The distance travelled by a particle moving with velocity v is $\Delta L = v\Delta t$, which can be squared to give $\langle \Delta L \rangle^2 = v^2\Delta t^2$, allowing the displacements due to Brownian motion and sedimentation to be added together:

$$\langle \Delta L \rangle^2 = v^2\Delta t^2 + 4D\Delta t$$

eq. 6

Fitting the calculated mean-squared-displacement of sedimenting gold particles using eq. 6 gives the velocity at which the gold particles move. An average of velocities was taken over 30 particles at each angle of incline investigated. This data is plotted against $\tan\theta$ in Figure 8, where θ is the angle of incline.

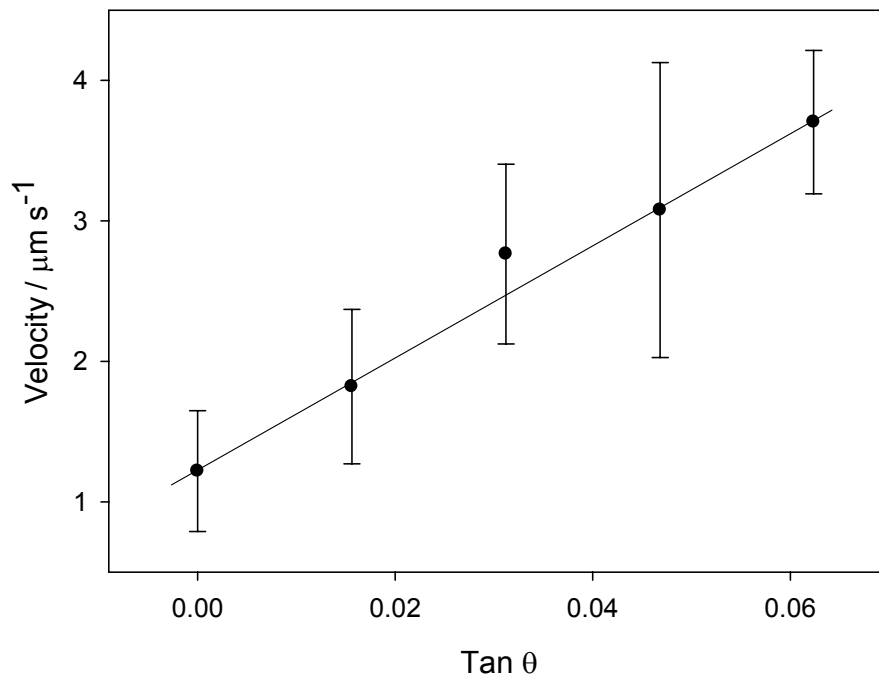


Figure 8 Sedimentation velocity of 4 μm gold particles on sloped glass substrates. The data points are at intervals of 0.9° incline. The bars show one standard of deviation in each direction.

A linear plot is obtained with the fastest velocities occurring at the largest angle of incline, as expected. At the largest angle measured, 3.6° , a velocity of $3.7\mu\text{m s}^{-1}$ was measured, which would make a very reasonable velocity for a particle to propel itself forward, comparable to some of the nanoswimmers discussed in the introduction.

Data points are at increments of 0.9° and show that even at the small angles studied, propulsive velocities are moderately fast. The fit of data points should pass through the origin, as at zero angle of incline the velocity of particles should be zero, but it does not. This is probably due to the microscope not being precisely oriented in the horizontal plane (level), even though an effort was made to level the microscope. Extrapolation of the fit gives an angle of incline of the microscope to be 1.0° .

The data plotted in Figure 8 should have a gradient of $2r^2(\rho_{particle} - \rho_{water})g/9\eta$ but instead has a gradient only $\frac{1}{4}$ of this value. This could be caused by the increased viscous resistance experienced by the gold particle when in close proximity to the glass substrate, as water is now squeezed through a gap between the particle and the surface. The close proximity of a substrate has been shown both numerically^{13,14} and experimentally^{15,16} to increase the viscous drag, which Faucheux and Libchauber¹⁷ found could decrease the diffusion coefficients of particles by up to a factor of 3.

To further investigate if eq. 6 adequately describes the behaviour of a particle migrating due to a gradient of height, the angle of incline was fixed at 1° and particles of different densities investigated. As the particles were of different sizes it was necessary to normalise the velocity by dividing by the radius of the particle-squared.

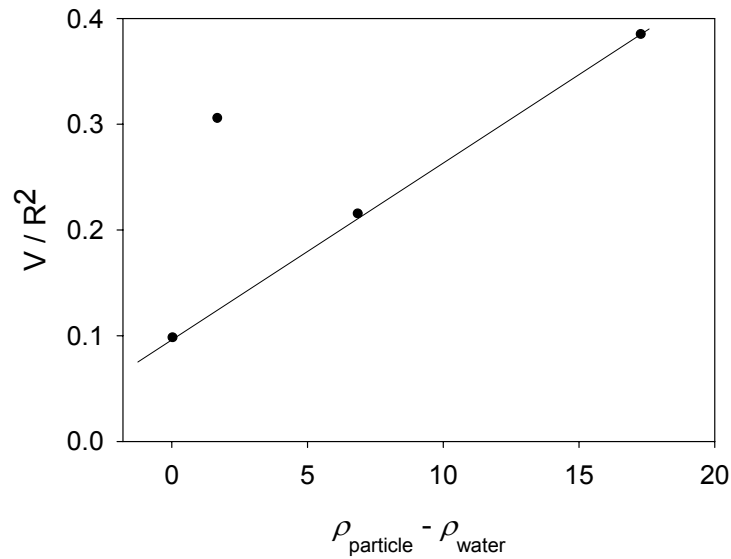


Figure 9 Sedimentation velocity of metal particles normalised by dividing by the radius-squared, against effective particle density. Data points are from left to right: Polystyrene, Aluminium, Iron and Gold.

Figure 9 shows this normalised velocity against density for particles of polystyrene, aluminium, iron and gold. Polystyrene has a low density (1.05 g cm^{-3}) so is nearly neutrally buoyant in water (1 g cm^{-3}) and so should not sediment to any great extent, although data captured did not agree and showed that polystyrene particles had an average velocity of $0.1 \mu\text{m s}^{-1}$. Analysis of captured trajectories showed that the polystyrene particles sometimes moved in directions against the gradient of the slope, highlighting that the observed motion may be due to small convection currents present in the observation chamber fluid rather than sedimentation.

Particles of iron and gold moved much faster, creating a linear trend in the data which coincides with the data point from polystyrene. Aluminium particles showed anomalous behaviour sedimenting much faster than they should in the trend of data other particles. These aluminium particles were the most polydisperse and so it was difficult to define their average radius to use in calculation of V/R^2 .

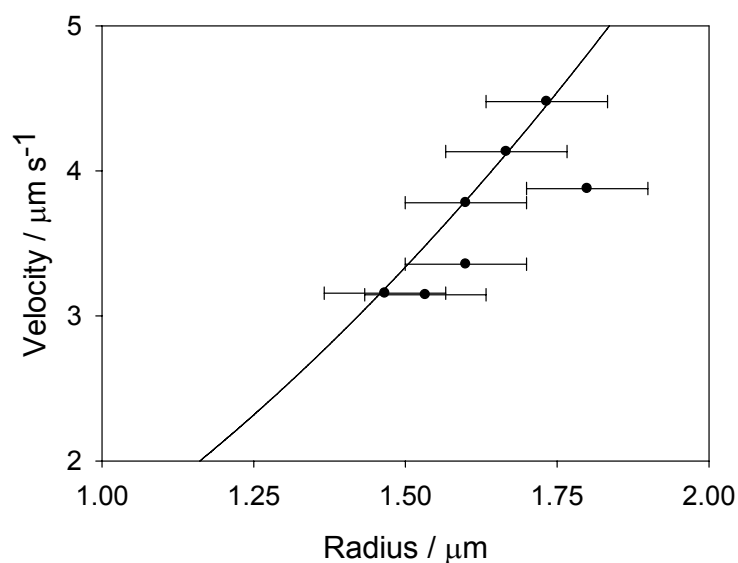


Figure 10 Sedimentation velocities of gold particles of different sizes. Bars represent the error of estimating the particle size using optical micrographs.

Figure 10 shows the measured velocity for gold particles of different size at a fixed angle of incline. A general trend of faster sedimentation can be observed with increasing particle radius. The particles which sediment the fastest at each radius form a trend line with the expected R^2 dependency. Particles which are observed to sediment slower than this value could be experiencing extra drag by coming into contact with the surface through their non-spherical shape or by surface contamination.

From these gathered trends in the data, it is possible to confirm that sedimenting particles do roughly obey eq. 5, although they sediment at around only a quarter of the predicted velocity. This is probably due to the higher viscous resistance experience at the surface due to the proximity of the glass surface. More importantly it has been shown that gold particles will respond to a small incline and be propelled down the slope moderately quickly. If surface modification can create these small inclines by increasing the charge of a surface, it should be possible to create a working implementation of the theoretical design.

4.5 Repulsion-Repulsion Surface Interaction Patterns

To investigate if gradients of surface charge can influence the position of small particles and be used in an implementation of the theoretical design, very sharp static gradients were created using photolithography. If these sharp gradients can influence the motion of small particles, it should be possible to use them to propel particles forward using these repulsive electrostatic interactions, as in the theoretical design.

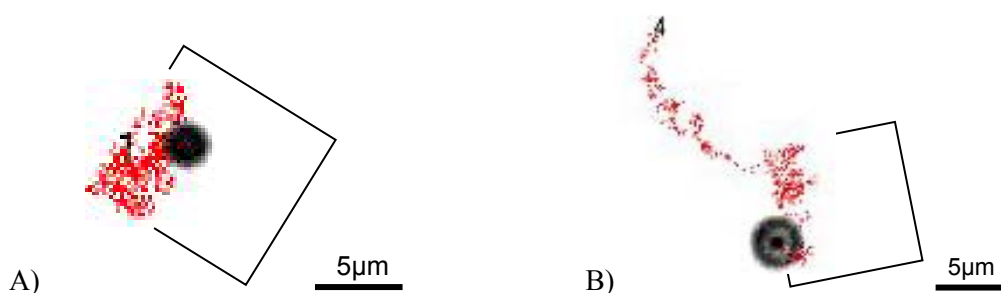


Figure 11 Trajectories of 4 μm gold particles on patterned surfaces of octadecane thiol / mercaptoundecanoic acid. Boxes drawn are a guide to the eye only and are smaller than the actual boxes which are 20x20 μm .

Patterned surfaces were created from octadecane thiol and mercaptoundecanoic acid on gold using a photomask that contains squares 20 μm x 20 μm . In this way a surface was created consisting of squares of octadecane thiol, having a zeta potential of $\sim -30\text{mV}$ at pH 7, separated by a grid pattern consisting of mercaptoundecanoic acid, having a zeta potential of $\sim -65\text{mV}$ at pH 7. A small gold particle dispersed above this surface should experience different strengths of electrostatic surface repulsion depending on which surface of the pattern they are above.

The trajectories of gold particles diffusing in water was followed using video microscopy and a LabView tracking script. Most of the gold particles diffused to give trajectories which were either approximately spherical or globular - as would be expected for a particle unperturbed by any surface patterning - or a 'wobbly' line as would be expected in the case of a particle sedimenting and undergoing Brownian motion. A few particles had unusually shaped trajectories which seemed to be influenced by the surface patterning.

Figure 11 shows the trajectories of two 4 μm gold particles undergoing Brownian motion on a surface which has been chemically patterned leading to a surface with a pattern of surface charges. In Figure 11A the particle seems to mark out the corner of a

square as if it were inside one of the square surface patterns and cannot escape. In Figure 11B a particle is seen to migrate from the top left into a region where it then marks out the corner of a square and again cannot seem to escape from this square.

It is not possible to know the position of the square patterns on the surface as they are not visible by light microscopy, so it can only be speculated what the surface patterning is around a particle. It was observed a few times that several particles captured in a movie marked out straight lines or corners which were parallel or perpendicular to each other and consistent with the surface patterning (not shown). Therefore it could be speculated that the surface patterning of charge is influencing the Brownian motion of particles.

This speculation is consistent with particle-surface interaction calculations which as already shown, predicts that gold particles should experience a difference in surface repulsion upon migrating between the two areas which make up the surface pattern, leading to a change in gravitation potential energy of around $15kT$. A particle which is inside a square of low surface charge should be reluctant to leave as it would have to gain energy, as seems the case in Figure 11A. A particle should be able to migrate into a square of lower surface charge as this results in a drop in energy but should not be able to escape once inside, as seems the case in Figure 11B.

With these results in mind, it is tempting to conclude that the patterned surface charge is influencing particles in the desired way. But other collected results and observations suggest that the observed particle influence is not due to patterns of surface charge. For example, if it is the surface charge which is influencing particle motion, then why don't all the particles behave in the same way and mark out square patterns in their trajectories?

Figure 12 shows the trajectory of another particle diffusing on a patterned surface. Although in this case the particle is a smaller, less dense $3\mu\text{m}$ iron particle on a surface pattern consisting of squares of unfunctionalised silica and a grid pattern of dodecyl silane. As can be seen in the figure, a particle diffuses giving an unusual trajectory which seems to mark out a pattern identical to that of the photomask used.

Firstly considering the parts of the trajectories shown in blue, four straight lines can be seen, two of which are parallel and coincide with each other, and two other lines which are perpendicular to the first lines and are also parallel. The distance separating the two blue regions is exactly $7\mu\text{m}$, which is also the width of the grid pattern on the photomask used. Due to this pattern of trajectory, the position of the surface pattern can be stated with fair confidence and that this pattern is influencing the particle diffusing above it, although not through electrostatic repulsion.

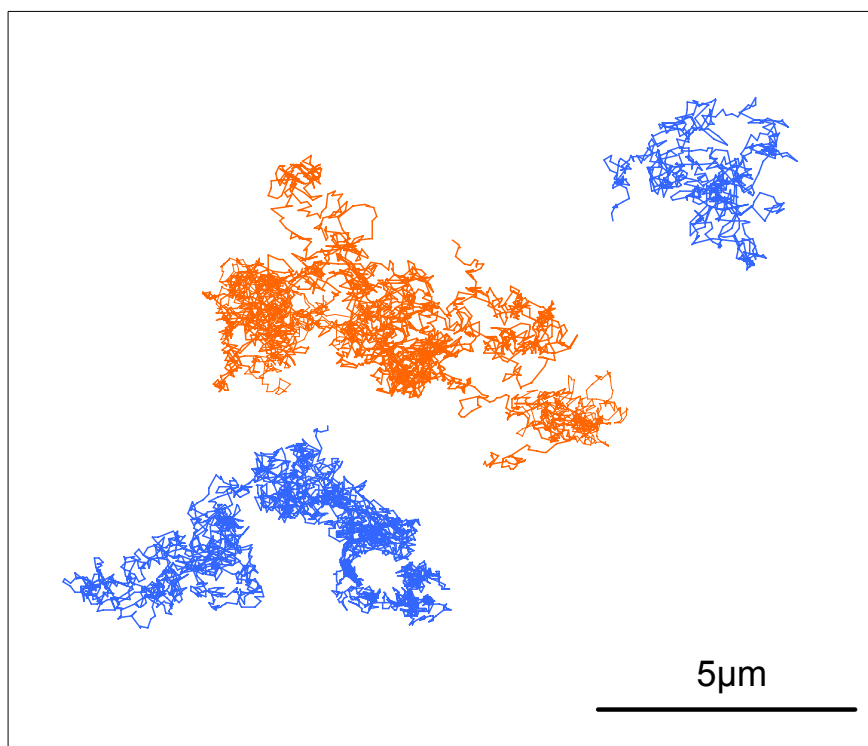


Figure 12 Trajectory of a 3µm iron particle on a patterned surface of dodecyl silane / bare silica over 30 minutes. The orange part of the trajectory has been moved upwards by 2µm.

In this surface pattern used, the areas of highest surface charge are inside the silica squares (zeta potential $\sim -70\text{mV}^{18}$, -40mV^{11}), and the areas of lowest surface charge on the grid pattern of dodecyl silane (zeta potential = $-30\text{mV}^{11,18}$). Therefore particles should be reluctant to enter the squares of silica, but are instead observed to be reluctant to leave these squares by crossing the interface between different chemically patterned areas. The part of the trajectory shown in orange corresponds to when the particle is repelled over a surface of low charge and shows again that the particle is reluctant to cross the interface between patterned regions. From these experiments it has been shown that the observed behaviour is not consistent with the particle-surface interaction calculations and therefore a different explanation is needed.

It was observed that in almost all of the experiments performed that a significant fraction of the dispersed particles adhered to the surface. This was attributed to surface contamination during the preparation of the patterned surfaces by ‘greasy’ molecules which are present in the air. This contamination lowers surface repulsions allowing particle and surface to come into contact and adhere. As the patterned surfaces typically contained a hydrophobic, low-surface-charge region and a hydrophilic, highly-charged region, the different regions have significantly different wetting properties to each other

and it was postulated that this surface contamination could be responsible for the observed influence on particle motion.

To investigate this, patterned surfaces consisting of mercaptoundecanoic acid and mercaptoundecanol were created. This gives a patterned surface where the surface charge is significantly different (-60mV vs. -18mV) but the wetting properties are very similar (static contact angles both $<10^\circ$). A typical trajectory of a diffusing gold particle on these hydrophilic-hydrophilic patterned surfaces is shown in Figure 13, which shows a particle which diffuses uninfluenced by the surface patterning. This experiment was repeated many times but not one particle was ever found which marked out a grid pattern while diffusing.



Figure 13 A 4 μ m gold particle diffusing on a patterned surface of mercaptoundecanoic acid / gold. Both regions of the surface pattern are hydrophilic.

Therefore it seems likely that as the calculated particle-surface interaction does not explain the observed behaviour, and that it is only observed when a surface pattern consisting of regions with different wettabilities is used, that it is caused by surface contamination. It was noticed that as patterned surfaces dry, the interface between the hydrophobic and hydrophilic region was often the last place to dry, meaning that any contamination could be concentrated into this interfacial region.

To summarise this section, it has been predicted by calculation of the repulsive forces acting on a 4 μ m gold particle that differences in surface charge of around 30mV should lead to differences in particle energies of around 15kT. Experiments which have created very small gradients of this difference in surface charge have shown that this surface charge cannot control the position and motion of gold particles. Therefore creating gradients of surface charge does not lead to the propulsion of small particles. Perhaps the particle-surface interaction calculations employed are correct in predicting a difference in surface repulsion, but predicts a difference which is larger than the actual difference.

Either way, electrostatic interactions are of no use in implementing the theoretical design as they cannot significantly influence particles.

The difference between the predicted behaviour and the observed behaviour could be attributed to surface roughness, which is often quoted as being responsible for differences between experiment and theory. Also surface contamination has been shown to be present on the surfaces investigated and could also contribute to the unexpected results.

4.6 Adhesion-Repulsion Surface Interaction Patterns

In the previous section, experiments have shown that gradients of electrostatic repulsions cannot control particles and are therefore of no use in implementing the theoretical design. In this section gradients of electrostatic interactions which change from attractive to repulsive shall be investigated.

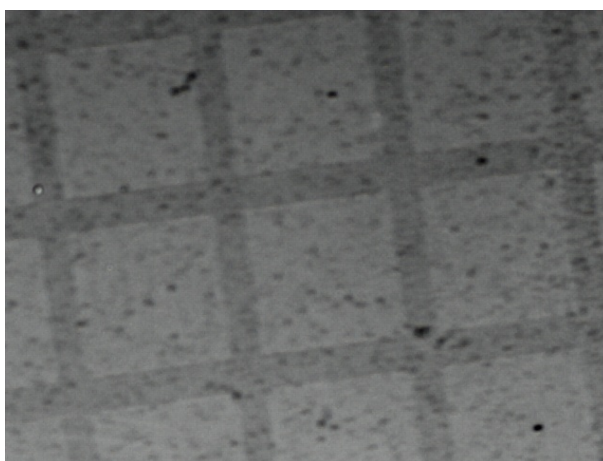


Figure 14 A patterned surface functionalised with silica particles

Using a combination of photolithography and the self assembly of silanes on silica, patterned surfaces were created with one cationically charged region and the other region anionically charged. In this way the surface is patterned with regions which have attractive or repulsive interactions with negatively charged particles.

Figure 14 shows a patterned surface which has been created consisting of anionically charged square regions of silica, separated by a grid pattern of cationic trimethylamino propyl silane. After formation of this patterned surface it was exposed to a solution of negatively charged silica nanoparticles. These particles should be attracted to the oppositely charged regions of the grid pattern and repelled away from the anionically charged regions of silica squares. In Figure 14 it is possible to see a pattern on the surface identical to the photomask used. Silica squares where silica particles do not adhere-to, appear lighter than the grid pattern where silica should adhere to. This is due to the silica particles dispersing light reducing the intensity reflected back, making these regions appear darker and shows the adhesive-repulsive surface interactions have controlled the position of small particles.

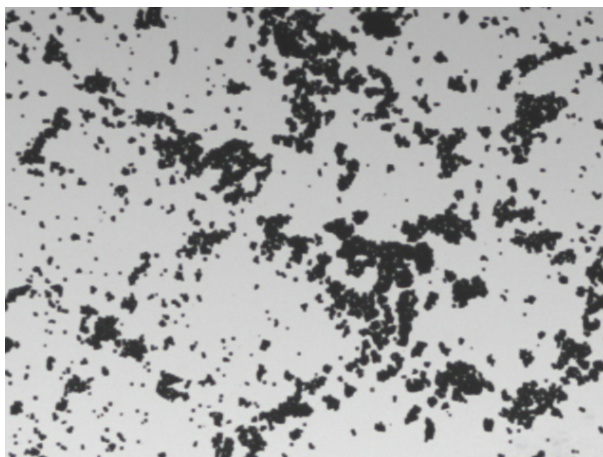


Figure 15 NMe₃ / SiOH surface functionalised with gold particles before agitation

Figure 15 shows an identically created patterned surface which has been exposed to 4 μ m gold particles functionalised with MUDA to make them negatively charged. As can be seen in the figure, only a weak pattern of particles has been created – there are particles in the anionic squares and the cationic surface of the grid has not been completely functionalised with oppositely charged gold particles.

This weak pattern is probably caused by the slow kinetics of pattern formation when large gold particles are used. An area of oppositely charged surface cannot become functionalised with particles until a gold particle diffuses into one of these areas and as the particles diffuse quite slowly, the formation of this pattern requires a long time. The rate at which particles migrate into an oppositely charged area can be increased by inclining the surface, leading to the gold particles being driven across the surface. Also inverting the patterned surface allows gold particles to sediment into areas of the adhesive surface which would otherwise be blocked by other gold particles nearby.

Figure 16 shows the same surface as in the previous figure but after the surface had been inclined and inverted at various angles for a few minutes. Now the pattern of gold particles has become much stronger, with the majority of the adhesive surface functionalised with gold particles. Some excess particles which have not been able to find a place on the adhesive surface are present in the repulsive interaction regions.

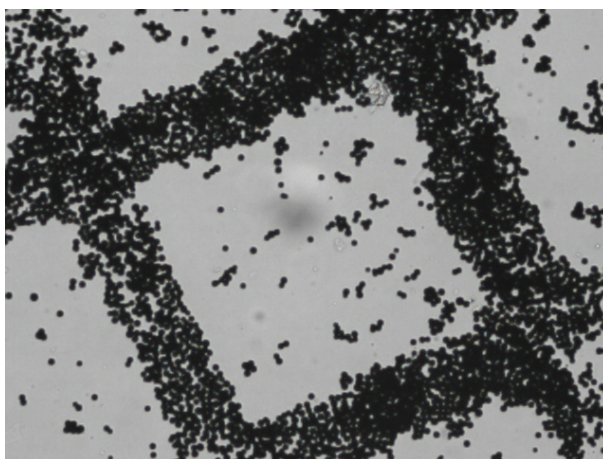


Figure 16 NMe_3 / SiOH patterned surface after agitation

These experiments show that attractive electrostatic interactions can be used to control the position of particles on a surface and that a gradient of interaction which changes from repulsive to adhesive does lead to the migration of particles down the gradient. If a chemical reaction could be used to alter adhesive regions into repulsive regions, this interaction could be used in an implementation of the theoretical design.

Particles would initially adhere to a surface through attractive electrostatic interactions, a motor particle would then release a chemical reagent to change the surface interactions from attractive to repulsive causing the particles to be released from the surface. Particles would then migrate down the created adhesion gradient to a region of the surface which is adhesive leading to propulsion of the particle.

Unfortunately, it has been shown that this chemical modification is not possible due to van der Waals force, meaning that particles cannot reversibly bind to surfaces. Whereas it has been shown in this section that a particle will migrate along a gradient of repulsive to adhesive interactions, this migration can only be used a single time. Therefore implementations of the theoretical design based on these interactions will not work.

4.7 Adhesion-Adhesion Surface Interaction Patterns

In the previous section it was shown that gradients of surface interactions which change interactions on the surface from repulsive to adhesive, can control the position of negatively charged gold particles. But also that, these created gradients cannot be used in implementing the theoretical design due to the irreversibility of adhesion to the surface caused by van der Waals force. In this section gradients of electrostatic interactions shall be investigated which change from attractive to more attractive, to see if these gradients can control particles through their surface interactions and if this could be used in an implementation of the theoretical design.

Patterned surfaces were created by photopatterning self-assembled monolayers of trimethylamino propyl silane and then back-filling the exposed areas of silica with dodecyl silane. In this way, patterned surfaces consisting of dodecyl silane squares separated by a grid pattern of cationically charged trimethylamino propyl silane were created.

MUDA functionalised 4 μ m gold particles were observed to adhere to the cationic trimethylamino propyl silane surface as expected due to the opposite surface charges. Gold particles should not adhere to surfaces of dodecyl silane, as the two surfaces are of like surface charge. But unexpectedly, gold particles were observed to adhere to the surface of dodecylsilane and did not undergo Brownian motion. This unexpected lack of colloidal stability leading to adhesion can be explained by the low surface charge of the dodecyl silane surface, the roughness of the gold particles, the moderately large force which particles exert on the surface due to their high density, and also contamination of the surfaces by dirt which reduces repulsive surface forces.

To make doubly sure that gold particles adhered to the dodecyl silane surface as well as the cationic trimethylamino propyl silane surface, a small amount of salt was added to the dispersion solution to suppress electrostatic repulsions. Therefore when gold particles sediment onto the created patterned surfaces, they experience an attraction to the cationic areas due to electrostatic forces and an attraction to dodecyl silane areas due to van der Waals force.

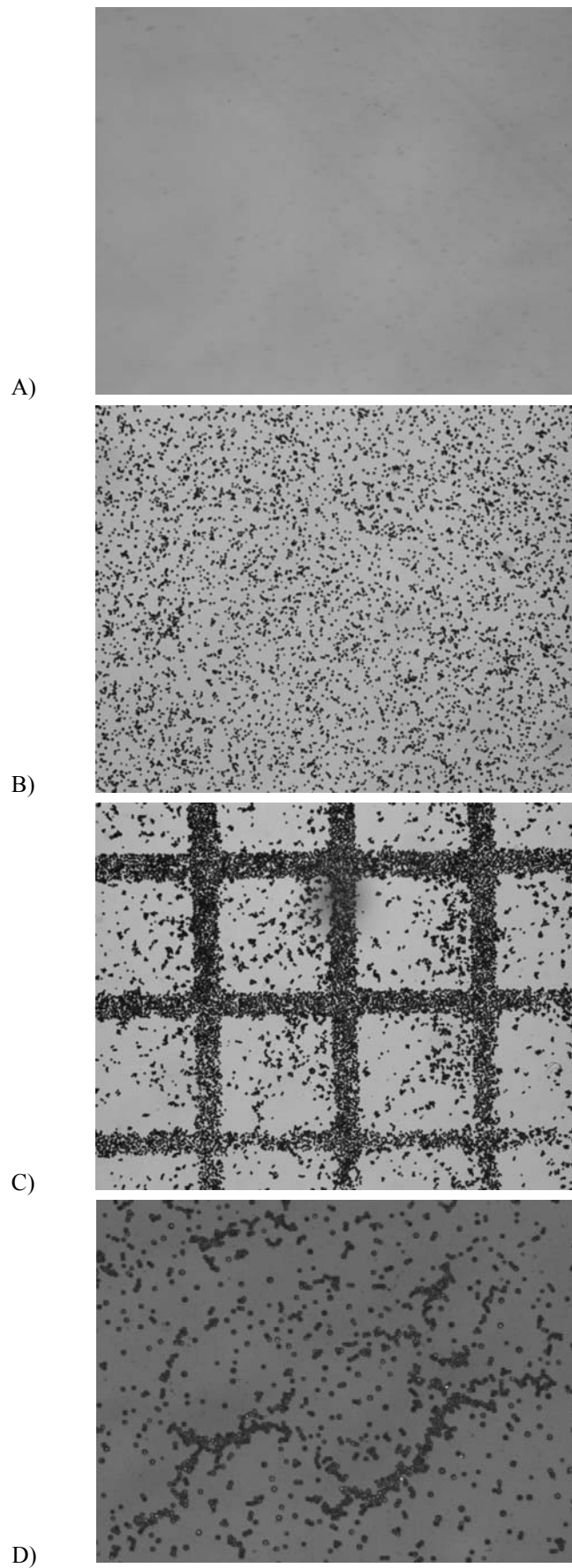


Figure 17 Prepared NMe_3 / Me Patterned Surface, when dry A); with MUDA functionalised particles added B); after agitation C); after sonication D).

Figure 17 shows the behaviour of MUDA functionalised gold particles dispersed on a patterned surface. After patterning using photolithography, no pattern on the surface is visible when examined by light microscopy as shown in Figure 17A. Upon adding the negatively charged gold particles dispersed in water, they sediment onto the patterned surface and adhere where they land. As shown in Figure 17B this leads to a random distribution of the particles on the surface and shows no pattern. Unlike earlier when patterns of adhesion / repulsion were investigated, particles cannot diffuse to the cationic areas as they are bound to the surface.

This surface with a random distribution of particles was then agitated by inclining the surface to an angle $\sim 45^\circ$ and tapping on the surface in a direction parallel with the surface with the palm of a hand. This was repeated many times, rotating the surface in between tapping so that the agitation was applied in all directions in a plane parallel to the surface. The surface was frequently inverted for a few seconds in between cycles of tapping. After a few cycles of this agitation a pattern started to appear on the surface consistent with the surface patterning by photolithography. Following many agitation cycles the pattern became stronger and appeared to reach an equilibrium pattern as shown in Figure 17C.

In this pattern, gold particles have accumulated in the areas of the surface which are cationic. As no extra particles were added to the surface during this step, the extra particles which have appeared must have originated from areas functionalised with dodecyl silane. This means that some particles must have migrated from one area of adhesion to another, breaking off from one location and re-adhering at another place.

After the particles and surface had been agitated to form the pattern observed in Figure 17C, the surface was agitated further by ultrasonic waves from a sonicator for 1 minute. This procedure resulted in a loss the patterned formed by the gold particles and they rearranged on the surface in an approximately random distribution, sometimes forming wavy lines of particles as shown in Figure 17D. As the previous pattern has been lost, particles must have migrated from areas of trimethylamino propyl silane to areas of dodecyl silane.

These results can be explained by the differences in adhesion experienced by the gold particles on the surface. When adhered to an area of dodecyl silane, particles experience attractive van der Waals forces, whereas when adhered to an area of trimethylamino propyl silane, they experience this attractive van der Waals force, as well as an extra attraction due to the electrostatic forces operating between oppositely charged surfaces. Giesbers et al¹⁹ have studied the forces acting between surfaces which are oppositely charged using similar self-assembled monolayers. They found that the force required to remove an anionic particle from cationic surface, the *pull-off force*, was relatively large at

30nN due to the acid-base pairing which occurs between surface immobilized groups. Whereas they found the pull-off force to remove an anionic particle from an anionic surface was small at 0.5nN, because there isn't any acid-base pairing.

Their results can be used to rationalize Figure 17. When particles sediment onto the surface from solution they adhere in the location which they land and are unable to migrate to more adhesive areas. This may be called the *kinetic product* as the outcome is dictated by kinetics. If this arrangement of particles is then agitated, forces are exerted on the bound particles. If this force is larger than the pull-off force, particles will be pulled off the surface and will re-adhere in another location. Conversely if the force is smaller than the pull-off force they will remain in the same location. In Figure 17C, the agitation must have lead to a force acting on the particles which is larger than the pull-off force for a particle on dodecyl silane, but smaller than the pull-off force for a particle on trimethylamino propyl silane. In this way particles could migrate from an area of low to high adhesion and accumulate in one area forming the pattern. This may be called the *thermodynamic product*, as the global energy of the system has been minimised.

Figure 17D, sonication has been used to agitate the particles and resulted in the formed pattern dispersing back into a random distribution of particles. Under these conditions the force exerted on the gold particles must be larger than pull-off force for a particle on both surfaces. In this way particles are removed from both low and high areas of adhesion and then re-adhere to both areas of the surface with approximately equal probability leading to no accumulation of particles in one area.

In an attempt to agitate the gold particles on the created surface in a way which gives a reproducible force of known strength, several methods were investigated. Firstly, the surface was attached to a piezo electric transducer with an alternating current passed through. Unfortunately the force exerted by the transducer was too small to remove the gold particles from the dodecyl silane surface, as judged from video microscopy. Secondly, the surface was attached to a vibrating motor which can exert vibrations of variable strength on the surface by controlling the applied voltage. This force was strong enough to remove gold particles from the surface but didn't lead to the formation of patterns after agitation. Therefore, currently the method of tapping with the palm of a hand is the best method to agitate the particles.

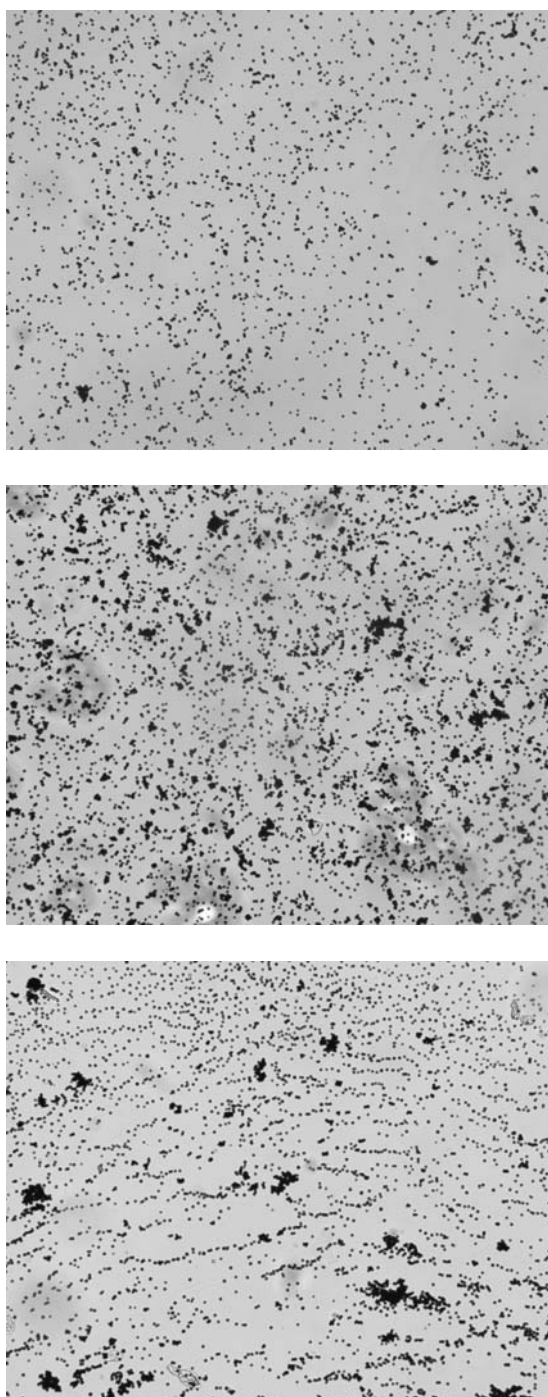


Figure 18 Patterned surface consisting of regions x and y, where x =NMe₃ and y = 50% NMe₃ 50% Me; pattern with added MUDA gold particles A); after agitation B); after sonication C).

Experiments were also performed on surface patterns consisting of areas of different chemical compositions. In these experiments areas of low adhesion were made more adhesive by adding 50 vol % trimethylamino propyl silane to the silane solution used to form the surface. This results in patterned surfaces which will have pull-off forces that

are closer together in magnitude than those already investigated. Figure 18 shows the results from these experiments. Again, upon adding the gold particles they adhere to the patterned surface where they land, giving the kinetic product as shown in Figure 18A. After agitation by hand the particles do not rearrange to form a pattern, as shown in Figure 18B. This may be because the pull-off forces are too similar and the agitation results in an approximately equal number of particles being removed from both adhesive areas. After sonication when large forces have been applied to the particles no pattern appears, as shown in Figure 18C. This is to be expected as the sonication results in a force which is larger than the pull-off force in both areas.

These experiments show that attractive electrostatic interactions can be used to control the position of particles on a surface if they are subjected to agitation of the correct strength. A gradient of interaction which changes from adhesive to more adhesive should lead to the migration of particles towards stronger adhesion.

If a chemical reaction could be used to alter adhesive regions into less adhesive regions, this interaction could be used to propel particles forward in an implementation of the theoretical design. But the particles would have to be pulled off the surface by some kind of agitation to allow them to migrate to areas of stronger adhesion. It is likely that this agitation would interfere with the distribution of the chemical species released by the motor particle making it of no use in implementing the theoretical design.

4.8 Summary and Conclusions

In this chapter electrostatic interactions have been investigated as a potential way to propel particles forward using surface interactions. Particle-surface interaction calculations were used to calculate the forces present between a charged surface and a small particle. It was identified that these interactions could be altered in a variety of ways but suggested that the best way to alter the interaction between particle and surface was to change the magnitude of surface charge. Calculations showed that the height above a surface at which a gold particle is positioned could be raised by 11nm by changing the surface charge from -30mV to -60mV. This would cause the particle to gain 15kT through gravitational potential energy.

Following the proposed route of altering the surface charge, different surfaces were created using the self-assembly of thiol molecules onto a gold surface. Investigation of the surface charges through the measurement of zeta potentials showed that surfaces had a variety of charges depending on the surface functionality. To convert a surface of low surface charge to one of high surface charge, it was suggested that a gold surface could be treated with mercaptoundecanoic acid or alternatively, a mercaptoundecanoic acid surface could have its surface charge increased by increasing the pH of the surrounding solution. In both cases it was measured that the surface charge would change by around 30mV.

To investigate if the proposed surface interactions would lead to the propulsion of small particles upon forming a surface interaction gradient, static gradients of these interactions were created in two ways:

Glass microscope slides were inclined at small angles to simulate the gradient of particle height created by the repulsive interactions. These were found to propel the particles forward at reasonable velocities, even when the angle of incline was of the order of a few degrees. The propulsion behaviour of particles was found to be described by a modified Svedburg equation, although observed velocities were only around a quarter of that predicted.

Very sharp static gradients of surface repulsion were created by patterning a surface using photolithography. Results showed that the patterned surfaces exhibited some control over the position of gold particles but this control was attributed to surface contamination rather than electrostatic interactions.

From these experiments it was concluded that electrostatic surface interactions could not control the position of particles repelled above them. So they could not be used to

drive particles forward through a surface gradient and are of no use in implementing the theoretical design.

Surface patterns of adhesion and repulsion, as well as patterns of adhesion-adhesion were also investigated. Both exhibited good control over particles using attractive electrostatic interactions and it was suggested that particles do migrate on surface gradients of repulsion to adhesion. On surface patterns of adhesion-adhesion, particles were able to migrate to areas of stronger surface interactions once agitation was applied, allowing the particles to break off the surface and move. But both of these gradients of surface interaction which include areas of adhesion are of no use in implementing the theoretical design. Gradients of repulsion to adhesion only allow particles to be propelled a small distance before they are irreversibly adhered to the surface. Gradients of adhesion to stronger adhesion are also of no use as agitation has to be applied to the surface to detach particles allowing them to move. It was proposed that this agitation would interfere with the distribution of the chemical species used to alter the surface interactions.

Overall, electrostatic interactions between particles and surfaces have been shown to be of little use in implementing the theoretical design. These negative results disagree with the positive results obtained from theory. These differences are probably due to real-life factors which are not considered in the theory, such as surface roughness and surface contamination, which alter the electrostatic interactions.

4.9 Experimental Details

Materials. All chemicals were purchased from Sigma-Aldrich and used as received except otherwise stated. Mercaptoundecanoic acid was purified by recrystallising from hot hexane. Aluminium spherical powder and Gold particles (3-5 μm) were purchased from Alfa Aesar and iron particles (2-3 μm) from PolySciences inc. Small gold particles (<1 μm) were purchased from Sigma-Aldrich.

Preparation of Silane Monolayers. Glass microscope slides were first cleaned by submersion in piranha solution for a few hours, followed by extensive rinsing with distilled water, and finally dried by placing in a hot oven for a few hours. These clean glass substrates were then functionalised with self-assembling silane monolayers by submersion in a 10 μM solution of either trichlorododecylsilane in dry toluene or a 10 μM solution of (3-aminopropyl) triethoxysilane in ethanol. After leaving the surfaces overnight they were then washed with an excess of the solvent used and dried under a stream of nitrogen gas. Surfaces of (3-aminopropyl) silane were converted to quaternised to create surfaces of trimethylamino propyl silane by submerging a 0.1M solution of methyl iodide in tetrahydrofuran overnight, then rinsed with an excess of ethanol and finally dried under a stream of nitrogen gas.

Monolayer quality was assessed by measuring the static contact angle of the surfaces with water.

Preparation of Gold Surfaces. Glass microscope slides were first cleaned by submersion in piranha solution for a few hours, followed by extensive rinsing with distilled water, and finally dried by placing in a hot oven for a few hours. These clean glass substrates were then placed in a thermal evaporator, a vacuum created giving a pressure typically lower than 10^{-6} Torr and then $\sim 5\text{nm}$ of chromium evaporated onto the surface to aid the binding of gold to the surface. Gold was then evaporated onto the surface to give a thickness of $\sim 15\text{nm}$. By evaporating a layer of metal onto the glass slide which is $<30\text{nm}$ allowed sufficient light to pass through the metal allowing diascopic lighting to be used when visualising the surface by optical microscopy.

Functionalisation of Gold Surfaces using Thiols. Gold surfaces were either used straight from the thermal evaporator or were otherwise cleaned by submersion in piranha solution for a few hours, followed by extensive rinsing and drying, before functionalising with thiols. A gold surface was introduced to a $\sim 10\mu\text{M}$ ethanoic solution of the desired thiol and left to self-assemble overnight before being rinsed with an excess of ethanol and dried under a stream of nitrogen. In this way gold surfaces were functionalised with

Mercaptoundecanoic acid, 4- or 2-mercaptovinyl pyridine, Mercaptoundecanol, Butane thiol or Octadecane thiol.

Photopatterning of Thiol or Silane Monolayer Surfaces. Electron microscopy grids were used as photolithography masks and were placed onto functionalised surfaces and weighed down using a small piece of quartz (2cm diameter x 0.2cm thickness). Surfaces were then exposed to a UV light source for 90 minutes, resulting in photo-oxidation in areas where UV light hit the surface. Surfaces were then rinsed with ethanol and dried using a stream of nitrogen. Static contact angle measurements on the surfaces with water showed that most of the thiol or silane monolayer is removed in the first 20 minutes of UV light exposure but that longer exposures of 90 minutes was required to remove the majority of the monolayer.

Observation of Aluminium, Gold or Iron Particles on Patterned and unpatterned Substrates. A small amount of the desired particles were dispersed in distilled water, then sonicated for one minute to aid dispersion. A drop of this solution was then sandwiched between a patterned substrate and a clean microscope slide using 0.1mm thick double-sided adhesive (Grace Bio-Labs). Particles on the substrate were then observed under a microscope (Nikon Ellipse ME2000) at 5x, 10x or 20x magnification using diascopic lighting. Movies of the motion were recorded using a Pixelink PL-A742 machine vision camera. The motion of particles was tracked after movie capture using a custom built LabView script which determined the position of particles in each frame of the movie.

Zeta Potential Measurements. Investigation of surface charge of thiol functionalised surfaces was investigated by measuring the zeta potential of small spherical gold particles. 1 μ m gold particles (Sigma-Aldrich) were functionalised by dispersion in a ~10 μ M ethanoic solution of the desired thiol, and stirred overnight. Particles were then purified by 5 repeat cycles of centrifuging, removing the supernatant, followed by redispersing in ethanol. Thiol functionalised particles were then dispersed in water adjusted to the correct pH using dilute solutions of hydrochloric acid or sodium hydroxide, and the zeta potential measured using Malvern ZetaSizer.

References

- (1) Zypman, F. R. *J. Phys.-Condes. Matter* **2006**, *18*, 2795-2803.
- (2) Hogg, R.; Healy, T. W.; Fuersten.Dw *Transactions of the Faraday Society* **1966**, *62*, 1638-&.
- (3) Bhattacharjee, S.; Elimelech, M. *J. Colloid Interface Sci.* **1997**, *193*, 273-285.
- (4) Dupin, D.; Fujii, S.; Armes, S. P.; Reeve, P.; Baxter, S. M. *Langmuir* **2006**, *22*, 3381-3387.
- (5) Israelachvili *Intermolecular & Surface Forces*; 2nd ed.; Academic Press.
- (6) Love, J. C.; Estroff, L. A.; Kriebel, J. K.; Nuzzo, R. G.; Whitesides, G. M. *Chemical Reviews* **2005**, *105*, 1103-1169.
- (7) Vezenov, D. V.; Noy, A.; Rozsnyai, L. F.; Lieber, C. M. *Journal of the American Chemical Society* **1997**, *119*, 2006-2015.
- (8) Yu, H. Z.; Xia, N.; Liu, Z. F. *Analytical Chemistry* **1999**, *71*, 1354-1358.
- (9) Bryant, M. A.; Crooks, R. M. *Langmuir* **1993**, *9*, 385-387.
- (10) Albert, A.; Barlin, G. B. *Journal of the Chemical Society* **1959**, 2384-2396.
- (11) Shyue, J. J.; De Guire, M. R. *Langmuir* **2004**, *20*, 8693-8698.
- (12) Abkarian, M.; Lartigue, C.; Viallat, A. *Phys. Rev. E* **2001**, *63*.
- (13) Brenner, H. *Chem. Eng. Sci.* **1961**, *16*, 242-251.
- (14) Goldman, A. J.; Cox, R. G.; Brenner, H. *Chem. Eng. Sci.* **1967**, *22*, 637-&.
- (15) Holmqvist, P.; Dhont, J. K. G.; Lang, P. R. *Physical Review E* **2006**, *74*.
- (16) Michailidou, V. N.; Petekidis, G.; Swan, J. W.; Brady, J. F. *Physical Review Letters* **2009**, *102*.
- (17) Faucheux, L. P.; Libchaber, A. J. *Physical Review E* **1994**, *49*, 5158-5163.
- (18) Hozumi, A.; Sugimura, H.; Yokogawa, Y.; Kameyama, T.; Takai, O. *Colloids and Surfaces a-Physicochemical and Engineering Aspects* **2001**, *182*, 257-261.
- (19) Giesbers, M.; Kleijn, J. M.; Stuart, M. A. C. *J. Colloid Interface Sci.* **2002**, *252*, 138-148.

5 Propulsion using Steric Interactions

5.1 Introduction

In this chapter implementations of the theoretical design shall be investigated which make use of the steric repulsions between two surfaces which are coated with a polymer brush. This will allow the interaction between a particle and a surface to be altered, and through creating of a gradient of this interaction, the particle to be propelled forwards.

Surfaces with attached polymer chains may be created in a variety of ways. For example a polymer can be adsorbed onto the surface from solution due to favourable interactions between the polymer and the surface. This leads to a polymer chain which is attached to the surface at a number of places and has loops of polymer between anchoring points. If two surfaces coated with adsorbed layers of polymer come into close proximity to each other, steric repulsions cause the surfaces to be repelled from each other. This has been extensively used to repel colloidal particles away from each other and prevent coagulation. If the surfaces are not completely saturated with adsorbed polymer, a single polymer chain can adsorb to both the surfaces bridging them together. This leads to an attraction between surfaces and can cause colloids to adhere to one another, known as *bridging flocculation*. Block copolymers can also be adsorbed onto the surface through favourable interactions with one block, which leaves the other block free to extend into solution while still tethered to the surface.

Alternatively, polymer chains can be adsorbed from solution and attached to the surface through a covalent bond. Commonly, polymer chains with terminal thiol groups are attached to gold surfaces or polymers with terminal silane groups attached to silica surfaces. This is known as the *grafting-to* approach¹. Polymer chains can also be grown from a surface functionalised with a polymerisation initiator².

The size of a polymer chain in a good solvent can be described by its radius of gyration as $R_g = aN^{3/5}$, where a is the size of a monomer unit and N the number of monomer units per polymer chain. When polymer chains are grafted to a surface and the distance between two chains is greater than the radius of gyration, they behave as isolated polymer

chains which are tethered to a surface. If however the distance between them is smaller than the radius of gyration, two or more polymer chains begin to come into contact and are forced to share the same volume. This results in the polymer chains being stretched in the direction perpendicular to the surface they are tethered to³. Now instead of an adsorbed polymer layer, the functionalised surface is known as a *polymer brush*.

Using Alexander – De Gennes theory, the force experienced between a small particle and a surface covered in a polymer brush due to steric repulsion can be calculated as^{4,5}:

$$\frac{F}{R} = \frac{16\pi kTL}{35s^3} \left[7\left(\frac{2L}{D}\right)^{5/4} + 5\left(\frac{D}{2L}\right)^{7/4} - 12 \right]$$

eq. 1

where R is the particle radius, S the average distance between polymer chains, D the separation between the two surfaces, L the brush thickness. This treatment is quite simplistic and does not take into account any charge on the polymer brush. More rigorous treatments have been developed⁶⁻⁸ but won't be used here.

From eq. 1 it is possible to see that the repulsive force that a small particle experiences depends only on the thickness of the polymer brush and the distance between polymer chains in the brush. Therefore to make use of polymer brushes in the theoretical design, one of these parameters will have to be changed via a chemical reaction.

Changing the grafting density from an initial high value to one lower could be readily achieved by the cleavage of covalent bonds holding polymer chains on the surface. But this would lower the repulsion experienced between a particle and surface, whereas the theoretical design requires the interaction to be made more repulsive i.e. increasing the grafting density. Increasing the grafting density would be difficult to achieve in practice and would have to make use of the grafting-from approach to grow extra polymer chains onto the surface, or the grafting-to approach to tether extra polymer chains to the surface.

It is therefore more desirable and synthetically more feasible to change the thickness of a polymer brush from an initially low value to a higher one. This can be achieved in a variety of ways such as changing the ionic strength or pH of the surrounding solution⁹ and will be discussed in more detail later in the chapter.

In this chapter, ways to create a particle and polymer brush surface which repel each other shall be investigated, followed by investigation if these repulsive interactions can control the position of a particle. Then chemical reactions which increase the height of a polymer brush shall be investigated and then finally ways to create potential motor particles which release a source of a surface-modifying chemical investigated.

5.2 Achieving Colloidal Stability on Polymer Brushes

For particles to be able to respond to gradients of steric repulsion created by a motor particle, both motor and target particles need to be repelled from the brush surface and have good colloidal stability towards coagulation between particle and brush surface.

Poly(dimethylamino ethyl methacrylate) (PDMA) brushes were created by surface-initiated Atom Transfer Radical Polymerisation, as explained in the experimental section of this chapter. Investigation of 4 μm gold particles and 20 μm silica particles as potential target or motor particles, revealed that they adhered to a PDEA brush surface and did not undergo Brownian motion. This is most likely caused by the negative surface charge of both gold (-35mV) and silica (-70mV)¹⁰, leading to a long ranged electrostatic attraction to the cationic PDMA surface. To achieve colloidal stability, the surfaces of gold and silica particles need to be altered so that they are cationic.

The following section describes how gold particles can be modified by polymer chains to become cationic and how silica particles can be modified by electrostatic self-assembly to become cationic. The colloidal stabilities of these resulting particles is then investigated.

Functionalisation of Gold Particles with PDMA-SH

Following a synthetic protocol by Rutland et al¹¹, dimethylamino ethyl methacrylate was polymerised using Reversible Addition Fragmentation Polymerisation (RAFT)^{12,13}. The ratio of chain transfer agent to radical initiator was increased from 2:1, which the authors found gave polydispersities of ~ 1.4 , to 5:1 as used by Armes et al¹⁴ for a similar monomer giving much better polydispersities. This protocol gave a polymer of 14,900g mol⁻¹, close to the targeted molecular weight of 15,700g mol⁻¹, a low polydispersity of 1.22 and a conversion greater than 95%.

The produced polymer had a terminal end group of dithio benzoate from the chain transfer agent used. This was converted to a thiol terminal end group by reduction using sodium borohydride, following a protocol by Summerlin et al¹⁵. This thiol terminated polymer was then used to modify the surface of 4 μm gold particles by mixing them together allowing a self assembled layer of poly(dimethylamino ethyl methacrylate) (PDMA) to form.

Smaller gold particles (500-1000nm) were also modified and used in analysis of zeta potentials of the modified surfaces. Before modification gold particles had a zeta

potential of -35mV and afterwards a zeta potential of +12mV at pH 7, indicating that the gold surface had been functionalised by the PDMA chains. A control experiment was carried out to determine if polymer chains could physically adsorb onto the gold surface and so if the thiol group was necessary, by mixing gold particles with PDMA without a thiol end group. Zeta potential measurements showed that without the terminal thiol group gold particles retained their original zeta potential of -35mV, indicating that the surface was unmodified and that the thiol group is necessary for modification.

Investigation of the modified gold particles on polymer brush surfaces showed that they sedimented onto the PDEA surface where they adhered to the surface and did not undergo Brownian motion. This result was unexpected as the steric forces generated between the two surfaces should repel the particle and surface apart. Inverting the brush surface so that it was upside down, revealed that the gold particles were adhered to the surface rather than simply in physical contact. Even at pH 3 where both the brush surface and the particle surface have a large cationic surface charge due to protonation of amine groups and so should strongly repel each other by electrostatic forces, gold particles did not undergo Brownian motion. Quaternisation of tertiary amine groups in the PDMA chains using methyl iodide gave particles with a permanent cationic surface charge (zeta potential = +30mV). These particles also adhered to the brush surface at all pH's.

Functionalisation of Silica Particles with Poly(ethylene imine) Hydrochloride by Electrostatic Self-assembly.

Silica particles (20 μ m) were investigated as particles which could possibly be used as the basis for a motor or target particle. As expected untreated silica particles adhered to polymer brush surfaces due to their opposite surface charge. Therefore particles were coated with a layer of oppositely charged poly(ethylene imine) through electrostatic self assembly¹⁶ in an attempt to make them cationically charged.

The created particles were unfortunately too large to have their zeta potential measured, as they sediment to the bottom of a dispersion very quickly. Investigation of the modified silica particles on polymer brushes showed that they did not adhere and were free to migrate from one area to another due to sedimentation or convection, thus confirming that they had been converted to cationic.

In this section particles have been created which are repelled away from a polymer brush surface and remain colloidally stable against surface coagulation. This will allow the particles to slide over the polymer brush surface, free of friction. These silica particles will form the basis of particles used for motor or target particles in the theoretical design.

5.3 Can Polymer Brushes Influence Small Particles?

To show that polymer brushes are able to repel small particles away from a surface and change the particle interaction from repulsive to more repulsive, gradients of surface repulsion were created. These were created by selectively patterning a surface with areas of polymer brush while leaving other areas unfunctionalised. This leads to a very sharp gradient of brush height at the interfaces of the pattern which mimics the desired gradient of surface interaction in the theoretical design.

By dispersing small particles on these patterned brush surfaces and observing if they are influenced by the surface repulsion gradients at the interfaces of the pattern, it should be possible to ascertain if steric interactions can be used in an implementation of the theoretical design.

Creating Patterned Polymer Brush Surfaces

To create surface patterns of polymer brushes photolithography was used to create a patterned initiator surface which was then amplified into a polymer brush by surface initiated Atom Transfer Radical Polymerisation (ATRP). The protocol is outlined in Figure 1 and full synthetic details of the preparation are given in the experimental section at the end of this chapter.

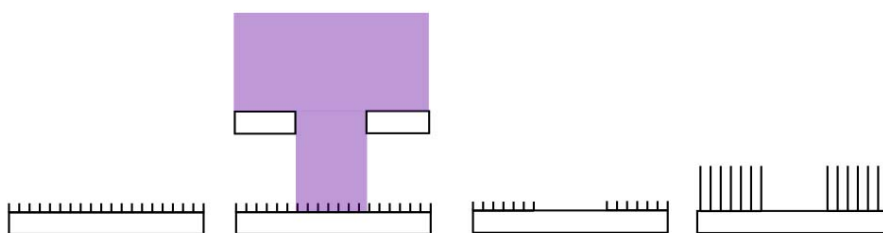


Figure 1 Preparation of patterned polymer brush surfaces. From the left: initiator monolayer formation on silicon; photopatterning; patterned initiator monolayer; amplification into polymer brush.

Two hours exposure time to the UV lamp was found to be optimal for the particular light source used. Surfaces functionalised with the silane initiator typically had a static contact angle with water of $\sim 90^\circ$, whereas after two hours exposure to the light source the

contact angle fell to $<10^\circ$ indicating that the hydrophobic silane monolayer had been removed exposing hydrophilic silanol groups. Passing water vapour over the patterned surface revealed a wetting pattern identical to the pattern of the photomask used.

This patterned silane initiator layer was then amplified into a patterned polymer brush surface by the growth of poly(*t*-butyl methacrylate) (PtBMA) via ATRP. In each polymerization reaction a reference surface containing an unpatterned ATRP initiator monolayer was included. This allowed determination of brush height by spectroscopic ellipsometry if it is assumed that brushes grow to the same height on both surfaces. After polymerization of *t*-butyl methacrylate, surfaces had brush thicknesses up to 100 nm depending on the amount of time allowed for polymerization. It was assumed that the grafting density of the polymer chains is high which leads to surfaces with tethered polymer chains which are stretched out to form a polymer brush rather than being in the mushroom regime. Parnell *et al*¹⁷ found a grafting density of 0.12 chains nm^{-1} using an identical initiator monolayer.

Hydrolysis of *t*-butyl methacrylate ester linkages using *p*-toluene sulfonic acid gave patterned polymer brushes of poly(methacrylic acid) (PMAA). Hydrolysis was confirmed by ellipsometric measurement of the dry brush height which reduced by around 60% suggesting that the polymer layer had lost volume due to the conversion of PtBMA to PMAA. Ellipsometric titration which showed the brush became pH responsive after hydrolysis with a pK_a of 6.9 (see later).

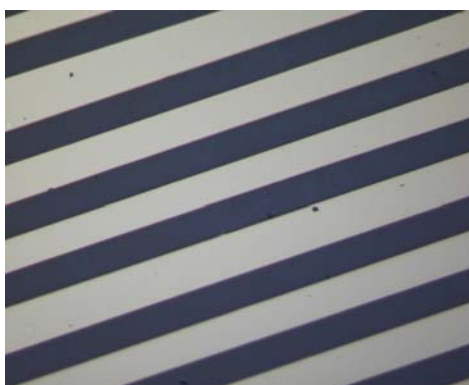


Figure 2 Optical micrograph of a patterned polymer brush surface.

Figure 2 shows an optical micrograph of a prepared patterned polymer brush of PMAA. Patterning of the surface can be clearly seen; dark blue regions are the polymer brush and white regions are due to the silicon surface. Interfaces between the two chemically

different regions look sharp and well defined which should produce well defined changes in particle interactions.

Controlling Particles which Undergo Brownian Motion

Following successful preparation of the patterned polymer-brush surfaces it was investigated if these surfaces can control the placement and motion of small particles which undergo Brownian motion in close proximity to the surface. Metal particles are much denser than water and sediment to a point above a surface at which their gravitational force (mg) is balanced by repulsive surface forces (electrostatic, steric or electro-steric) acting upwards. By functionalising the surface with a polymer brush it is possible to repel a dense metal particle further away from the surface causing it to gain gravitational potential energy (mgh), as shown in Figure 3. Therefore surface patterns of polymer brushes should result in patterns of particle energies. Metal particles will position themselves in the lowest energy areas where there isn't polymer brush and once inside these areas, particles which undergo Brownian motion shouldn't be able to escape providing the energy barrier due to the gain in height (mgh) is large enough.

Gold particles (3-5 μ m) dispersed in water at pH 10 were investigated as they underwent Brownian motion near to the patterned surfaces using optical microscopy. These particles are sufficiently large and dense enough that raising an individual particle by a small height results in a change in energy of the same order as the thermal energy kT . An often quoted number in sedimentation experiments is the height a particle has to be raised to increase its energy by the thermal energy kT , called the gravitational length. For the gold particles used, this is 0.7 nm, highlighting the fact that a gold particle only needs to be raised a few nanometres by a polymer brush to encounter a significant energy barrier. Conversely a polystyrene particle of the same size has a gravitational length of 250 nm and therefore needs to be raised significantly higher to result in a large change in energy.

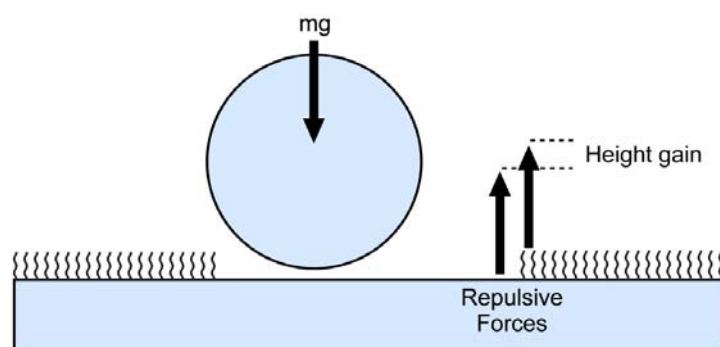


Figure 3 Schematic representation of a particle on a patterned polymer brush surface and the forces acting on the particle.

Observation of the gold particles showed that they sedimented onto the surface within a fraction of a second, where they adhered to the surface and did not undergo Brownian motion, remaining in the same position for the entire observation period (~20 minutes). This observation is surprising as it was expected that gold particles which are negatively charged due to the adsorption of hydroxide ions (Zeta potential = -37mV) and the surface which is also negatively charged due to the ionization of silanol groups or methacrylic acid (>99.9% at pH 10), to strongly repel each other and not come into contact^{18,19}. If the surface is inverted upside down, the gold particles remained on the surface showing that they are attached rather than simply in contact.

Iron particles (2-3 μ m diameter) were also investigated and although they are less dense than gold particles they are still dense enough to have a small gravitational length of 4-15 nm. Around half the particles showed similar behaviour to gold and adhered to the surface. The remaining half remained colloidally stable towards surface aggregation and diffused from one area to another due to Brownian motion. This colloidal instability was attributed to contamination of surfaces during synthesis or observation which lowers surface charge allowing particles to come into contact with the surface and can also tether a particle and surface together by bridging between the two surfaces, so called bridging flocculation. Polymer brushes have been reported to be highly resistant to adsorption of macromolecules and proteins²⁰ but in this case there seems to be some contamination of the surface leading to particles adhering to surfaces. Gold particles are possibly less colloidally stable towards surface aggregation than iron due to the higher mass of particles, which press particle and surface together with a force 21x larger than for iron.

Iron particles which did not become immobilized to the surface were repelled from the surface through a combination of electrostatic and steric forces. Their equilibrium height

above the surface is the point at which the repulsive surface force acting upwards is equal to the gravitational force (mg) acting downwards²¹. While in this energy minima above the surface, the particles are free to undergo Brownian motion while simultaneously translating along the surface to lower regions due to the surface not being precisely level.

Figure 4A shows trajectories of particles undergoing Brownian motion in close proximity to a patterned brush surface during 30 minutes of observation. The particles were free to migrate inside the squares of bare silicon (light areas) but could not pass onto the polymer brush layer surrounding the square (dark areas). To migrate outside the silicon square the particle must be raised above the polymer brush which acts as an electro-steric barrier repelling the particle upwards. In this way the position and motion of particles were precisely controlled by the polymer brush.

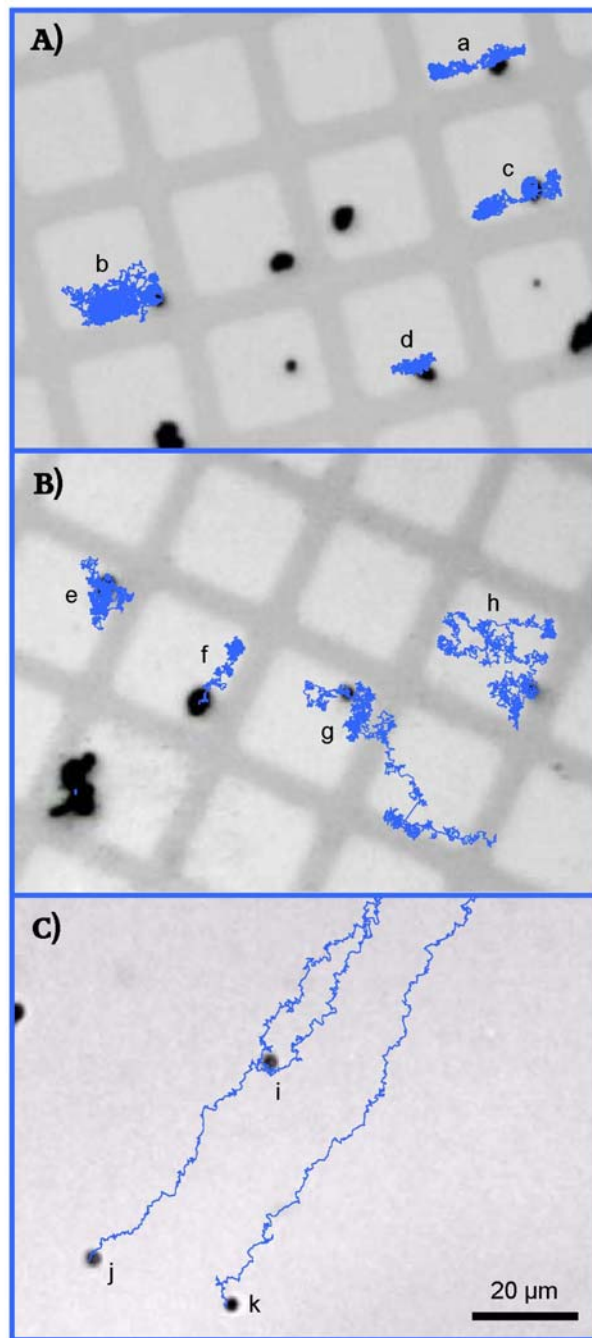


Figure 4 Trajectories of iron particles on a) 97 nm patterned brush, b) 39nm patterned brush, c) patterned silane monolayer

The poly(methacrylic acid) brush acts as a physical barrier repelling the dense particle ($\rho = 7874 \text{ kg m}^{-3}$) further away from the surface causing it to gain gravitational potential energy. For a $3\mu\text{m}$ diameter iron particle the gain in gravitational potential energy can be calculated as $\Delta E = mgh$. The height the particle has been repelled away from the surface h , is estimated to be equal to the measured ellipsometric brush thickness. This is a

valid estimation if the particle does not compress the polymer brush. Therefore $\Delta E = 20kT$ for the transfer of a $3\mu\text{m}$ iron particle from a silicon square onto a 97nm high brush. From a Boltzmann distribution of energies only $10^{-7}\%$ of $3\mu\text{m}$ particles have this energy at any one time and therefore most collisions between the particle and polymer brush result in repulsion back into the silicon squares and confinement of the particle. When in contact with the brush-boundary it can be calculated that iron particles collide with the polymer brush with a mean instantaneous velocity of $205\mu\text{m s}^{-1}$ using the equation $v = \sqrt{kT/\text{Mass}}$ ²², with a frequency of $70,042 \text{ s}^{-1}$ using the equation $n = v^2/4D$ ²², where v is the mean instantaneous velocity and D the diffusion coefficient. It is perhaps surprising that good control of particle motion can be achieved under these conditions especially as the height of the brush is so small – 5% of the particle diameter.

Figure 4B shows the trajectories of particles diffusing on a patterned polymer brush of smaller height (39nm) in which the energy barrier caused by the repulsion of the polymer brush is smaller at $8kT$. It can be seen that motion of the particles is strongly influenced by the brush and that particles remain inside the silicon squares for long periods of time. The two particles labelled *E* and *F* remain confined for the duration of the observation whereas particles *G* and *H* are confined and then escape from squares. This behaviour can be explained by the size distribution of iron particles ($2\text{-}3\mu\text{m}$) and the energy barrier being proportional to the particle radius cubed. $2\mu\text{m}$ particles experience only a small energy barrier of $2kT$ whereas larger $3\mu\text{m}$ particles experience a larger barrier of $8kT$. The diameter of particles which remain confined were measured as $E = 3.2\mu\text{m}$ and $F = 3.9\mu\text{m}$, and the two that escape as $G = 2.2\mu\text{m}$ and $H = 2.1\mu\text{m}$ as judged from the movie optical micrograph.

Figure 4C shows particle trajectories on a silane patterned surface without a polymer brush. It can be seen that the particles move a distance from top to bottom through a combination of diffusion and drift from sedimentation along the surface, which isn't precisely oriented in the horizontal plane. The angle of incline can be calculated from the modified Svedburg equation

$$\theta = \tan^{-1}\left(\frac{9\eta}{v2r^2(\rho_{particle} - \rho_{water})}\right)$$

to be small at 0.16° . It is also possible to see the effect of gravity in Figure 4A biasing particle positions to the lowest part of a square. The distance travelled by particles is large enough that several interfaces between bare silicon and the silane monolayer must have

been crossed without the particle being perturbed by the pattern. This control experiment shows that the confinement of particles observed in Figure 4A and the influence of particle motion in Figure 4B is caused by the polymer brush rather than the underlying silane pattern. Comparison of Figure 4A and B shows that the degree of particle control is influenced by the height of polymer brush and mass of iron particle, not by differences between silicon and PMAA.

Patterned surfaces of poly(methyl methacrylate) were also created which are insoluble in water, unlike the poly(methacrylic acid) brushes, and identical behaviour of iron particles was observed on these surfaces. This suggests that the identity of the polymer brush is not significant and simply acts as a physical barrier to the particle and neither is the modulus of the brush; poly(methyl methacrylate) is ‘hard’ like the silicon surface whereas solvated poly(methacrylic acid) is ‘soft’.

Analysis of particle motion by a custom built LabView script which finds the position of particles in each frame of the movie allows the mean-squared-displacement (MSD) of particles to be found. Following analysis by Bickel²³ it is expected that the diffusion behaviour of particles on patterned surfaces will follow Einstein’s equation $MSD = 4D\Delta t$ at short time scales, where they are unperturbed by the surface pattern, then at long time scales the MSD to plateau to $800\mu\text{m}^2$, as this is the largest dimension of the silicon box squared.

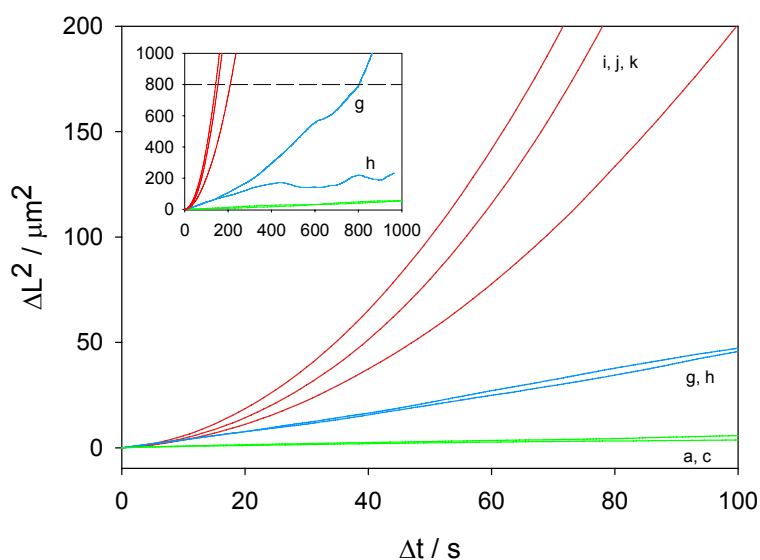


Figure 5 Mean-squared displacements of particles shown in Figure 4. Insert is at long time scales.

Figure 5 shows the mean-squared-displacement of particles in Figure 4 at short time scales (0 - 50 seconds). Particles *G* and *H* give a straight line indicating Brownian like diffusion from which a diffusion coefficient of $0.11\mu\text{m}^2\text{ s}^{-1}$ is found for both particles in close agreement to that calculated from the Stokes-Einstein equation of $0.15\mu\text{m}^2\text{ s}^{-1}$, considering the proximity of the surface which Faucheux and Libchaber²⁴ claim can reduce the diffusion coefficient by as much as 2/3. Whereas particles *I*, *J* and *K* give a curved MSD, characteristic of a particle undergoing a combination of Brownian motion and sedimentation at velocity v fitting the equation $\text{MSD} = 4Dt + (vt)^2$. As there is not a brush interface nearby to arrest their sedimentation, they can have large MSD's unlike on patterned surfaces. Particles *A* and *C* (shown) and *B*, *D*, *E* and *F* (not shown) have MSD's which give linear plots but which have a diffusion coefficient around 10x slower than that expected from the Stokes-Einstein equation. It is not clear why these particles diffuse so slowly but visual inspection of Figure 4 shows that these particles spend most of the observation period in close proximity to the brush interface which may hinder their diffusion.

The insert in Figure 5 shows the MSD calculated at much longer time intervals up to 1000 seconds. Computing the MSD for time scales as long as the experiments it is found that the MSD curves becomes noisy due to insufficient data points and observation time, even though data is based on an average of over 4600 data points taken over 30 minutes. A point of interest is that particles which appear to be confined by the square pattern in Figure 4 have an MSD which does not exceed the largest dimension of the silicon regions squared ($800\mu\text{m}^2$), whereas particles *G* and *I*, *J*, *K* have MSD's which exceed this distance, thus confirming the visual observation that the particles are confined to the inside of silicon squares.

Kim *et al*²⁵ studying the Brownian motion of less dense silica particles on topographically patterned silica surfaces, found the diffusion coefficient of particles at long time scales to be reduced by the energy barrier (ΔE) to $D = D_o \exp(-\Delta E)$. If this is also true in these experiments, diffusions coefficients at long time scales will be reduced 5 billion-fold.

Although calculated energy barriers of 20kT have been calculated for the thickest polymer brush by differences in ellipsometric height, they are only an estimate due to differences in the surface charge of silicon and poly(methacrylic acid). If the surface charge is greater on silicon, the difference in height will be smaller than expected and therefore also the energy barrier, conversely if the charge is lower on silicon, the difference in height and the energy barrier will be larger.

These experiments show that a small difference in the height at which a dense particle hovers above a surface can be created using polymer brushes and that this difference in height can be used to control the position of particles undergoing Brownian motion. When the energy barrier is small as in Figure 4B, particles can ‘hop’ over the interface by Brownian motion whereas if the energy barrier is larger as in Figure 4A particles are totally controlled by the polymer brush interfaces.

If one of these polymer brush interfaces could be caused to move along the surface by a chemical reaction, the positions in which particles can diffuse should also be moved along the surface leading to the desired propulsion of particles. The difference in energy between the two heights of the propagating polymer brush must be sufficiently high to prevent particles from hopping over the interface. Although conversely when the difference in height is small and particles can diffuse over the interface after a certain amount of time, interesting behaviour may be observed. This may lead to behaviour in which the particle is propelled by the surface wave, then diffuses over the interface and ceases to be propelled, followed by the surface gradient being re-established and propulsion being resumed. This method of propulsion would be synonymous with that of bacteria which propel themselves using a ‘run and tumble’ strategy.

Controlling Particles which are Propelled along Patterned Surfaces

Following the successful control of particles which undergo Brownian motion by patterned surfaces, the behaviour of larger 20 μm silica particles whose motion is not dominated by Brownian motion was investigated. As the particles do not migrate very far by Brownian motion it was necessary to move them across the surface so that they came into contact with the polymer brush interfaces. Being denser than water, silica particles sediment downwards to a position close to the patterned surface, where the gravitational force acting downwards is balanced by the electrostatic or electrosteric forces acting upwards. By inclining the substrate to the angle θ from the horizontal (see Figure 6), particles can be driven across the surface by a combination of the gravitational force and the surface repulsions which act perpendicular to the inclined surface.

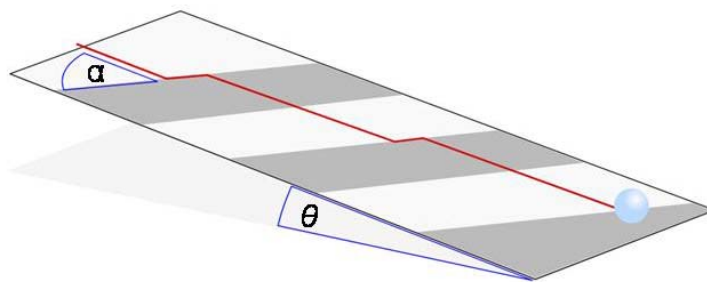


Figure 6 Schematic representation of a silica particle sedimenting across a patterned polymer brush surface.

In the following experiments an inclination angle of $\theta = 4.5^\circ$ was chosen, which, following analysis of particle trajectories by a custom made LabView script, propelled the silica particles at a uniform velocity of $\sim 2 \mu\text{m s}^{-1}$ down the sloped surface. This velocity is surprisingly slow, only $\sim 10\%$ of the velocity predicted by the modified Svedberg equation $\frac{2r^2(\rho_{\text{Silica}} - \rho_{\text{H}_2\text{O}})g}{9\eta} \tan \theta$. Even taking into account the proximity of the substrate to the particle which Goldmann *et al*²⁶ have predicted can increase the viscous drag on a spherical particle by a factor of 3, particles are still only driven along the surface at around half the predicted velocity. A considerable amount of research has gone into the study of friction on polymer brushes^{11,27} which could explain the slow motion, although it is not expected that the particle and brush will come into contact, instead they should remain separated by electrostatic repulsion.

While being driven across the patterned substrate particles travel from areas of bare silicon to areas of poly(methacrylic acid) (PMAA) functionalised silicon and vice versa. The angle α is defined as the angle between the direction in which particles are driven along the substrate due to sedimentation and the orientation of pattern interfaces. Figure 7 shows the trajectories of silica particles driven across a patterned substrate with different angles of incidence α , at pH 10. Three different behaviours result depending on this angle.

When the angle α is large as in Figure 7 top, $\alpha = 82^\circ$, the particle travels over both the silicon-to-brush and brush-to-silicon interface relatively unperturbed. This type of behaviour can be called *Non-compliant* (N), as the particle does not follow the brush pattern. The particle velocity remains constant on passing over both interfaces neither speeding up or slowing down.

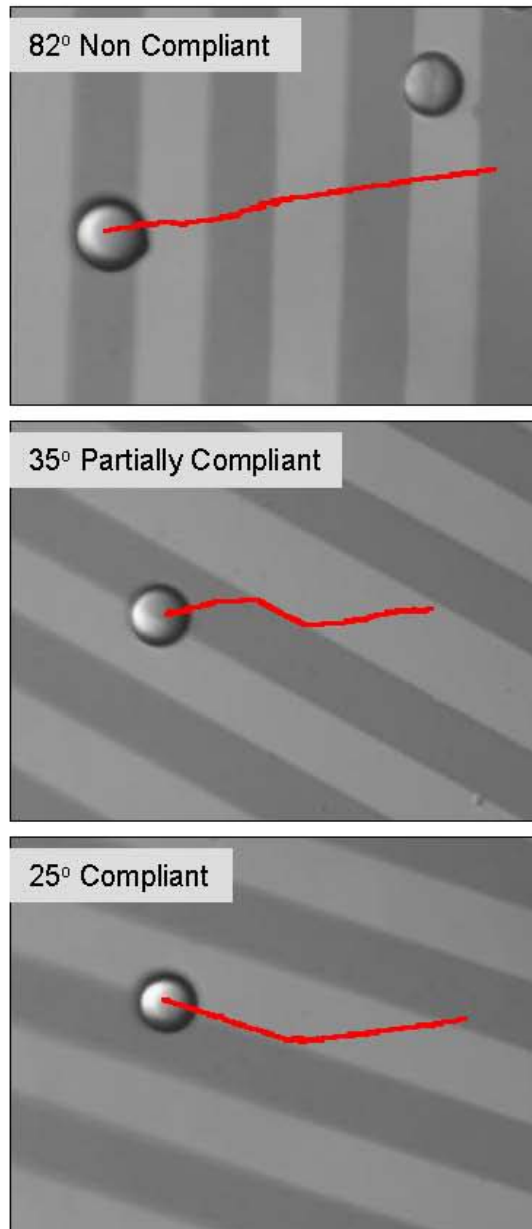


Figure 7 Trajectories of silica particles sedimenting across patterned PMAA brush substrates at different angles of incidence. Top 82° , middle 35° , bottom 25° .

When α is smaller as in Figure 7 middle, $\alpha = 35^\circ$, the behaviour changes and the particle is perturbed by the patterned substrate. The particle sediments across the silicon surface in the direction of gravity until its centre reaches the brush interface, at which point its motion is deflected to follow the direction of the interface. After sliding along the interface for some distance, motion is resumed in a direction parallel its original course of motion. Upon reaching the opposite side of the parallel bar pattern, the particle travels

over the brush-to-silicon surface unperturbed. This type of behaviour can be called *Partially Compliant (P)*.

When α is small as in Figure 7 bottom, $\alpha = 25^\circ$, particle behaviour changes once again. Now particles travel along the silicon surface in the direction of gravity until their centre-point meets the brush interface, at which point they change direction and sediment in the direction of the brush interface. Unlike at larger angles they do not pass over the interface after a certain distance but instead continue to sediment along the same interface. This type of behaviour could be called *Compliant (C)*.

The behaviour of silica particles sedimenting along patterned surfaces at different angles of incidence is summarised in Figure 8. At small angles the behaviour is wholly Compliant, and at large angles wholly Non-compliant, and between these two regimes is Partially Compliant behaviour. The cross-over between these behaviours are not well defined and two different behaviours occurring at the same angle has been observed, which can be attributed to differences between individual particles and also the brush height at different positions on the surface. Whilst the difference between compliant and non-compliant behaviour is instantly obvious, this is not the case for partially compliant and compliant behaviour. Particles may travel a large distance along the interface before passing over and resuming their original course, meaning that many particles which were thought to be compliant are actually partially compliant.

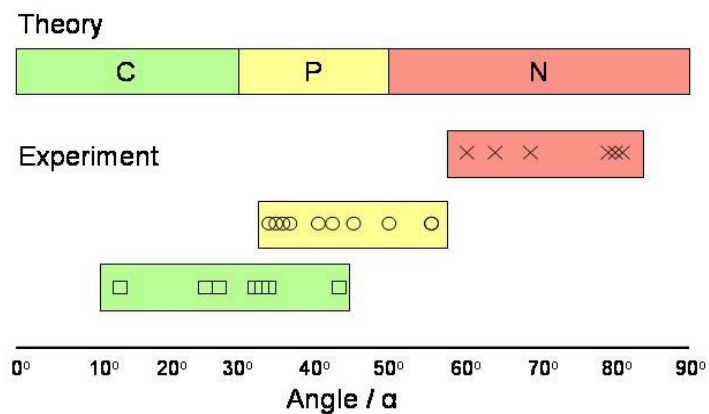


Figure 8 Behaviour of Silica particles at different angles of incidence α . See text for explanation of theory. Green – compliant (C), Yellow – partially-compliant (P), Red – non-compliant (N).

The three different behaviours of silica particles observed can be explained by calculating the forces exerted on a silica particle undergoing sedimentation across a

patterned surface. Taking a classical mechanics approach which treats the polymer brush as an incompressible slab, rather than invoking a more complex polymer physics approach, provides useful results. Gravity and the electrostatic repulsion from the inclined silicon surface result in the force F' , which pushes particles down the surface towards the silicon-brush interface (from left to right in Figure 9). Resolving the force F' so that it is perpendicular to the brush interface gives a force, F . Gravity and the electrosteric repulsion from the PMAA brush result in the force f , which pushes particles away from the silicon-brush interface, in a direction anti-parallel to the force F (see Figure 9). A full derivation of these forces using trigonometry is given in appendix 1.

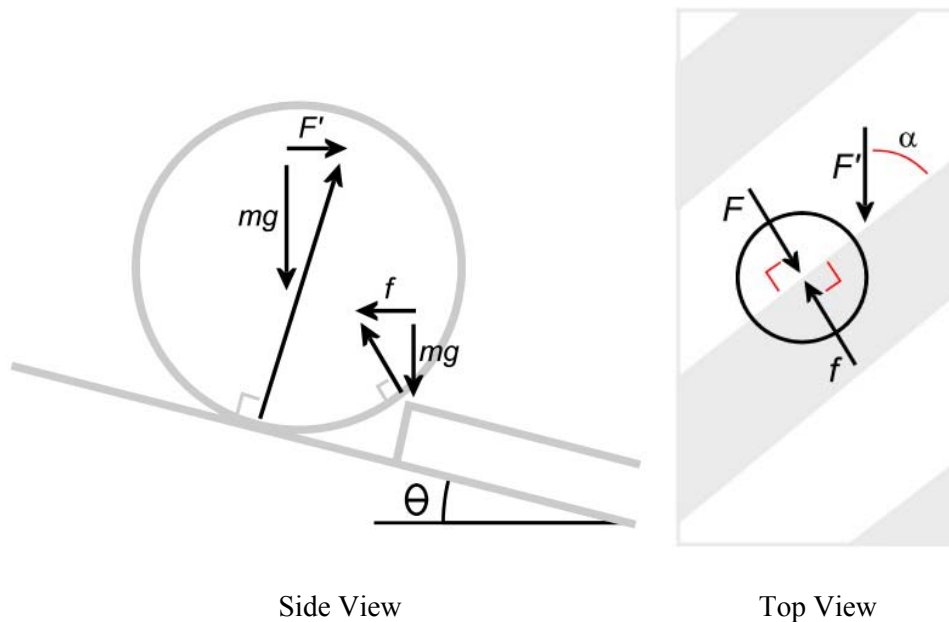


Figure 9 Schematic representation the forces F and f acting on a silica particle which has sedimented along the patterned surface to come into contact with the brush interface.

Comparison of these two forces rationalises the observed behaviour. At large α angles F is larger than f , so particles are forced over the silicon-brush interface onto the polymer brush, resulting in Non-compliant behaviour. At $\alpha = 90^\circ$, F is 3.2 pN and 1.5x larger than f which is 2.1 pN. At small α angles F is smaller than f , meaning that particles cannot pass over the silicon-brush interface and must sediment without crossing the interface resulting in Compliant behaviour.

The angles at which Partially compliant behaviour is observed coincides well with the angle at which F is approximately equal to f . Between $\alpha = 30-50^\circ$, F / f is 0.9-1.1 and experimental results show that partially-compliant behaviour occurs around the same

angles, between 30° and 60° . If the polymer brush was highly regular and of uniform height all over the surface, this behaviour regime would not exist – Compliant behaviour would change directly to Non compliant as F becomes larger than f . Therefore the observed behaviour can be attributed to defects or inhomogeneity in the polymer brush height over the surface. This variation in height will cause f to be smaller than the mean value and allow particles to pass over interfaces giving partially-compliant behaviour, rather than the expected compliant behaviour. At small angles where F is small, the variation in height needed to allow a particle to pass over an interface is large, whereas at large angles where F is large, the variation needed in height is small.

It is expected that defects in the brush surface cause a reduction in height and these defects have a distribution of sizes. Consistent with this hypothesis, the distance particles travel along the interface before reaching a defect large enough to allow them to pass over the interface increases as the angle increases. As shown in Figure 10, the distance a particle slides along the interface before passing over it is $0\mu\text{m}$ at angles larger than $\sim 60^\circ$, consistent with non-compliant behaviour, then increases as the angle of incidence, and so the force F is reduced, up to a point at around $\sim 30^\circ$ where the particles slide indefinitely along the brush interface giving compliant behaviour.

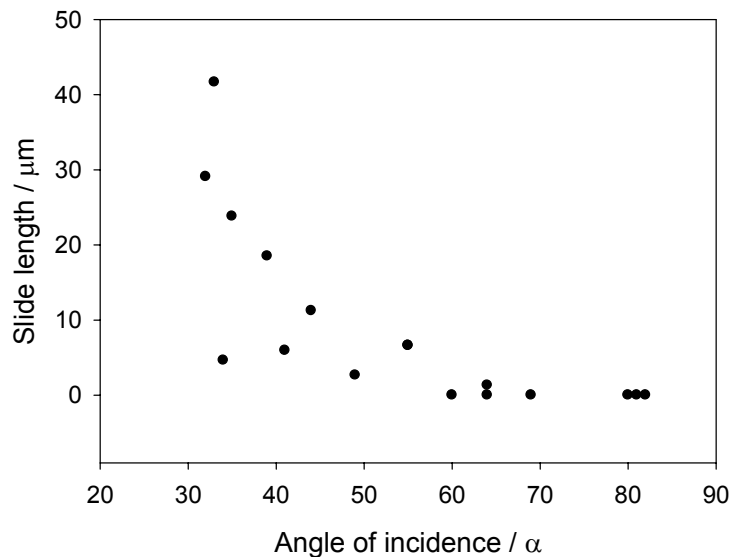


Figure 10 The length silica particles slide along a brush interface before resuming their original course of motion at different angles of incidence. Data is shown for particles which give partially compliant and non compliant behaviour.

Partially compliant behaviour also appears to occur at larger angles than expected, which could be caused by a polymer brush height which is larger than anticipated.

Ellipsometry has been used to measure the brush height but the true brush height may be slightly thicker due to the top of the polymer brush having a low segment density and therefore only a small difference in refractive index which is undetected by the polarised light of the ellipsometer.

The hypothesis that Brownian diffusion is the cause of partial compliance can be discounted by comparing this experiment with the previous on small particles diffusing over a polymer brush interface. In that experiment, the energy barrier was a few kT . In this current work, the much larger silica particles, which slide along a silicon-brush interface do not diffuse over the interface because the energy barrier is much larger at $700kT$ and the diffusion coefficient of $20\mu\text{m}$ silica particles is much smaller, meaning that there is a very small probability of particles diffusing over the interface. Also particles do not diffuse over the silicon-brush interface when they show compliant behaviour, which they should if diffusion was the explanation to this behaviour.

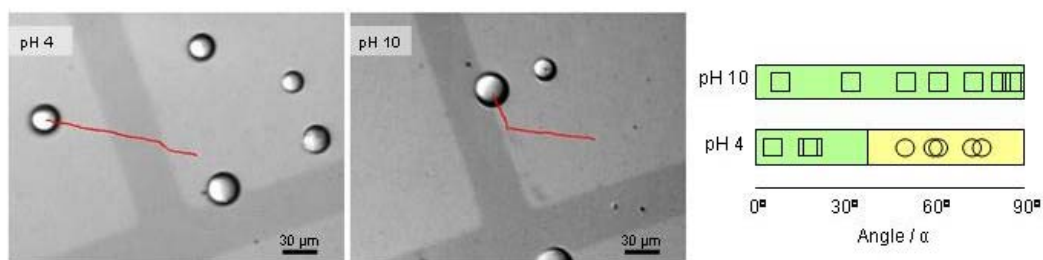


Figure 11 Behaviour of silica particles at pH 4 (left) and pH 10 (middle) with an angle of incidence 63° in both cases. Right - Behaviour of particles at different angles of incidence, squares indicate compliant behaviour and circles partially compliant behaviour.

Poly(methacrylic acid) brushes are pH responsive meaning that brush thickness increases with the degree of ionisation of the methacrylic acid groups (see Figure 11). The behaviour of particles on patterned substrates at different pH values has been investigated. Figure 11 shows two silica particles which sediment across a patterned surface at pH 4 and 10, in both cases the angle of incidence was 63° . At pH 4 methacrylic acid groups in PMAA are mostly protonated and so the polymer brush is mostly uncharged and collapses to 75 nm in height. Under these conditions silica particles show partially compliant behaviour. At pH 10 methacrylic acid groups are mostly deprotonated and the brush swells to 116 nm and is highly charged. Now under these conditions, particles show compliant behaviour. This interesting pH dependant behaviour is potentially useful in creating ‘valves’ which divert the flow of particles depending on pH.

It was also observed that silica particles are much less colloiddally stable at pH 4 than pH 10 and are prone to adhering to both the silicon and PMAA surfaces. This seems reasonable considering the isoelectric point of silica is pH 3, meaning that the surface has only a small surface charge at pH 4 and that the PMAA brush is not ionised at pH 4 nor can it selectively adsorb ions from solution as an insoluble polymer brush can¹⁹. It should be noted that study of the surface forces between a similar polyacid covered surface and silica spheres showed only repulsive interactions at all pH values²⁸ whereas in these experiments silica particles adhered to brush surfaces.

It was observed that particles sometimes slide along the silicon surface into the silicon-brush interface and then are immobilised by adhering to PMAA. This mostly occurred at pH 4 at large angles of incidence where the forces pressing particle and surface together are large and the colloidal stability poor due to the low surface charge. This is also potentially useful for creating 'gates' which decide if particles are allowed to pass depending on the solution pH.

It has also been observed that patterned poly(methacrylic acid) brushes are capable of assembling particles into clusters or lines as they sediment along an interface. Figure 12 shows the edge of a patterned surface in which particles have sedimented along a brush interface by compliant behaviour to the edge of the pattern where they encounter a corner in the pattern (the light areas are the wells). The corner traps the particle as the force F , is smaller than f . Other particles then sediment along the same interface and collide with the first trapped particle, transferring their gravitational force F through the line of particles formed to the corner interface. In this fashion the force pushing the first particle towards the brush can be multiples of F .

In Figure 12a two particles have sedimented into a corner where they remain trapped as F is smaller than f . Two further particles then sediment into the corner increasing F to become larger than f (Figure 12b). Following a rearrangement of the particles, one of them is ejected from the corner over the interface, which reduces the force F acting on the corner particle to be less than f . Now the remaining three particles are trapped in the corner once again. As two or three particles always remain at the corner it is possible to say that f is between 3 and 4 times the size of F . In this way, patterned polymer brush surfaces can act as particle assemblers, directing particles of an initially random distribution to specific locations and assemble them into microstructures such as lines or clusters. The patterned surface acts as a microbalance, measuring the forces exerted on the polymer brush interface; the force exerted on the interface is small at around 3.2 pN.

The patterned surface could also be considered to be a *Boolean operator* for the function *greater than*, as the patterned surface measures if F is greater than f and either

traps particles or allows them to pass depending on the outcome of this inequality. By trapping particles in a corner the brush maintains a fixed number of particles at a specific location also highly useful in the fields of microfluidics.

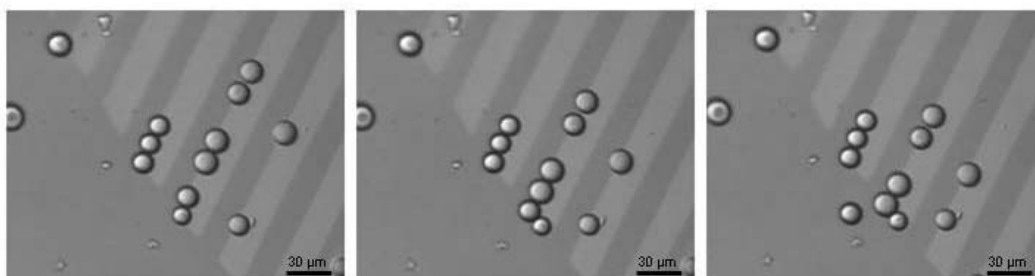


Figure 12 Three sequential micrographs showing the behaviour of silica particles at the corners of the grid pattern.

Finally it was investigated how particles behave on the patterned surfaces when propelled along by a flow of water rather than gravity, as would be the case if the surfaces were used in a microfluidic device. Under these conditions the particles show Non compliant behaviour and pass over the silicon-brush interface unperturbed at all angles. The behaviour is the same at all flow rates including one which propels particles at the same velocity at which they are propelled by sedimentation along a sloped surface. This difference in behaviour was attributed to the flow-streamlines of the water over the corrugated surface; at the interfaces the flow of water is not parallel to the silicon surface giving a lift force which pushes particles over the interfaces even when F is smaller than f . This result is somewhat disappointing considering the rapidly expanding field of microfluidics and the need to manipulate small particles in these devices.

Summary of Controlling Particles using Steric Forces

Patterned surfaces of polymer brushes were successfully prepared using photolithography allowing the creation of very short, sharp gradients of brush repulsion from the surface. It was shown through the investigation of the Brownian motion of small particles on these prepared surfaces that they could influence and control where a particle could move. For the surfaces to be able to control the motion of particles well, the difference in height of the polymer brush and silicon surface needed to be moderately

large to give a large difference in gravitational potential energy between the two surfaces. It was also found that particles could ‘hop’ over a brush interface if the difference in height was small.

It was also shown that patterned surfaces can control larger particles which do not undergo Brownian motion to any appreciable extent. Although now it is surface repulsion at the brush interface rather than the difference in gravitational potential energy which leads to particle control. It was shown that ‘gates’ or ‘valves’ could be created making use of the pH response of PMAA chains.

From the experiments shown in this section it has been shown that a particle can be controlled by repulsive surface interactions. From this it can be stated that a polymer brush surface should be capable of propelling a particle across its surface; if the position of a brush interface could be moved, the position of particles around it would also have to move, leading to propulsion of the particles. Methods to move the location of a surface repulsion gradient by altering brush height, shall be investigated in the next section.

5.4 Altering the Thickness of a Polymer Brush by pH

In the previous sections it has been shown that polymer brushes can control the placement and motion of particles by repelling them away from a surface causing them to gain gravitational potential energy. Therefore if the surface pattern could change over time, it should be possible to propel a particle across a brush surface away from an area of high repulsion to an area of lower surface repulsion. To achieve this, a surface repulsion gradient must be created by a chemical reaction, which either increases the height of a polymer brush or creates a polymer brush on the surface.

Changing the repulsion experienced by a particle from a polymer brush by changing the pH of the surrounding shall therefore be investigated in this section.

Swelling Polymer Brushes by Chemical Modification

Uncharged non-ionic polymer chains may adsorb water into their polymer matrix due to energetically favourable enthalpic interactions between a water molecule and a polymer segment²⁹, causing the polymer chains' occupied volume to swell and increase. This swelling due to favourable enthalpic interactions is counterbalanced by the energetically unfavourable stretching of polymer chains, which limits the increase in volume. In polymer chains which are charged due to the dissociation of functional groups, extra water can be accommodated into the polymer matrix due to the entropically favourable hydration of ion pairs and the increased ionic strength inside the matrix which causes an osmotic pressure into the brush layer³⁰. Therefore converting an initially non-ionic or neutral polymer chain to a charged ionic polymer chain leads to an increase in volume of the polymer and brush thickness.

Conversion of a neutral polymer chain to a charged polymer chain can be achieved by the reversible protonation or deprotonation of weak acid or weak base groups within a polymer chain. This strategy is taken in this section where polymer chains of poly(methacrylic acid) and poly(diethylamino ethyl methacrylate) are exposed to solutions of different pH. Polymer chains can also be chemically converted to become charged by an irreversible chemical reaction such as the quaternisation of poly(diethylamino ethyl methacrylate) using methyl iodide which will also be investigated.

Strategies such as these have been used to create polymer hydrogels which exhibit large changes in their volume in response to changes in pH as the polymer chains become

ionised³¹. Others have made use of these changes in volume to create objects capable of performing useful tasks such as converting chemical energy to mechanical actuation³²⁻³⁴.

5.4.1 Swelling by Deprotonation of Polyacid Brushes

Poly(methacrylic acid) can be deprotonated by the addition of a base such as sodium hydroxide as shown in Figure 13 schematically. This changes a neutral polymer chain to a strongly charged anionic polymer chain and an increase in the amount of counterions and water in the brush layer.

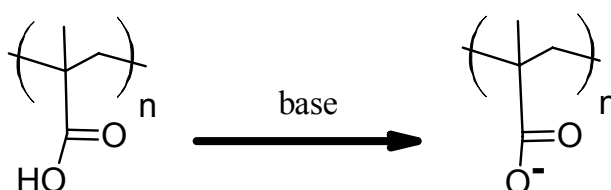


Figure 13 Deprotonation of neutral poly(methacrylic acid) leading to an anionically charged polymer chain.

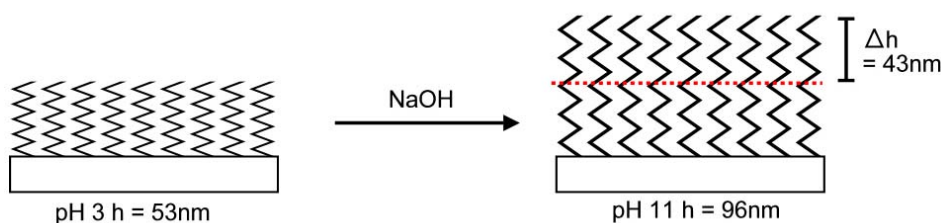


Figure 14 Schematic of poly(methacrylic acid) brush swelling in response to the addition of sodium hydroxide as the pH is changed from 3 to 11.

Figure 14 depicts results showing how the height of a PMAA brush changes upon addition of sodium hydroxide. At pH 3 a typical PMAA brush had a height of 53nm as measured by spectroscopic ellipsometry. At this low pH value, carboxylic acid groups in the PMAA brush are mostly protonated and so polymer chains are mostly un-ionised. Upon increasing the pH of the surrounding liquid by the addition of sodium hydroxide, the fraction of carboxylic acid groups that are deprotonated in the polymer chains gradually increases leading to an increase in the brush height. At pH 11 the height of the

polymer brush increased to 96nm. This gives an increase in height of the polymer brush on changing the pH of $\Delta h = 43\text{nm}$.

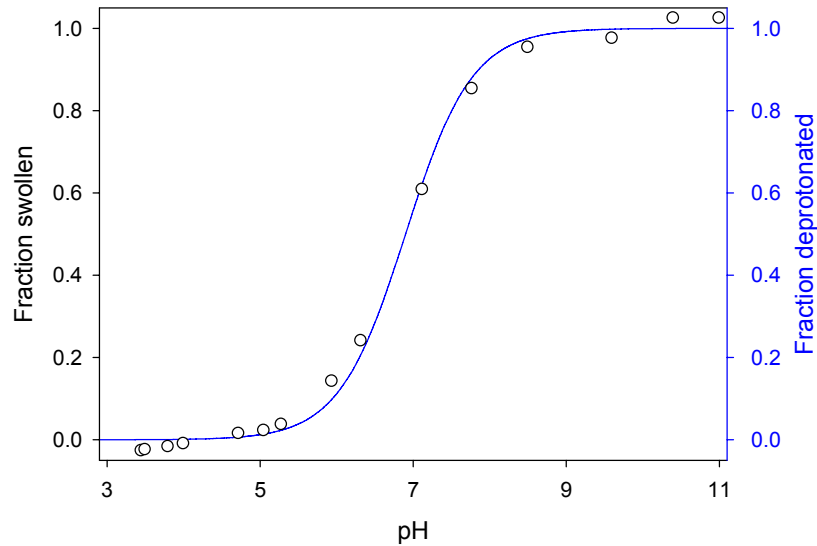


Figure 15 Fraction of a PMAA brush swollen vs. pH studied using HCl / NaOH by spectroscopic ellipsometry. The blue line is the fraction of carboxylic acid groups deprotonated based on a pK_a of 6.9 .

The extent to which the polymer brush is swollen can be defined by a fraction of swelling, given by:

$$\text{Fraction swollen} = \frac{h_{pH} - h_{\min}}{h_{\max} - h_{\min}} \quad \text{eq. 2}$$

where h_{pH} is the height or thickness of the polymer brush at a particular pH, h_{\min} is the lowest height of the polymer brush found over the pH range and h_{\max} is the largest height of the polymer brush over the pH range.

To investigate how the height of a polymer brush changes with pH of the surrounding liquid, an ellipsometric titration was performed on a typical PMAA brush. Figure 15 shows the fraction swollen of a poly(methacrylic acid) brush over a range of pH values obtained by the ellipsometric titration. The brush was introduced to a liquid cell initially at pH ~3, allowed to reach equilibrium over 15 minutes and the brush height measured. Then drops of sodium hydroxide solution were added to increase the pH, the brush allowed to reach equilibrium again and the height was measured.

As already stated, the brush height changes from 53nm at pH 3 to 96nm at pH 11 due to the ionisation of carboxylic acid groups in the polymer chains. The transition is most pronounced around pH 7 close to the expected pK_a of 5.5-6³⁵.

Figure 15 also shows that the brush height can only be changed significantly by altering the pH close to the pK_a of the polymer chains. For example changing the pH from 3 to 5 doesn't significantly alter the fraction of the brush which is swollen, whereas altering the pH from 6 to 8 drastically changes the fraction swollen of the polymer brush.

When data in Figure 15 is fitted with the fraction of PMAA deprotonated (ionised) using the equation:

$$\text{Fraction Deprotonated} = \frac{10^{pH - pK_a}}{10^{pH - pK_a} + 1} \quad \text{eq. 3}$$

a good fit is achieved using a pK_a of 6.9 . Showing that the fraction of brush swollen is directly related to the fraction of the polymer chain which is deprotonated and so charged. Conveniently the pK_a of the brush is close to pH 7, meaning that the amount of sodium hydroxide that needs to be added to the solution surrounding the brush to alter the fraction of brush swelling is small.

For example to change the fraction of swelling from 0.1 to 0.9 by altering the pH from 6 to 8 requires $9.9 \times 10^{-7} \text{ mol dm}^{-3}$ of sodium hydroxide to be added. Whereas if the pK_a of the polymer brush was lower at $pK_a = 2$, to achieving the same change in the fraction swollen of the brush, the pH would have to be changed from pH 2 to 4, requiring an addition of $9.9 \times 10^{-3} \text{ mol dm}^{-3} \text{ NaOH}$, 10,000x more than when the pK_a is 6.9 .

The pH response highlighted above could be used to propel particles across a surface. If a motor particle could be created which releases sodium hydroxide, this particle could swell a polymer brush under a target particle from 53nm to 96nm, a difference in height of $\Delta h = 43\text{nm}$. If the target particle was constructed of a dense material such as gold of diameter $4\mu\text{m}$, swelling the brush would cause the particle to be raised by 43nm and gain gravitational potential energy (mgh) of 62 kT. If the motor particle could create a linear gradient of deprotonation over a length the same as the target particle's diameter, this would result in a propulsive force of 0.13 pN, enough to propel the particle forward through solution at a velocity of $3.8\mu\text{m s}^{-1}$.

To create this gradient of surface repulsions, the motor particle must release a base such as sodium hydroxide. This can be either from a source of base stored inside the particle or by generating base via a chemical reaction catalysed by the motor particle.

5.4.2 Swelling by Protonation of Polybase Brushes

In direct contrast to polymer brushes containing weak acid groups, polymer brushes containing weak base groups swell at low pH and collapse to a smaller height at high pH, due to the protonation / deprotonation of tertiary amine groups as shown schematically in Figure 16.

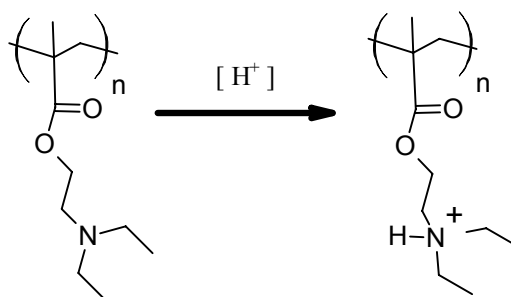


Figure 16 Protonation of poly(diethylamino ethyl methacrylate) polymer chains leading to the formation of cationic polymer chains by the addition of acid.

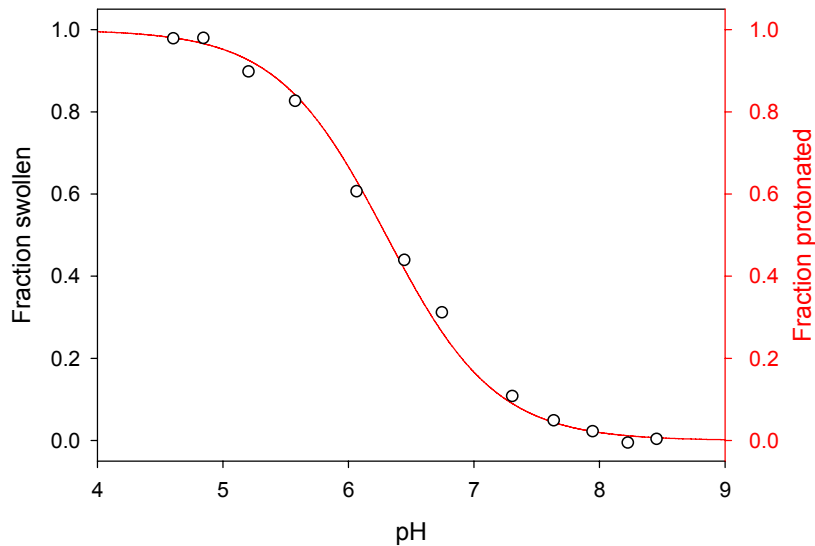


Figure 17 Fraction of a PDEA brush swollen vs. pH studied using HCl / NaCl by spectroscopic ellipsometry. The red line is the fraction of amine groups protonated based on a pK_a of 6.3 .

Figure 17 shows the calculated fraction swollen of a poly(diethylamino ethyl methacrylate) (PDEA) using eq. 2, at different pH values. As with PMAA brushes the results are fitted well by the fraction ionised (protonated) using a pK_a of 6.3 (Fraction protonated = 1 – fraction deprotonated). Armes et al³⁶ found a pK_a of 7.3 for a PDEA homopolymer by titration, which is one pH unit higher than the pK_a measured in these experiments. This is possibly due to confinement of polymer chains in the polymer brush which makes it more difficult to ionise (protonate) a polymer chain, thus requiring a higher concentration of acid.

Data in Figure 17 was obtained from a polymer brush of smaller thickness (24nm at pH 8.5) than the PMAA brushes investigated, which gave a smaller increase in height of $\Delta h = 10\text{nm}$. This height increase would lead to an increase in the gravitational potential energy of a $4\mu\text{m}$ gold particle of $\Delta E = 14kT$. Investigation of thicker PDEA brushes should yield larger increases in height (Δh) but these brushes gave ellipsometric data which could not be fitted with a model and so the height of the polymer brush could not be inferred from the model fitting of the data. It is not known why the model did not fit these data. Adding extra Cauchy layers, grading the layer or adding surface roughness did not improve the fit.

5.4.3 Kinetic Investigation of PDEA Brushes Swollen by Acid

It is important to find out how quickly a polymer brush can respond to changes in pH to ascertain if the response will be of use in implementing the theoretical design. Ideally the brush should change relatively quickly to create fast propulsion. If the change requires a significant amount of time particles may move away from the brush area being modified by the chemical reaction, either by Brownian motion if the particles are relatively small or by sedimentation if they are larger.

To investigate the response of a polymer brush to a stimulus of acid, kinetic ellipsometry was used. A PDEA brush initially surrounded by water at pH 8 had an amount of hydrochloric acid added at $t = 0$ sec and ellipsometric data captured every 3 seconds. Depending on the amount of acid added, the pH of the solution changed from 8 to either 4, 3.7 or 3.4. A thick polymer brush was used as the change in height Δh is greatest for a thicker brush, but this meant that ellipsometric data could not be fitted with a Cauchy layer model as already discussed above. Therefore the raw data captured has been used to investigate brush swelling kinetics.

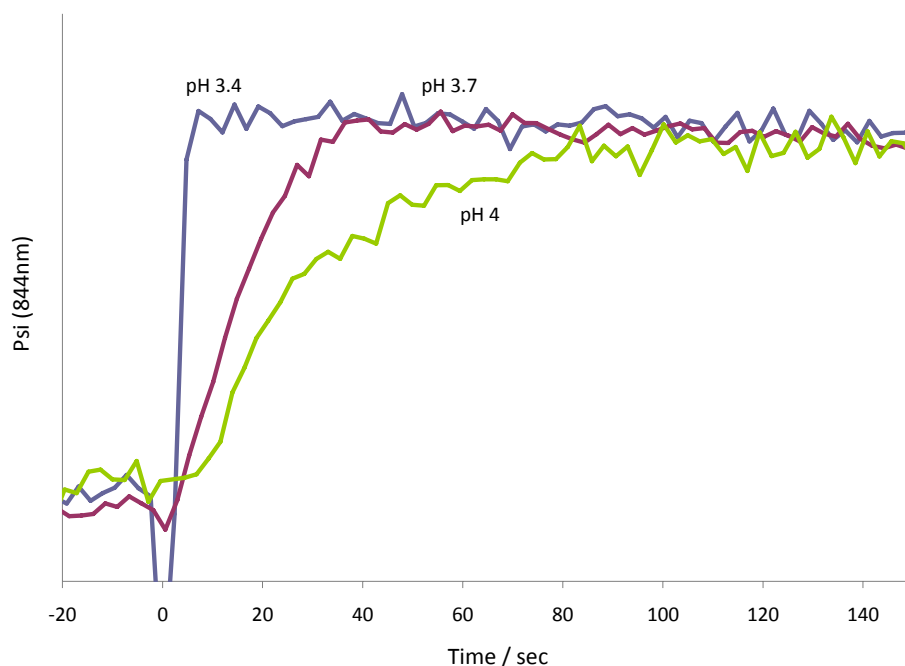


Figure 18 Kinetic ellipsometry results of swelling a poly(diethylamino ethyl methacrylate) brush initially at pH 8 by adding different amounts of HCl at $t = 0$ sec, which results in a final pH as shown in the diagram.

Figure 18 shows the measured ellipsometric parameter ψ at a wavelength of 844nm over time for the experiment described. Upon addition of the acid at $t = 0$, ψ starts to increase from its initial value and eventually after a certain amount of time fluctuates around a new higher value. Without inferring the height of the polymer brush by fitting the data with a model it cannot be said if the polymer brush is increasing or decreasing in height, but logically and from experiments carried out on thinner polymer brushes which can be fitted with a Cauchy layer model, it is possible to say that the change in ψ reflects the change in the polymer brush height from initially a small height before $t = 0$ to a larger height after.

From this data, it is possible to see that polymer brushes respond relatively quickly to a drop in pH. The response is slowest when the pH is changed from 8 to 4 taking around 80 seconds and fastest for a pH drop from 8 to 3.4, which seems to be complete within 10 seconds and a drop from pH 8 to 3.7 is intermediate at around 40 seconds. In all cases the drop in pH results in a fraction of ionisation (protonation) greater than 0.99, but the rate of change is different depending on the pH drop.

This result seems reasonable as a pH drop from 8 to 3.4 requires the addition of twice as much acid as the drop from 8 to 3.7, which in turn, requires twice as much acid as the drop from 8 to 4. Proportionally the response of the brush seems to take twice as long for

a drop of pH 8 to 4 (~80 sec) compared to a drop from pH 8 to 3.7 (~40 sec), which takes four times as long as a drop from pH 8 to 3.4 (~10 sec).

Parnell et al³⁷ have studied the response of PMAA brushes to a change in pH using Atomic Force Microscopy to image the brush layer and found that the response was fast, taking around 6 seconds to complete when averaged over an area of a few micrometers, but was even faster when the response at one particular point was measured, taking less than a second. These results correlate well with the gathered experimental results from ellipsometry.

Siegel found that rate at which polymer gels swell can be increased by adding certain small molecules to the solution such as buffers³⁸. These buffers increase the concentration of dissociating acid molecules while maintaining the same pH, increasing the speed of protonation. Also charged molecules such as strong acids are thought to be repelled from the charged polymer matrix, whereas buffer molecules are weak acids so are not completely ionised when dissolved in water, allowing them to enter into the polymer matrix.

The results obtained show that the response of a PDEA brush is relatively fast and so could be used in the implementation of the theoretical design. Desirably the response of

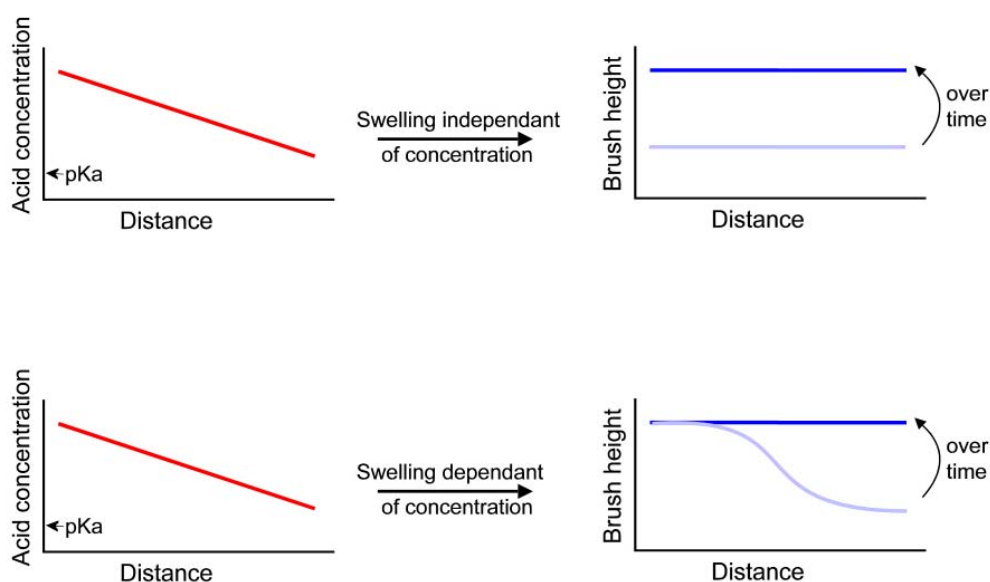


Figure 19 Schematic of how a poly(diethylamino ethyl methacrylate) brush will swell in response to a linear concentration gradient of acid if the rate of swelling is independent or dependant on the concentration of acid, when the concentration of acid is above the pK_a .

the polymer brush is faster at higher concentrations of acid meaning that the repulsive interaction gradient caused by the release of acid from a motor particle will be greater than if the rate of brush swelling was independent of acid concentration.

Figure 19 shows schematically the swelling of a PDEA brush in response to a linear gradient of acid produced by a potential motor particle. If the rate of swelling is independent of the concentration of acid, the brush swells homogeneously in the regions where $\text{pH} > \text{pK}_a$. Any propulsive force acting on particles is due to the slope of polymer brush height, so a brush which swells homogeneously results in a propulsive force of 0. Whereas if the brush swells faster at higher concentrations of acid, the resulting swelling is no longer homogeneous, as the brush swells faster where there is a higher concentration of acid. This gives a sloped surface as the brush swells, which eventually returns to a flat surface at long times when the brush has had enough time to swell at the lower concentrations of acid. Therefore the sloped surface gives an extra propulsive force while it is swelling.

5.4.4 Particles which Create Gluconic Acid

To create a motor particle for this design, it will be necessary to create a particle which either releases acid or creates acid via a chemical reaction catalysed on a particle's surface. As shall be shown later, a particle which releases acid would quickly run out of its supply of acid so it is more desirable to create a particle which produces acid via a catalytic reaction on its surface.

Glucose oxidase is an enzyme which oxidises glucose to gluconic acid and hydrogen peroxide using dissolved oxygen (see Figure 20). Therefore immobilisation of this enzyme onto a particle will lead to a motor particle which creates a local high concentration of gluconic acid, which in turn protonates the surrounding polymer brush causing particles to be repelled upwards.

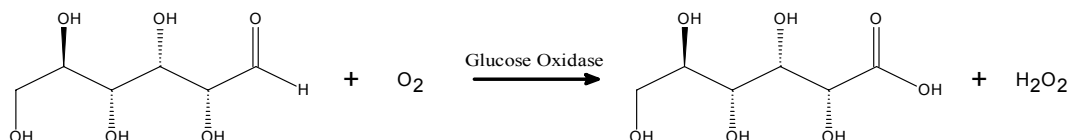


Figure 20 Oxidation of glucose to gluconic acid by glucose oxidase

Following a protocol by Hou et al³⁹, styrene and glycidyl methacrylate were copolymerised under emulsion conditions in an attempt to create latex particles with pendent epoxy groups at the surface, through which glucose oxidase could be attached by reaction of amine groups in the enzyme and the epoxy group to form an amine linkage (see Figure 21). Although the reaction resulted in latex particle formation there seemed to be little incorporation of the glycidyl methacrylate into the particles, as the reaction mixture became viscous, indicating polymer in solution rather than contained in the particles. ¹H NMR analysis of the produced particles could not distinguish any peaks from glycidyl methacrylate due to the overlapping peaks from styrene and the steric stabiliser added to the reaction poly(n-vinyl pyrrolidone).

Following production of the particles, they were mixed with glucose oxidase in an attempt to functionalise particles with the enzyme, and were then purified from the free enzyme by centrifuge. The particles were then assayed to find if they had become functionalised with the enzyme and if the enzyme was still capable of catalysing the reaction. A colorimetric assay by Rauf⁴⁰ was used in which the hydrogen peroxide produced by the oxidation of glucose is used in a second enzymatic reaction to oxidise 4-aminoantipyridine creating a red dye. The appearance of this dye can be measured over time using a UV-Vis spectrometer.

Using this assay with the produced particles in a glucose solution gave a negative result – the initially colourless solution remained colourless even after 24 hours indicating that the particles were not converting glucose to gluconic acid. Whereas this assay gave a positive result when the enzyme glucose oxidase was tested, indicating the production of gluconic acid.

This result informs us that either no enzyme has become immobilised onto the latex particles or that enzyme has been immobilised onto the surface but is denatured and unable to catalyse the reaction, meaning that the produced particles are of no use as a motor particle.

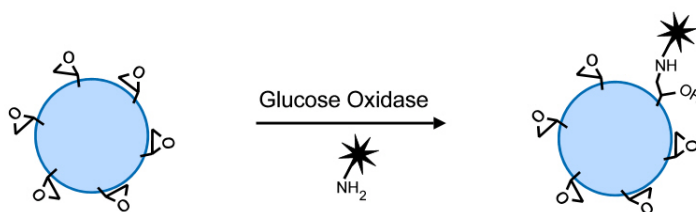


Figure 21 Immobilisation of glucose oxidase onto poly(styrene-co-glycidyl methacrylate) particles.

An alternative scheme by Caruso et al⁴¹ was testing in which glucose oxidase is immobilised onto a latex particle through electrostatic self-assembly⁴². In this scheme a negatively charged latex particle was produced by surfactant-free emulsion polymerisation⁴³ and was then coated with a layer of oppositely charged poly(ethylene imine) (PEI) giving a 'hairy' cationic particle. Zeta potential measurements showed that the particle had a zeta potential of -35 mV before PEI was adsorbed and then a zeta potential of +35 mV afterwards, showing that the surface of the particle had been functionalised with the PEI. Onto this cationic particle was then adsorbed glucose oxidase which is negatively charged (see Figure 22). Particles were then separated from glucose oxidase in solution by repeated centrifuge-redispersion cycles.

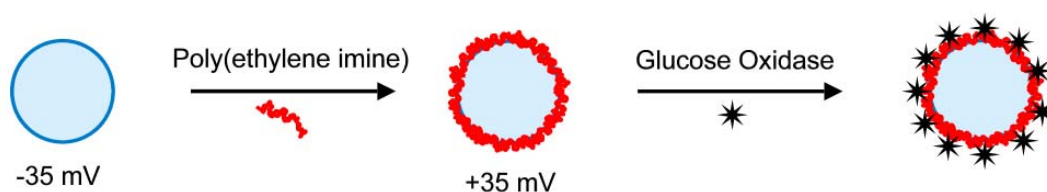


Figure 22 Schematic representation of the production of glucose oxidase functionalised polystyrene particles by electrostatic self-assembly.

Investigation of the particles using the colorimetric assay gave a positive result within minutes showing that the particles were functionalised with the enzyme and that it had retained its enzymatic activity. To make doubly sure that the enzyme was attached to the particle surface and not simply in solution, the particles were centrifuged and redispersed a further three times to remove any enzyme in solution. Even after these extra purification steps the particles still assayed positively showing that the enzyme is attached to the surface of the particle.

5.4.5 Measuring the Rate of Gluconic Acid Released

Following the successful immobilisation of glucose oxidase onto polystyrene particles, the rate of gluconic acid production per particle was found by monitoring the amount of red dye produced in the colorimetric assay over time. Using a UV-Vis spectrometer the absorbance of a cell containing particles, glucose and the assay ingredients was monitored at a wavelength of 505 nm over time. The measured absorbance was then converted to an

amount of dye, by producing a calibration graph of measured absorbance vs. amount of dye. As one mol of dye is produced from one mol of hydrogen peroxide, and that the oxidation of glucose produces one mol of gluconic acid and one mol of hydrogen peroxide, the amount of dye produced to the amount of gluconic acid produced can be calculated:

$$\text{Absorbance} \times \text{Conversion factor} = \text{mol dye}$$

eq. 4

$$\text{mol dye} = \text{mol H}_2\text{O}_2 = \text{mol Gluconic Acid}$$

Figure 23 shows the amount of gluconic acid produced over time. The plot is linear showing that the amount of gluconic acid produced by the functionalised particles is constant over the course of the measurement and that analysis of the slope of the line will yield the rate of reaction. This was found to be $4 \times 10^{-7} \text{ mol min}^{-1}$, which if divided by the number of particles in the cuvette gives a rate of $8.8 \times 10^{-17} \text{ mol min}^{-1}$ per particle.

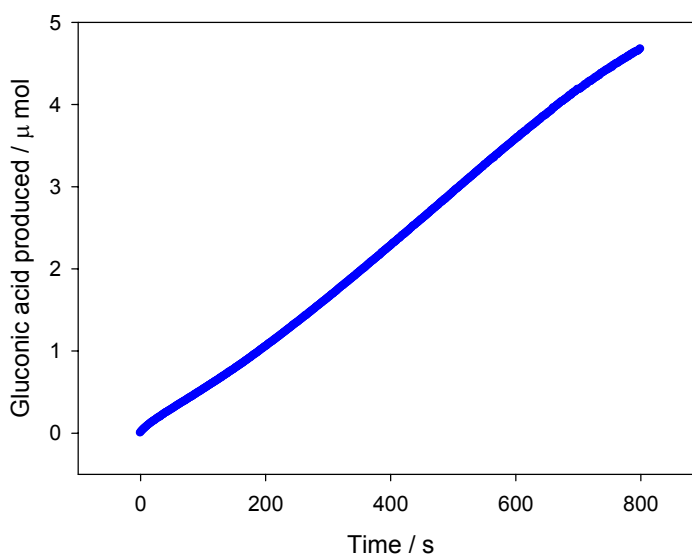


Figure 23 Colorimetric assay of the rate of production of gluconic acid by glucose oxidase functionalised particles in 32 mM glucose.

5.4.6 Concentration of Gluconic Acid around a Motor Particle

For a particle to be propelled along a polymer brush surface it must release acid, which protonates amine groups causing the brush to swell and increase in thickness. For the brush to swell by any appreciable amount the pH surrounding the brush must be lower than the pK_a of the brush which has been found to be 6.9 . For a particle which produces acid at a certain rate, the concentration of acid around the particle will should follow the equation:

$$\text{Conc}_{(r,t)} = \frac{\text{Rate}}{4\pi Dr} \operatorname{erfc} \frac{r}{\sqrt{4Dt}} \quad \text{eq. 5}$$

where concentration is measured in mol m^{-3} , Rate is the rate of gluconic acid production (mol s^{-1}) and D diffusion coefficient ($\text{m}^2 \text{s}^{-1}$) of gluconic acid. erfc is the complimentary error function.

After a sufficient amount of time, the concentration around the iron particle should reach a steady state, as the amount of gluconic acid released by the particle is equal to the amount removed from the vicinity of the particle by diffusion, and should obey the equation:

$$\text{Conc}_{(r)} = \frac{\text{Rate}}{4\pi Dr} \quad \text{eq. 6}$$

as t becomes infinitely large $r/\sqrt{4Dt} = 0$ and $\operatorname{erfc}(0) = 1$. The concentration of gluconic acid changes by less than 1% when $\operatorname{erfc} r/\sqrt{4Dt} = 0.99$, or when $r/\sqrt{4Dt} = 0.01$. This occurs in less than a second at distances up to $r = 500\text{nm}$. Therefore at all times observed by video microscopy the concentration of gluconic acid around a particle should follow eq. 6 and be highest at the surface and decrease at a rate proportional to $1/r$ to 0 some distance away from the particle.

Figure 24 shows the concentration of gluconic acid around one of the created polystyrene particle functionalised with glucose oxidase calculated using eq. 6. The diffusion coefficient of gluconic acid in water was estimated from the molecule's size using the Stokes-Einstein equation, although this value may be too low due to the anomalously fast diffusion of protons through water via the 'proton shuttle' mechanism. The rate used was that measured for the particles using the colorimetric assay, which is likely to be an overestimation of the rate achieved by particles while observed under the microscope due to the stagnant conditions. This difference arises because the reaction

liquid was stirred by convection currents while being investigated in the colorimetric assay, meaning that particles had a constant supply of reactants, whereas when observed under the microscope particles will be in stagnant conditions and the rate of reaction shall be severely restricted by the diffusion of reactants to the catalytic particles.

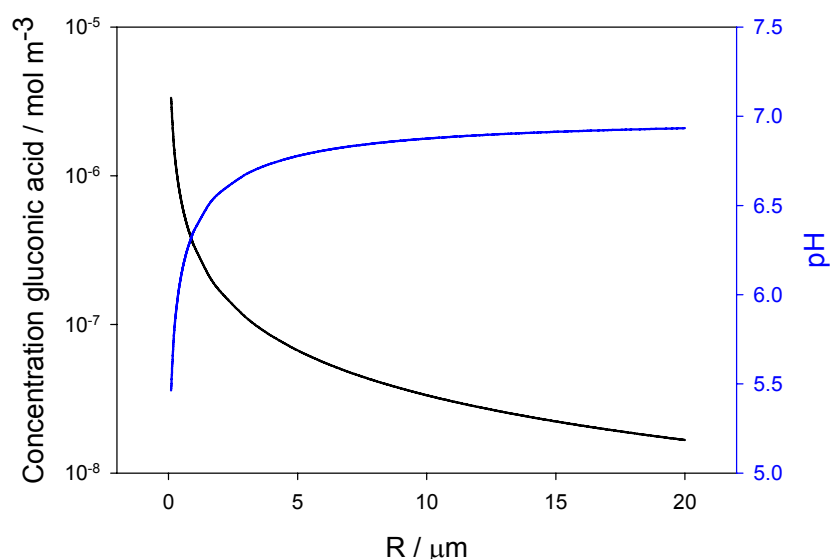


Figure 24 Concentration of gluconic acid around a particle functionalised with glucose oxidase and the resulting pH change around the particle from an initial pH of 7.

Figure 24 shows that the chemical reaction catalysed by glucose oxidase immobilised to a particles surface leads to an increase in the concentration of gluconic acid around the particle, which is highest at its surface and decrease to zero infinitely far away from the particle. The pH of solution surrounding a glucose oxidase functionalised particle can be calculated by adding the concentration of protons due to gluconic acid to the concentration of protons from water at pH 7:

$$\text{pH} = -\log[\text{H}^+] \quad \text{eq. 7}$$

$$[\text{H}^+] = [\text{Gluconic acid}] + 10^{-7} \quad \text{eq. 8}$$

The pH is lowest at the particle surface and increases back to the bulk pH of 7 at distances larger than $\sim 10\mu\text{m}$. To swell the PDEA brush the particle must release acid at a sufficient rate to lower the pH of the solution below that of the brushes pK_a of 6.3, which

is at a distance of $r \sim 100\text{nm}$ away²¹. As can be seen from Figure 24, this is achieved by the glucose oxidase functionalised particles and is in fact achieved for distances up to $r = 1\mu\text{m}$. Therefore if glucose oxidase functionalised particles were used as motor particles on PDEA brushes they would be able to swell the brush underneath themselves.

To achieve propulsion of itself and a target particle, the motor particle must swell the polymer brush underneath the target particle to create a gradient of repulsion. Using a combination of the glucose oxidase functionalised particle as the motor particle and a $4\mu\text{m}$ gold particle as the target particle, the brush must be swollen at a distance of $r = 4.5\mu\text{m}$. Calculation of the pH at this point using eq. 6, 8 and 10 gives $\text{pH} = 6.74$, which is only slightly lower than the bulk pH and is above the pK_a of 6.3 .

If instead the developed PEI coated silica particles ($20\mu\text{m}$) are used as the target particle, the distance over which the brush must be swollen rises to $15\mu\text{m}$. At this large distance the concentration of gluconic acid is very low giving pH 6.9, well above the pK_a .

Rearranging eq. 6 it is possible to calculate the rate needed to give a $\text{pH} < \text{pK}_a$ at a distance of r . Calculating the rate required to give $\text{pH} < \text{pK}_a$ at $r = 4.5\mu\text{m}$, gives a rate which is 5.4x faster than that measured by the colorimetric assay. Recalculating for a pH which is one pH unit below the pK_a leading to a PDEA brush that is 90% swollen gives a rate which is 66x faster than the measured rate. Calculating for the larger silica particles, $r = 15\mu\text{m}$, gives rates which 18x than the measured rate for the pH to equal the pK_a and a rate 220x faster to lower the pH one unit below the pK_a .

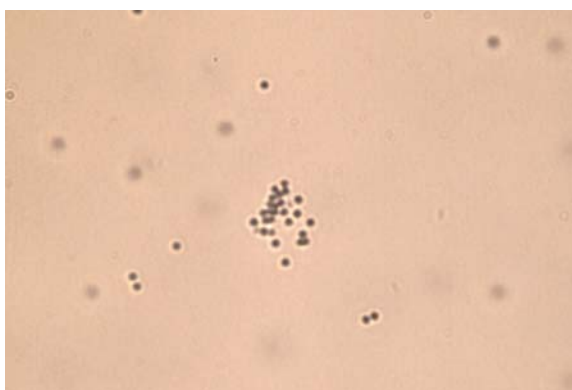


Figure 25 An optical micrograph of glucose oxidase functionalised polystyrene particles in a solution of glucose with universal indicator added to the solution to image the concentration profile of gluconic acid formed around particles.

In an attempt to visualise the concentration profile of gluconic acid formed around particles functionalised with glucose oxidase, a universal indicator solution was added to

functionalised particles dispersed in water and visualised under a microscope. The universal indicator changes colour depending on the surrounding pH of the solution from green at neutral pH to red at low pH. Figure 25 shows an optical micrograph of this experiment at a time when the catalytic particles and glucose have been in contact for 5 minutes. No increase in red colour can be observed around the particles even when they are clustered together, instead the whole of the image has a pink colour indicating that the solution has become acidic throughout and not just around the functionalised particles.

This result seems to contradict the results of calculating the concentration profile around particles using eq. 6. This difference in result can be rationalised considering that the particles are small compared to the thickness of the observation chamber (1 μ m vs. 100 μ m), meaning that any red corona due to the release of gluconic acid around the particles will also be small in comparison to the total volume. Visualising this small volume of red dye may not be possible due to the small amount of light which it adsorbs compared to the large amount of light adsorbed by the observation cell liquid. Therefore the concentration profile of gluconic acid may well be that calculated by eq. 6 but this concentration profile cannot be visualised using optical microscopy.

The height of a PDEA brush around a motor which release gluconic acid can be calculated using eq. 6 to calculate the concentration of gluconic acid around the particle, followed by eq. 7 and 8 to find the pH around the particle, and using eq. 3 to calculate the fraction of ionisation (protonation). It was found earlier that the fraction of ionisation was equal to the fraction of swelling, so using eq. 2 and inputting approximate minimum and maximum heights of the polymer brush ($h_{min} = 50$ nm and $h_{max} = 100$ nm) finally gives the height of the polymer brush around a glucose oxidase functionalised motor particle. The distance from the catalytic particle is converted to the distance along a flat brush surface using the relation:

$$d_{(\mu m)} = \sqrt{R^2 - 1.6^2} \quad \text{eq. 9}$$

where 1.62 is the radius of the glucose oxidase functionalised particle + the separation distance between the particle and surface (~ 100 nm).

Figure 26 shows this calculated polymer brush height around a particle positioned at $d = 0$, 100nm above the surface. It should be noted that this calculation did not take into account the different rates of swelling of a polymer brush at different concentrations of acid, nor the distribution of gluconic acid around the particle at short time scale before a steady state has been achieved. It has also not taken into account that diffusion of the

acid molecules away from the catalytic particle may be blocked by the surface and that the concentration profile will be affected by the close proximity of the surface to the particle.

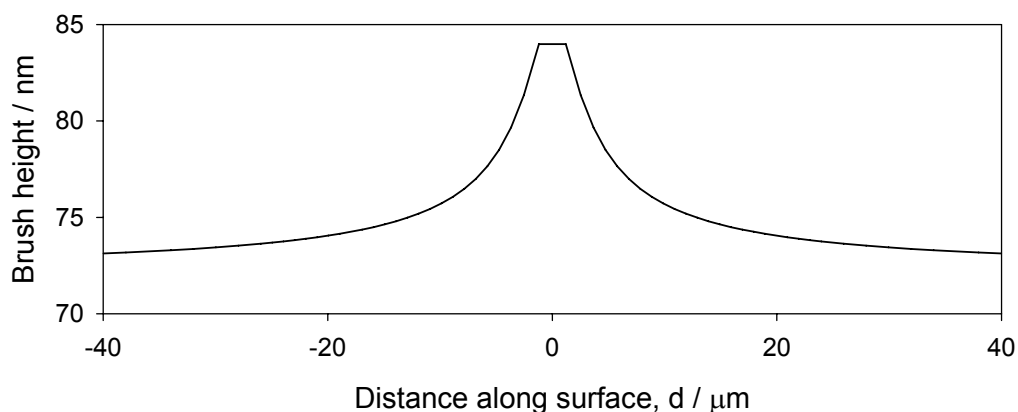


Figure 26 Height of a PDEA brush around a glucose oxidase functionalised particle positioned 100nm above the surface at $d = 0$, at timescales long enough for a steady state of gluconic acid to form around the particle and the polymer brush to reach its equilibrium height.

As can be seen from Figure 26, the polymer brush height is increased underneath the glucose oxidase functionalised particle due to the high concentration of gluconic acid present. Then the brush height drops significantly at distances away from the motor particle. Even at a distance of $20\mu\text{m}$ along the surface the brush is swollen to 73nm, 15nm higher than its bulk height at pH 7 of 58nm.

Propulsion of particles will be caused by slopes on the surface created by protonating the polymer brush increasing its height. The motor particle positioned at $d = 0$ will not experience a propulsive force as the brush height at this position is uniform and symmetrical about the particles centre. Whereas a target particle positioned some distance away will experience a brush surface which is sloped to some extent. Close to the motor particle this slope is greatest and at distances of $d > 20\mu\text{m}$ is very small, effectively zero.

The velocity created by a dense particle sedimenting down this slope can be calculated using the modified Svedburg equation²²:

$$v = \frac{2r^2(\rho_{particle} - \rho_{water})}{9\eta} \tan \theta \quad \text{eq. 10}$$

where r is the particles radius, η viscosity of water and θ the angle created from horizontal by the sloped surface.

If a 4 μm gold particle was used as the target particle, it would be positioned at $d = 4.5\mu\text{m}$ and would experience a slope of $1.1\text{nm } \mu\text{m}^{-1}$ giving a $\theta = 0.06^\circ$. Using eq. 10 it can be calculated that this slope would propel the gold particle at a velocity of only 19nm s^{-1} . If a 20 μm silica particle was used as the target particle, it would be positioned at $d = 11.5\mu\text{m}$ and would experience a smaller slope of 0.012° . This would lead to a propelled velocity of 5nm s^{-1} .

Therefore from these experiments it can be stated that glucose oxidase functionalised particles cannot produce gluconic acid sufficiently fast enough to enable a propagating wave or particle-surface interaction to be created. Any propulsion created will be too slow to distinguish from Brownian motion or sedimentation.

5.4.7 Particles which Release a Stored Source of Acid

An alternative way to creating a local high concentration of acid, is to create a particle containing a source of acid which can be released into the surrounding liquid. Acids such as hydrochloric acid are miscible with water meaning that a particle containing this acid must regulate its rate of release, otherwise it would all be released instantaneously and would quickly diffuse away.

To circumvent this problem, a particle containing an acid which is only slightly soluble in water can be used. Now the acid can only transfer from the particle to the surrounding water if its concentration in the water is below its maximum solubility. Therefore the acid will regulate its own release into solution to always maintain a saturated solution at its surface.

Benzoic acid is a hydrophobic molecule so has a solubility in water of only 24mM. A particle of benzoic acid will therefore dissolve in water at a rate which gives a concentration of 24mM at the particle surface and cannot dissolve faster as the solution surrounding the particle is saturated with benzoic acid. If the particle dissolves in water at pH 8 it should give a solution of 24mM benzoic acid, converting the pH of the solution to pH 2.9 ($\text{pK}_a = 4.21$).

To investigate if benzoic acid particles could be used as a self-regulating source of acid and therefore be used as a motor particle, the following experiments were performed. Firstly to find the drop in pH that benzoic acid would cause, an excess of benzoic acid was added to water and allowed to reach equilibrium overnight. Before the addition of the acid the pH was measured to be 8 and then 24 hours after the addition of benzoic acid pH 3.1, in close agreement with the expected pH of 2.9 .

To create a particle of benzoic acid a precipitation method was attempted. Benzoic acid was dissolved in a minimum amount of hot water to give a saturated solution. This solution was then cooled leading to the precipitation of benzoic acid from solution. This method formed small needle-like crystals of benzoic acid, rather than the desired spherical shape. It was anticipated that if this process occurred very quickly perhaps benzoic acid would precipitate as spherical particles, but even if the solution was cooled very quickly using liquid nitrogen, needle-like crystals still appeared.

Particles of paraffin wax containing benzoic acid were attempted to be created by dissolving benzoic acid in molten paraffin wax, followed by emulsifying the molten wax in water using surfactant and cooling to form solid particles. But as the molten particles were cooled benzoic acid precipitated out of solution in the aqueous phase forming needle-like crystals.

As neither of these preparation methods had been success it was found that the best method to form small particles of benzoic acid which had a small aspect ratio (short needles or cubes rather than long needles) was simple grinding of benzoic acid in a pestle and mortar. This result gave thicker, short particles of benzoic acid than the two other methods used.

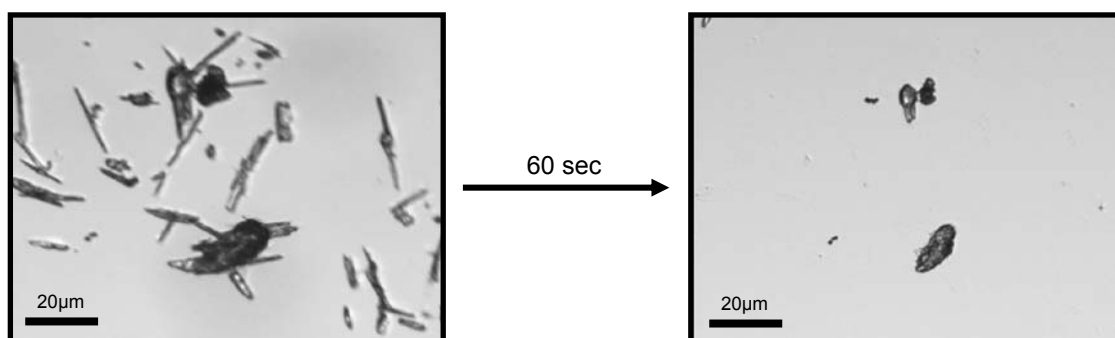


Figure 27 Optical micrographs of ground benzoic acid particles dissolving in water without any convection currents. The image on the left was taken a few seconds after introducing water to the cell and the image on the right 60 seconds after the water was introduced.

To investigate the predicted self-regulation of the rate at which benzoic acid is released into solution, a small amount of the ground particles were placed in a microscope observation chamber, water at pH 8 added and the resulting behaviour captured by optical microscopy.

Figure 27(left) shows the prepared benzoic acid particles a few seconds after water has been introduced to the observation chamber. The particles dissolved at a rate which maintains a saturated solution of benzoic acid at the particle's surface and therefore maintains pH ~ 3 at the particle surface. After 60 seconds most of the small particles have dissolved releasing all of their contained benzoic acid into solution, as shown in Figure 27 (right). It is expected from the results of experiments carried out on the Brownian motion of particles, that convection currents were negligible in the chamber and that benzoic acid was removed from the particles vicinity by diffusion alone.

This experiment confirms results gathered in section 5.4.6 that the rate at which acid must be generated or released from a potential motor particle is very high. While particles of benzoic acid are able to achieve this high rate of release, they use up their supply of acid very quickly, meaning that experiments into the propulsion of particles caused by this release of acid must be carried out also very quickly.

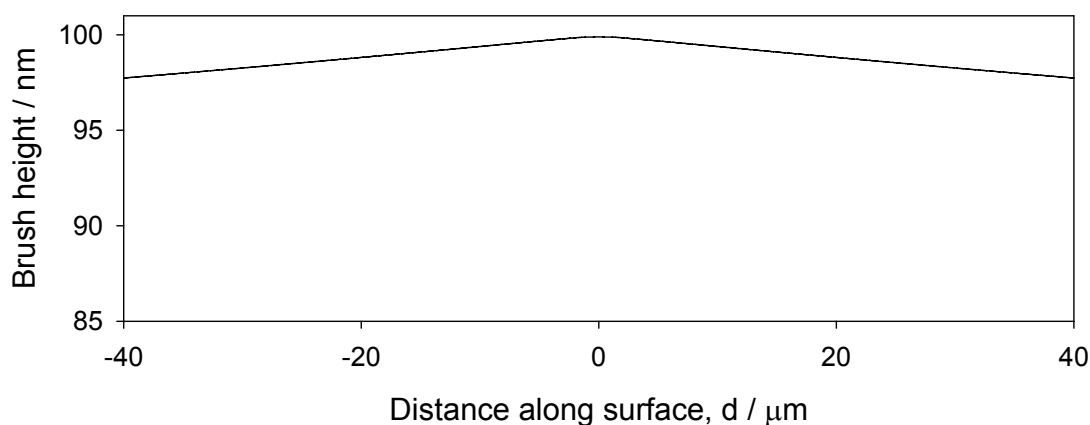


Figure 28 Height of a PDEA brush around a particle of benzoic acid positioned 100nm above the surface at $d = 0$, at timescales long enough for a steady state of benzoic acid to form around the particle and the polymer brush to reach its equilibrium height.

Using the procedure outline in the text above, the height of a PDEA brush around a particle of benzoic acid is shown in Figure 28. Due to the high rate of release and the quick diffusion of benzoic acid away from the particle, the polymer brush is highly

swollen not only underneath the particle but also at large distances away. The slope of the brush is small leading to propulsion of a potential target particle at a velocity of 1 nm s^{-1} for both a $4 \mu\text{m}$ gold particle and a $20 \mu\text{m}$ silica particle.

Ways to alter the thickness of a polymer brush by changing the pH of the surrounding solution have been proposed and investigated. It has been found that a change in pH can drastically alter the thickness of a polymer brush quickly, leading to changes in a particles energy of tens of kT . Ways to generate a local change in pH by creating potential motor particles which either produce or release acid have been investigated. In cases where acid was generated through a catalytic chemical reaction, the rate of reaction necessary to surround the particle with acid was found to be higher than the catalytic particles could achieve. This was overcome by creating particles which released a store of acid from their interior, but these particles could only maintain the required rate of release for 60 seconds.

Investigation of the shape of the created surface interaction gradient showed that glucose oxidase functionalised particles cannot surround themselves with enough acid to create fast propulsion. Particles of benzoic acid create surface interaction gradients which are too diffuse to create fast propulsion.

5.5 Swelling by Chemical Modification with Methyl Iodide

Polymer brushes of poly(diethylamino ethyl methacrylate) can be swollen by an irreversible chemical reaction which leads to the ionisation of the polymer chains. One such reaction is the quaternisation of tertiary amine groups in the polymer chains to quaternary amine cations using methyl iodide as shown in Figure 29. This reaction converts a neutral water-insoluble polymer brush to a cationic water-soluble brush.

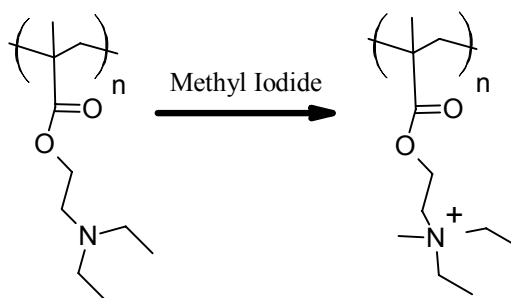


Figure 29 Quaternisation of poly(diethylamino ethyl methacrylate) by reaction with methyl iodide.

To create a motor particle which is capable of releasing methyl iodide and so swell a PDEA brush to a larger thickness, droplets of methyl iodide were created. Due to the low solubility of methyl iodide in water the droplet should regulate its own rate of release as discussed for benzoic acid particles above.

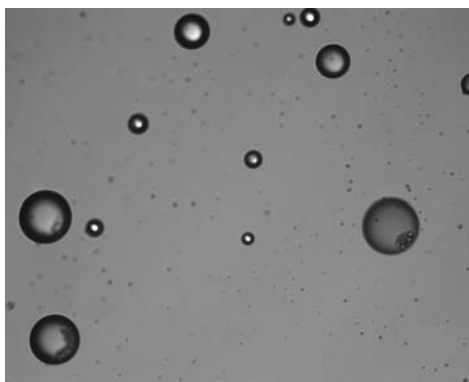


Figure 30 Optical micrograph showing methyl iodide emulsion droplets created by stirring with surfactant

To generate these particles methyl iodide was added slowly to a solution containing surfactant while being vigorously stirred. This resulted in methyl iodide emulsion droplets in a wide range of sizes from $\sim 100\mu\text{m}$ to $1\mu\text{m}$ and presumably also droplets that are smaller than can be observed by light microscopy, as shown in Figure 30.

Study of the droplet sizes generated showed that there was no correlation between droplet size and the concentration of surfactant in the solution. At low concentrations of surfactant incomplete emulsification of methyl iodide occurred, presumably because there is an insufficient amount of surfactant present to stabilise the increase in surface area generated by emulsifying methyl iodide.



Figure 31 Brownian motion of a methyl iodide droplet on a PDEA brush.

The produced methyl iodide emulsion droplets were investigated to see if they were colloidally stable towards surface coagulation. It was found through video microscopy shown in Figure 31 that particles were able to undergo Brownian motion on the surface of PDEA brushes, meaning that they could respond to a generated gradient of brush height and potential be of use as a motor particle. The droplets are also quite dense ($\rho = 2.3 \text{ g ml}^{-1}$) meaning that they sediment to the bottom surface of observation chambers where they are required, and that they should sediment along a sloped brush surface although much slower than the dense target particles prepared.

In the prepared dispersion of methyl iodide droplets, water is saturated with methyl iodide and so the concentration is uniform throughout the liquid and around particles. To be used as motor particles, droplets of methyl iodide must create a concentration gradient around themselves, meaning that the prepared dispersion must be diluted to reduce the concentration of methyl iodide in the water to effectively zero. Then with the liquid no longer saturated, particles will release methyl iodide creating the desired concentration gradient. It was not studied how long emulsion droplets are able to release methyl iodide at the required rate before they run out of their stored supply but this may only be a short

period of time, meaning that the particles must be diluted and any motion created by the particles studied very quickly.

To investigate how quickly the quaterisation of PDEA occurs, kinetic ellipsometry was used to measure the ellipsometric parameters over time as an amount of methyl iodide was added. A thick PDEA brush was used to give the largest change in brush height possible but this meant that data could not be fitted with a model to infer the brush's height over time. Instead changes in the raw data of ψ at 844nm was used to find how the polymer brush changed over time.

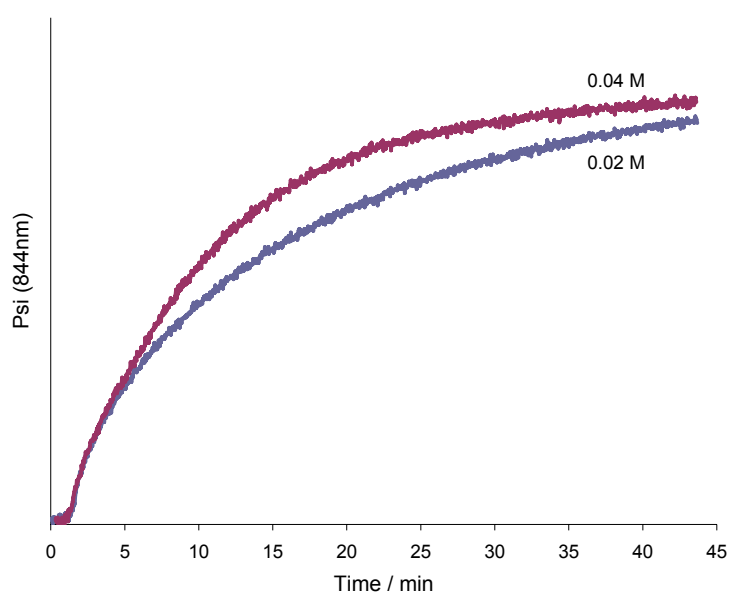


Figure 32 Kinetic ellipsometry results of swelling a poly(diethylamino ethyl methacrylate) brush initially in water at pH 8 by the addition of methyl iodide at $t = 0$ min, which give the final solution concentrations shown in the diagram.

Figure 32 shows the measured values of ψ at 844nm for a PDEA brush with different amounts of methyl iodide added to the surrounding solution at $t = 0$. As can be seen, the brush takes a few minutes to respond to the added methyl iodide before ψ can be seen to increase. This is possibly due to the amount of time taken by the added methyl iodide to mix thoroughly with the solution around the brush. When an amount of methyl iodide is added to the solution resulting in a concentration of 0.04M, the solution is saturated with methyl iodide. So this is the highest concentration of methyl iodide that can be used to modify a polymer brush and should give the fastest rate. At this concentration the transformation of the polymer brush is slow and takes 45 minutes before ψ can be seen to

plateau to its new higher value. At the lower concentration of 0.02M methyl iodide the reaction is slower and seems to be incomplete even after 45 minutes.

This is much too slow to be of much use in the implementation of theoretical design. A motor particle which releases methyl iodide will have migrated a large distance away by Brownian motion and or sedimentation before the brush is swollen to any extent. If this chemical transformation could result in propulsion this also would be extremely slow due to the slow rate of reaction.

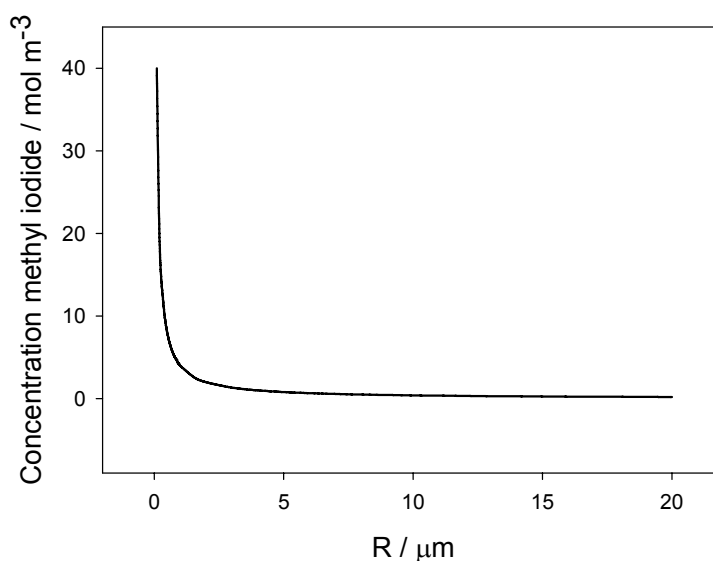


Figure 33 Concentration of methyl iodide around an emulsion droplet of methyl iodide

Figure 33 shows the concentration of methyl iodide around an emulsion droplet of methyl iodide calculated using eq. 6 and adjusting the rate of release so that the concentration very close to the surface equalled the maximum solubility of methyl iodide in water (0.04 mol dm^{-3} or 40 mol m^{-3}). The concentration is highest close to the particle and rapidly decays away from the particle. At a distance of $3.2 \mu\text{m}$, where a target particle would be positioned if made of gold, the concentration has fallen to 1.3 mM . Whereas at a distance of $11 \mu\text{m}$ where a target particle of silica would be positioned, the concentration has fallen to $4 \times 10^{-4} \text{ M}$.

From kinetic ellipsometry it has been shown that the modification of a polymer brush at concentrations of 0.02-0.04M methyl iodide is far too slow to be of use as a way to swell a polymer brush. So at the concentrations underneath a target particle highlighted above, the reaction will be even slower and of no use in implementing the theoretical design.

5.6 Creating a Polymer Brush by Grafting-to

A particle could also be raised above a surface by the creation of a polymer brush underneath particles. Methods of creating a polymer brush are split into two distinct methods: *grafting-from* where monomer is polymerised from an initiator species tethered to the substrate and *grafting-to* where a polymer chain is attached to the surface through a covalent bond.

The *grafting-from* approach usually requires elevated temperatures, airless conditions if ATRP is used, and is normally slow, taking a few hours to form a polymer brush of significant height. For these reasons the *grafting-from* approach is not suitable for use in implementing the design. The *grafting-to* approach does not require any of these stringent conditions and can be done from aqueous solution at room temperature, so is a much more appealing method for use in implementation of the theoretical design.

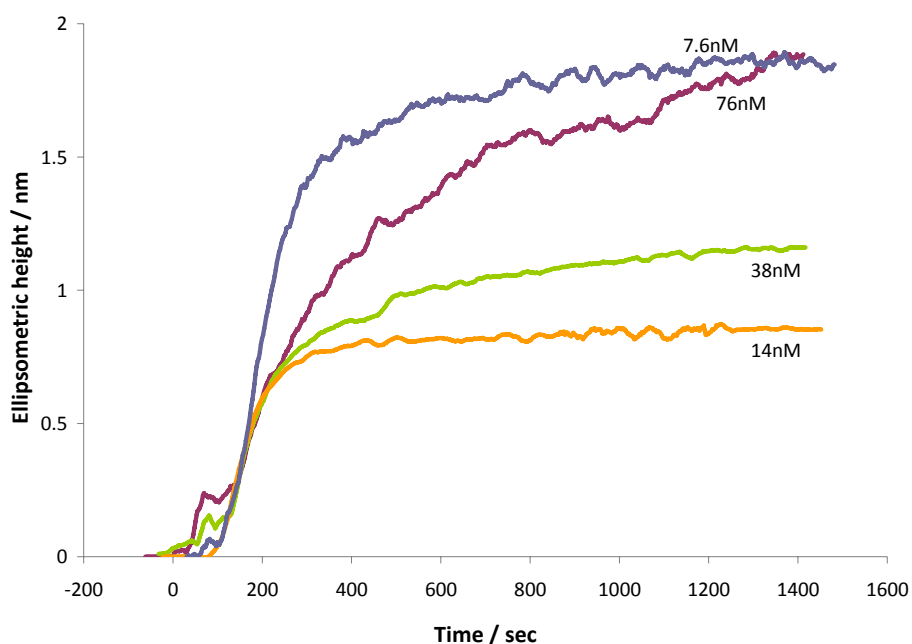


Figure 34 Kinetic ellipsometry results for the grafting of thiol terminated PEO to a gold surface at different concentrations of the polymer in water.

To investigate if this approach could be used to form a polymer brush underneath particles repelling them from the surface and changing the interaction between a particle and surface to more repulsive, poly(ethylene oxide) with a terminal thiol group was introduced to a gold surface to form an adsorbed polymer layer.

Figure 34 shows kinetic ellipsometry results for a gold surface being functionalised with the PEO-SH chains. It can be seen that the process of self-assembly is slow requiring around 300 seconds to complete. This is undesirable for the design as the interaction between the surface and particle should be altered as fast as possible. A slow change means that particles can move away from its initial position by Brownian motion possibly interfering with the propulsive mechanism.

The height of the adsorbed polymer layer is also very thin at only a couple of nanometres at all concentrations investigated. This height is insufficient to create a sizable change in particle energy, raising a $4\mu\text{m}$ gold particle by 2nm gives a change in energy of only $3kT$. If a constant gradient of this energy difference was created over one particle diameter ($4\mu\text{m}$) as in the theoretical design this would lead to a propulsive velocity of only $0.1\mu\text{m s}^{-1}$. During which time the particle would be undergoing Brownian motion. Using Einstein's equation it can be calculated that the particle would diffuse $1.4\mu\text{m}$ in 1 second – a distance 14x larger than that produced from the propulsive force.

Investigation of the concentration dependence on the kinetics give mixed results. Generally increasing the concentration of the polymer increased the thickness of the adsorbed layer without altering the initial rate of formation. Although the thickest polymer layer was observed for the lowest concentration investigated indicating the spread of results.

In all concentrations investigated, adsorption of thiol terminated poly(ethylene oxide) onto a gold surface gave an adsorbed layer with a final thickness which was too thin, and a rate of self-assembly that was too slow for this method to be of any use in implementing the theoretical design.

Taylor and Jones⁴⁴ investigated creating polymer functionalised surfaces in an identical fashion to that described, and also found that *grafting-to* from aqueous solution gave a thin adsorbed polymer layer. They found by adding non thiol-terminated PEO to the aqueous solution, that the thickness of the adsorbed polymer layer could be increased significantly. While this is useful for creating thick polymer brushes, it is of little use in implementing the theoretical design, as the added PEO increases the viscosity of the liquid meaning that a target and motor particle would encounter significantly more viscous drag when moving through the liquid and move very slowly.

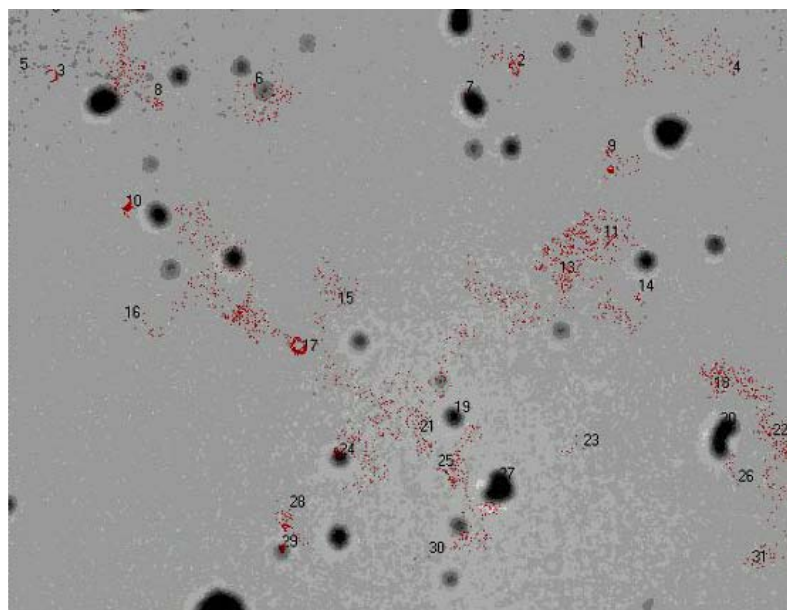


Figure 35 Brownian motion of gold particles on a patterned surface of mercaptoundecanol and thiol terminated PEO.

To investigate if an adsorbed layer of thiol terminated PEO which creates a gradient of surface repulsion is capable of propelling a particle along a surface, very sharp gradients of adsorbed PEO were created using photolithography as follows. Firstly a self-assembled monolayer of mercaptoundecanol (MUD) was created and then patterned using photolithography to remove selected areas of MUD. The areas of removed thiol were then backfilled with thiol terminated PEO giving a grid shaped surface pattern, with squares containing tethered PEO and grid lines containing MUD.

The Brownian motion of gold particles dispersed in water on these surfaces was then investigated and their position tracked using a custom made LabView script as shown in Figure 35. If the adsorbed PEO layer is capable of controlling the position of gold particle undergoing Brownian motion as studied with PMAA brushes earlier, then they should be able to be able to propel particles as well. In Figure 35 particles undergo Brownian motion giving a random motion of the particles, the particle trajectories do not mark out a clear pattern dictated to them by the surface but it perhaps possible to see a weak pattern due to the surface patterning.

These results highlight the earlier results from ellipsometry that adsorbed PEO chains do not form a layer of sufficient thickness to create a significant change in the repulsion of a dense particle away from a surface. Due to this reason, as well as their relatively slow self-assembly on a gold surface, creating a polymer brush by the grafting-to approach is not suitable for use in implementing the theoretical design.

5.7 Summary and Conclusions

In section 5.2 it was shown that small particles could be modified making them colloidally stable towards surface aggregation on polymer brush surfaces. Modification was unsuccessful at achieving colloidal stability for 4 μm gold particles but successful for larger 20 μm silica particles. Achieving this colloidal stability has allowed particles to respond to surface repulsions and be able to migrate along surface repulsion gradients.

To mimic a gradient of surface repulsion by a polymer brush, photolithography was used in section 5.3 to create patterned polymer brush surfaces. Investigation of iron particles on these surfaces showed that the particles responded to the created surface gradients and would not pass over a brush-silicon interface. These results were explained by calculating the gain in gravitational potential energy of the particle being repelled away from a surface. It was found that the polymer brush needed to repel the particle far enough away from the surface to cause a gain in gravitational potential energy of greater than $8kT$ for good control of the particles to be achieved and to prevent particles ‘hopping’ over an interface.

The prepared surfaces also showed good control over larger 20 μm silica particles which diffuse by Brownian motion much slower. Three different types of behaviour were observed depending on the angle a particle sedimented into a brush interface. Although in this case calculating the relevant forces F and f acting on the particle explained the behaviour, rather than the gain in gravitational potential energy. ‘Gates’ were created using these surfaces which decide whether to allow a particle to pass depending on the solution pH, as well as identifying that brush interfaces could act as a microbalance and count the number of particles at a specific location.

Following proof that particles responded to gradients of surface repulsion, chemical reactions which could create these gradients were investigated. Polymer brushes of poly(methacrylic acid) were found to swell in response to an increase in pH and gave increases in height of 43nm leading to differences in particle energy of $62kT$. Polymer brushes of poly(diethylamino ethyl methacrylate) were found to swell in response to a decrease in pH. The height of polymer brushes was found to be directly proportional to the fraction of ionisation of the polymer chains, although pK_a values were shifted either up or down by ~ 1 pH unit compared to literature values.

Investigation of poly(diethylamino ethyl methacrylate) brushes swelling in response to added acid showed that the brush changed its height quickly, completing within a few seconds but was also dependant upon the amount to acid added. Therefore the chemical

reaction was identified as a possible way to alter the interaction between a surface and particle which could be used to propel particles forward.

To create a motor particle which released acid, swelling a polymer brush leading to propulsion, the enzyme glucose oxidase was successfully immobilised onto a polystyrene particle. Measurement of the rate at which these created motor particles produced gluconic acid and mathematical analysis of the result showed that this rate was not fast enough to create a low pH around the particle. Due to this slow rate of acid generation and the fast diffusion of protons away from the particle, only a small gradient of brush height would be created underneath a target particle resulting in propulsion of the particles at a velocity of only 19nm s^{-1} .

Particles of benzoic acid were created by grinding in a pestle and mortar to act as motor particles capable of releasing a store of acid. These particles were calculated to be able to release acid very quickly creating a low pH around themselves, although it was found by experiment that these particles ran out of their stored supply of acid within 60 seconds. Calculation of the pH around particles and conversion of this pH to a polymer brush height, showed that a polymer brush would be mostly swollen in the proximity of the motor particle and not sloped. Therefore no propulsion of particles would result.

Quaternisation of poly(diethylamino ethyl methacrylate) brushes using methyl iodide was investigated as an alternative chemical reaction to increase surface repulsion. Motor particles containing reactant were created by emulsifying methyl iodide in water. Investigation of the reaction kinetics showed that it was slow, taking around 40 minutes to complete, meaning that it would be of no use in creating propulsion through repulsive surface interactions.

Finally, the grafting-to approach was investigated as a possible way to create a polymer brush on a surface increasing surface repulsions. Kinetic ellipsometry of thiol terminated poly(ethylene glycol) on gold surfaces showed that an adsorbed polymer layer was slow to form and only had a thickness of 2nm, meaning that this approach was not suitable for implementation of the theoretical design. Optical microscopy of gold particles diffusing on a patterned surface of grafted-to PEO confirmed this showing little control over particles.

From the experiments performed, the repulsive interactions between a polymer brush and a particle has been identified between as able to influence and control particles. These repulsive surface interactions have been shown to be altered by chemical reactions such as protonation and quaternisation using methyl iodide. Motor particles which are able to release acid or methyl iodide and modify a polymer brush surface have been created, but none of these created particles were able to create a gradient of surface repulsion. In all

cases the rate of release of the reagent from the particle was found to be too low or the rate at which this reagent modified the surface too slow. Motor particles of benzoic acid were created which could release acid at the required rate but these too were calculated not to produce a gradient of surface repulsion due to the fast diffusion of protons away from the particle. This would give a very broad gradient resulting in slow propulsion masked by Brownian motion and sedimentation.

5.8 Experimental Details

Materials. All chemicals were purchased from Sigma-Aldrich and used as received except the silane initiator [11-(2-Bromo-2-methyl) propionyl] undecyl trichlorosilane which was synthesised according to Matyjaszewski *et al*⁴⁵. Silica particles (20µm) were purchased from Kisker bio-tech. Gold particles (3-5 µm) were purchased from Alfa Aesar and iron particles (2-3 µm) from PolySciences inc.

Preparation of Silane Initiator Monolayers. Silicon (100) wafers were cut into small pieces and cleaned by submerging in piranha solution for several hours, rinsed with water then ethanol and dried in an oven overnight. The clean silicon was then functionalized with the silane initiator [11-(2-Bromo-2-methyl) propionyl] undecyl trichlorosilane by submerging in 10ml of 5 µM solution of the silane initiator in dry toluene and 100µl of triethylamine added. After 6 hours immersion time the silicon substrates were removed from the solution, washed with dry toluene then ethanol and blown dry in a nitrogen stream.

Preparation of Patterned Silane Initiator Monolayers. The initiator functionalized silicon substrates were patterned by contact photolithography which removed the silane monolayer in selected areas by exposure to UV light from a halogen light source using a TEM grid (Agar Scientific) weighed down with a quartz slide as a photo-lithography mask⁴⁶. Following photo-oxidation the substrate was washed with toluene then ethanol and blown dry in a nitrogen stream. Patterned substrates were used immediately. Patterning of the substrate was confirmed to be successful by visual examination of the substrates after polymerisation which showed a pattern of light and dark areas in an identical pattern as the photomask used.

Preparation of Poly(methacrylic acid) Polymer Brushes. Acidic monomers such as methacrylic acid cannot be polymerised directly by ATRP, as the acidic conditions protonate amine ligands making the copper catalyst ineffective at polymerising monomer. Therefore the indirect two step method of polymerising t-butyl methacrylate to form a poly(t-butyl methacrylate) brush followed by conversion to a poly(methacrylic acid) brush by hydrolysis was used as described below.

i) Atom Transfer Radical Polymerization of t-butyl methacrylate from Silane initiator Monolayers. 10ml t-butyl methacrylate, 5ml 1,4-dioxane and 100µl pentamethyldiethyltriame were added to a reaction tube (Radley's) with a cross-hair stirrer bar. Either an unpatterned silicon substrate or a patterned silicon substrate along with an unpatterned silicon substrate were suspended in the reaction solution using stainless steel wire. The solution was then purged with nitrogen while being stirred for 30

minutes to remove oxygen. After 30 minutes 50 milligrams of copper(I) chloride was added while the nitrogen flow was maintained. The tube was resealed and purged with nitrogen for a further 5 minutes, then heated to 50°C and left to react for 14 hours. Polymerization was quenched by opening the tube allowing oxygen to enter.

Following polymerization substrates were rinsed with copious amounts of 1,4-dioxane and sonicated in several washings of dilute acetic acid to remove copper(II) followed by washing with water and ethanol.

ii) Hydrolysis of Poly(t-butyl methacrylate) to Poly(methacrylic acid). Substrates with grafted poly(t-butyl methacrylate) were suspended in a reaction tube using stainless steel wire and 15ml of 0.2M p-toluene sulfonic acid in 1,4-dioxane added. The mixture was then heated to reflux and left to react for 24 hours. After which substrates were washed with excess 1,4-dioxane then ethanol and dried in a nitrogen stream. Hydrolysis of poly(t-butyl methacrylate) to poly(methacrylic acid) was confirmed by a reduction in ellipsometric thickness by around 60% and ellipsometric titration which showed that the brush became pH responsive with a pKa of 6.9 .

Atom Transfer Radical Polymerization of diethylamino ethyl methacrylate from Silane initiator Monolayers. 10ml diethylamino ethyl methacrylate, 5ml 1,4-dioxane and 100µl pentamethyldiethyltriame were added to a reaction tube (Radley's) with a cross-hair stirrer bar. A initiator functionalised silicon substrate was suspended in the reaction solution using stainless steel wire. The solution was then purged with nitrogen while being stirred for 30 minutes to remove oxygen. After 30 minutes 50 milligrams of copper(I) chloride was added while the nitrogen flow was maintained. The tube was resealed and purged with nitrogen for a further 5 minutes, then heated to 50°C and left to react for 14 hours. Polymerization was quenched by opening the tube allowing oxygen to enter.

Following polymerization substrates were rinsed with copious amounts of 1,4-dioxane and sonicated in several washings of dilute acetic acid to remove copper(II) followed by washing with water and ethanol.

Observation of Gold, Iron or Silica Particles on Patterned and unpatterned Substrates. A small amount of the desired particles were dispersed in distilled water adjusted to the appropriate pH using dilute sodium hydroxide or hydrochloric acid. In the case of gold or iron particles the dispersion was then sonicated for one minute to aid dispersion. A drop of this solution was then sandwiched between a patterned substrate and a clean microscope slide using 0.1mm thick double-sided adhesive (Grace Bio-Labs). Particles on the substrate were then observed under a microscope (Nikon Ellipse ME2000) at 10x magnification using episcopic lighting. Movies of the motion were recorded using a Pixelink PL-A742 machine vision camera at 10 frames per second for

100 seconds. The motion of particles was tracked after movie capture using a custom built LabView script which determined the position of particles in each frame of the movie.

Spectroscopic Ellipsometry Measurements. The thickness of polymer brushes were determined on unpatterned substrates using a J.A. Woollam spectroscopic ellipsometer and fitting data with a Cauchy layer model when dry or a Effective Medium Approximation (EMA) consisting of a Cauchy material and water when wet.

Kinetic Spectroscopic Ellipsometry Measurements. Kinetic measurements were taken using *Complete Ease* software which capture ellipsometric data 3 times per second, data was then fitted with an EMA layer model. Substrates were submerged in water and allowed to reach equilibrium for at least 10 minutes before the measurement was started and data was normally captured for 5 minutes before any chemical stimulus such as methyl iodide was carefully added to the liquid.

Spectroscopic Ellipsometry Measurements on Gold substrates. Gold substrates were prepared by thermally evaporating a thin layer of chromium (~5nm) followed by a layer of gold (~30nm) onto a clean glass microscope slide. These slides were then cut up into 1cm square pieces and labelled. At the start of an experiment, ellipsometric data of the gold substrate to be use was captured and converted to a *B-spline* using the *Complete Ease* software. This data was then used as a substrate in further modelling of the surface using a Cauchy or EMA layer model.

Preparation of PDMA functionalised gold particles by immobilisation of thiol terminated polymer synthesised by Reversible Addition Fragmentation Polymerisation. 3g dimethylamino ethyl methacrylate, 6mg AIBN, 0.042g 2-cyano-2-propyl dithiobenzoate and 6ml of 1,4-dioxane were added to a reaction tube with a magnetic stirrer bar. Nitrogen was bubbled through the solution while being stirred for 30 minutes to remove oxygen after which the tube was heated to 90°C for 24 hours. ¹H NMR analysis showed that the reaction had gone to greater than 95% conversion.

The reaction mixture was then precipitated into 50ml of cold diethyl ether, filtered to remove the liquid and then dried in a desiccator over night. Gel permeation chromatography using tetrahydrofuran as the solvent showed the produced polymer to have an M_n of 14,900 g mol⁻¹, close to the targeted molecular weight of 15,700 g mol⁻¹. The polydispersity was low at 1.22 characteristic of a living polymerisation.

The produced polymers terminal group was converted from dithiobenzoate to a thiol by reduction using sodium borohydride. 0.12g of the as produced polymer was mixed with 10 ml of aqueous 0.1M NaBH₄ and left for 24 hours to react. 100µl of this solution was then added to a dispersion of ~5mg gold particles dispersed in 1ml water and allowed to

react overnight resulting in PDMA functionalised gold particles. These particles were purified by three repeat centrifugation-redispersion cycles in water.

Analysis of the particles zeta-potential showed a change from -35mV before functionalisation to +12mV after functionalisation.

Preparation of micron sized polystyrene-co-glycidyl methacrylate particles via dispersion polymerisation. Following Hou *et al*³⁹, 60ml ethanol, 0.2g AIBN, 0.4g poly(n-vinyl pyrrolidone) and 13g styrene were added to a 250 ml 3-necked round bottom flask fitted with reflux condenser and magnetic stirrer bar. Nitrogen was then bubbled through the reaction solution for 30 minutes to remove oxygen after which the mixture was heated to 70°C. After 3 hours reaction time 0.5g glycidyl methacrylate in 15ml ethanol was added to the reaction after first being degassed. The reaction was then allowed to continue for a further 14 hours before the reaction was quenched by opening to the air. The produce latex particles were purified by 5 repeat cycles of centrifugation-redispersion in water. The first 3 cycles gave off a viscous supernatant. Dynamic light scattering showed the particles to have a mean diameter of 1.37µm and a polydispersity of 0.21. Peaks from polystyrene, poly(n-vinyl pyrrolidone) and poly(glycidyl methacrylate) were not distinguishable by ¹H NMR analysis.

Immobilisation of glucose oxidase onto polystyrene-co-glycidyl methacrylate particles. Following Hou *et al*³⁹, 50mg poly(styrene-co-glycidyl methacrylate) particles and 5mg glucose oxidase were mixed in 2 ml water for 2 hours before the particles were separated from the free enzyme by 3 repeat cycles of centrifugation-redispersion in water.

Preparation of micron sized polystyrene particles via surfactant-free emulsion polymerisation.⁴³ 50ml water, 5g styrene and 2mg NaCl were added to a 3-necked 250ml round bottom flask fitted with reflux condenser and magnetic stirrer. The flask was then heated to 60°C while being degassed by bubbling nitrogen through the liquid for 30 minutes. Then 50mg of ammonium persulfate dissolved in 2 ml water was injected through a side arm initiating polymerisation. The mixture was then allowed to react overnight which gave a white milky liquid with a hard skin on top. This was passed through a sieve to remove large lumps and then the particles were purified by 3 repeat cycles of centrifugation-redispersion in water.

Preparation of glucose oxidase functionalised particles by electrostatic self-assembly. Following a method by Caruso *et al*,⁴¹ 200µl of the particles prepared above were added to 1 ml of 1mg ml⁻¹ poly(ethylene imine) hydrochloride solution while being vigorously stirred and allowed to mix for 30 minutes. After which time the particles were separated from the mixture by 3 repeat cycles of centrifugation-redispersion in water. Zeta potential measurements showed a change from -35mV to +35mV indicating that the surface of particles had been functionalised with poly(ethylene imine). The particles

were then added to a solution of 2mg glucose oxidase in 1 ml water and allowed to mix for 1 hour before the particles were separated from the mixture by 3 repeat cycles of centrifugation-redispersion in water.

Colourmetric assay of glucose oxidase functionalised latex particles. A colourmetric assay by Rauf *et al*⁴⁰ was used to find the catalytic output of glucose oxidase functionalised particles. In this assay the by product of the reaction hydrogen peroxide is used to oxidise a dye molecule via a second catalytic reaction using horse radish peroxidase, the production of this dye is then monitored via UV-Vis spectroscopy. In detail, a solution consisting of 32mg glucose, 16mg 4-aminoantipyridine, 1mg horse radish peroxidase, 5ml water and 100µl of 40mM phenol solution was created. A quartz cuvette was then filled with this solution and 100µl of 10wt % solids glucose oxidase particle solution added, then the adsorbance at 505nm was measured over time using a UV-Vis spectrometer.

Preparation of Benzoic Acid Particles by Precipitation. 0.5g benzoic acid was added to a 250ml flask filled with ~20ml water and heated so that the water boiled while being stirred. Hot water was then added to this flask until slowly until all of the benzoic acid had dissolved (~150ml), giving a transparent liquid. This flask was then allowed to cool back to room temperature while being stirred which gave a turbid white mixture. Alternately the solution was cooled rapidly by transferring a small amount of the liquid to a test tube and submerging in liquid nitrogen while taking care not to freeze the mixture. These process gave needle-like crystals approximately 1µm x ~20-100µm.

Preparation of Benzoic Acid / Paraffin Wax Particles. 0.1g benzoic acid was mixed with 0.1g paraffin wax in a 50ml sample tube and then heated to 70° while stirred with a magnetic stirrer bar until a transparent homogenous solution was obtained. Then 1.8ml of boiling water containing 1% sodium dodecylsulfonate was added and the stirring rate increase to emulsify the molten wax. After 30 stirring the solution was allowed to cool back to room temperature. This procedure gave spherical droplets with a large size distribution of paraffin wax as well as needle-like particles of benzoic acid.

Preparation of Benzoic Acid Particles by Grinding. Benzoic acid powder was ground by hand in a pestle and mortar for a few minutes giving rectangular crystals approximately 1µm x 10µm.

Preparation of Patterned Surface Functionalised with Thiol Terminated Poly(ethylene glycol). Glass microscope slide were cleaned using piranha solution, rinsed and dried. These clean microscope slides were then loaded into a thermal evaporator and ~5nm chromium followed by ~15nm gold evaporated onto them. Gold surfaces were then introduced to a 10mM ethanolic solution of mercaptoundecanol (MUD) and left overnight before being rinsed with ethanol and dried. Photopatterning

was achieved by exposing a MUD surface to UV light using a TEM grid as a photomask for 2 hours. Following photopatterning surfaces were then submerged into a solution of 100mM aqueous solution of thiol terminated poly(ethylene glycol), left overnight then rinsed with copious amount of water and blown dry.

References

- (1) Zdyrko, B.; Luzinov, I. *Macromol. Rapid Commun.*, **32**, 859-869.
- (2) Edmondson, S.; Osborne, V. L.; Huck, W. T. S. *Chem. Soc. Rev.* **2004**, *33*, 14-22.
- (3) Huang, H. Q.; Rankin, S. E.; Penn, L. S.; Quirk, R. P.; Cheong, T. H. *Langmuir* **2004**, *20*, 5770-5775.
- (4) Kamiyama, Y.; Israelachvili, J. *Macromolecules* **1992**, *25*, 5081-5088.
- (5) DeGennes *Acad. Sci. Ser. 2* **1985**, *300*, 839.
- (6) Israels, R.; Leermakers, F. A. M.; Fleer, G. J.; Zhulina, E. B. *Macromolecules* **1994**, *27*, 3249-3261.
- (7) Zhulina, E. B.; Birshtein, T. M.; Borisov, O. V. *Macromolecules* **1995**, *28*, 1491-1499.
- (8) Biesheuvel, P. M. *J. Colloid Interface Sci.* **2004**, *275*, 97-106.
- (9) Ruhe, J.; Ballauff, M.; Biesalski, M.; Dziezok, P.; Grohn, F.; Johannsmann, D.; Houbenov, N.; Hugenberg, N.; Konradi, R.; Minko, S.; Motornov, M.; Netz, R. R.; Schmidt, M.; Seidel, C.; Stamm, M.; Stephan, T.; Usov, D.; Zhang, H. N. In *Polyelectrolytes with Defined Molecular Architecture I*; Springer-Verlag Berlin: Berlin, 2004; Vol. 165, p 79-150.
- (10) Hozumi, A.; Sugimura, H.; Yokogawa, Y.; Kameyama, T.; Takai, O. *Colloids and Surfaces a-Physicochemical and Engineering Aspects* **2001**, *182*, 257-261.
- (11) Nordgren, N.; Rutland, M. W. *Nano Letters* **2009**, *9*, 2984-2990.
- (12) Moad, G.; Rizzardo, E.; Thang, S. H. *Polymer* **2008**, *49*, 1079-1131.
- (13) Perrier, S.; Takolpuckdee, P. *Journal of Polymer Science Part a-Polymer Chemistry* **2005**, *43*, 5347-5393.
- (14) He, L.; Read, E. S.; Armes, S. P.; Adams, D. J. *Macromolecules* **2007**, *40*, 4429-4438.
- (15) Sumerlin, B. S.; Lowe, A. B.; Stroud, P. A.; Zhang, P.; Urban, M. W.; McCormick, C. L. *Langmuir* **2003**, *19*, 5559-5562.
- (16) Chen, W.; McCarthy, T. J. *Macromolecules* **1997**, *30*, 78-86.
- (17) Parnell, A. J.; Martin, S. J.; Dang, C. C.; Geoghegan, M.; Jones, R. A. L.; Crook, C. J.; Howse, J. R.; Ryan, A. J. *Polymer* **2009**, *50*, 1005-1014.
- (18) McCormack, D.; Carnie, S. L.; Chan, D. Y. C. *J. Colloid Interface Sci.* **1995**, *169*, 177-196.
- (19) Israelachvili *Intermolecular & Surface Forces*; 2nd ed.; Academic Press.

- (20) Ma, H. W.; Hyun, J. H.; Stiller, P.; Chilkoti, A. *Adv. Mater.* **2004**, *16*, 338-+.
- (21) Prieve, D. C.; Frej, N. A. *Langmuir* **1990**, *6*, 396-403.
- (22) Berg, H. C. *Random Walks in Biology*; Princeton University Press, 1983.
- (23) Bickel, T. *Physica A* **2007**, *377*, 24-32.
- (24) Faucheux, L. P.; Libchaber, A. J. *Physical Review E* **1994**, *49*, 5158-5163.
- (25) Kim, M.; Anthony, S. M.; Granick, S. *Phys. Rev. Lett.* **2009**, *102*, 4.
- (26) Goldman, A. J.; Cox, R. G.; Brenner, H. *Chem. Eng. Sci.* **1967**, *22*, 637-&.
- (27) Liberelle, B.; Giasson, S. *Langmuir* **2008**, *24*, 1550-1559.
- (28) Drechsler, A.; Synytska, A.; Uhlmann, P.; Elmahdy, M. M.; Stamm, M.; Kremer, F. *Langmuir*, *26*, 6400-6410.
- (29) Flory, P. I. *Journal of Chemical Physics* **1942**, *10*, 51-61.
- (30) De, S. K.; Aluru, N. R.; Johnson, B.; Crone, W. C.; Beebe, D. J.; Moore, J. *Journal of Microelectromechanical Systems* **2002**, *11*, 544-555.
- (31) Chen, G. H.; Hoffman, A. S. *Nature* **1995**, *373*, 49-52.
- (32) Topham, P. D.; Howse, J. R.; Mykhaylyk, O. O.; Armes, S. P.; Jones, R. A. L.; Ryan, A. J. *Macromolecules* **2006**, *39*, 5573-5576.
- (33) Topham, P. D.; Howse, J. R.; Crook, C. J.; Parnell, A. J.; Geoghegan, M.; Jones, R. A. L.; Ryan, A. J. *Polymer International* **2006**, *55*, 808-815.
- (34) Topham, P. D.; Howse, J. R.; Crook, C. J.; Armes, S. P.; Jones, R. A. L.; Ryan, A. J. *Macromolecules* **2007**, *40*, 4393-4395.
- (35) Khare, A. R.; Peppas, N. A. *Biomaterials* **1995**, *16*, 559-567.
- (36) Butun, V.; Armes, S. P.; Billingham, N. C. *Polymer* **2001**, *42*, 5993-6008.
- (37) Parnell, A. J.; Martin, S. J.; Jones, R. A. L.; Vasilev, C.; Crook, C. J.; Ryan, A. J. *Soft Matter* **2009**, *5*, 296-299.
- (38) Firestone, B. A.; Siegel, R. A. *Journal of Applied Polymer Science* **1991**, *43*, 901-914.
- (39) Hou, X. H.; Liu, B. L.; Deng, X. B.; Zhang, B. T.; Chen, H. L.; Luo, R. *Analytical Biochemistry* **2007**, *368*, 100-110.
- (40) Rauf, S.; Ihsan, A.; Akhtar, K.; Ghauri, M. A.; Rahman, M.; Anwar, M. A.; Khalid, A. M. *Journal of Biotechnology* **2006**, *121*, 351-360.
- (41) Caruso, F.; Schuler, C. *Langmuir* **2000**, *16*, 9595-9603.
- (42) Decher, G. *Science* **1997**, *277*, 1232-1237.

- (43) Goodwin, J. W.; Hearn, J.; Ho, C. C.; Ottewill, R. H. *Colloid and Polymer Science* **1974**, 252, 464-471.
- (44) Taylor, W.; Jones, R. A. L. *Langmuir*, 26, 13954-13958.
- (45) Matyjaszewski, K.; Miller, P. J.; Shukla, N.; Immaraporn, B.; Gelman, A.; Luokala, B. B.; Siclovan, T. M.; Kickelbick, G.; Vallant, T.; Hoffmann, H.; Pakula, T. *Macromolecules* **1999**, 32, 8716-8724.
- (46) Herzer, N.; Hoepfener, S.; Schubert, U. S. *Chem. Commun.*, 46, 5634-5652.

6 Summary, Discussion and Conclusions

6.1 Summary

In chapter 2 the feasibility of the theoretical design was assessed and changes necessary to make the design work suggested. It was found that particles could adhere to oppositely charged surfaces but could not be spontaneously released due to van der Waals force. From investigation of the frictional forces between the particle and surface it was also found that a particle could not slide across a surface without encountering a large frictional force. To overcome these problems it was suggested that the particle-surface interaction be changed from a totally adhesive interaction, to one in which the particle is either initially attached to the surface and then repelled, or an interaction where the particle is totally repelled away from the surface at all times.

The modification of the surface by the controlled release of nanoparticles from a microcapsule was also discussed and investigated. It was found that nanoparticles could not be released from a microcapsule at a controlled rate using existing synthetic techniques, and that nanoparticles do not significantly change the properties of a surface into which they adhere. The fraction of surface functionalisation was also found to be low at around 22%. To overcome these problems it was suggested that the nanoparticles be substituted for a chemical species which alters the surface. Furthermore the chemical species should be generated by a chemical reaction rather than be released, allowing a larger surface area to be modified.

In chapter 3 these changes to the theoretical design were taken heed of and an implementation of the design created based on repulsive van der Waals forces. In this implementation the particle-surface interaction consisted of only a single contribution from van der Waals forces, which Lifshitz theory predicted could be changed from an attractive to a repulsive interaction, allowing particles to be released from a surface.

Experiments showed that metal particles could be repelled away from a silica surface when dispersed in bromobenzene, and attracted to the surface when dispersed in a mixture of benzene and bromine. A chemical reaction was identified to convert the particle-surface interaction from adhesive to repulsive, which is catalysed by iron particles. It was also found that the adhesion of iron particles to a silica surface may be irreversible due to the contamination of surfaces. In all experiments, no propulsion of particles was observed.

Measurement of the rate of reaction occurring on the catalytic iron particles and calculation of the concentration of bromobenzene around the particle showed that the concentration was not high enough to release particles from the silica surface. This was caused by the rate of reaction and fast diffusion of bromobenzene away from its source. To make the implementation work, an unphysically high rate of reaction was found to be needed.

In chapter 4 an implementation of the theoretical design based on repulsive electrostatic forces was investigated. Calculations of the particle-surface interaction showed that a particle could be repelled further away from a surface by increasing the charge of a surface. Meaning that the particle-surface interaction became more repulsive with increasing surface charge and that particles should migrate down a gradient of surface charge to areas of low surface charge.

Gradients of electrostatic repulsion were mimicked by inclining a glass microscope slide at an angle. It was found that moderately fast propulsion velocities could be created by a small incline in the surface, suggesting that particles should migrate down a gradient of surface charge. Very short and sharp electrostatic gradients were also created by photo-patterning surfaces. Investigation of the behaviour of particles on these surfaces showed that the electrostatic interactions did not significantly influence the particles and so could not be used in an implementation of the theoretical design.

In chapter 5 implementations of the theoretical design based on repulsive steric interactions were investigated. Polymer brush surfaces were used to repel dense particles away from the surface and gradients of steric repulsion were created by photolithography. These steric gradients were found to be able to significantly influence particles and control their motion, meaning that they are useful in implementing the theoretical design.

The repulsion experienced by a particle could be altered by changing the thickness of the polymer brush using a chemical reaction such as protonation, deprotonation or quaternisation using methyl iodide. Kinetic studies showed that quaternisation with

methyl iodide was too slow to be of any use in implementing the theoretical design, whereas protonation was fast and could be used.

Potential motor particles were created by immobilising glucose oxidase onto particles. Investigation of the rate of reaction and calculation of the pH around the motor particle showed that the rate of reaction was too slow to swell the polymer brush and create propulsion. Particles of benzoic acid were created which were capable of releasing acid at the required rate but optical microscopy showed that these particles ran out of their store of acid within a minute and so were of no use.

The grafting-to approach was also investigated to find out if it could be used in an implementation of the theoretical design. Kinetic ellipsometry showed that the polymer layer created formed too slowly and was of insufficient thickness to be of use.

6.2 Discussion

It is informative to compare the results gathered from all implementations of the theoretical design investigated and the preliminary results gathered in chapter 2 to find common reasons why all implementations failed.

Substituting a Repulsive Interaction for an Adhesive Interaction

In the theoretical design the interaction between the particle and surface changes from initially attractive to become less attractive when the surface is modified by the nanoparticles released from the motor particle. As was shown in chapter 2 this interaction needs to be modified to allow the particle to be repelled from the surface and migrate down the gradient of surface interaction. In all of the experimental work carried out in this study, a repulsive interaction has been used to repel the particle away from the surface. In chapter 3 this interaction was initially attractive and then changes to be repulsive, whereas in chapters 4 and 5, particle-surface interactions were investigated which were totally repulsive.

This necessary change has consequences for the scope of the propulsion created. When surface-particle interactions are totally repulsive, as in chapters 4 and 5, a relatively large and dense particle must be used. This is because the change in particle energy is due to

the gain in gravitational potential energy as the particle is repelled further away from the surface against gravity.

When a surface-particle interaction which is initially attractive and is then converted to repulsive upon release of a chemical, as in chapter 3, the particle should also be large and dense to maximise the change in particle energy as it is raised off the surface. The particle could also be neutrally buoyant when this interaction is used and instead of relying on gravity to propel the particle forward its mobility can be used. When the particle is adhered to the surface its mobility is zero and when repelled away from the surface non-zero, meaning that the particle should migrate from areas of repulsion to areas of adhesion.

As has been shown in the later half of chapter 3, surface interactions which change from adhesive to less adhesive could be used to implement the theoretical design, if the particles are agitated in a way which pulls them off the less adhesive surface without pulling them off the strongly adhesive surface. This agitation needs also to not interfere with the distribution of nanoparticles or chemical species around the motor particle which creates the surface interaction gradient. Achieving this agitation of particles in practice without perturbing the distribution of nanoparticle / chemical species may be very difficult.

It has therefore been shown that the attractive particle-surface interaction in the theoretical design could be substituted for a partially or totally repulsive interaction. Both van der Waals force and steric forces were found to be able to change the particle-surface interaction and control the position of particles on surfaces, whereas electrostatic interactions were found to be incapable of influencing the position of particles.

Using Solid Particles instead of Hollow Microcapsules

In the theoretical design the target and motor particles consist of a membrane which encapsulates a liquid inside. The authors suggest that these particles could be something like particles created by the layer-by-layer deposition of polyelectrolytes¹. In all implementations of the theoretical design investigated and the preliminary studies of chapter 2, solid particles have been used.

Although solid particles initially seem completely different to hollow ones, they do in fact behave in a similar way. For example in chapter 2, it was found that particles cannot adsorb onto a surface and then spontaneously release due to van der Waals force, and it may be thought that using a hollow particle may help in this situation. But it does not, as the thickness of the membrane in hollow particles created by layer-by-layer deposition is around 30nm² and as van der Waals force is severely retarded at distances greater than

15nm, the interaction depends predominantly on the structure of the particle very close to the surface. Therefore adhesion of a hollow or solid particle due to van der Waals force is identical as they both have a similar structure in the first 30nm above the surface.

A case in which solid and hollow particles do not behave identically is when the thickness of the membrane is very thin, as in a phospholipid vesicle. Marra and Israelachvili³ studied the surface forces between lipid bilayers and found that van der Waals forces were smaller than expected but still caused adhesion of the two bilayers when forced together. Although van der Waals force is smaller than when using a solid particle it is still present and leads to irreversible adhesion.

In all implementations of the theoretical design used in this work, large dense solid particles have been used. This means that the orientation of the surface along which particles travel is limited to being exactly level and perpendicular to the gravitational force. Particles can no longer travel in a vertical direction as they could if neutrally buoyant particles were used.

Using Chemical Reagents instead of Nanoparticles

In the theoretical design the surface is altered by the adsorption of nanoparticles which are released from the motor microcapsule. As was discussed in chapter 2, the release of nanoparticles from a microcapsule is not currently synthetically feasible and experiments showed that nanoparticles do not significantly alter the properties of surfaces, so an alternative mechanism was used. In this alternative method nanoparticles are replaced with a chemical species which modifies the surface, which allows the scope of the surface modification to be vastly increased due to the breadth of chemical modifications known. To prevent a motor particle quickly running out of its supply of encapsulated chemical, as was shown to be the case in chapter 5 with benzoic acid, catalytic reactions were used to create the chemical species, with the catalyst immobilised on the motor particles surface. This allows the motor particle to act as a source of the chemical species almost indefinitely, rather than the 60 seconds observed for benzoic acid particles.

This substitution has significant effects which may change the design so much, that it is no longer adequately modelled by the computational work. The diffusion coefficient of the species which modifies the surface has been increased 10-100 times by this substitution, meaning that the chemical species migrates away from the motor particle much faster than nanoparticles would. This alters the concentration of the chemical species around the particle making the interaction gradient more diffuse reducing the propulsive force generated. It also increases the rate at which the substance must be released into solution to create a local high concentration around the motor particle. If

the diffusion coefficient is increased by 100, then the rate at which the substance is released must also be increased by 100 to maintain the same concentration at a specific point.

With all implementations of the theoretical design investigated, it was the concentration of the active chemical species around the motor particle which ultimately resulted in the implementation not working. In chapter 3 it was found that the rate of bromination by iron particles needed to be 7,600 times faster to surround the particle with bromobenzene and convert the attractive surface interaction to repulsive. In chapter 5 it was found that the rate of gluconic acid production needed to be 66 times faster to swell the polymer brush underneath particles.

Therefore from these results it seems that substituting a chemical species for nanoparticles is not a suitable alternative to the problem and is the main reason why implementations did not succeed in producing propulsion. It is disappointing that electrostatic repulsions could not significantly influence particles, as this would have allowed the self assembly of thiols on gold to be used. This chemical reaction has been shown to be moderately fast at very low concentrations, meaning that the rate of release from a potential motor particle could be very low and practically possible.

Getting to Time = Zero in the Computational Models

All computational modelling used by Balazs et al, starts with a motor and a target capsule positioned next to each other on the surface, and then at the start of the modelling nanoparticles are released from the motor capsule. Getting to this arrangement in real life implementations of the design is challenging. As was shown in chapter 2, a motor and a target particle rarely come into close proximity with each other on the surface if the concentration of particles is low. If the concentration is raised, target and motor particles are observed in close proximity to each other but there is now also many other particles in close proximity to the pair of particles, blocking their path and interfering with the surface interaction gradient created.

Getting a motor capsule to start to release nanoparticles at a specific time is also challenging. De Geest et al⁴ have created microcapsules which rupture and release encapsulated nanoparticles, but the exact time when this occurs cannot be controlled. In this work particles have been created which create a chemical species by a catalytic reaction on their surface, they release the chemical species constantly and cannot be turned on or off.

Several approaches could be taken to help improve the chances of an implementation of the theoretical design succeeding. Firstly, optical tweezers⁵ could be used to precisely

position a motor and target capsule in close proximity overcoming the problem of the two capsules rarely being found close together. Secondly, motor capsules should be developed which can be triggered by an external stimulus to start releasing a chemical substance. Ideally this release should be triggered by a stimulus of light of a particular wavelength, as this can be applied instantaneously unlike a chemical stimulus which requires time to diffuse. Perhaps a photo-catalytic reaction could be used to generate the chemical species.

6.3 Conclusion

Using a particle-surface interaction which changes from adhesive to less adhesive, would not result in the propulsion of a particle along a surface. As was found in chapter 2, adhesion is irreversible and particles cannot slide along surfaces without encountering significant friction. Nanoparticles cannot be released from a microcapsule without rupturing the membrane and these nanoparticles also do not significantly change the properties of a surface onto which they adsorb, meaning that they do not alter the particle-surface interaction.

It has been shown in chapter 3 that van der Waals forces can be used to change the particle-surface interaction from adhesive to repulsive. Iron particles can convert a mixture of benzene and bromine to bromobenzene but were shown to not be able to surround themselves with a sufficient amount of bromobenzene to be repelled from the surface, due to the high diffusion coefficient and rate of reaction.

Repulsive electrostatic forces cannot be used to change the particle-surface interaction in implementing the theoretical design, as they were found to be unable to significantly influence a particle. Adhesive electrostatic forces were found to be able to control particles but are of no use in implementing the theoretical design as adhesion to their surface is irreversible.

Steric repulsion can be used to precisely control the position and motion of small particles which sediment onto their surface. As shown in chapter 5, these steric repulsions can be altered through a chemical reaction such as protonation or quaternisation, meaning that the interaction can be used to implement the theoretical time. Motor particles can be created with an attached enzyme which catalyses the production of acid, but the rate of reaction is too slow to lower the pH of the surrounding solution below the pK_a of the polymer brush enabling it to swell. Changing steric repulsions by quaternisation using methyl iodide gives a rate of reaction which is slow compared to the diffusion of methyl iodide away from the motor particle, meaning that it cannot create a suitable surface interaction gradient. The grafting-to approach was found to not significantly change the surface repulsions.

Implementations where a suitable interaction was found ultimately failed because of the high rate of release needed from a motor particle to surround itself with a high concentration of the chemical species. This is due to the large diffusion coefficient of small molecules. Therefore substituting a chemical species for the nanoparticles used in the theoretical design has allowed surfaces to be modified, changing particle-surface

interactions, but means that surface interaction gradients cannot be created due to the faster diffusion of the smaller species.

6.4 Future Work

Further investigation into creating an implementation of the theoretical work could take a number of directions. Computational modelling of the implementations of the theoretical design used in this study may prove useful in suggesting changes to the theoretical design which make it feasible. Using computational modelling a wide variety of variables can be changed and measurements made that are not possible experimentally. For example, throughout this study the concentration of chemical species around a motor particle has been calculated using equations which do not account for the effects of the nearby target particle or the proximity of the surface. Computational modelling could take into account these effects and compute the exact concentration profiles around particles.

A way must be found of creating a surface interaction gradient by the release of a substance from a particle. It has been shown that nanoparticles cannot be used because they do not alter surfaces significantly. Chemical species cannot be used either as they diffuse away too fast to create the desired gradient, therefore some other method of creating the surface interaction gradient must be found.

Developing surface interaction gradients along which a single polymer chain is propelled may allow a particle to be tethered to the surface and also be propelled along. This research direction was not pursued and may enable propulsion of particles as long as the particle remains repelled above the surface.

Particle-surface interactions which change from adhesive to less adhesive may be able to propel a particle forward. As was shown in chapter 5, particles can migrate from an area of weak to strong adhesion if some method of pulling the particles off weak adhesion areas can be found. This method should not pull the particles off areas of strong adhesion and also should not interfere with the distribution of nanoparticles or chemical species released from the motor particle.

References

- (1) Decher, G. *Science* **1997**, *277*, 1232-1237.
- (2) Lensen, D.; Vriezema, D. M.; van Hest, J. C. M. *Macromolecular Bioscience* **2008**, *8*, 991-1005.
- (3) Marra, J.; Israelachvili, J. *Biochemistry* **1985**, *24*, 4608-4618.
- (4) De Geest, B. G.; De Koker, S.; Demeester, J.; De Smedt, S. C.; Hennink, W. E. *Polymer Chemistry*, *1*, 137-148.
- (5) Dholakia, K.; Reece, P.; Gu, M. *Chem. Soc. Rev.* **2008**, *37*, 42-55.

Appendix 1: Calculation of the forces F and f in Chapter 5.

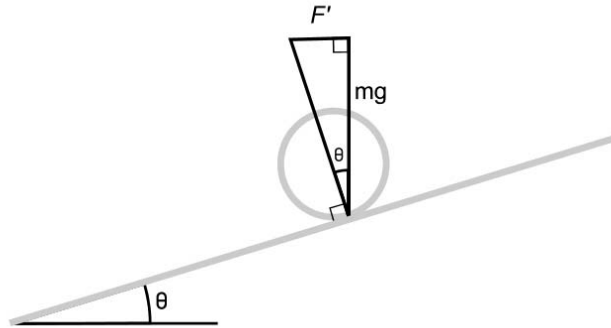


Figure 1

To calculate the force propelling a silica particle down a surface inclined at the angle θ , a triangle can be drawn as in figure 1. The gravitational force of the particle (mg) (mass = dry mass – mass of water displaced) acts downwards and the surface repulsions either electrostatic or steric act on the particle normal to the inclined surface. Therefore the force F' propelling the particle from right to left can be calculated as:

$$F = mg \tan \theta \quad \text{eq. 1}$$

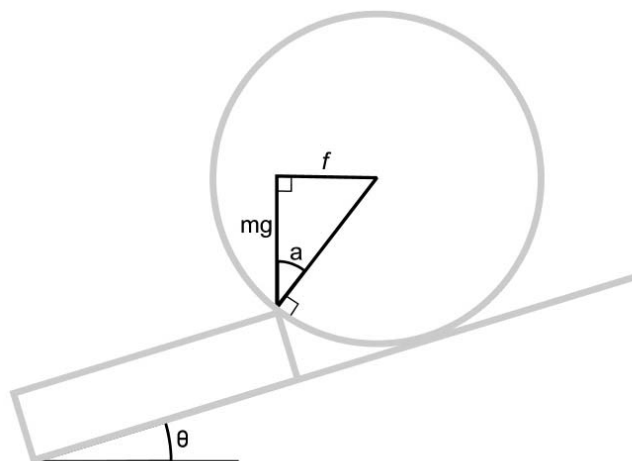


Figure 2

To calculate the force acting on particles by a polymer brush, the brush layer is treated as an incompressible slab. A triangle can be constructed as in figure 2. The gravitational force acts downwards and the repulsion from the polymer brush layer acts in a direction normal to the particles surface. Therefore the force acting on the particle f by the polymer brush antiparallel to the driving force F can be calculated as:

$$f = mg \tan(a) \quad \text{eq. 2}$$

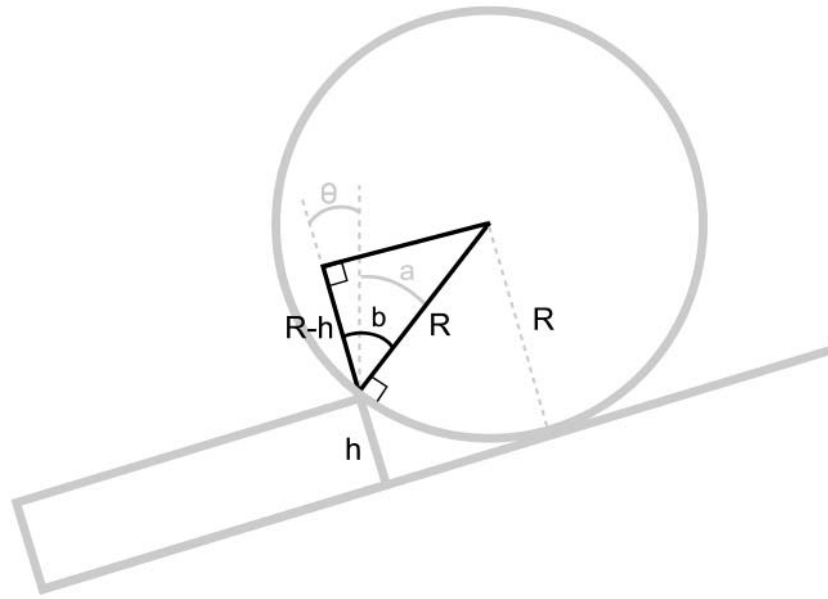


Figure 3

To find the angle a it is necessary to create another triangle as shown in figure 3, where R is the radius of the particle and h is the height of the polymer brush estimated from spectroscopic ellipsometry. The angle b can be calculated from a ratio of particle radius and brush height:

$$b = \cos^{-1}\left(\frac{R-h}{R}\right) \quad \text{eq. 3}$$

And then the angle a can be calculated by:

$$a = b - \theta \quad \text{eq. 4}$$

When $\alpha = 90^\circ$ f and F' are antiparallel whereas at all other angles the forces are not antiparallel, as shown in antiparallel to the propulsive force f needs to be calculated using the equation:

$$F = F' \cos(90^\circ - \alpha) \quad \text{eq. 5}$$

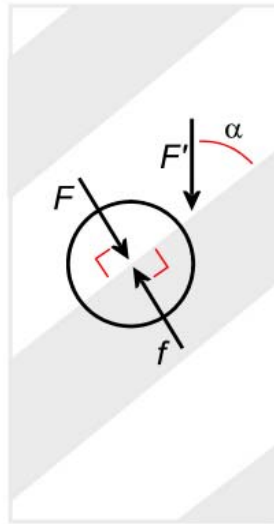


Figure 4

Calculation of F and f in this work

Using the values radius = $10\mu\text{m}$, density = $2000 - 1000 = 1000 \text{ kg m}^{-3}$ and $\theta = 4.5^\circ$

$$F = 3.2 \text{ pN}$$

Taking the height of the polymer brush to be the value found by ellipsometry $h = 85\text{nm}$.

$$f = 2.1 \text{ pN}$$

So when $\alpha = 90^\circ$, f is smaller than F at 2.1 pN allowing particles to pass over brush interfaces, giving *non-compliant* behaviour. F is approximately equal to f at angles between $30 - 50^\circ$ giving *partially compliant* behaviour. When $\alpha < 30^\circ$ F is smaller than f , resulting in *compliant behaviour*.